Université de Liège

Faculté des Sciences Appliquées

Analysis of simple connections in steel structures subjected to natural fires

Thèse présentée par François Hanus en vue de l'obtention du grade de

Docteur en Sciences Appliquées

Année Académique 2009-2010

MEMBERS OF THE JURY

Prof. Jean-Pierre JASPART (President of the Jury)
University of Liège, Department of Architecture, Geology, Environment and Constructions
Bât. B52, Chemins des Chevreuils, 1
4000 Liège – Belgium

Prof. Jean-Marc FRANSSEN (Promoter of the Thesis)
University of Liège, Department of Architecture, Geology, Environment and Constructions
Bât. B52, Chemins des Chevreuils, 1
4000 Liège – Belgium

Prof. Jean-Claude DOTREPPE
University of Liège, Department of Architecture, Geology, Environment and Constructions
Bât. B52, Chemins des Chevreuils, 1
4000 Liège – Belgium

Prof. André PLUMIER
University of Liège, Department of Architecture, Geology, Environment and Constructions
Bât. B52, Chemins des Chevreuils, 1
4000 Liège – Belgium

Dr. Bin ZHAO
Centre Technique Industriel de la Construction Métallique, Service Recherche Incendie
Espace Technologique – L'Orme des merisiers – Immeuble Apollo
91193 Saint-Aubin - France

Prof. Luís SIMÕES DA SILVA
University of Coimbra, Department of Civil Engineering
Rua Luis Reis Santos – Polo II da Universida – Pinhal de Marrocos
3030-688 Coimbra - Portugal

Dr. Olivier VASSART
ArcelorMittal, Research and Development, Structural Long Products
Rue de Luxembourg, 66
4009 Esch-sur –Alzette – GD Luxemburg

Abstract

Until recently, investigations on the fire resistance of steel joints have been neglected by structural engineers under the arguments that the design resistance of connections at room temperature is usually higher than the resistance of the connected members and that the temperature increases more slowly in the joint zone (high concentration of mass, low exposure to radiative fluxes) than in the adjacent beams and columns. However, brittle failures of connection components have been observed especially during the cooling phase of real fires for two main reasons: the high sensitive and non-reversible character of the resistance of bolts and welds at elevated temperatures and the development of high tensile thrusts. The present thesis is a contribution to the understanding of the thermo-mechanical behaviour of simple connections in steel beam-to-column joints subjected to natural fire conditions, with a special attention to the behaviour of these connections during the cooling phase.

The distribution of temperature in joints has been analysed by use of numerical models built in SAFIR software. The simplified methods presently mentioned in the Eurocodes are discussed and new methods, calibrated on the results of numerical simulations, are proposed in the present work to predict the temperature profile in steel beams and joints covered by a flat concrete slab under fire.

An existing method aimed at evaluating the distribution of internal forces in restrained steel beams (and by extension, in joints) under natural fire has been analysed in detail. Several modifications have been added in order to improve this method and to extend its field of application. The final version of this analytical method has been implemented and validated against numerical results.

An experimental programme aimed at characterising the mechanical behaviour of bolts and welds under heating and subsequent cooling is described in the present thesis. The properties of the tested specimens, the thermal loading applied to these specimens, the test set-ups and the results of the tests are reported in detail. Mechanical models for bolts loaded in tension or in shear have been calibrated on the experimental results. The loss of resistance of bolts and welds due to their non-reversible behaviour under heating and subsequent cooling has been quantified.

Finally, a large part of the thesis is dedicated to the development of component-based models representing the action of common simple connections under natural fire conditions and to the analysis of the behaviour of these connections as a part of a sub-structure or large-scale structure. These simple models can be used for parametric analyses because it conciliate a reasonable time of definition of the data, an acceptable time of simulation and a good degree of accuracy of the results. Recommendations for the design of connections have been defined. The ductility of connections has a major influence on

the occurrence of connection failures and classes of ductility for connections, dependant of the fire loading, have been defined in this work.

Résumé

Jusque très récemment, la recherche sur la résistance au feu des assemblages métalliques a été délaissée par les ingénieurs sous le prétexte que la résistance de calcul des assemblages à froid est habituellement supérieure à celle des éléments connectés et que l'échauffement est plus lent dans la zone d'assemblage que dans les poutres et colonnes adjacentes (grande concentration de matière, exposition réduite aux flux radiatifs). Toutefois, les ruptures fragiles de composants d'assemblages sont observées, notamment durant la phase de refroidissement pour deux raisons principales : caractère sensible et non-réversible des boulons et des soudures aux élévations de température et apparition d'efforts de traction importants. La présente thèse s'inscrit comme une contribution à la compréhension des phénomènes gouvernant le comportement des assemblages simples poutre-poteau sous conditions de feu naturel. Une attention spéciale est portée au comportement de ces assemblages durant la phase de refroidissement.

La distribution de température dans les assemblages a été analysée grâce à des modèles numériques mis au point dans le programme SAFIR. Les méthodes simplifiées actuellement mentionées dans les Eurocodes actuels sont discutées et de nouvelles méthodes, calibrées sur les résultats numériques, sont proposées dans ce travail pour prédire le profil de température dans les poutres et assemblages métalliques couverts d'une dalle en béton sous feu.

Une méthode existante destinée à évaluer la distribution des efforts internes dans les poutres en acier restraintes (et par extension, dans les assemblages) sous feu naturel a été analysée en détail. Plusieurs modifications ont été proposées pour améliorer cette méthode et étendre son champ d'application. La version finale de cette méthode analytique a été implémentée et validée avec des résultats numériques.

Une série de tests expérimentaux destinée à caractériser le comportement mécanique des boulons et des soudures sous échauffement et refroidissement est décrite dans cette présente thèse. Les propriétés des spécimens testés, le traitement thermique qui leur est appliqué, le montage des essais et les résultats obtenus sont rapportés en détail. Des modèles mécaniques pour les boulons soumis à traction ou cisaillement sont calibrés sur les mesures expérimentales. La perte de résistance des boulons et des soudures causée par leur comportement non-réversible sous échauffement et refroidissement a été quantifiée.

Finalement, une large part de la thèse a été dédiée au développement de modèles basés sur la méthode des Composantes pour représenter l'action des assemblages simples courants sous feu naturel et

l’analyse de leur comportement dans une sous-structure ou une structure complète. Ces modèles simples permettent de concilier un temps de définition des données raisonnable, un temps de calcul acceptable et un bon niveau de précision des résultats. Des recommandations pour le dimensionnement des assemblages ont été énoncées. Il est démontré que la ductilité des connections a une influence majeure sur l’apparition de ruptures dans les assemblages et des classes de ductilité, dépendant du chargement au feu, ont été définies dans ce travail.

Table of contents

List of Figures

List of Tables

Acknowledgement

The present thesis is the output of four years of researches at the University of Liège in collaboration with other research centers of Europe. All the persons that have contributed to this teamwork are gratefully acknowledged.

My gratitude goes firstly to Prof. Jean-Marc Franssen, promoter of this thesis, for his support and the guidance of my researches. His experience in the field of structural fire engineering and numerical modelling has been a precious source of inspiration. The advices of Prof. Jean-Pierre Jaspart and Dr. Jean-François Demonceau have also been a considerable help for the successful completion of this work.

I am grateful for the work provided by Giuliani Zilli (Centro Sviluppo Materiali, Italy), Arnoud Breunese (Efectis Nederland, The Netherlands), Bin Zhao (CTICM, France) and technicians in order to ensure the right achievement of experimental work.

I would like to thank my former and current colleagues of the "Fire Group" of the University of Liège for the interesting discussions and pleasant moments we had: Nuno Lopes, Thi-Bin Chu, Jean-Baptiste Lansival, Christophe Peigneux, Thomas Gernay, Alain Alonso Ipiña and, more particularly, David Janssen withwhom I shared an office room during four years.

Last but not least, I want to thank my parents and Jehanne for their continuous support and apologize to my family and friends for the insufficient time and attention devoted to them during both my under-graduate and post-graduate studies.

Notations

Latin Upper Case Letters

A Cross-section area of beam. Tensile stress area of bolt

A_f Floor surface

A_m Surface area per unit length of steel members

A_m/V Section factor for unprotected members

$(A_m/V)_b$ Box value of the section factor for unprotected members

A_s Reduced section area of the bolt

A_t Total area of the compartment

$A_{top\text{-}bottom}$ Area of heat transfer between the top and bottom flanges

$A_{transfer\ slab}$ Area of heat transfer between top flange and concrete slab

A_v Area of vertical openings

A_{vc} Shear area of column

E Young's modulus

E_b Young's modulus of bolts

F_{ij} View factor between two surfaces

F_{pl} Plastic axial force

F_{Rd} Plastic resistance of a component or a row

F_T Axial force in the beam

F_{pb} Proportional tensile force of bolts

$F_{S,Rd}$ Maximal friction force trnadsferred by a non-preloaded bolt

F_{tb} Tensile force in bolts at the point of inflexion of the descending branch

F_{ub} Ultimate tensile force of bolts

$F_{v,Rd}$ (= R_b) Design resistance of bolts in shear

$F_{w,Rd}$ Design resistance of welds in shear

G Self-weight load

I Second moment of inertia

I_y Second moment of inertia according to the horizontal axis

K Level of axial restraints. Stiffness of a component in a bolt or compressive row. Stiffness of a bolt or compressive row

K_A Axial stiffness of the surrounding frame

$K_{A,beam}$ Axial stiffness of the beam

K_{ini} Initial stiffness of a component or a row

K_R Rotational stiffness of the surrounding frame

L Length

L_b Bolt elongation length

M Bending moment

$M_{c,Rd}$ Design bending moment of the beam section

M_P Externally applied free bending moment

M_R Restraint bending moment

M_t Thermally-induced bending moment

M_T Mid-span bending moment

$M_{j,Rd}$ Design resisting moment of the joint without axial forces

$M_{j,Sd}$ (or $M_{j,Ed}$) Bending moment applied to the joint

N Axial force

$N_{j,Rd}$ Design axial force of the joint

$N_{j,Sd}$ (or $N_{j,Ed}$) Axial force applied to the joint

N_t Thermally-induced axial force

O Opening factor

Q Quantity of heat

R_b (= $F_{v,Rd}$) Design resistance of bolts in shear

$R_{u,b}$ Ultimate resistance of bolts in shear

S_b (or $S_{b,v}$) Initial stiffness of the force-displacement diagram of bolts in shear

$S_{b,t}$ Initial stiffness of the force-displacement diagram of bolts in tension

$S_{st,b}$ Strain-Hardening stiffness of the force-displacement diagram of bolts in shear

S_j Tangent rotational stiffness of a joint

$S_{j,ini}$ Initial rotational stiffness of a joint

T_f Failure temperature (or test temperature)

T_u Up temperature (reached at the end of the heating phase)

V Volume. Shear force

V_{Ed} Shear force applied to the joint section

W Section modulus

Latin Lower Case Letters

a Weld thickness

b Thermal absorptivity of the total enclosure. Width

$b_{eff,c,wc}$ Effective width of the column in the compression zone

$b_{eff,t,wc}$ Effective width of the column in the tension zone

c Specific heat

c_f Coefficient of interpolation for the beam deflection profile

d Nominal diameter of bolt. Depth

d_{M16} Nominal diameter of a reference M16 bolt

d_p Thickness of fire protection material

d_{pb} Proportional deformation of bolts in tension

d_{tb} Deformation of bolts in tension at the point of inflexion of the descending branch

d_{ub} Ultimate deformation of bolts in tension

d_{yb} Yield deformation of bolts in tension

e_1 End distance from the centre of a fastener hole to the adjacent end of any part, measured in the direction of load transfer

e_2 End distance from the centre of a fastener hole to the adjacent end of any part, measured perpendicularly to the direction of load transfer

f_p Proportional limit of stress

f_y Yield strength

f_u Ultimate strength

f_{ub} Ultimate strength of bolts

h Height

h_{eq} Weighted average of window heights on all walls

$h_{net,d}$ Design value of the net heat flux accounting for thermal exchanges by convection and radiation

k Stiffness coefficient of a joint component

k_b Conversion factor accounting for heat transfers in the neighbouring component parts of the compartment. Reduction factor for bolts strength

k_c Conversion factor depending on the material of structural cross-sections

k_E Reduction factor for Young's modulus of carbon steel

k_ε Reduction facor on the emissity accounting for shadow effect

$k_{nr,b}$ Reduction factor for the non-reversible behaviour of bolts and welds

$k_{nr,w}$ Reduction factor for the non-reversible behaviour of welds

k_p Reduction factor for the proportional limit of carbon steel

k_w Reduction factor for welds strength

l_{eff} Effective length

n_b Number of shear planes

n_{comp} Number of components in a bolt or compressive row

$q_{f,d}$ Design value of the fire load

$q_{t,d}$ Design value of the fire load related to the floor surface

r_c Root radius

t Time

t* Fictive time

$t_{e,d}$ Equivalent time

w Weld

w_f Ventilation factor

z Vertical deflection. Lever arm between the tension and compression resistances

$z_{C.G.}$ Level of the gravity centre of the beam section

Greek Upper Case Letters

ΔL Variation of beam length

ΔL_m Variation of beam length due to mechanical deformations

ΔL_t Variation of beam length due to thermal deformations

$\Delta l/l$ Thermal elongation

ΔT Variation of temperature

Δt Time interval

Ψ Combination factor

Greek Lower Case Letters

α Coefficient of thermal expansion. Angle

α_c Coefficient of heat transfer by convection

β Ratio between the initial and strain-hardening stiffnesses of bolts in shear. Transformation parameter to account beam-end moments on shear panel

β_w Correlation factor

γ_M Partial safety factor for material property

δ Mid-span deflection

δ_b Elastic deformation of bolts

$\delta_{u,b}$ Ultimate deformation of bolts

$\delta_{f,b}$ Failure deformation of bolts (end of the descending branch)

ε Strain

ε_m Material emissivity

ε_f Fire emissivity

ε_t Thermal elongation

η Ratio between the elastic and ultimate deformations of bolts in shear. Stiffness modification factor

θ Temperature. Rotation

κ Ratio between the elastic and ultimate resistance of bolts in shear

λ Thermal conductivity

λ_p Plate slenderness

μ Slip factor

ρ Unit mass. Reduction factor for plate buckling

σ Constant of Stefan Boltzmann ($5.67*10^{-8}$). Normal stress

τ Shear stress

τ_{ub} Maximum allowed shear stress in bolts

ϕ Configuration factor

χ Curvature

ω Reduction factor for interaction with shear in column web panel

Sub-script

b Beam. Bolt

c Column

el Elastic

f Flange

i Row

j Component

m Mechanical

max Maximal

propor Related to the proportional limit of carbon steel

p Plate

pl Plastic. Related to the yield strength of carbon steel

ref Related to the reference time

t Thermal

u Ultimate

w Web

Abbreviations

YS Yield strength

UTS Ultimate tensile stress

1 Introduction

1.1 Concepts of Fire Safety Engineering

The control of fire by humans definitely enabled them to improve their level of well-being and theirs conditions of life. Fire helped them to generate heat and light, to cook, to produce some new materials and to develop new technologies. However, fire has also been a source of danger for humans in numerous dramatic cases. By the consequence of evil-minded acts or off-guard moments, fire sometimes becomes out of control and has two serious consequences: the death of persons and the destruction of material goods. During the second part of the 20th century, an effort was made to develop and apply more active and passive measures in order to limit the damages caused by fire. In Belgium, a major fire occurred in the Department Store "Innovation" (1967) where 322 people died. This highlighted the necessity of integrating Fire Engineering in the design of medium and high-rise buildings and encouraged authorities of the country to react by investigating more deeply on the behaviour of structures under fire conditions.

The distinction is made here between two concepts because confusion may arise from these different terminologies: Fire Safety Engineering and Structural Fire Engineering [Bailey, 2004]. Fire Safety Engineering is a global and multi-discipline science aimed at limiting the death of people and damages in buildings subjected to fire. By example, active and passive measures are taken to prevent the spread of fire, provide sufficient load-bearing capacity of structural elements. The analysis of the reaction to fire of elements included in a compartment and the toxicity of the combustion gases produced by the fire are also disciplines of the Fire Safety Engineering. Structural Fire Engineering is one of these disciplines and is aimed at analysing the effects of fire on a structure and designing members under the combination of thermal and mechanical loadings applied in case of fire.

A general analysis of Structural Fire Engineer consists of three basic steps: the modelling of the fire, the thermal analysis and the structural analysis. The modelling of the fire is a calculation of the gases temperature in a room or a compartment under fire scenarios as a function of the fire load, the dimensions of the compartment, the presence of openings, the material properties of walls and of the ceiling, etc. The thermal analysis is aimed at predicting the distribution of temperature in the different members of the structure. Finally, the structural analysis is a verification of the resistance and/or fire-separating function of structural elements under the combination of thermal and mechanical loadings.

Initially, the fire resistance of structural elements have been determined experimentally and compared to the requirements of legal prescriptions [Dotreppe, 1983]. However, the cost and the time needed for

these tests are considerable and testing all the real configurations of building is inconceivable. New processes, based on scientific work, have been developed. As a first step, empirical tables or formulae have been defined on the basis of fire tests performed under standard fires. Then, simplified calculation methods based on simple theories have been proposed to obtain safe design rules. Finally, numerical methods necessitating the use of computers have appeared. The real behaviour of structures under fire can be approached accurately by the use of Finite Element Methods. These methods lead to very good predictions but they are time-consuming and necessitate a financial investment. In present research projects, experimental tests and numerical tools are used to calibrate theories and deduce some design methods for usual practical applications.

1.2 Fire resistance of steel structures and steel connections

In comparison with other types of constructions, unprotected steel structures lose rather quickly their stability when submitted to elevated temperatures. The main explanation to this is the relative thinness of individual elements. The fast heating of structural elements induces a rapid reduction of their mechanical properties. Consequently, steel structures are often thermally-protected by insulating materials or intumescent paints [B.S., 1990]. However, the cost of fire protection is considerable: the increase of cost may reach 30% of the bare steelwork [Lawson, 2001]. Consequently, architects and engineers try to adapt the design of steel structures or to use composite action in order to optimize or avoid the use of fire-protecting materials [Wang, 1998 and Bailey, 1999].

During the last decades, the fire research projects carried out on steel buildings and supported by the European Coal and Steel Community were focused on the fire behaviour of single steel structural members: [ECSC, 1988; ECSC, 1995a and ECSC, 1995b]. The next fire research projects were aimed at investigating on the behaviour of global steel structures: [ECSC, 1999 and ECSC, 2000]. The joints behaviour under fire loading has not been studied so extensively. Until recently (see ENV 1993-1-2 [CEN, 1995]), it was considered as unnecessary to study the behaviour of joints in structures subjected to fire conditions because the less severe exposition and the presence of more material in the joint zone induce lower temperatures in that zone than in the connected members. The large amount of joints typologies, the large number of parameters influencing their behaviour and the difficulty to realize experimental tests are other explanations to the lack of sufficient knowledge of joints behaviour under fire conditions.

The collapse of WTC Twin Towers on the 11th of September 2001 has highlighted the possibility of connection failures and their detrimental effects on structures. Some experts have alleged that the failure of connections between truss beams and edge columns has played a significant role in the final

global collapse of the two towers. Furthermore, the damaged connections (distorted bolts and holes bearing) were documented as a failure mode of the WTC5, a 45-storey building that collapsed several hours after WTC 1 and 2 under the unique effect of fire [LaMalva, 2009]. Some investigations were conducted during the last years, mainly in Europe, on the behaviour of joints under fire. The first design rules have been established from the Component Method, firstly developed for joints at room temperature. This method has been adapted to accommodate with the design of joints under fire loading [Simões da Silva, 2001a].

Some real-scale tests performed in Cardington [Wald, 2005] and Vernon [ECSC, 2000] have also shown that steel and composite connections could become a weak point under fire conditions, especially during the cooling phase. Up to now, few researches have been focused on that phase (Figure 1-1). Failures of steel or steel-concrete composite structures may occur in connection components during the cooling phase due to the tensile forces created in steel beams after significant plastic deformations have been undergone during the heating phase (Figure 1-2). In fact, the plastic deformations in steel beams during the heating phase of a fire cause a significant contraction of the beam. During the cooling stage, high tensile forces are created and this may induce damage of the connection components [Bailey, 1996].

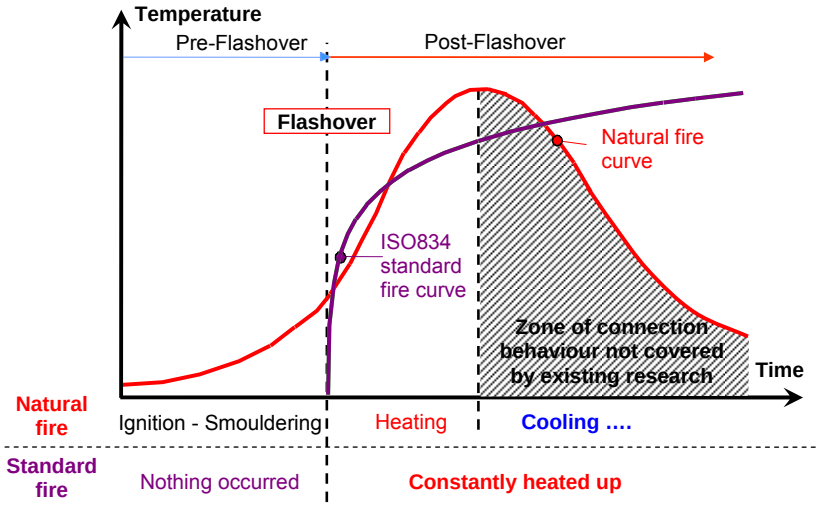

Figure 1-1 : Field of application of existing research work on connections in fire

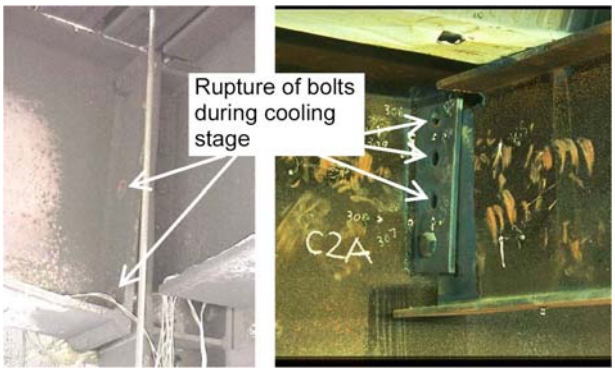

Figure 1-2 : Failure of bolts in steel connections subjected to natural fire

In the past, several research works have already been performed on the behaviour of steel connections under standard fire conditions. One of the first works carried out in this field was aimed at investigating the behaviour of different types of steel connections by means of standard fire tests [Kruppa, 1976]. Some years later, a research project was focused on behaviour of bolts at elevated temperatures [Riaux, 1980]. More recently, a series of research programmes on the behaviour of connections under fire have been carried out in United Kingdom. A brief summary is made hereafter.

- **Experimental and analytical work on the behaviour of bolts and welds at elevated temperatures [Latham, 1993 and Kirby, 1995].** These tests have demonstrated that, at elevated temperatures, the reduction of the bolts and welds resistance is more important than the reduction of resistance of carbon steel. On the basis of the results of these experimentations, specific reduction factors for bolts and welds have been integrated into the EN 1993-1-2 [CEN, 2004a] ;

- **Experimental work on bolted connections under standard fire exposure [Wainman, 1995].** Extended end-plate, flush end-plate and web cleats connections have been tested with or without fire protection under ISO fire. All the tests have been stopped because of beam vertical deflections, before any failure in the joint components ;

- **Experimental, analytical and numerical research works on the behaviour of bolted beam-to-column joints at the Universities of Manchester [Liu, 1996 and Liu, 1999b] and Sheffield [Leston-Jones, 1997; Al-Jabri, 2000; Spyrou, 2002; Block, 2006, Sarraj, 2007; Yu, 2009a; Yu, 2009b; Yu, 2009c and Yu, 2009d].** Liu developed the first finite element model, made of shell elements, able to predict the mechanical response of typical joints at elevated temperatures. The experimental investigations realised at the University of Sheffield are focused on the behaviour of isolated joints. Leston-Jones conducted eleven tests on flush end-plate connections (steel and composite) in order to develop some moment-rotation relationships for these connections. Additional tests performed by Al-Jabri

allowed studying the influence of parameters such as the size of members, the dimensions of the end-plate and the characteristics of composite slab. Spyrou investigated separately the performance at elevated temperatures of the tension zone (45 T-stub tests) and compression zone (29 tests on column webs under transversal compression). This led to simplified analytical models for the two zones and a component-based model integrated in the Vulcan software. This experimental and analytical work has been extended to joints subjected to axial forces by Block. Sarraj developed a component spring-model for fin-plate connections. Very recently, Yu realised experimental tests on simple connections (fin plate, web cleats and header plate connections) under a combination of tensile forces and bending moment at elevated temperatures. He developed a component-based model for web cleats connections and a yield-line model for header plate connections.

- **Experimental, analytical and numerical investigations about the influence of connections behaviour on the performance of steel and composite beams under fire conditions at the University of Manchester [Liu 1998; Liu, 1999a; Liu, 2002; Yin, 2005a and Yin, 2005b]**. Experimental tests have been performed by Liu on a "rugby goal post" sub-structure in order to investigate the role of typical connections (flush end-plate and web cleats connections) on the behaviour of steel beams under fire conditions. The development of catenary action preventing the running away of beams has been highlighted by this experimental programme. The enhancement of the fire resistance of beams with moment resisting connections by reduction of the mid-span bending moment has also been demonstrated. A simplified method for the analysis of catenary in restrained beams has been developed by Yin.

In all the mentioned research work, the cooling phase has almost not been considered. Block has treated the effects of unloading and cooling in his component-based model but few experimental results are available.

In parallel, the behaviour of steel joints under natural fire conditions has been investigated experimentally and numerically at the University of Coimbra [Santiago, 2008d]. Six tests have been performed on steel sub-structures under the reproduced thermal conditions of the 7th Cardington fire test. The influence of joints typologies on the behaviour of the frame has been analysed. The brittle failures of joint components during the heating and cooling phases have been observed. This work was focused on rigid and semi-rigid connections.

A complete review of the analytical and experimental research work realised on the performance of beam-to-column joints in fire is available in [Al-Jabri, 2008]. In the present work, individual detailed states of the art have been realised about the prediction of temperature in steel beams and joints (see

Chapter 2), the prediction of internal forces in axially and rotationally restrained beams subjected to fire (see Chapter 3), the resistance of bolts and welds at elevated temperatures (see Chapter 4) and the behaviour of steel connections at room and elevated temperatures (Chapter 5 is completely dedicated to this state-of-the-art).

The results of all the mentioned research works have led to the introduction of design rules in the fire part of Eurocode 3 [CEN, 2005a] and constructional details in the fire part of Eurocode 4 [CEN, 2005b]. However, the ductility performance of connections, that is proved to be a key parameter for the prediction of the fire resistance of connections, has not been included in these present Eurocodes and the design procedures provide insufficient information to designers in order to avoid the failure of typical connections during both the heating and cooling phases of a natural fire. The behaviour of simple connections under fire conditions, commonly used in steel structures, has only been studied very recently and the interaction with the surrounding elements has always been ignored.

The objective of this thesis is to analyse the behaviour of common types of simple steel connections under natural fire accounting for the presence of the surrounding members and to propose some new recommendations for the design of these connections under natural fire. A special attention will be paid to the ductility of connections and the risk of failure occurrence during both the heating and cooling phases. The content and the objectives of the chapters of this thesis are described in § 1.3.

1.3 Thesis Layout

The present thesis contains nine chapters and five appendices. The division of the work approximately corresponds to the chronology followed by an engineer to evaluate the fire resistance of a structure under natural fire conditions. Chapter 1 is a global introduction to the concepts of Fire Safety Engineering and Structural Fire Engineering and to the behaviour of steel structures under fire conditions. A special attention is paid to the behaviour of steel connections, and the problem of connection failures during the cooling phase, treated in the present work, is introduced. A recapitulation of the main researches realised on the behaviour of steel connections and steel structures up to now is made.

Chapter 2 contains a large review of available models for fire representation and of the prediction of the distribution of temperature in steel members and beam-to-column joints. Different modifications or improvements to the existing methods are proposed for the evaluation of temperature in joints under natural fire.

The objective of Chapter 3 is the development of a simple method able to predict the evolution of the distribution of internal forces in axially and rotationally-restraints beams under natural fire that does not require time-consuming numerical simulations. This part is based on the work realised recently at the University of Manchester [Yin, 2005a and 2005b; Li, 2006]. Modifications and improvements made by the author are aimed at predicting accurately the distribution of bending moments, even in cases where the resisting bending moment of the joint is limited.

Chapter 4 presents the results obtained from series of isothermal tests performed on bolts and welds under heating and subsequent cooling conditions. These tests, performed at the Centro Sviluppo Materiali were aimed at quantifying how bolts and welds recover their strength during the cooling phase of a natural fire. The tests results are analysed and discussed in this thesis. Afterwards, analytical models characterising the force-displacement relationships of bolts in tension or shear at elevated temperatures are proposed on the basis of the results obtained from experimental tests.

Chapter 5 is a review of the existing models for steel joints at room and elevated temperatures. Special attention is paid to the Component Method included in the Eurocode recommendations for the calculation of the resistance and the stiffness of commonly used connections at room temperature. This state-of-the-art also sums up the experimental, analytical and numerical investigations on the mechanical behaviour of isolated joints under fire conditions.

Chapter 6 presents four new tests performed on steel sub-structures under heating and subsequent cooling in order to analyse the behaviour of connections during the cooling phase [Efectis France, 2007a and 2007b; Efectis NL, 2009]. Bilinear and Nonlinear Fibre Models based on the Component Method are proposed, integrated into SAFIR software for the numerical modelling of simple connections under natural fire conditions and validated against experimental results and against results obtained by use of other numerical models. This chapter also includes parametric analyses and recommendations for the design of these connections.

Chapter 7 is a case study showing how the developments and recommendations presented in this thesis can be included into the current fire design methodology. Existing and proposed design methods are applied to a complete frame.

Chapter 8 contains the general conclusions of the thesis and the perspectives for future investigations on the behaviour of steel connections under natural fire conditions.

Finally, Chapter 9 is a list of references.

The outline of the thesis is represented on Figure 1-3. White frames are related to the work realised in the past, blue frames show the contributions of the present thesis and green frames are a combination of work realised previously to this thesis and during this thesis.

Figure 1-3 : Schematic representation of the outline of the thesis

2 Distribution of temperature in steel and steel-concrete composite beams and joints

2.1 Overview of Fire Modelling

The development of a fire in a compartment necessitates the simultaneous presence of fuel, oxygen and of a heat source, the three elements frequently referred to as "fire triangle". It is necessary that at least one of these elements is absent to avoid a fire starting or to extinguish it. It is difficult to avoid or limit the presence of oxygen and fuel in a compartment. In consequence, active and passive measures usually consist to reduce and control the presence of heat sources. Active control refers to the actions taken by a person or by automatic devices to extinguish a fire and/or prevent the growth of others (by example, the activation of a sprinkler system). Passive control refers to fire control by systems that do not require any operation by people or automatic control (by example, the protection of structural members by insulating materials). A typical time-temperature curve for the complete process of fire development inside a typical room without fire suppression is divided in four stages (Figure 2-1): the ignition or incipience, the growth, the burning and the decay [Buchanan, 1999 and Cadorin, 2003].

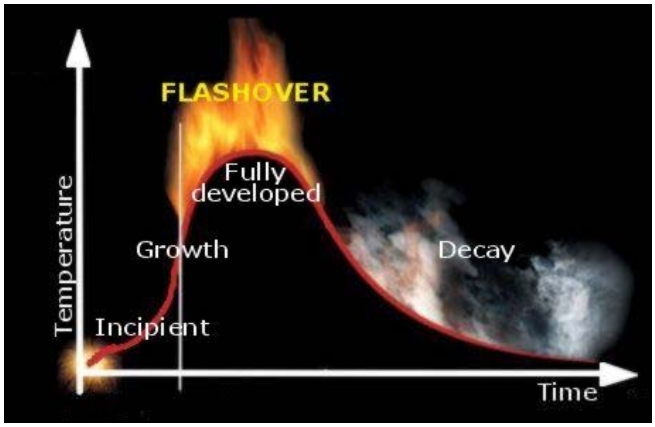

Figure 2-1 : Time-temperature curve for full process of fire development

The **ignition** is followed by a quick increase of temperature due to the exothermic nature of fire reaction. This process can be either flaming or smouldering combustion. The fire remains localised during that period. Then, the **growth phase**, takes place. Firstly, the fire spreads slowly to combustible surfaces, then more rapidly as the fire growths and heat is exchanged between hot gases and other fuel items. At that point, the situation can evolve towards one the two following possibilities: either the elevation of temperature is such that the flashover occurs and provokes the ignition of all the objects

of the compartment, or the temperature rise is not sufficient to cause the flashover and the fire remains localised. The **fully-developed** period is characterized by a stabilisation of the temperature. The fire is called ventilation-controlled or fuel-controlled depending on the fact that the rate of heat release is respectively limited by the quantity of oxygen or the quantity of combustible materials. Finally, the temperature decreases slowly during the cooling phase or **decay phase**.

Three categories of models are used for the analysis of dynamics in a compartment fire and are shortly described hereafter, classified by increasing degree of difficulty [Cadorin, 2003]:

- Analytical Models are based on simple theoretical developments or correlations obtained from experimental results. They have the form of simple equations, suitable for hand calculations, and can be classified as nominal, equivalent time or parametric temperature-time curves.

- Zone models is the name given to the models where the compartment analysed is divided in zone(s) in which the temperature is assumed to be uniform. The equations of energy and mass balances are solved numerically.

- Field models are based on fundamental principles and implemented in very complex softwares. This type of model may involve few simple calculations in some cases or require huge number of calculations and extensive calculation time in other cases, like CFD analyses.

The detailed description of the two most complex models and the investigations performed in the field of fire modelling is not realised within the present work. For more information about fire modelling, the reader is referred to specific works about Zone models [Cadorin, 2003] and Field models [Olenick, 2003]. Analytical models are described in § 2.2.

For situations with large compartments and/or a limited quantity of combustibles, the fire remains localised near the source of the fire during a long period of time and the flashover phenomenon could even be avoided. Under this type of fire, some specific models [Hasemi, 1995] exist in the informative Annex C of the EN 1991-1-2 to analyse the thermal effects on horizontal structural elements accounting for the fire loading, distance from the fire sources, the flame impacting the ceiling or not, etc. The development of new methods [Haller, 2006] and the realisation of experimental tests [Sokol, 2008] are aimed at improving the calculation of the thermal distributions in a steel column exposed to localised fire but validations and improvements to these methods are still needed.

A heat transfer is an exchange of thermal energy from a hot object to a cool object. In a compartment where a fire is burning, the evolution of the distribution of temperature in structural elements is due to

three types of heat transfer. Conduction is the transfer of heat by direct contact of matter. This type of heat transfer has no influence on the average temperature of an isolated structural element but causes a redistribution of temperatures inside the element. The differential equation for a tri-dimensional case is (Eq. 2-1).

$$\frac{\partial}{\partial x}\left(\lambda(\theta)\frac{\partial\theta}{\partial x}\right)+\frac{\partial}{\partial y}\left(\lambda(\theta)\frac{\partial\theta}{\partial y}\right)+\frac{\partial}{\partial z}\left(\lambda(\theta)\frac{\partial\theta}{\partial z}\right)+\frac{\partial Q}{\partial t}=\rho c(\theta)\frac{\partial\theta}{\partial t} \quad \textbf{2-1}$$

where λ is the thermal conductivity, ρ is the density, c is the specific heat and $\partial Q/\partial t$ is the heat produced (or consumed) inside the volume.

Convection is the transfer of heat energy due to the movement of molecules within fluids. Convective exchanges between occur at the interface between steel elements and hot gases. The convective flux q_c is proportional to the difference between the gases temperature θ_g and the element temperature θ_m (Eq. 2-2). In the EN 1991-1-2 [CEN, 2002a], the coefficient of heat transfer by convection α_c is recommended to 25 W/m²K for standard curve, to 35 W/m²K for simple natural fire models and to 50 W/m²K for the hydrocarbon fire. On the unexposed side of separating members, $\alpha_c = 4$ should be used if the effects of heat transfer y radiation are explicitly taken into account and $\alpha_c = 9$ should be used when assuming that this coefficient contains the effects of heat transfer by radiation.

$$q_c=\alpha_c\left(\theta_g-\theta_m\right) \quad \textbf{2-2}$$

Finally, radiation is the transfer of heat energy through empty spaces. All the objects radiate and the radiating flux from one element to another is the difference between the received flux and the emitted flux. The radiative flux q_r is proportional to the difference between the effective radiation temperature θ_r to the power 4 and the element temperature θ_m to the power 4 (Eq. 2-3).

$$q_r=\phi\,\sigma\,\varepsilon_m\,\varepsilon_r\left(\left(\theta_r+273\right)^4-\left(\theta_m+273\right)^4\right) \quad \textbf{2-3}$$

where ϕ is the configuration factor, σ is the Stefan-Boltzmann constant ($5.67*10^{-8}$ W/m²K⁴), ε_m is the material emissivity, ε_f is the fire emissivity and the temperatures θ_r and θ_m are given in Celsius degrees.

The EN 1991-1-2 recommends to use a resultant emissivity equal to 0.8 unless a value is given in the Eurocode dedicated to the type of element analysed, like in EN 1993-1-2 [CEN 2004a] where $\varepsilon_m = 0.7$ for steel.

2.2 Analytical models for Fire Modelling

2.2.1 Nominal fire curves

Nominal fire curves define the evolution of the gas temperature after the flashover as a function of time without accounting for the characteristics of the compartment analyses. This type of curves was historically used as a reference for normative prescriptions to allow some reasonable comparisons between the results performed on different elements or in different laboratories. Because of the intensive use of these curves, they continue to be used in practical applications. These curves are usually quite different from real conditions. The use of nominal fire curves assumes that the temperature is uniform in the compartment and does not include any cooling phase. For common applications, the use of these curves is a safe assumption but the under-estimation of the fire resistance of an element can be important.

In the actual draft of Eurocodes, three types of nominal temperature-time curves are defined [CEN, 2002a]. The **ISO 834 fire curve** (Eq. 2-4) is the most commonly-used nominal curve and is based on experimental results obtained with wood based fires and cellulosic fires. For fire scenarios where a faster rate of initial increase in temperature is observed, like the burning of gasoline or plastics, the **standard hydrocarbon fire curve** (Eq. 2-5) should be used [(*)]. Finally, the **fire curve of external fire** (Eq. 2-6) is recommended to be applied to peripheral walls.

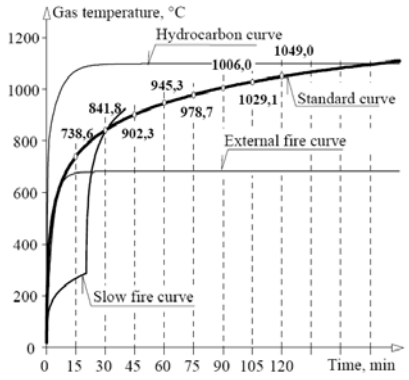

$\theta_{gas,ISO} = 20 + 345 \log_{10}(8t + 1)$	**2-4**
$\theta_{gas,HC} = 20 + 1080\left(1 - 0.325e^{-0.167t} - 0.675e^{-2.5t}\right)$	**2-5**
$\theta_{gas,ext.} = 20 + 660\left(1 - 0.687e^{-0.32t} - 0.313e^{-0.38t}\right)$	**2-6**

Figure 2-2 : Nominal fire curves [Wald, 2005]

[*] In some circumstances, the use of the Majorated Hydrocarbon Curve should be recommended for representing the action of severe fires. In this curve, the coefficient 1080 of Eq. 2-5 is substituted by 1280.

2.2.2 Equivalent-time fire curves

A lot of fire tests are performed on structural elements submitted to standard fire curves and thus, it is interesting to relate real fires to standard tests. The concept of equivalent fire severity was thus introduced, stating that the effect of a real fire on a structure is equivalent to the effect of a standard fire curve during a period of time, the equivalent-time.

A wide variety of equivalent-time formulas exists and is presented in reviews [Law, 1997 and CEC, 1999]. The method proposed in the informative Annex F of EN 1991-1-2 [CEN, 2002a] is a modified version of a formula based on the ventilation parameters of the compartment and the fuel load [Pettersson, 1976]. This method is applicable to reinforced concrete, protected steel and unprotected steel. The equivalent time of ISO fire exposure is defined by Eq. 2-7.

$t_{e,d} = \left(q_{f,d} \; k_b \; w_f \right) k_c$	**2-7**

where $q_{f,d}$ is the design fire load density, k_b is the conversion factor accounting for the heat transfer in the neighbouring component parts of the compartment, w_f is the ventilation factor and k_c is another conversion factor depending on the material of the structural cross-sections.

2.2.3 Parametric fire curves

Parametric fire curves are time-temperature relationships that provide an estimation of the evolution of temperature in the compartment considering the influence of the following parameters: geometry of the compartment, characteristics of materials constituting walls and ceilings, fire loading, area and position of the openings. The use of these curves implies that the temperature is assumed to be uniform in the compartment. Contrary to nominal and equivalent-time curves, the parametric curves include a cooling phase.

The most widely-used parametric fire curve is the one suggested by the Annex A of EN 1991-1-2. During the heating phase, the gas temperature is given by Eq. 2-8 as a function of the fictive time t*, calculated with Eqs 2-9 to 2-12.

$\theta_{gas} = 20 + 1325 \left(1 - 0.324\, e^{-0.2 t^*} - 0.204\, e^{-1.7 t^*} - 0.472\, e^{-19 t^*} \right) \quad [°C]$	**2-8**
$t^* = t \Gamma \quad [h]$	**2-9**
$\Gamma = \dfrac{(O/b)^2}{(0.04/1160)^2} \quad [-]$	**2-10**
$O = \dfrac{A_v \sqrt{h_{eq}}}{A_t} \quad where \quad 0.02 \le O \le 0.2 \quad [m^{1/2}]$	**2-11**

$b = \sqrt{c\,\rho\,\lambda} \quad where \quad 100 \le b \le 2200 \quad [J/m^2\,s^{1/2}\,K]$	**2-12**

In the previous equations, c, ρ and λ are respectively the specific heat, the density and the thermal conductivity of boundary of enclosure. A_t, A_v and h_{eq} are the total area of enclosure (walls, ceiling and floors), the total area of vertical openings and the weighted average of window heights.

The duration of the heating phase t^*_{max} is determined as a function of the fire load and the opening factor (Eqs 2-13 to 2-15). A calculation method for the design fire load density $q_{f,d}$ related to the floor surface A_f is proposed in the Annex E of the EN 1991-1-2. In Eq. 2-15, $q_{t,d}$ is the design fire load density related to the total surface A_t. In case of fuel controlled fire, t_{max} is determined by the value of t_{lim} in Eq. 2-14 and t* must be calculated by Eq. 2-16 (instead of Eq. 2-9). Depending on the rate of growth of the fire, the value of t_{lim} is 15 min (fast), 20 min (medium) or 25 min (slow). In case of ventilation controlled fire, t_{max} higher than t_{lim}. If the three conditions O > 0.04; $q_{t,d}$ < 75 and b < 1160 are simultaneously fulfilled, Γ_{lim} is multiplied by k, given in Eq. 2-19.

$t^*_{max} = t_{max}\,\Gamma \quad [h]$	**2-13**
$t_{max} = \max\left[\left(0.2*10^{-3}\,q_{t,d}/O\right); t_{lim}\right] \quad [h]$	**2-14**
$q_{t,d} = q_{f,d}\,A_f/A_t \quad [MJ/m^2] \quad where \quad 50 \le q_{t,d} \le 1000$	**2-15**
$t^* = t\,\Gamma_{lim} \quad [h]$	**2-16**
$\Gamma_{lim} = \left(O_{lim}/b\right)^2 / \left(0.04/1160\right)^2 \quad [-]$	**2-17**
$O_{lim} = 10^{-4}\,q_{t,d}/t_{lim} \quad [m^{1/2}]$	**2-18**
$k = 1 + \left(\frac{O-0.04}{0.04}\right)\left(\frac{q_{t,d}-75}{75}\right)\left(\frac{1160-b}{1160}\right) \quad [-]$	**2-19**

During the cooling phase, the gas temperature is given by Eqs 2-20 to 2-22 where t*, t^*_{max} and x are respectively given by Eqs 2-16, 2-23 and 2-24.

$\theta_{gas} = \theta_{max} - 625\left(t^* - t^*_{max}\,x\right) \quad [°C]$	*for*	$t^*_{max} \le 0.5$	**2-20**
$\theta_{gas} = \theta_{max} - 250\left(3 - t^*_{max}\right)\left(t^* - t^*_{max}\,x\right) \quad [°C]$	*for*	$0.5 \le t^*_{max} \le 2$	**2-21**
$\theta_{gas} = \theta_{max} - 250\left(t^* - t^*_{max}\,x\right) \quad [°C]$	*for*	$t^*_{max} > 2$	**2-22**
$t^*_{max} = 0.2*10^{-3}\,q_{t,d}/O \quad [h]$			**2-23**
$if\ t_{max} > t_{lim}\ then\ x = 1\ \ else\ x = t_{lim}\,\Gamma/t^*_{max} \quad [-]$			**2-24**

2.3 Prediction of temperature in steel and composite beams and joints: state-of-the-art

2.3.1 European recommendations for the prediction of temperature in steel beams (EN 1993-1-2)

In the European standards dedicated to the design of steel and composite structures under fire, the temperature in unprotected steel sections is calculated by the Lumped Capacitance Method [Incropea, 2005]. The equilibrium is stated between the quantity of heat received by the steel cross-section $\Delta Q_{transferred}$ and the quantity of heat consumed by this section $\Delta Q_{heating}$ to increase its own temperature by $\Delta\theta_{a,t}$ during an incremental interval of time Δt (Eq 2-25).

$\Delta Q_{transferred} = \dot{h}_{net,d}\, k_{sh}\, A_m\, \Delta t = c_a\, \rho_a\, V\, \Delta\theta_{a,t} = \Delta Q_{heating}$	**2-25**

A_m and V are the surface area and the volume of steel per unit length of the member, c_a and ρ_a are the specific heat and the unit mass of steel and $h_{net,d}$ is the design value of the net heat flux accounting for thermal exchanges by convection and radiation. The correction factor for shadow effect k_{sh} in concave-shaped sections is determined by Eq. 2-26 for I-sections under nominal fire and Eq. 2-27 for other cases. $(A_m/V)_b$ is the box value of the section factor. This factor is used to limit the quantity of energy reaching the surface of the heated member by the quantity of energy travelling through the smallest box surrounding the section. Strictly speaking, the correction should only be applied to the radiative part of the heat flux whereas k_{sh} is applied to the convective part of the flux in Eq 2-25 [Franssen, 2009].

$k_{sh} = 0.9\,(A_m/V)_b / (A_m/V)$	**2-26**
$k_{sh} = (A_m/V)_b / (A_m/V)$	**2-27**

For steel sections covered by insulating materials, the calculation method of the EN 1993-1-2 is similar to Eq. 2-25 but the equation is a little bit different (Eq. 2-28 and 2-29). Due to the low value of the thermal conductivity of insulating materials, it is reasonable to assume that the temperature at the external surface of these materials is the same as the one of the gases. Thus, the design value of heat fluxes $h_{net,d}$ and the shadow factor k_{sh} are not considered in protected sections.

$\phi = \frac{c_p\, \rho_p}{c_a\, \rho_a}\, d_p\, \frac{A_p}{V}$	**2-28**

$$\Delta\theta_{a,t} = \frac{\lambda_p \; A_p/V}{d_p \; c_a \; \rho_a} \frac{h_{net,d}}{1+\phi/3} \Delta t - \left(e^{\phi/10} - 1\right) \Delta\theta_{g,t} \qquad with \;\; \Delta\theta_{a,t} \geq 0 \;\; if \;\; \Delta\theta_{g,t} \geq 0 \qquad \textbf{2-29}$$

c_p, ρ_p, λ_p, d_p and A_p are respectively the specific heat, the specific mass, the thickness and area per unit length of fire protection material. $\Delta\theta_{g,t}$ is the increase of gas temperature during the time interval Δt.

2.3.2 Eurocode recommendations for the prediction of temperature in steel-concrete composite beams (EN 1994-1-2)

Eurocode recommendations for steel-concrete composite elements [CEN, 2005b] states that the assumption of a uniform distribution of temperature in protected and unprotected steel profiles of a steel-concrete composite beam is not valid anymore because of the presence of a concrete slab. The profile temperature is calculated by using Eq. 2-25 and a new expression of the shadow factor k_{sh} (Eq. 2-30 and Figure 2-3). In the expression of k_{sh}, the interface between the upper flange and the concrete slab is considered as an adiabatic frontier.

$$k_{sh} = 0.9 \left(\frac{e_1 + e_2 + b_1/2 + \sqrt{h_w^2 + \left(b_1 - b_2\right)^2/4}}{h_w + b_1 + e_1 + e_2 + b_2/2 - e_w} \right) \qquad \textbf{2-30}$$

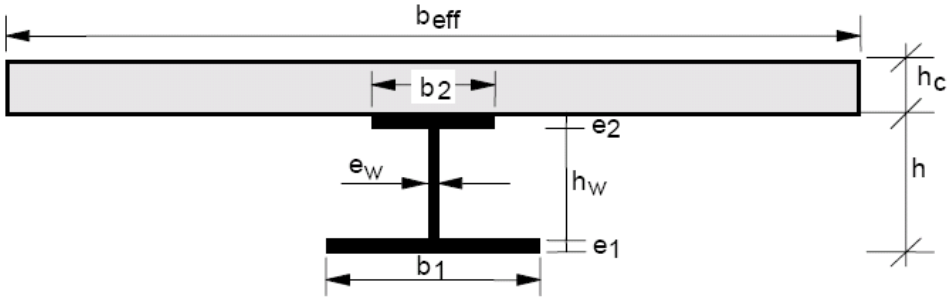

Figure 2-3 : Elements of the cross-section of a steel-concrete composite beam [CEN, 2005b]

For protected and unprotected composite beams, EN 1994-1-2 recommends to use Eq. 2-29 separately for the different parts of the steel section and to consider a "local" section factor of the flange or the web $A_{p,i}/V_i$ instead of the "global" section factor A_p/V (Eqs 2-31 to 2-33), except for members with box-protection where a uniform temperature may be assumed over the height of the profile. For the section factor of the upper flange, the interface between the upper flange and the concrete slab is considered as an adiabatic frontier when at least 85% of the upper flange is in contact with the slab or when any void formed between the upper flange and a profiled steel deck is filled with non-combustible material. The temperature of the beam web may be taken as equal to that of the lower flange if the beam depth h does not exceed 500 mm.

$A_{p,i}/V_i = 2\,(b_1 + e_1)/b_1\,e_1$	*for the lower flange*	**2-31**
$A_{p,i}/V_i = (b_2 + 2\,e_2)/b_2\,e_2$	*for the upper flange* $(contact \geq 85\%)$	**2-32**
$A_{p,i}/V_i = 2\,(b_2 + e_2)/b_2\,e_2$	*for the upper flange* $(contact < 85\%)$	**2-33**

2.3.3 Eurocode recommendations for the prediction of temperature in steel and composite joints (EN 1993-1-2)

Concerning the distribution of temperature in joints, EN 1993-1-2:2004 mentions that it may be assessed using the local A/V value of the parts forming that joint or, as a simplification, by assuming a uniformly-distributed temperature calculated with the maximal value of the ratios A/V of the connected steel members in the vicinity of the joint. In beam-to-column and beam-to-beam steel joints with beams supporting any type of concrete floor, the distribution of temperature may be obtained from the temperature of the bottom flange at mid-span. The ratio between the temperature in the joint zone at a vertical abscissa h and the temperature of the bottom flange at mid-span is given in Figure 2-4 for beam depths lower than or equal to 400 mm (left profile) and beam depths higher than 400 mm (right profile).

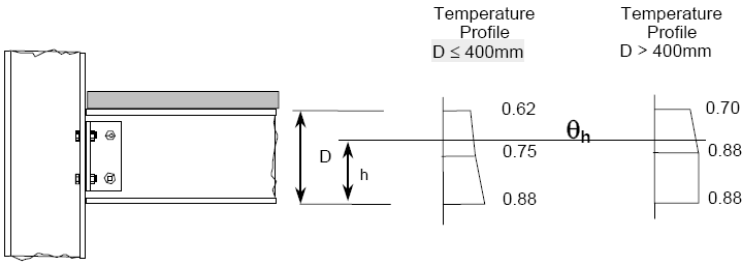

Figure 2-4 : Temperature profile of a beam-to-column or beam-to-beam joint supporting a concrete floor as a function of the temperature of the bottom flange at mid-span [CEN, 2004a]

2.3.4 Recent investigations on the prediction of connection temperatures

Numerical investigations performed with the use of SAFIR program [Franssen, 2003] have demonstrated that the local effects of bolts can clearly be neglected when evaluating the distribution of temperature in a joint [Franssen, 2004]. They also show that the use of the local massivity values of the components comprising the connection, as recommended in the Eurocodes, is not acceptable because the order of magnitude of the components dimensions is too small in comparison to the order of magnitude of the connected members dimensions. A simplified assumption is discussed and validated for representing the thermal insulation.

Experimental tests have been carried out at the University of Manchester on assemblies of one column and four beams with a concrete slab on top [Dai, 2007]. In these tests, the steel members were all

unprotected and the gas temperature followed the standard ISO 834 fire curve during 60 minutes. The cooling phase has not been considered. The different types of connections tested are flush and flexible end-plate, fin plate and double web cleats. Comparisons have been made between the experimental measurements and the temperatures obtained by the use of three different methods [K. Anderson, 2009]. The temperatures calculated with the "Eurocode Percentages Method" are much different from test results and this method seems unreliable. The Lumped Capacitance Method showed good correlation with average connection temperatures but more work is expected for the prediction of temperature in individual connection elements and the definition of the volume of beams and columns that should be included in calculations made with the Lumped Capacitance Method. The numerical simulations performed with the finite element package Abaqus [Abaqus, 2009] have given a good agreement with experimental results and have shown that the inclusion of the concrete slab only affects the temperature of the upper flange of the beam.

A series of fire tests on composite steel joints assemblies with different types of connections and fire protection schemes have also been carried out recently at the University of Manchester [Dai, 2008]. The influence of protecting the bolts or not on the temperature of other components is studied and a quantity called "exposure factor" is defined to calculate the temperature of unprotected bolts in protected joints.

2.4 Numerical model for thermal analyses

2.4.1 Brief description of SAFIR program - Thermal module [Franssen, 2005]

SAFIR is a special purpose computer program for the analysis of structures under ambient and elevated temperatures conditions. It was developed at the University of Liege and is based on the Finite Element Method. The analysis of a structure exposed to fire consists of a thermal analysis, a torsional analysis for 3-D BEAM elements (if necessary) and a structural analysis. Thermal analyses are performed with 2-D or 3-D SOLID elements. The three types of heat transfers described previously are taken into consideration with SAFIR. The consideration of radiative transfers between two solid elements requires the definition of "VOID elements" and this tool is not available in 3-D thermal analyses. The radiative transfers between solid elements and hot gases are automatically considered in 2-D and 3-D thermal analyses.

2.4.2 Thermal properties of steel (EN 1993-1-2: 2004)

The density of steel is 7850 kg/m³ and remains constant with temperature. The relative elongation $\Delta l/l$, specific heat c_a and thermal conductivity λ_a of carbon steel are only dependent from steel temperature

θ_a. The values given for these parameters in the EN 1993-1-2 are given in Eqs 2-34 to 2-42 and represented on Figures 2-5 to 2-7. The peak value of the specific heat at 735°C is due to phase change of carbon steel at this temperature.

$\Delta l/l = 1.2*10^{-5}\,\theta_a + 0.4*10^{-8}\,\theta_a^2 - 2.416*10^{-4}$	$for\ 20°C \le \theta_a \le 750°C$	**2-34**
$\Delta l/l = 1.1*10^{-2}$	$for\ 750°C \le \theta_a \le 860°C$	**2-35**
$\Delta l/l = 2*10^{-5}\,\theta_a - 6.2*10^{-3}$	$for\ 860°C \le \theta_a \le 1200°C$	**2-36**

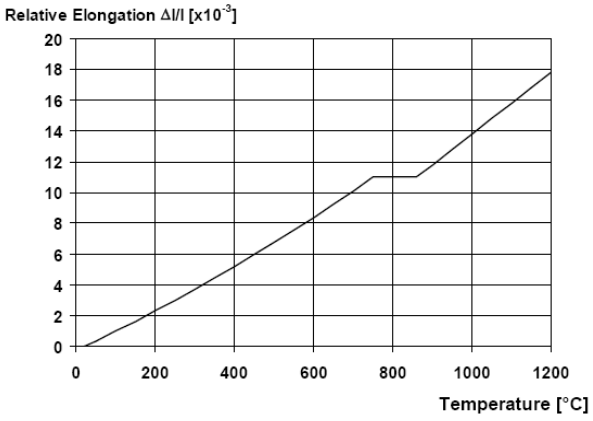

Figure 2-5 : Relative elongation of carbon steel as a function of temperature [CEN 2004a]

$c_a = 425 + 0.773\theta_a - 1.69*10^{-3}\,\theta_a^2 + 2.22*10^{-6}\,\theta_a^3 \ \ J/kgK$	$for\ 20°C \le \theta_a \le 600°C$	**2-37**
$c_a = 666 + \dfrac{13002}{738 - \theta_a} \ \ J/kgK$	$for\ 600°C \le \theta_a \le 735°C$	**2-38**
$c_a = 545 + \dfrac{17820}{\theta_a - 731} \ \ J/kgK$	$for\ 735°C \le \theta_a \le 900°C$	**2-39**
$c_a = 650 \ \ J/kgK$	$for\ 900°C \le \theta_a \le 1200°C$	**2-40**

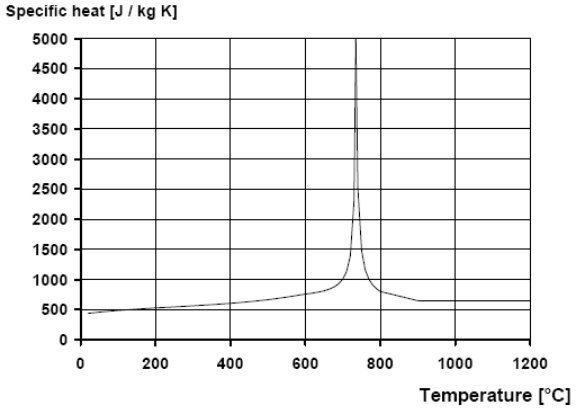

Figure 2-6 : Specific heat of carbon steel as a function of temperature [CEN 2004a]

$\lambda_a = 54 - 3.33 * 10^{-2}\,\theta_a \;\; W/mK$	$for\ 20°C \le \theta_a \le 800°C$	**2-41**
$\lambda_a = 27.3 \;\; W/mK$	$for\ 800°C \le \theta_a \le 1200°C$	**2-42**

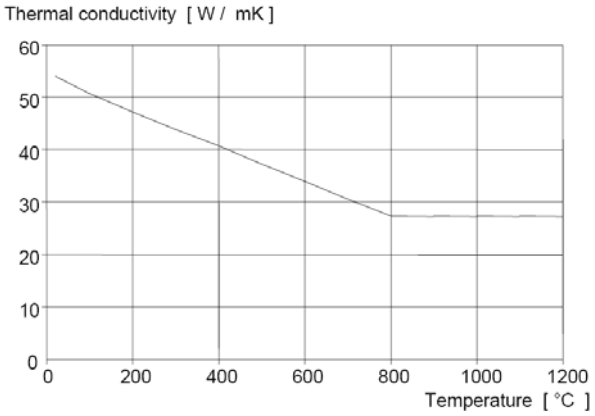

Figure 2-7 : Thermal conductivity of carbon steel as a function of temperature [CEN 2004a]

2.4.3 Thermal properties of concrete (EN 1992-1-2:2004)

The density of concrete depends on the nature of aggregates and the mix design but the density of normal concrete (in opposition to lightweight concrete) is about 2300 kg/m³. When heated to 100°C the density of concrete will be reduced by up to 100 kg/m³ due to the evaporation of free water, otherwise the density does not change much at elevated temperature (see recommended values of the EN 1992-1-2 in Eqs 2-43 to 2-46). A significant exception is made with calcareous aggregate which decompose above 800°C with a corresponding decrease in density [Buchanan, 1999].

$\rho(\theta) = \rho(20°C)$	$for\ 20°C \le \theta \le 115°C$	**2-43**
$\rho(\theta) = \rho(20°C) * (1 - 0.02\,(\theta - 115)/85)$	$for\ 115°C \le \theta \le 200°C$	**2-44**
$\rho(\theta) = \rho(20°C) * (0.98 - 0.03\,(\theta - 200)/200)$	$for\ 200°C \le \theta \le 400°C$	**2-45**
$\rho(\theta) = \rho(20°C) * (0.95 - 0.07\,(\theta - 400)/800)$	$for\ 400°C \le \theta \le 1200°C$	**2-46**

In normal concrete, the contribution of aggregate to the total thermal expansion goes from 65% to 80% [Bažant, 1996]. Types of aggregate that contains high quantities of silica, such as quartzite and sandstone, have a high coefficient of thermal expression [Browne, 1972]. This explains the differences between the thermal elongation of concretes made of siliceous and calcareous aggregate in EN 1992-1-2 (Figure 2-8).

For siliceous aggregate:

$\Delta l/l = -1.8*10^{-4} + 9*10^{-6}\,\theta + 2.3*10^{-11}\,\theta^2$	*for* $20°C \le \theta \le 700°C$	**2-47**
$\Delta l/l = 14*10^{-3}$	*for* $700°C \le \theta \le 1200°C$	**2-48**

For calcareous aggregate:

$\Delta l/l = -1.2*10^{-4} + 6*10^{-6}\,\theta + 1.4*10^{-11}\,\theta^2$	*for* $20°C \le \theta \le 805°C$	**2-49**
$\Delta l/l = 12*10^{-3}$	*for* $805°C \le \theta \le 1200°C$	**2-50**

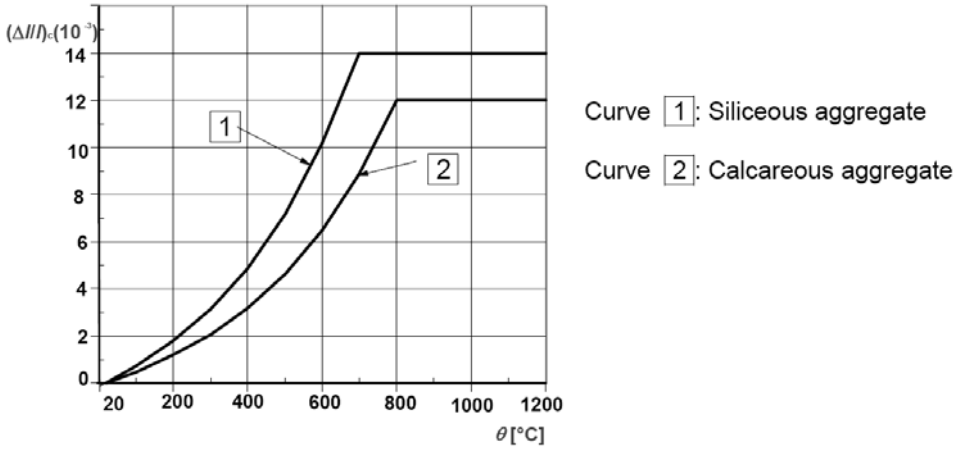

Figure 2-8 : Thermal elongation Δl/l of concrete as a function of temperature [CEN, 2004c]

The specific heat of concrete c_p varies in a broad range, depending on the moisture content u [Schneider, 1988]. Unless the moisture content is 0%, a peak value of the specific heat is observed between 100°C and 200°C because the water is driven off during the heating process. This is shown on Figure 2-10 for three values of the moisture content. The type of aggregate has no influence on the specific heat of concrete.

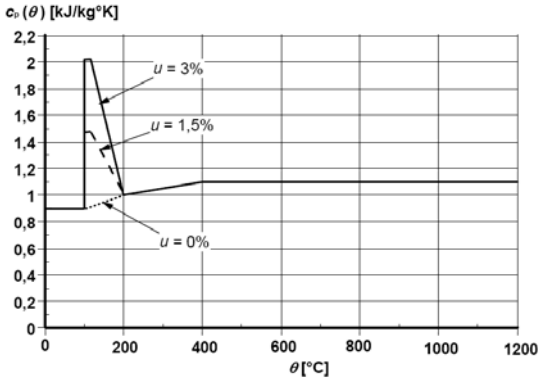

Figure 2-9 : Specific heat of concrete c_p as a function of temperature [CEN, 2004c]

The specific heat c_p of dry concrete (u = 0%) with siliceous or calcareous aggregate may be determined from the Eqs 2-51 to 2-54. Where the moisture content is not considered explicitly in the calculation method, the function given for the specific heat of concrete with siliceous or calcareous aggregates may be modelled by a constant value, $c_{p,peak}$ (Eqs 2-55 to 2-57), between 100°C and 115°C followed by a linear decrease between 115°C and 200°C.

$c_p = 900 \ \ J/kgK$	$for\ 20°C \le \theta \le 100°C$	**2-51**
$c_p = 900 + (\theta - 100) \ \ J/kgK$	$for\ 100°C \le \theta \le 200°C$	**2-52**
$c_p = 1000 + (\theta - 200)/2 \ \ J/kgK$	$for\ 200°C \le \theta \le 400°C$	**2-53**
$c_p = 1100 \ \ J/kgK$	$for\ 100°C \le \theta \le 1200°C$	**2-54**

$c_{p,peak} = 900 \ \ J/kgK$	$for\ u = 0\%$	**2-55**
$c_{p,peak} = 1470 \ \ J/kgK$	$for\ u = 1.5\%$	**2-56**
$c_{p,peak} = 2020 \ \ J/kgK$	$for\ u = 3\%$	**2-57**

The thermal conductivity of concrete is depending on the thermal conductivity of aggregate and the moisture content. At ambient temperature, the thermal conductivity of concrete with siliceous aggregates is higher than that with limestone [Blundell, 1976]. Higher values of the moisture content leads to higher values of the thermal conductivity because the thermal conductivity of air is very much less than that of water [Zoldners, 1971]. Under elevated temperatures, the thermal conductivity decreases as the temperature increases because of the loss of moisture during heating.

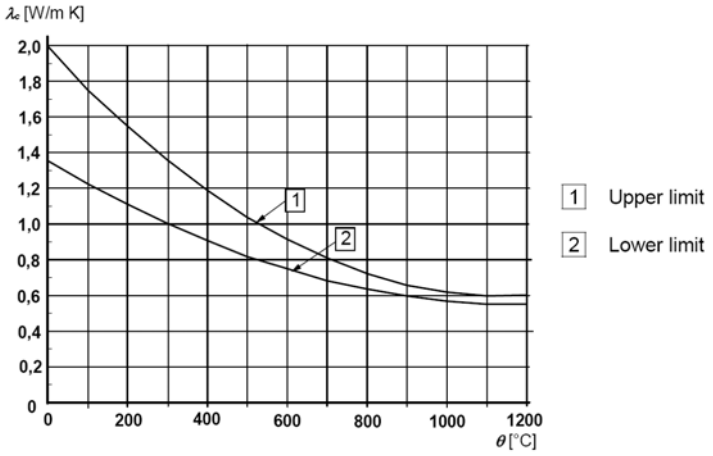

Figure 2-10 : Thermal conductivity of concrete as a function of temperature [CEN, 2004c]

2.4.4 Concepts of view and configuration factors

In the Lumped Capacitance Method described in the EN 1993-1-2 (Eq. 2-25), the shadow factor k_{sh} is used to account for the real exposition of steel I-shape profiles to fire, especially to radiative fluxes. In finite element models, boundary conditions are usually applied on the contour of heated elements and it is difficult to integrate the concept of shadow factor in the model. Although this is not specifically recommended in the Eurocode, Franssen recommends the use of one the two following procedures in advanced calculation models to introduce the concept of shadow effect [Franssen, 2009]:

- The values of the coefficient of convection and the emissivity of steel are multiplied by k_{sh} on the whole perimeter of the section, ensuring the same boundary conditions for the advanced model as for the Lumped Capacitance Method.

- The view factors between, on one hand, a surface of the real concave section where the energy arrives and, on the other hand, the surface of the box contour through which the energy passes, is calculated for each surface of the concave section. The coefficient of convection and the emissivity of the material are then multiplied by the relevant view factor depending on their position.

The view factor F_{ij} between, on one side, the internal surface of the flanges and the web and, on the other side, the surface of the box contour around the flanges, is calculated according to the rule of Hottel, valid in 2-D cases (Eq. 2-58 and Figure 2-11).

$$F_{ij} = \frac{\overline{AD} + \overline{BC} - \overline{AC} - \overline{BD}}{2\,\overline{AB}} \qquad \textbf{2-58}$$

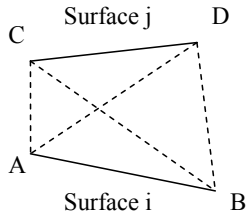

Figure 2-11 : Rule of Hottel [Franssen, 2009]

For external or 3-D applications, the view factor is substituted by the configuration factor. According to Annex G of the EN 1991-1-2, the configuration factor ϕ measures the fraction of the total radiative heat leaving a radiating surface that arrives at a receiving surface. Its value depends on the size of the radiating surface, on the distance from the radiating surface to the receiving surface and on their relative orientation (Figure 2-12).

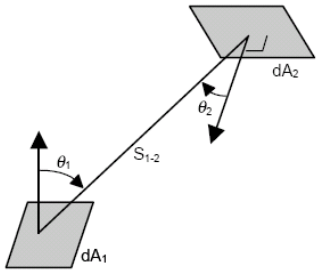

Figure 2-12 : Configuration factor between two infinitesimal surface areas

The mathematical form of the configuration factor is given in Eq. 2-59 for two infinitesimal surfaces:

$d\phi_{d1-d2} = \dfrac{\cos\theta_1 \cos\theta_2}{\pi S_{1-2}^2} dA_2$	**2-59**

The expression of the configuration factor ϕ for rectangular surfaces situated in two parallel planes or two perpendicular planes is given in the part G.3 of the Annex G dedicated to external members (Figure 2-13 - Eqs 2-60 and 2-61).

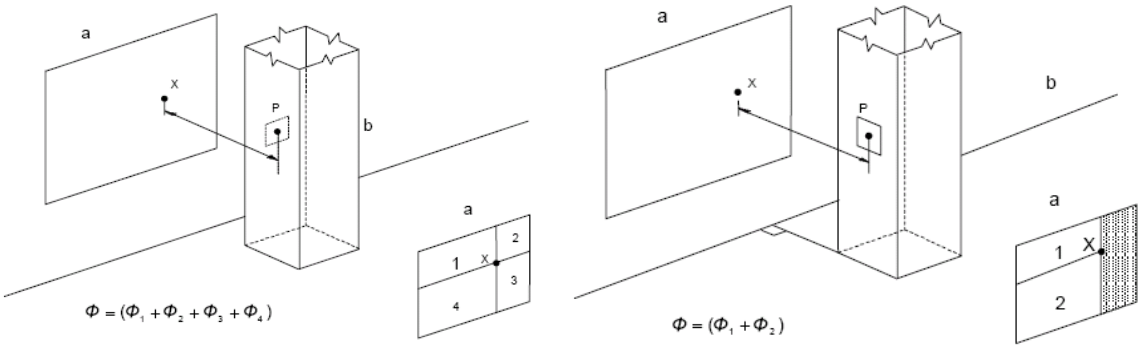

Figure 2-13 : Evaluation of the configuration factor for a receiving surface parallel (left) or perpendicular (right) to the plane of the radiating surface

$\phi = \dfrac{1}{2\pi}\left[\dfrac{a}{\left(1+a^2\right)^{0.5}}\tan^{-1}\left(\dfrac{b}{\left(1+a^2\right)^{0.5}}\right) + \dfrac{b}{\left(1+b^2\right)^{0.5}}\tan^{-1}\left(\dfrac{a}{\left(1+b^2\right)^{0.5}}\right)\right]$	**2-60**
$\phi = \dfrac{1}{2\pi}\left[\tan^{-1}(a) - \dfrac{1}{\left(1+b^2\right)^{0.5}}\tan^{-1}\left(\dfrac{a}{\left(1+b^2\right)^{0.5}}\right)\right]$	**2-61**

In the present work, the reduction factor k_ε on the relative emissivity applied to one zone is proportional to the configuration factor ϕ between that zone and the fictitious surface delimited by the extremities of the beam flanges (hatched surface on Figure 2-14). The coefficient 0.9 included in the

formula giving the shadow factor (Eq. 2-26) is kept in the Eq. 2-62 for the evaluation of the reduction factor k_ε.

$\varepsilon_{m,steel} = 0.7 * k_\varepsilon = 0.7 * 0.9 * \phi$	**2-62**

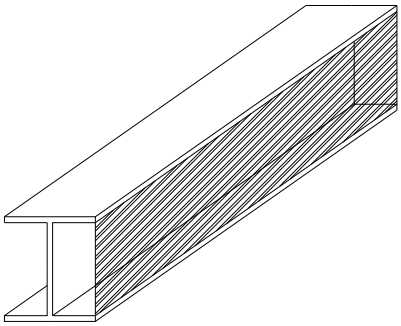

Figure 2-14 : Fictitious surface delimited by the extremities of the beam flanges

As an illustration to this, the configuration factor ϕ of the three parts (top flange, web and bottom flange) of an IPE300 beam connected to a HEA 300 column has been calculated analytically as a function of the distance from the end-plate and is represented on Figure 2-15. For thermal analyses in the SAFIR software, the configuration factor ϕ is assumed to be constant by zones, as represented on the same figure with "stairs-shape" curves.

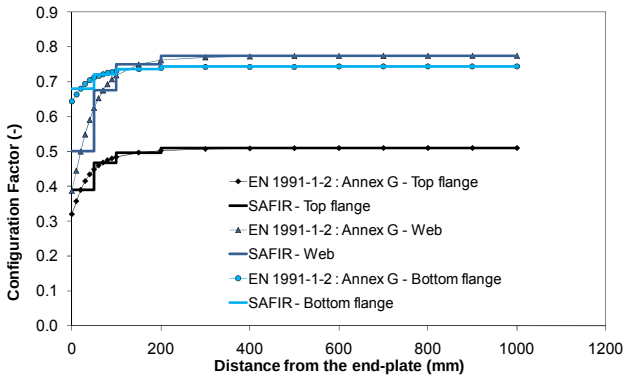

Figure 2-15 : Analytical and simplified expressions of the configuration factor ϕ as a function of the longitudinal abscissa

A short verification of the thermal model based on the concept of configuration factor is made hereafter. This validation consists in a comparison between the temperatures in the top and bottom flanges obtained, on one side, with a 3D-model in nodes situated far away from the joint, and on the other side, in a 2-D model where the emissivity of steel is multiplied uniformly by the value of the shadow factor k_{sh}. In the 2-D and 3-D models, the presence of the concrete slab is considered. The

temperature in a flange is read at equidistance from the vertical axis of symmetry of the beam and the extremity of the flange.

The correlation between the results obtained under a 2-hour standard ISO 834 fire with the two models is very good (Figure 2-16) and confirms that the calculations made by using the configuration factor leads to the same results than with the shadow factor. It also shows that, under quick fires like the standard ISO curve, using of a uniform reduction factor on the steel emissivity is good assumption.

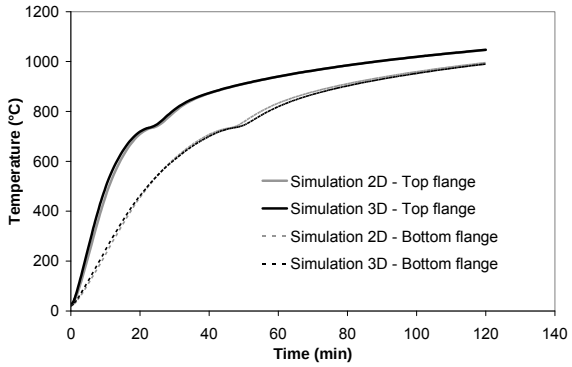

Figure 2-16 : Temperature in the top and bottom flanges under ISO fire obtained by 2-D and 3-D models

The above-mentioned validation of the model is not complete because it is not demonstrated that, for both 2-D and 3-D models, the shadow effect can be incorporated in the model by reducing the steel emissivity. However, this procedure has already been recommended in other publications [Franssen, 2009].

2.5 New proposals for prediction of temperature in steel and composite beams and joints

2.5.1 Objectives and methodology

The distribution of temperature in a beam-to-column joint zone under natural fire is very complex and depends on a large amount of parameters: type and geometry of the connections, geometry of the connected elements, characteristics of the fire, etc. It would be unrealistic to search for a method as simple as the “Eurocode Percentages Method” for predicting accurately the distribution of temperature in any existing joints subjected to any fire curve but it is admitted that the current existing rules are too crude and that the use of numerical simulations is a time-consuming operation that cannot be applied to daily applications. Between these two extreme boundaries, the Lumped Capacitance Method

accounts for more parameters to evaluate the temperature in the joint zone but a unique temperature is defined for the joint zone.

Another important aspect of the distribution of temperature in steel and composite joints is the real influence of a concrete slab. In case of steel beams covered by a non-collaborating concrete slab or composite beam, Eq. 2-25 ignores the heat flux between the top flange and the concrete slab. Preliminary numerical simulations have been performed in order to measure the influence of a concrete slab on the temperature in a steel element, independently of the fire exposition. Bi-dimensional analyses of a 150mm x 10mm flange, heated on three sides, have been realised in SAFIR with and without concrete slab on the top of the flange. In these analyses, the fire curve follows the standard ISO 834 fire curve.

In the case with no concrete slab, the temperature is approximately uniform in the flange and can be calculated by the Lumped Capacitance Method, stating that the heat transfers received by convection and radiation are consumed to increase the temperature of the flange. In the second case, a part of the heat received by the steel section is transferred to the concrete slab. Figure 2-17 shows (a) the temperatures in the steel flange with and without concrete slab under standard ISO fire and (b) the ratio between, on one side, the heat transferred from the steel section to the concrete slab and, on the other side, the heat received by the steel section during a small interval of time. These two graphs underlines that the flux between the beam and the slab is significant and should not be neglected. The sharp discontinuity of the proportion of heat transferred to the slab near 735°C corresponds to the peak of specific heat of steel (Figure 2-6).

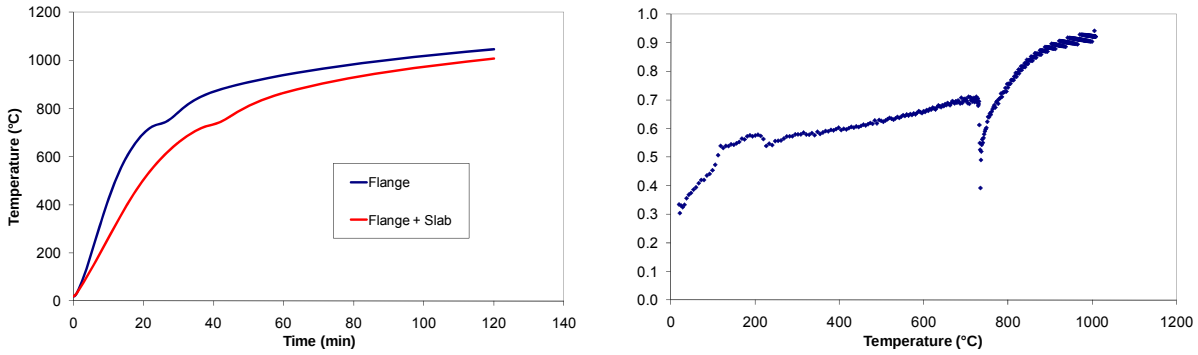

Figure 2-17 : (a) Evolution of temperature in flange – (b) Proportion of heat transferred to the slab

The objective of this chapter is to add new developments to the Lumped Capacitance Method or to find a new method that would enable to calculate the distribution of temperature in the different parts of steel beams and beam-to-column joints, taking into account the presence of a flat concrete slab on the top of the beam. The work is firstly focused on the temperature of the bottom flange in the mid-span section of the beam and then, in the joint zone at the same level. Secondly, the thermal analyses

are concentrated on the determination of the temperature of the upper flange in the beam section and in the joint zone. Finally, the results are extrapolated to the complete beam section and the complete joint zone.

2.5.2 References Cases

The building a 3-D model in a FE program such as SAFIR for thermal analyses in joints and the running of the numerical simulations are time-consuming operations. Thus, a limited number of cases have been modelled. The majority of the simulations have been made with two models with one type of connections: flush end-plate connections. In simple connections, the material discontinuity between the beam and column flanges induces some modifications in the zone of beam flanges. As a first step, it has been chosen to consider flush end-plate connections where this local effect does not exist. Paragraph 2.5.6 is dedicated to simple connections. The bolts have not been represented in the numerical models. The differences between the two models are the dimensions of the connected members and connecting elements. The first one is representative of a building where the beam span is quite small (around 6 metres) and the second one of a frame where this distance is much longer (around 12 metres).

The beam section, the column section and the dimensions of the plate (in mm) used in the reference cases are given in Table 2-1. The thickness of the flat concrete slab is 120 mm. The two models are represented on Figure 2-18.

Case n°	Beam	Column	Plate
1	IPE 300	HEA 300	200*380*10
2	IPE 550	HEM 300	410*625*25

Table 2-1 : Geometrical data of the reference cases

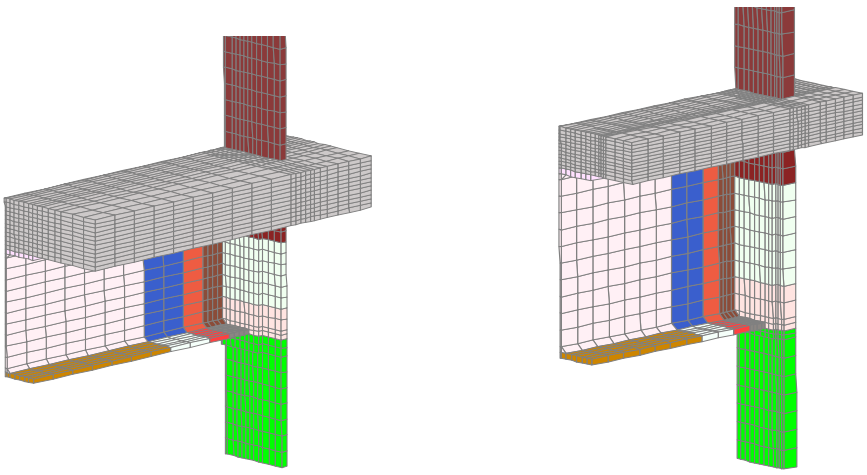

Figure 2-18 : FE models of the reference cases n°1 (left) and n°2 (right)

The validity and the degree of precision of the simple analytical methods proposed in this work will be demonstrated by comparisons between the temperatures obtained analytically and numerically. In these comparisons, the temperature of the gases follows two types of time-temperature curves: the standard ISO-834 curve (Eq. 2-4) and parametric curves (Eq. 2-8). The parametrical curves considered are characterised by a coefficient $\Gamma = 1$ and durations of the heating phase equal to 30, 60, or 90 minutes (Figure 2-19). During the heating phase, the parametric curves with $\Gamma = 1$ are similar to the standard ISO curve.

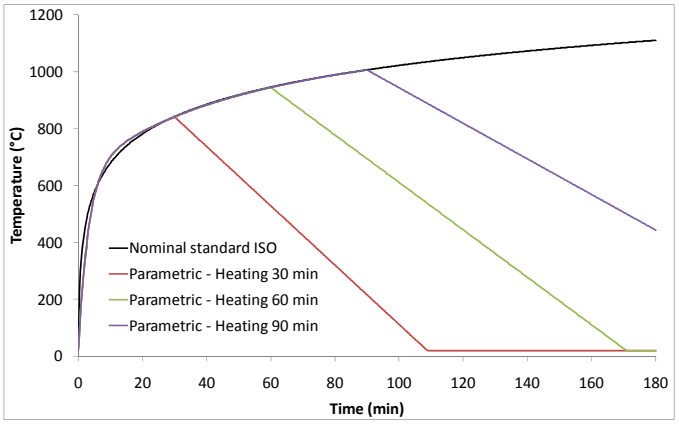

Figure 2-19 : Nominal and parametric fire curves used for the validations of the analytical methods

2.5.3 Analytical prediction of temperature in the bottom flange

2.5.3.1 Evaluation of temperature in 2-D beam sections

In the recommendations of the EN 1994-1-2 (Eqs 2-31 to 2-33), the steel beam is divided into individual parts and the ratio $A_{p,i}/V_i$ of the bottom flange is the ratio between the whole perimeter of this flange and its cross-section area. It is proposed to calculate the temperature in the bottom flange by the Lumped Capacitance Method, considering the ratio A_m/V of the flange heated on 4 sides (a) or the ratio A_m/V of the beam heated on 4 sides for the evaluation of the shadow factor (b). It should be mentioned that the shadow factor k_{sh} is not the same in (a) and (b) because the beam has a concave shape. The presence of the concrete slab is neglected for the moment.

The results obtained by the Lumped Capacitance Method with the two ratios A_m/V are compared with the results given by the 2-D model on Figure 2-20. The steel beam and the concrete slab are represented in the numerical model and the reduction of the emissivity is uniform in the steel section. The two values of the ratios A_m/V lead to good predictions as the three curves obtained numerically and analytically are almost superposed.

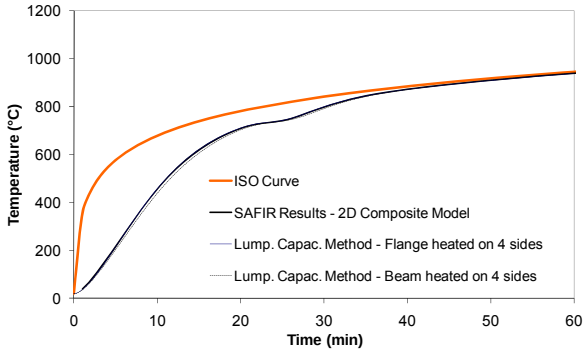

Figure 2-20 : Temperature in the bottom flange – Comparison between the Lumped Capacitance Method and SAFIR simulations

2.5.3.2 *Evaluation of temperature in 3-D joint zones*

2.5.3.2.1 Adaptations to the Lumped Capacitance Method for 3-D calculations

According to [Anderson, 2009], the Lumped Capacitance Method leads to very good results for the prediction of temperature in the joint zone. However, the parts of the joint integrated in the zone considered for the evaluation of the ratios A_m/V and the point of reference for the comparison with experimental results have not been clearly mentioned. Two ratios A_m/V are proposed here to predict the temperature at the junction between the beam bottom flange and the flush end-plate.

In the Method A1, the heated volume includes a length l_b of the beam bottom half, the lower half of the end-plate and a length l_c of one half of the column, as shown on Figure 2-21. The values of the distances l_b and l_c are the lengths of the beam and of the column in which the presence of the joint zone has a significant influence on the temperature profile (Eqs 2-63 and 2-64).

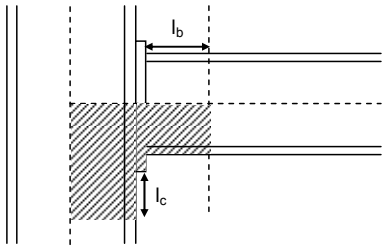

Figure 2-21 : Heated perimeter and heated section for the evaluation of the (A/V) ratio (Method A1)

The shadow factor k_{sh} and the ratio $(A_m/V)_{perimeter}$, given in Eqs 2-65 and 2-68, are inserted in the General Equation of the Lumped Capacitance Method (Eq. 2-25).

$l_b = h_b/2$	**2-63**
$l_c = \max\left(h_c/2\,;\,b_c/2\right)$	**2-64**
$A_{m,perimeter} = l_b\left(h_b + 2b_b\right) + t_p\left(b_p + h_p\right) + \left(l_c + \frac{h_b}{2}\right)\left(h_c + 2b_c\right) - \frac{A_b}{2}$	**2-65**
$A_{m,box} = \left(t_p + l_b\right)\left(h_b + b_b\right) + 2\left(l_c + \frac{h_b}{2}\right)\frac{h_c}{2} + \left(\left(l_c + \frac{h_b}{2}\right)b_c - \frac{h_b}{2}b_b\right)$	**2-66**
$V = \frac{A_b\,h_b}{4} + \frac{b_p\,h_p\,t_p}{2} + \frac{A_c}{2}\left(\frac{h_b}{2} + \frac{l_c}{4}\right)$	**2-67**
$k_{sh} = 0.9\left[\left(A_m/V\right)_{box}/\left(A_m/V\right)_{perimeter}\right] = 0.9\left[A_{m,box}/A_{m,perimeter}\right]$	**2-68**

where b_b, h_b and A_b are the width, the height and the cross-section area of the beam section; b_c and h_c are the width and the height of the column section; b_p, h_p and t_p are the width, the height and the thickness of the end-plate; $A_{perimeter}$, A_{box} and V are the area of the zone contour, the area of the smallest box surrounding the zone and the volume of the zone considered in the Lumped Capacitance Method.

A second adaptation of the Lumped Capacitance Method is based on the developments for a 2-D beam section. It has been demonstrated in § 2.5.3.1 that using the A_m/V ratio of a beam section heated on the four faces for predicting the temperature in the bottom flange leads to good results. As a very simple procedure, it is proposed to divide the ratio A_m/V obtained for 2-D sections by two for the bottom flange situated at the junction with the end-plate (Method A2). It is based on the rough assumption that the exposure to fire is divided by two in the joint zone.

2.5.3.2.2 Comparison between analytical and numerical results

The results given by Methods A1 and A2 have been compared to numerical results obtained with the two joint configurations under the standard ISO curve and parametric fire curves including a cooling phase (Figure 2-22). Analytical methods (A1 and A2) and numerical results show a good agreement under ISO fire. Due to the lower massivity of the beam and column sections, the temperature reaches fire curve earlier in the bottom flange of the IPE 300 beam.

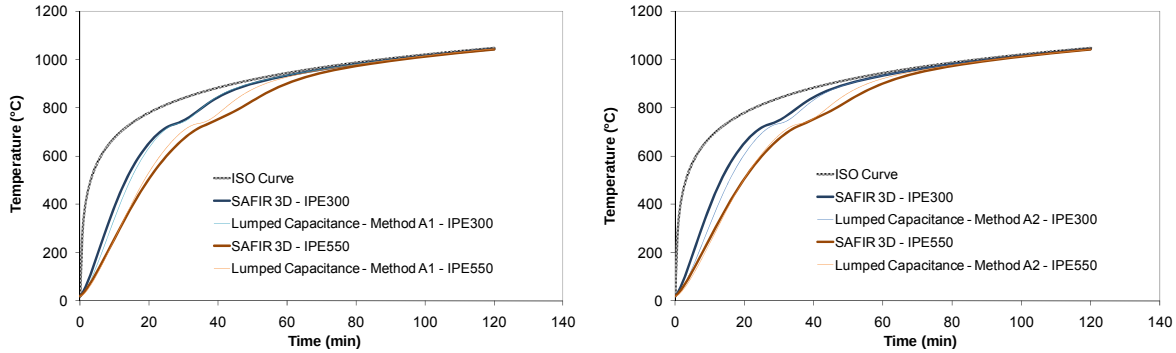

Figure 2-22 : Temperature in the bottom flange at the junction with the flush end-plate under ISO fire

The two Reference Cases have been analysed under parametric fire curves for two durations of the heating phase: 30 and 60 minutes. Figures 2-23 and 2-24 show that the prediction of temperature at the level of the bottom flange is good with the two proposed methods during heating and cooling phases. The differences between the temperatures calculated numerically and analytically are slightly higher with the Method A2 during the cooling phase of Reference Case n°2. This effect is low and can be explained by the fact that Method A2 does not account for the geometry of the column. Small differences are observed at the end of the cooling phase with Methods A1 and A2 and are explained as follows. The discontinuities obtained in the numerical simulations when the ambient temperature comes back to 20°C are due to the fact the coefficient of convection shifts to the "cold value" in the numerical simulations while this coefficient is kept constant in the analytical calculation. Such a discontinuity in the value of the coefficient of convection is in accordance with the Eurocodes recommendations but does not reflect the reality. The discussion about this aspect will not be extrapolated here.

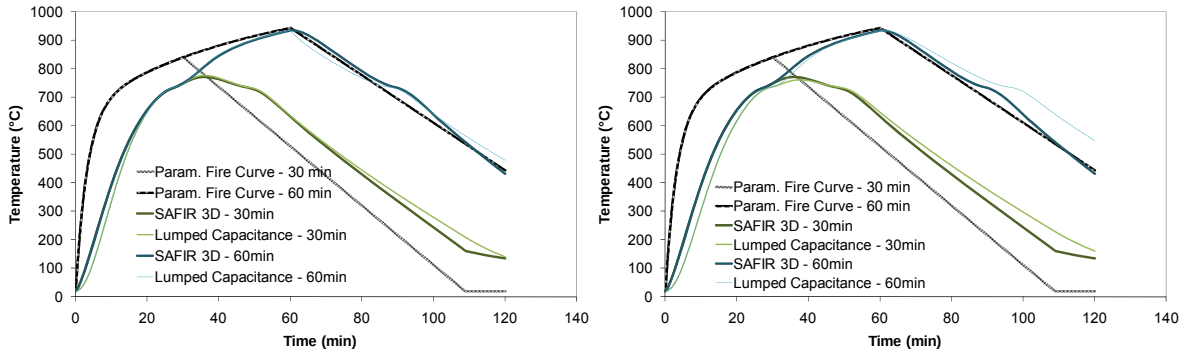

Figure 2-23 : Temperature in the bottom flange at the junction with the end-plate under parametric fires with Method A1 - (a) IPE 300 – (b) IPE 550

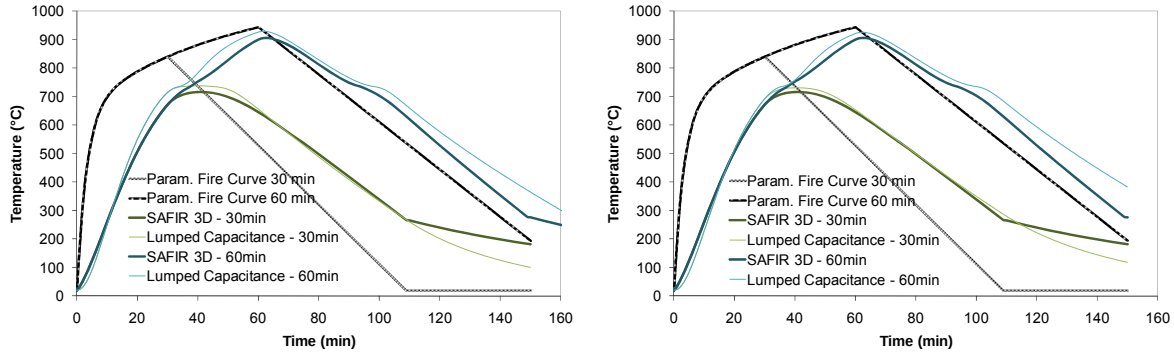

Figure 2-24 : Temperature in the bottom flange at the junction with the end-plate under parametric fires with Method A2 - (a) IPE 300 – (b) IPE 550

2.5.4 Analytical prediction of temperature in the top flange

2.5.4.1 Methods adapted from the Lumped Capacitance Method

2.5.4.1.1 Evaluation of temperature in 2-D beam sections

Proposal of a new shadow factor for the top flange

The ratio $A_{p,i}/V_i$ considered for the top flange is similar to the one used previously for the bottom flange except that the heated perimeter does not include the face that is in contact with the slab. This means that this frontier is assumed to remain adiabatic during the fire. The refined procedure proposed by Franssen and based on the rule of Hottel for advanced calculation models is used here for the evaluation of a shadow factor applied to the top flange (Figure 2-25 and Eqs 2-69 & 2-70).

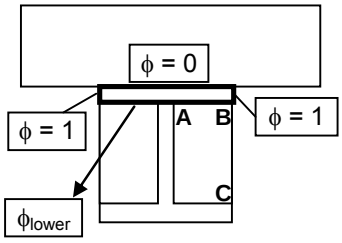

Figure 2-25 : Procedure based on view factors for the determination of the shadow factor

$\phi_{lower} = \dfrac{\overline{AB} + \overline{BC} - \overline{AC}}{2\overline{AB}}$	**2-69**
$k_{sh} = 0.9 \dfrac{\sum_i \phi_i l_i}{\sum_i l_i}$	**2-70**

By using this new procedure, the shadow factor of the top flange $k_{sh,top}$ passes from 0.65 (flange heated on 3 sides) to 0.48 (Hottel rule) in a IPE 300 cross-section. The Lumped Capacitance Method has been tested with these two values of the shadow factor for the prediction of the temperature in the top flange of the IPE 300 beam under standard ISO and parametric fire curves (Figure 2-26).

Under ISO fire, the Lumped Capacitance Method used with the shadow factor evaluated according to Eq. 2-70 gives a good prediction of the temperature in the top flange of the beam during the first part of the fire. After 45 minutes, the accuracy of the results is limited because the disregard of the heat transfer from the top flange to the concrete slab influences the temperature of the top flange (differences up to 90°C between numerical and analytical results). However, this simple method is conservative and leads to realistic values of the temperature in the top flange. The accuracy of this method is less good at high temperatures but the unprotected beam has probably already lost its stability when the temperature of the top flange reaches 700°C.

Comparisons between analytical and numerical results under parametric fire curves including a cooling phase are plotted for durations of the heating phase of 30 minutes (Figure 2-27a) and 60 minutes (Figure 2-27b). The correlation is not very good at the end of the heating phase and during the cooling phase, for the two values of the shadow factor.

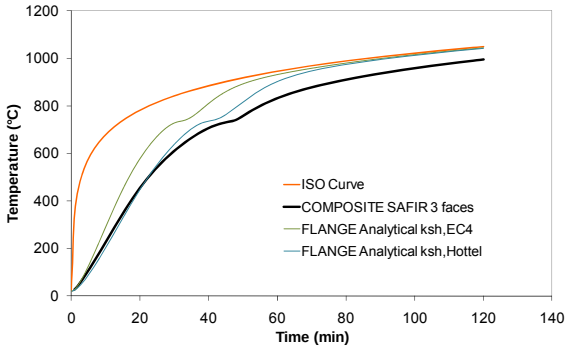

Figure 2-26 : Temperature in the top flange (IPE 300) – Analytical and numerical results

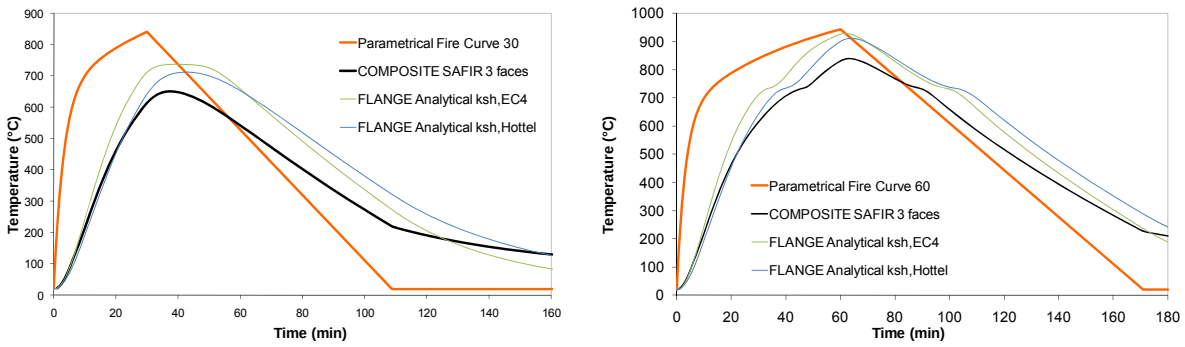

Figure 2-27 : Temperature in the top flange (IEP 300) – Analytical and numerical results

2.5.4.1.2 Evaluation of temperature in 3-D joint zones

Adaptations of the Lumped Capacitance Method

The applicability of two adapted versions of the Lumped Capacitance Method for the evaluation of temperature in the beam top flange at the junction with the flush end-plate and the column has been tested. In the Method B1, the thermal equilibrium is stated in a zone including a length l_b of the beam bottom half, the lower half of the end-plate and a length l_c of one half of the column. This zone is hatched on Figure 2-28. Method B2 consists in evaluating the A_m/V ratio of the 2D beam section following the rule of Hottel, in dividing this ratio by 2 and finally in calculating the temperature with the Lumped Capacitance Method.

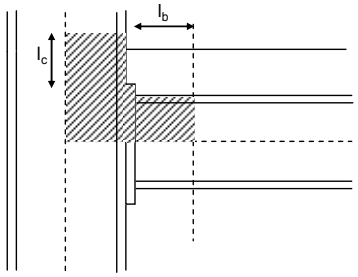

Figure 2-28 : Heated perimeter and heated section for the evaluation of the A_m/V ratio (Method B1)

$l_b = h_b/2$	**2-71**
$l_c = \max\left(h_c/2\,;\,b_c/2\right)$	**2-72**
$A_{m,perimeter} = l_b\left(h_b + b_b\right) + t_p\left(b_p + h_p\right) + \frac{h_b}{2}\left(h_c + 2b_c\right) - \frac{A_b}{2}$	**2-73**
$A_{m,box} = \left(t_p + l_b\right)\left(h_b + b_b\right) + 2\frac{h_b}{2}\frac{h_c}{2}$	**2-74**
$V = \frac{A_b h_b}{4} + \frac{b_p h_p t_p}{2} + \frac{A_c}{2}\left(\frac{h_b}{2} + \frac{l_c}{4}\right)$	**2-75**
$k_{sh} = 0.9\left[\left(A_m/V\right)_{box}/\left(A_m/V\right)_{perimeter}\right] = 0.9\left[A_{m,box}/A_{m,perimeter}\right]$	**2-76**

Under standard ISO fire, the temperature of the top flange is significantly over-estimated by the Method B1. The temperature of the top flange becomes similar to the ISO fire curve after approximately 60 minutes whereas the temperatures obtained numerically are about 200°C below the gas temperature (Figure 2-29). The non-consideration of the heat transfers between the top flange and the concrete slab is the source of such discrepancies. With Method B2, the temperature is under-estimated during the first 45 minutes and over-estimated during the rest of the fire. The differences between these analytical results and the numerical results are lower with Method B2 but this method is not conservative during a large period of the fire (Figure 2-30).

The application of Methods B1 and B2 under a parametric fire curve including a cooling phase also leads to large differences with regard to numerical results (Figure 2-31). During the cooling phase, the temperature is over-estimated with Method B1 but the differences with numerical results decreases with time. This is due to the fact that the heat transfers go from the slab to the top flange during the cooling phase and that these transfers are not considered in the analytical method. With Method B2, the prediction of temperature is acceptable during the heating phase but the cooling down of the top flange is too slow thereafter.

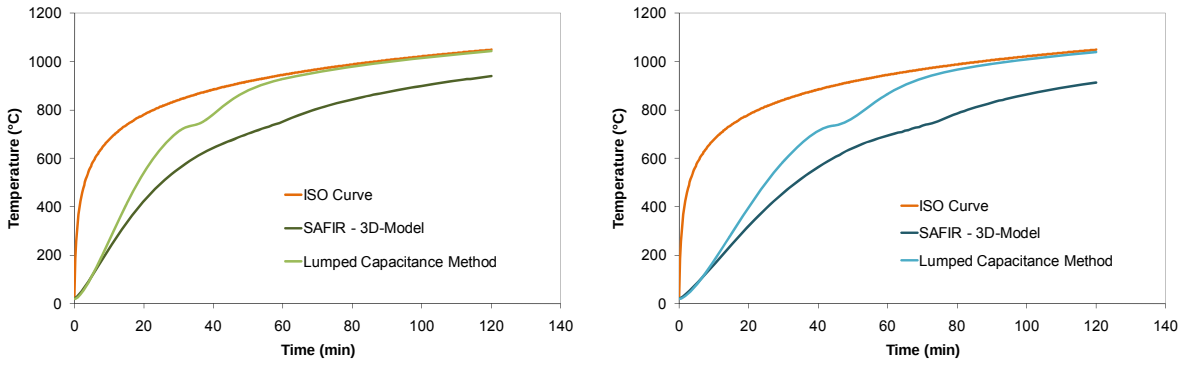

Figure 2-29 : Temperature in the top flange at the junction with the flush end-plate under ISO fire with Method B1 - (a) IPE 300 – (b) IPE 550

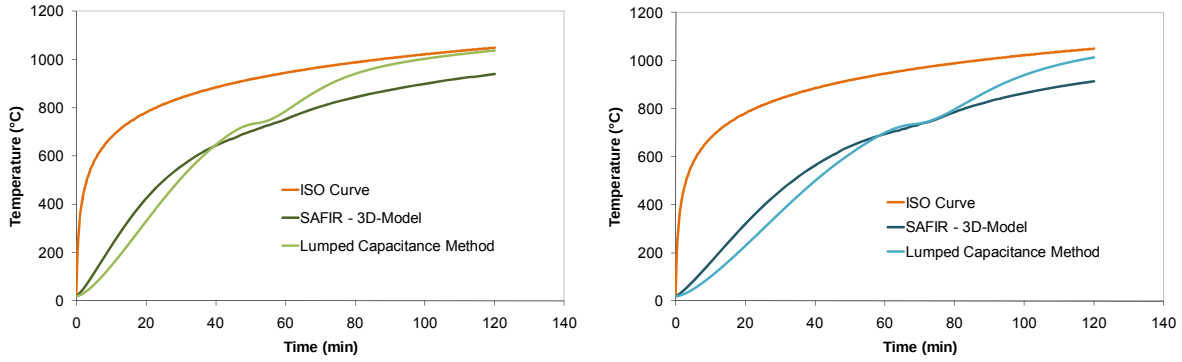

Figure 2-30 : Temperature in the top flange at the junction with the flush end-plate under ISO fire with Method B2 - (a) IPE 300 – (b) IPE 550

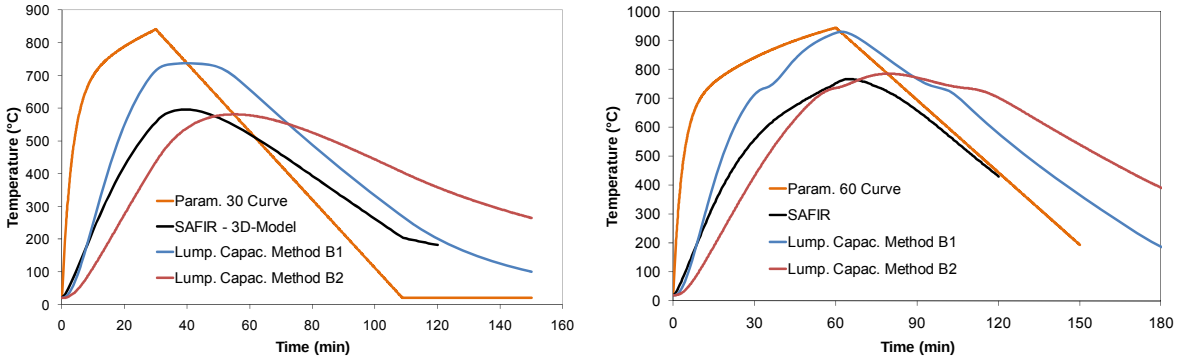

Figure 2-31 : Temperature in the top flange at the junction with the flush end-plate under parametric fire curves (EN 1991-1-2 Annex A) IPE 300 - (a) Heating = 30 min – (b) Heating = 60 min

2.5.4.2 Composite Section Method

2.5.4.2.1 Evaluation of temperature in 2-D beam sections

As a conclusion of the § 2.5.4.1, neglecting the presence of the concrete slab and the heat transfer between the top flange of the beam and the concrete slab leads to inaccurate predictions of the temperature at the top flange level, especially in the joint zone. In the Composite Section Method, it is proposed to include a part of the concrete slab in the heated zone (Figure 2-31). Indeed, in this new adapted version of the Lumped Capacitance Method, the heated section is composed of the upper half of the steel beam and a trapezoidal part of the concrete slab (Eq. 2-77). The heated perimeter is equal to the beam height so that the upper half of the heat fluxes from each vertical side of the box surrounding the beam are taken into account.

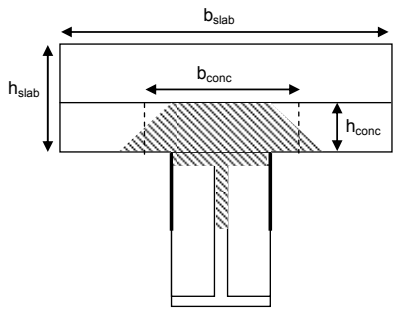

Figure 2-32 : Heated perimeter and heated section considered in the Composite Section Method

$b_{conc} = b_b + h_{conc}$	**2-77**

The Equation 2-3 of the Lumped Capacitance Method representing the equilibrium between the heat received by the section during a time step Δt and the quantity of energy consumed (or produced) by this section $Q_{heating}$ to increase (or decrease) the uniform temperature of the zone becomes:

$$\Delta Q_{transferred} = \dot{h}_{net,d}\, h_b\, \Delta t = \left(c_c\ \rho_c\ A_{conc} + c_a\ \rho_a\ A_b/2\right)\Delta\theta_{a,t} = \Delta Q_{heating} \qquad \textbf{2-78}$$

where A_b and A_{conc} are respectively the surface areas of the beam and the concrete zone integrated in the heated zone per unit length of the member, h_b is the beam height, c_c and ρ_c are the specific heat and the unit mass of concrete, c_a and ρ_a are the specific heat and the unit mass of steel and $h_{net,d}$ is the design value of the net heat flux accounting for thermal exchanges by convection and radiation.

After calibration of the Composite Section Method, the height of concrete integrated in the heated zone h_{conc} is expressed by Eq. 2-79 during the heating phase, where t_{fb} is the thickness of the beam flange and t_0 defines the speed of variation of h_{conc}, inversely related to t_{fb} (Eq. 2-80).

$$h_{conc} = \min\left(20 + 110\left(\frac{t}{t_0}\right); h_{slab}\right)\ [mm] \qquad \textbf{2-79}$$

$$t_0 = 60\left(\frac{10}{t_{fb}}\right)\ [\min] \qquad \textbf{2-80}$$

At the end of the heating phase, the temperature is equal to T_{max} and the height of concrete integrated in the heated zone h_{conc} has reached $h_{conc,max}$. During the cooling phase, the height h_{conc} decreases linearly until reaching 20 mm when temperature comes back to 20°C. The height h_{conc} is represented on Figure 2-33 for two cases, depending if h_{conc} reaches the slab thickness during the heating phase (bold line) or not (dotted line).

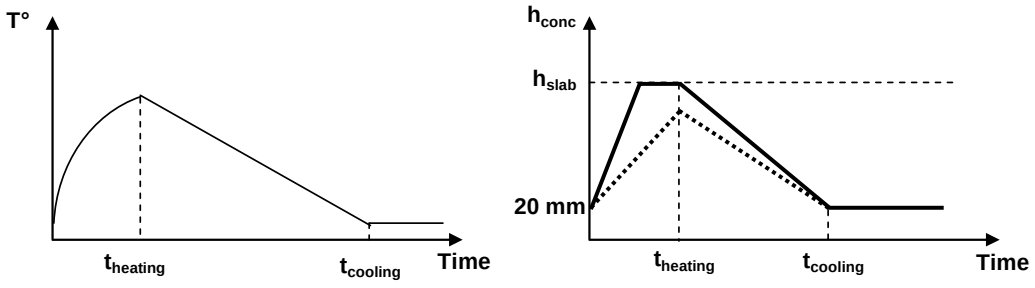

Figure 2-33 : Height of the "heated concrete slab" during a parametric fire

It should be mentioned that this method does not make the assumption that the temperature is uniform in the concrete slab. This method assumes that the variation of temperature ΔT is uniform in the heated zone during a time step Δt. At the next time step, the dimensions of the heated zone are modified and

new “cold parts” are included into the heated zone. Consequently, the temperature is not uniform in the heated zone. This simple method is not aimed at calculating the distribution of temperature in the concrete slab but this procedure could be continued in other researches.

Figure 2-34 shows the comparison between the evolution of temperature in the beam top flange predicted by the Composite Section Method and the numerical results obtained from SAFIR software. On the left, an IPE 300 steel section is subjected to several parametric fire curves (Figure 2-34a). On the right, three types of sections are tested under ISO standard fire curve (Figure 2-34b). The good correlation between the numerical and analytical results tends to validate the Composite Section Method for typical beam sections during the heating phase of parametric fire curves.

The application of the Composite Section Method leads to less good results during the cooling phase. The temperature starts to decrease earlier in numerical results. Figure 2-35 gives a comparison between analytical and numerical results under the parametric curve $\Gamma = 1$ for three durations of the heating phase. The Method A1 (Figure 2-35a) seems to give higher temperatures than the Composite Section Method (Figure 2-35b) during the heating phase but the results given by these methods are both higher than what is obtained numerically during the cooling phase.

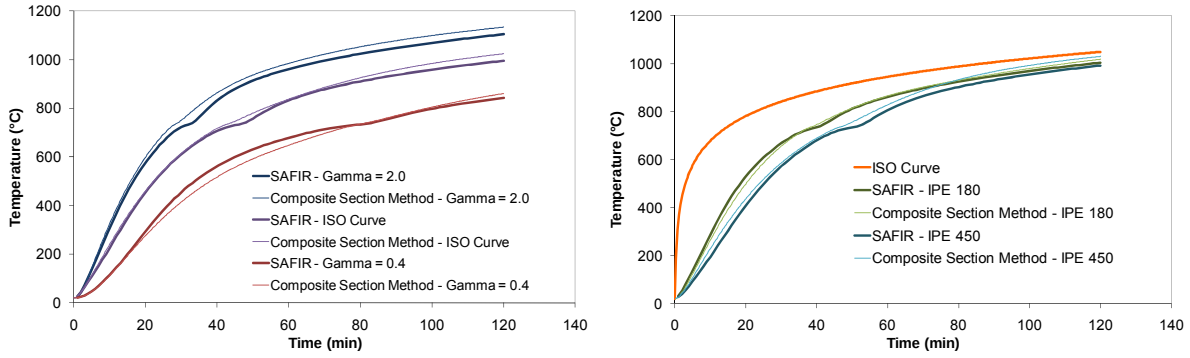

Figure 2-34 : Influence of the fire curve (a) and the beam height (b) on the temperature in the top flange

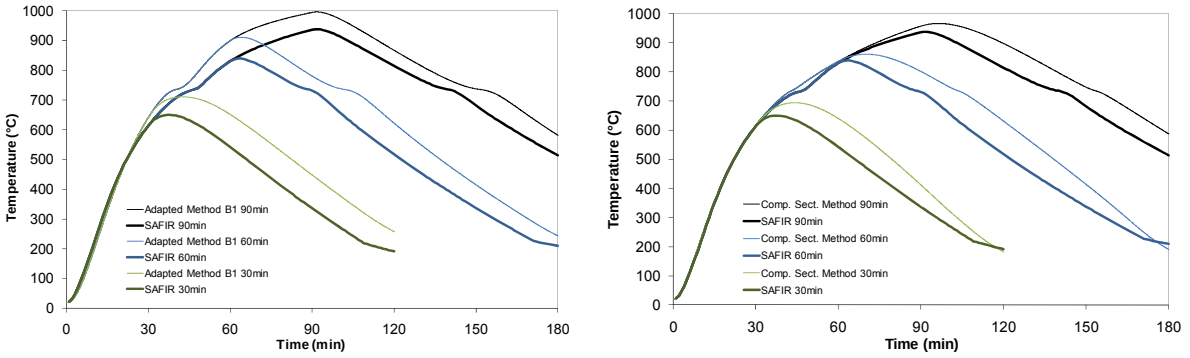

Figure 2-35 : Comparison of Method B1 and “Composite Section” Method under parametric fire curves

2.5.4.2.2 Evaluation of temperature in 3-D joint zones

Extension of the "Composite Section Method" to 3-D joint zones

The extension of the Composite Section Method to 3-D joint zones necessitates the definition of a 3-D heated zone. The volume of this heated zone chosen includes a length l_b of the steel beam and of the concrete trapezoidal section situated on the top of the beam, a part of the concrete slab situated between the column flanges (height = h_{conc}, length = h_{conc}) and a part of the column (height = $h_b/2 + 20 + 2*(h_{conc} - 20)$). Due to the high thermal conductivity of steel, the considered height of the column embedded in concrete is assumed to increase twice quicker than the height of concrete slab h_{conc} included in the heated volume (Figure 2-36).

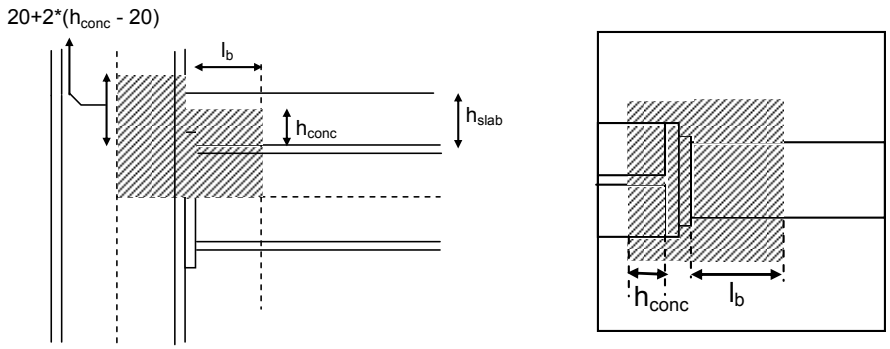

Figure 2-36 : Heated perimeter and heated section for the evaluation of the A_m/V ratio

Similarly to 2-D cases, the temperatures at the junction between the beam top flange and the column predicted by the Composite Section Method are in agreement with the numerical results (Figure 2-37) during the first part of the standard ISO fire curve (around 70 minutes). After this period, the analytical method tends to reach the fire curve while the gap between the top flange temperature and the fire curve decreases very slowly in the numerical simulations.

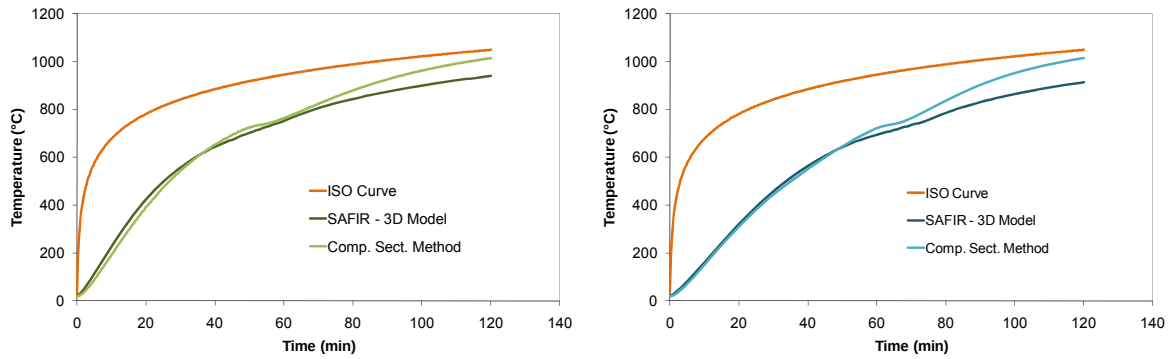

Figure 2-37 : Temperature in the top flange at the junction with the flush end-plate under ISO fire with Composite Section Method - (a) IPE 300 – (b) IPE 550

The Composite Section Method predicts the temperature of the top flange correctly during the heating phase of parametric fire curves but a delay is observed during the cooling down (Figure 2-38). This delay is due to the fact that the heat transfers between the top flange and the rest of the beam section are not explicitly taken into account. In reality, heat is transferred from the bottom flange to the top flange during the heating phase and the beginning of the cooling phase. During the heating phase, the heat exchanges between the flanges and the gases are of paramount importance and neglecting the heat transfers between the two flanges has no influence on the results. During the cooling phase, this statement is not true anymore because the differences of temperature between the flanges and the gases are lower. The heat transfers between the two flanges should be considered during that phase. Moreover, the direction of the heat transfers between the top and the bottom flanges is modified during the cooling phase, as explained hereafter.

The exposure of the bottom flange to fire is high and this flange reaches higher temperatures than the top flange during the heating phase of the fire. As a consequence of the high exposure to fire, the bottom flange is also cooled down rather quickly in comparison with the top flange at the beginning of the cooling phase. This means that the quantity of heat transferred from the bottom flange to the top flange decreases until the temperature is equal in the two flanges (Figure 2-39). Thereafter, the bottom flange becomes colder than the top flange the heat transfers go from the top flange to bottom flange. The fact that heat transfers between the top and bottom flanges are not taken into account in the Composite Section Method explains why the temperature of the top flange decreases more rapidly in the numerical simulations than predicted analytically. Figure 2-39 shows that the temperature starts to decrease in the two flanges at the same moment.

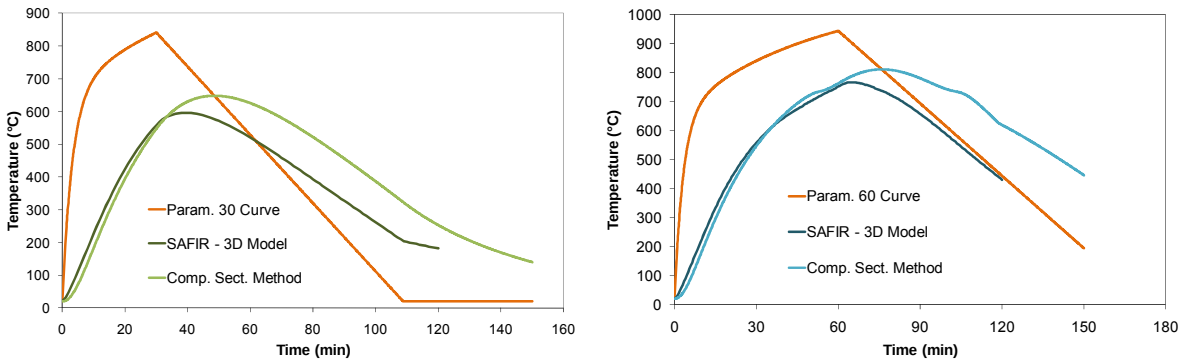

Figure 2-38 : Temperature in the bottom flange at the junction with the end-plate under natural fire with Composite Section Method - (a) $t_{heating}$ = 30 min – (b) $t_{heating}$ = 60 min

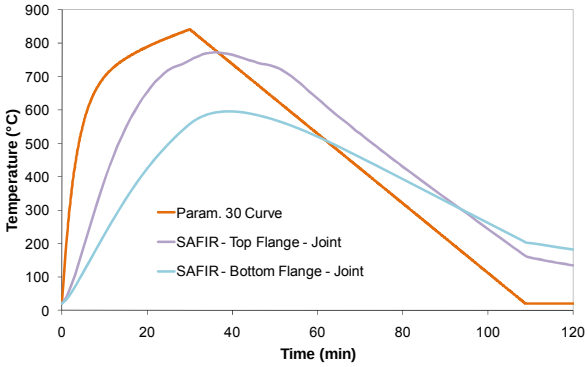

Figure 2-39 : Temperature in the beam flanges in the joint obtained numerically

2.5.4.3 *Heat Exchange Method*

2.5.4.3.1 Global description of the Heat Exchange Method

The applicability of the Lumped Capacitance Method and Composite Section Method to evaluate the temperature in the beam top flange (mid-span or joint sections) is limited because the heat transfers between this top flange on one side and the other parts of the steel section and/or the concrete slab on this other side are not taken into account. Thus, a new method is proposed where the heat ΔQ_{gas} exchanged between the top flange and the gas, the heat $\Delta Q_{top\text{-}bottom}$ exchanged between the top flange and the concrete slab and the quantity of heat $\Delta Q_{concrete}$ transferred between the top flange and the other parts of the steel section are calculated individually. The variation of the temperature during a time step Δt is obtained by use of Eq. 2-81.

$$\Delta Q_{transferred} = \Delta Q_{gas} + \Delta Q_{top-bottom} + \Delta Q_{concrete} = c_a \rho_a V \Delta \theta_{a,t} = \Delta Q_{heating} \quad \text{2-81}$$

2.5.4.3.2 Procedure for the prediction of temperature in 2D beam sections

Heat exchange between the top flange and the gas

The analysis of the heat transferred by convection and radiation between the top flange and the gas has already been mentioned previously and is, in the Eurocode recommendations, the unique type of heat transfer considered. In the present method, it is proposed to consider the heated perimeter shown on Figure 2-40 for 2-D beam sections (Eqs 2-82 & 2-83).

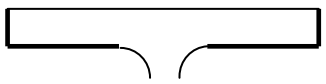

Figure 2-40 : Heated parameter for heat exchange between the top flange and the gas

$A_m = 2\,t_f\ + b_b\ - t_{wb} - 2\,r_c$	**2-82**
$V = b_b\,t_{fb}$	**2-83**

The quantity of energy transmitted to (or emitted by) the top flange by exchange with the gas is (Eq. 2-84):

$\Delta Q_{gas} = \dot{h}_{net,d}\,k_{sh}\left(b_b + 2\,t_f - t_w - 2\,r_c\right)\Delta t$	**2-84**

The shadow factor is calculated through the evaluation of the view factors of the top flange faces (§ 2.5.3.1 – Eq. 2-70).

Heat exchange between the top flange and the other parts of the steel beam

The results of numerical simulations show that the distribution of temperature in a composite beam is approximately uniform in the web and the bottom flange of the steel beam (Figure 2-41). A gradient of temperature is observed at the junction between the web and the top flange and heat is transferred by conduction in that zone.

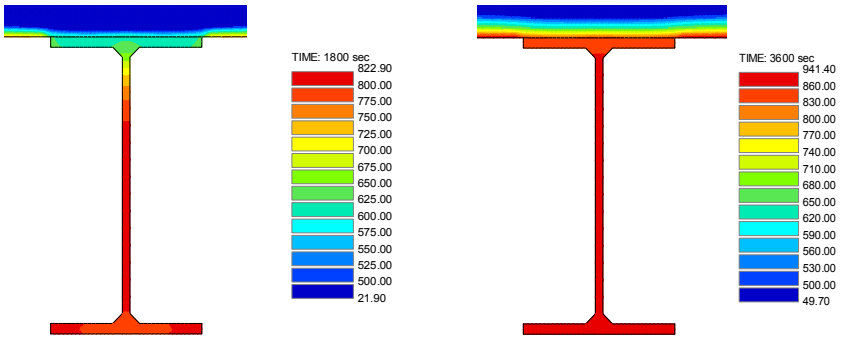

Figure 2-41 : Thermal distribution in a composite beam under ISO fire – (a) 30 min – (b) 60 min

Eq. 2-85 is proposed to evaluate the heat transfer between the top flange and the rest of the steel section during a given time step Δt. This energy can be positive (heat received by the top flange) or negative (heat lost by the top flange).

$\Delta Q_{top-bottom} = \lambda \dfrac{\left(T_2 - T_1\right)}{x}\,t_w\,\Delta t$	**2-85**

where λ(T) is the thermal conductivity of steel, x is the length of heat transfer (chosen equal to the radius of the root fillet), T_1, T_2 are the temperatures in the top and bottom flanges and t_{wb} is the thickness of the beam web. The temperature of the bottom flange T_2 is evaluated with the simplified version of the Lumped Capacitance Method exposed in § 2.5.3.1, considering the complete I-profile cross-section heated on its four faces.

Heat exchange between the top flange and the concrete slab

The quantity of heat transferred from the beam top flange to the concrete slab is quite difficult to estimate because the distribution of temperature in the concrete slab is not uniform. It is proposed here to calculate this quantity as a function of two parameters: the temperature of the top flange and the parameter Γ used to determine the shape of the parametrical fire curves in the Annex A of the EN 1991-1-2. Numerical simulations of a flange covered by a slab and submitted to fire have been performed (Figure 2-42). The quantity of heat transferred from the top flange to the slab has been obtained by calculating the difference between the quantity of heat received by the flange from the gases and the quantity of heat consumed to increase its temperature. The flux is the ratio between the heat transferred and the contact surface.

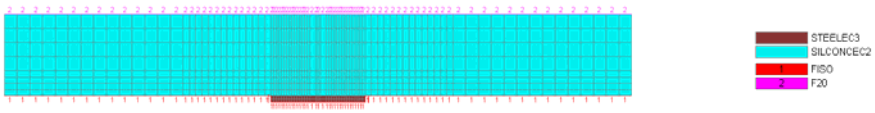

Figure 2-42 : Numerical model used to calculate the heat flux between the top flange and the concrete slab

This procedure has been followed for the heating phase of several parametric curves (Γ varies between from 0.4 to 2) and the evolution of the heat fluxes from the flange to the slab is plotted on Figure 2-43. Simple analytical expressions have been defined in order to approach the heat fluxes deduced from the results of numerical simulations (Equations 2-86 to 2-88 - Table 2-2). The strong discontinuities observed on Figure 2-43 around 735°C are due to the peak value of the specific heat of steel at this temperature (Figure 2-6).

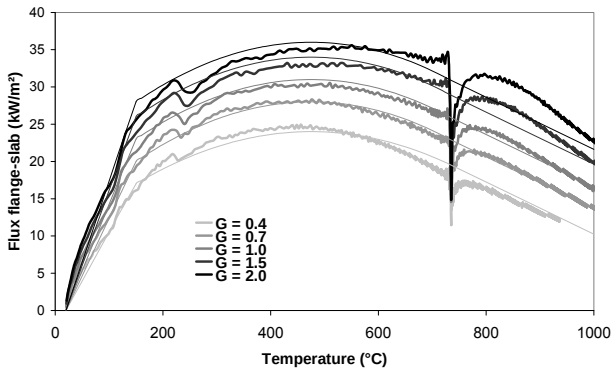

Figure 2-43 : Flux from top flange to concrete slab during the heating phase of a parametric fire curve

$\phi_{heating}(T) = \phi_{150}\dfrac{(T-20)}{(150-20)} \quad ; \quad T \le 150°C$	**2-86**
$\phi_{heating}(T) = \phi_{475} - (\phi_{475} - \phi_{150})\left(\dfrac{475-T}{325}\right)^2 \quad ; \quad 150°C \le T \le 730°C$	**2-87**

$$\phi_{heating}(T) = \phi_{475} - 0.616*(\phi_{475} - \phi_{150}) - 0.035*(T - 730) \quad ; \quad T \geq 730°C$$ **2-88**

	Γ = 0.4	Γ = 0.7	Γ = 1	Γ = 1.5	Γ = 2
	Flux (kW/m²)	Flux (kW/m²)	Flux (kW/m²)	Flux (kW/m²)	Flux (kW/m²)
20	0	0	0	0	0
150	17	20	23	26	28
475	24	28	31	34	36

Table 2-2 : Tabulated data of ϕ_{150} and ϕ_{475} in function of the parametric fire curve

Formulae of Equations 2-86 to 2-88 have been extracted from the numerical results obtained with a flange thickness equal to 10 mm. The influence of the flange thickness is limited and must not be considered in these analytical formulae (Figure 2-44).

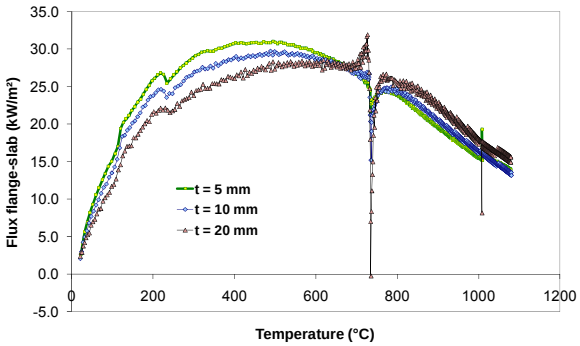

Figure 2-44 : Flux between the top flange and the concrete slab – Influence of the flange thickness

During the cooling phase, the distribution of temperature in the slab depends on the history of the thermal loading because the evolution of the flux is not reversible. The procedure realised for heating phases has been reiterated with parametric fire curves including a cooling phase (Figure 2-45). Two different cases are considered here: $t_{heating}$ = 30 minutes and $t_{heating}$ = 60 minutes. Analytical expressions of the flux during the cooling phase have been extracted from those results (Equation 2-89).

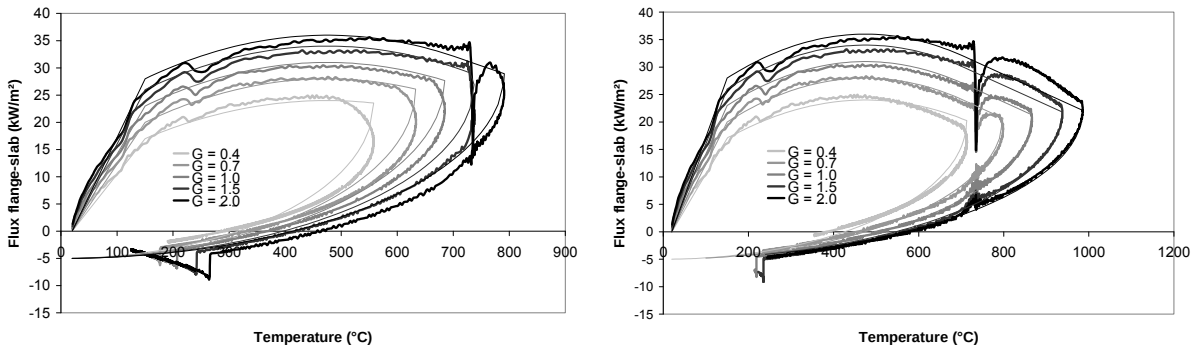

Figure 2-45 : Flux from top flange to concrete slab during the cooling phase of a parametric fire curve – (a) $t_{heating}$ = 30 min – (b) $t_{heating}$ = 60 min

$$\phi_{cooling}(T) = \phi_{\max} - (\phi_{\max} + 5)\sqrt{1 - \left(\frac{T}{T_{\max,heating}}\right)^2} \quad ; \quad 20°C \le T \le T_{\max,heating}$$ **2-89**

The quantity of heat ΔQ_{slab} exchanged between the top flange and the concrete slab during a time step Δt is (Eq. 2-90):

$$\Delta Q_{slab} = b_b \, \phi \, \Delta t$$ **2-90**

2.5.4.3.3 Validation of the Heat Exchange Method in 2-D beam sections

The temperatures of the top flange obtained with Heat Exchange Method and numerical results show a good agreement for the two reference cases under ISO fire, as shown in Figure 2-46. The Heat Exchange Method also gives good correlations with the SAFIR results under parametric fire curves, even during the cooling phase. The results obtained in the two reference cases and two durations of the heating phase are plotted on Figures 2-47 ($t_{heating}$ = 30 minutes) and 2-48 ($t_{heating}$ = 60 minutes). The delay observed with other methods at the beginning of the cooling phase has disappeared and the differences between the two curves remain small during the complete duration of the fire.

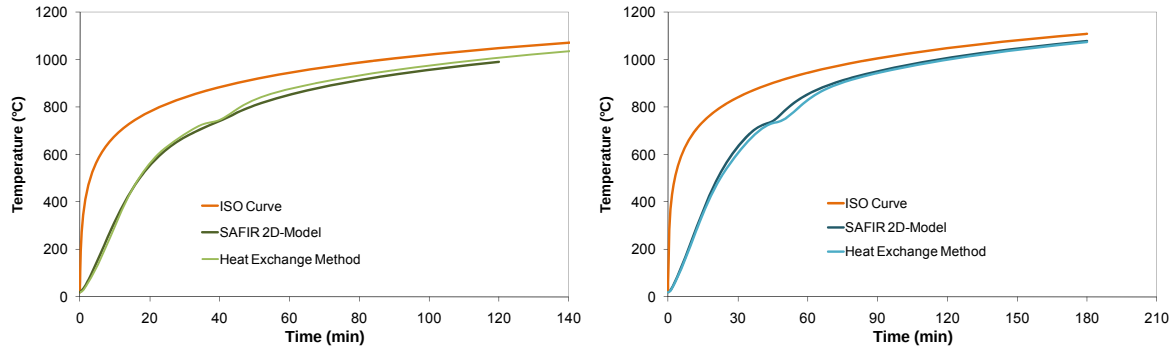

Figure 2-46 : Top flange temperatures obtained numerically and analytically – (a) IPE 300 – (b) IPE 550

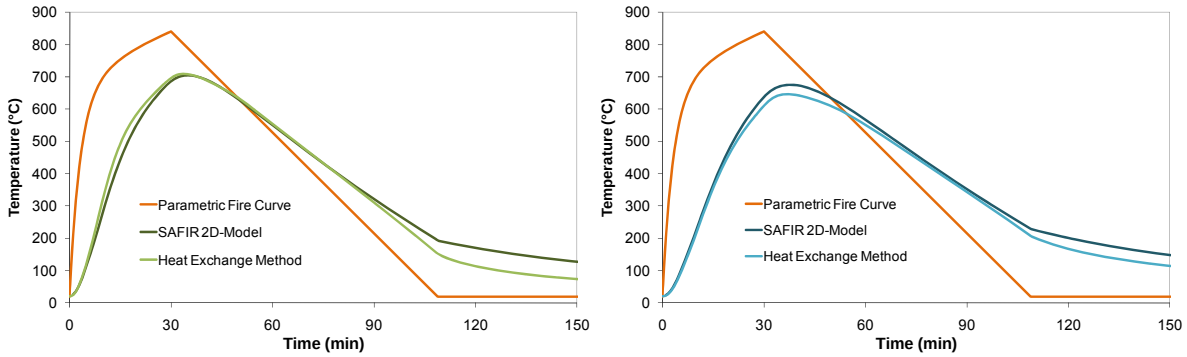

Figure 2-47 : Temperatures of the top flange obtained numerically and analytically – $t_{heating}$ = 30 min - (a) IPE 300 – (b) IPE 550

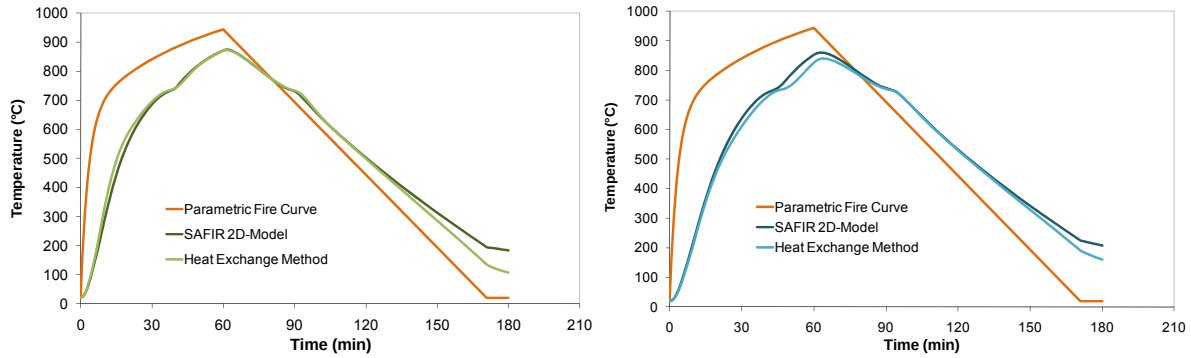

Figure 2-48 : Temperatures of the top flange obtained numerically and analytically – $t_{heating}$ = 60 min - (a) IPE 300 – (b) IPE 550

2.5.4.3.4 Procedure for the prediction of temperature in 3-D joint zones

In 3-D joint cases, the Heat Exchange Method states the equilibrium between the heat received (or emitted) by a zone through energy transfers with surrounding elements and the energy consumed to increase (or decrease) its own temperature. This zone is the same as the one considered with the previous methods and includes a part of the beam, a part of the end-plate and a part of the column (reminded in Figure 2-49).

The heat exchange $\Delta Q_{top\text{-}bottom}$ between the top flange and the other steel parts (rest of the column and bottom half of the beam) is supposed to exist through a cross-section $A_{top\text{-}bottom,}$ evaluated by Eq. 2-91. The vertical plane including weak axis of the column is supposed to be adiabatic by symmetry (similar to 3-D numerical model). The heat transfers to the top part of the column are supposed to be small enough in comparison with the fluxes between the "top flange" zone and the slab (Eq. 2-94) so that they are not considered.

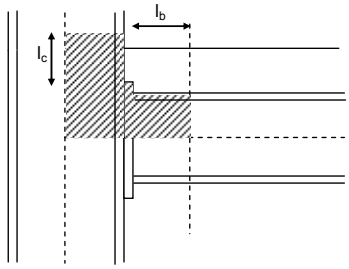

Figure 2-49 : Heated perimeter and heated section for the evaluation of the A_m/V ratio (Method B1)

$A_{top-bottom} = l_b\, t_{wb} + t_p\, b_p + A_c/2$	**2-91**
$\Delta Q_{top-bottom} = \lambda \dfrac{(T_2 - T_1)}{x} A_{top-bottom}\, \Delta t$	**2-92**

where t_p, b_p are the thickness and the width of the end-plate, $\lambda(T)$ is the thermal conductivity of steel, x is the length of heat transfer (chosen equal to the radius of the root fillet), T_1, T_2 are the temperatures in the top and bottom flanges, A_c is the cross-section area of the column and t_{wb} is the thickness of the beam web. The temperature T_2 is evaluated by use of the Lumped Capacitance Method A1 (§ 2.5.3.2.1 - Figure 2-21).

The expression of the heat flux between the top flange and the concrete slab is similar to the one used for 2-D cases. In joint zones, the cross-section $A_{transfer\ slab}$ on which heat transfers develop and the total heat transfer are given in Eqs 2-93 & 2-94.

$A_{transfer\ slab} = l_b\ b_b + t_p\ b_p + \left(\min\left(h_{slab}\ ; l_c\right)\right) * \left(h_c + 2b_c\right)$	**2-93**
$\Delta Q_{transfer\ slab} = \phi\ A_{transfer\ slab}\ \Delta t$	**2-94**

The temperatures at the junction between the top flange and the end-plate under standard ISO fire obtained by numerical simulations and by the Heat Exchange Method are plotted on Figure 2-50. The Heat Exchange Method leads to slightly higher temperatures than the finite element models, especially for the IPE 550 cross-section after more than 60 minutes but the correlation between the numerical and analytical results is good.

Under parametric fire curves including a cooling phase, temperatures predicted analytically in the top flange near the joint are still a little bit higher than numerical results. However, differences are small, even during the cooling phase (Figures 2-51 & 2-52).

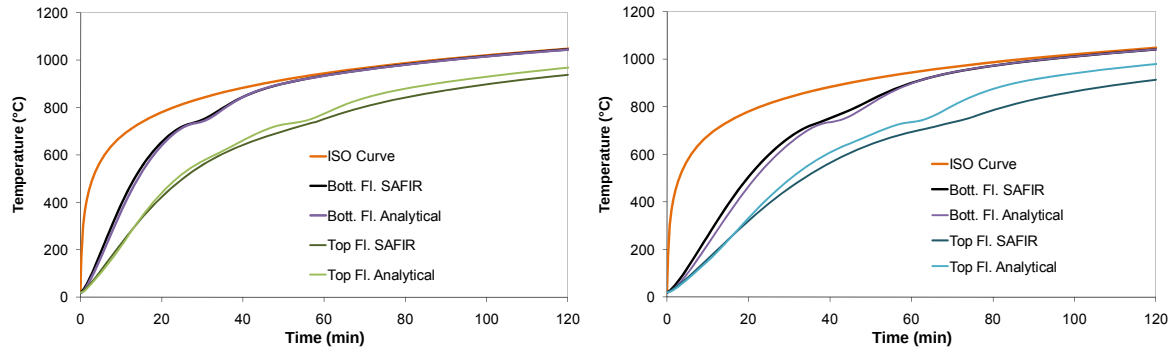

Figure 2-50 : Temperatures of the top flange predicted numerically and analytically – (a) IPE 300 – (b) IPE 550

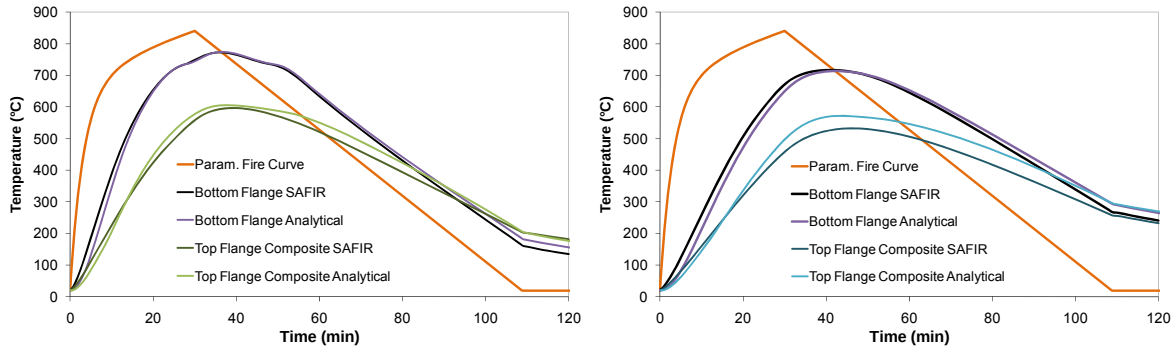

Figure 2-51 : Comparison between temperatures of the top flange obtained numerically and analytically – $t_{heating}$ = 30 min - (a) IPE 300 – (b) IPE 550

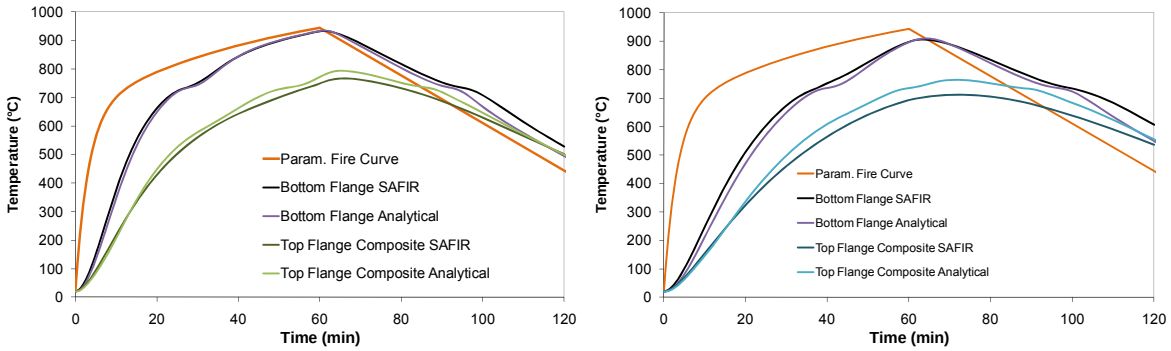

Figure 2-52 : Comparison between temperatures of the top flange obtained numerically and analytically – $t_{heating}$ = 60 min - (a) IPE 300 – (b) IPE 550

2.5.5 Interpolation between the top and bottom flanges

Up to here, the distribution of temperature in beam sections and joint zones has been characterized by the temperatures at the level of the top and bottom flanges. A simple method is proposed here to interpolate temperature between these two values calculated analytically. The results given by this method are compared to those obtained by use of SAFIR. For 2-D beam sections, the reference temperatures of the finite element model are taken on the vertical axis of symmetry of the steel profile. For 3-D joints zones, the reference temperatures of the model are read on the external surface of the end-plate at a distance $b_b/4$ of the vertical plane of symmetry of the beam (Figure 2-53), where b_b is the width of the beam flange. In usual joints, bolts are situated close to this reference line.

The simple method proposed here consists in assuming that the temperature profile is bilinear on the beam height as plotted on Figure 2-54. Figures 2-55 to 2-58 show comparisons between the temperatures interpolated from analytical and numerical results. Comparisons have been made under the standard ISO curve (t = 15, 30 and 60 minutes) and during the cooling phase of the parametric fire curve with $\Gamma = 1$ and $t_{heating}$ = 30 minutes (t = 60, 90 and 120 minutes). Figures 2-55 to 2-58 show that

this bilinear profile is an acceptable assumption in the analysed cases. However, it is noted that the temperature of the beam web is slightly under-estimated after 15 minutes in the massive beam section. This is in agreement with the recommendation of the EN 1994-1-2 stating that the temperature of the web can be taken as equal to that of the bottom flange if the beam height does not exceed 500 mm.

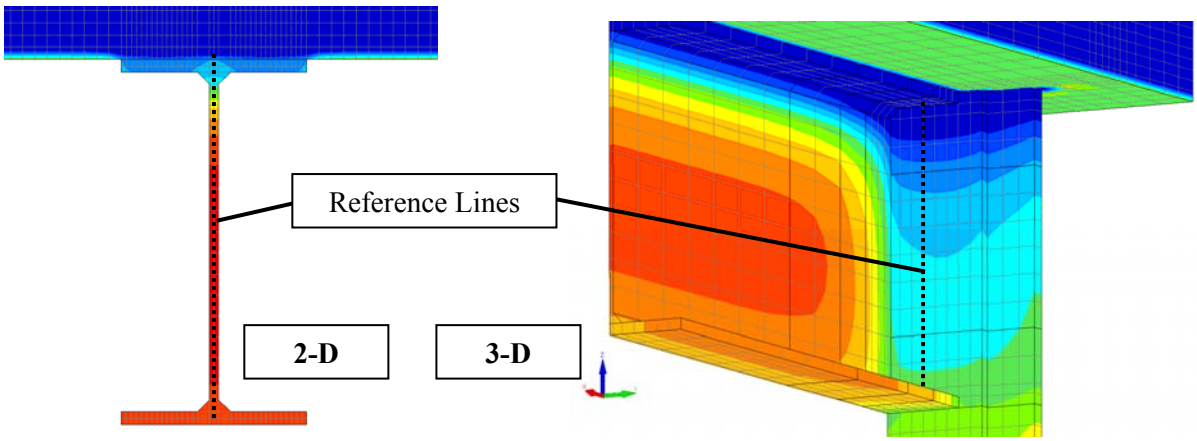

Figure 2-53 : Reference lines for temperature interpolation between the levels of top and bottom flanges

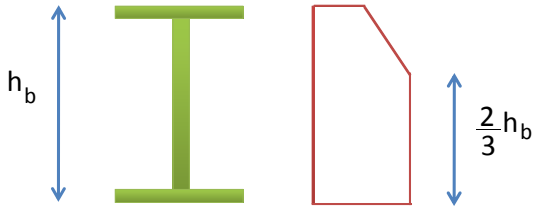

Figure 2-54 : Simple temperature profile between the levels of the top and bottom flanges

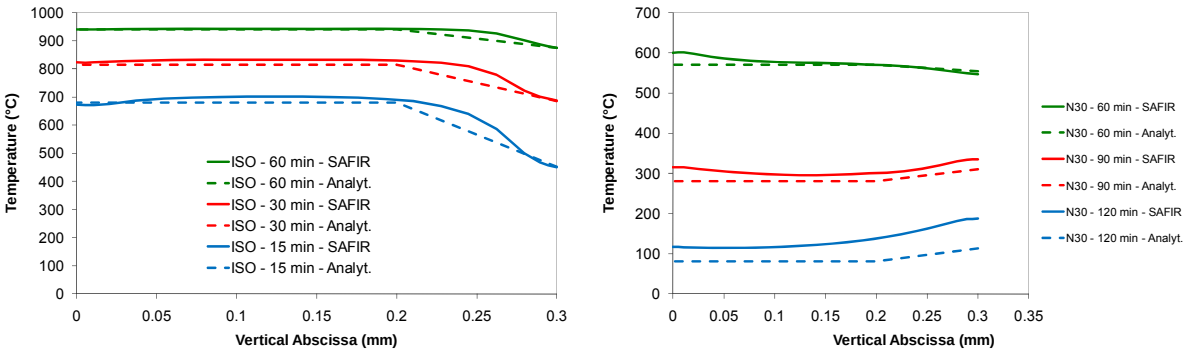

Figure 2-55 : Temperature profiles in the IPE 300 beam under ISO fire and parametric fire curves

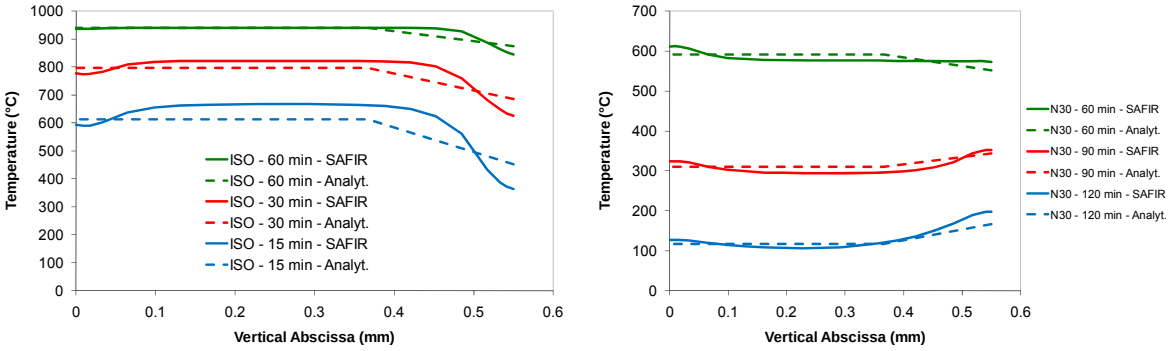

Figure 2-56 : Temperature profiles in the IPE 550 beam under ISO fire and parametric fire curves

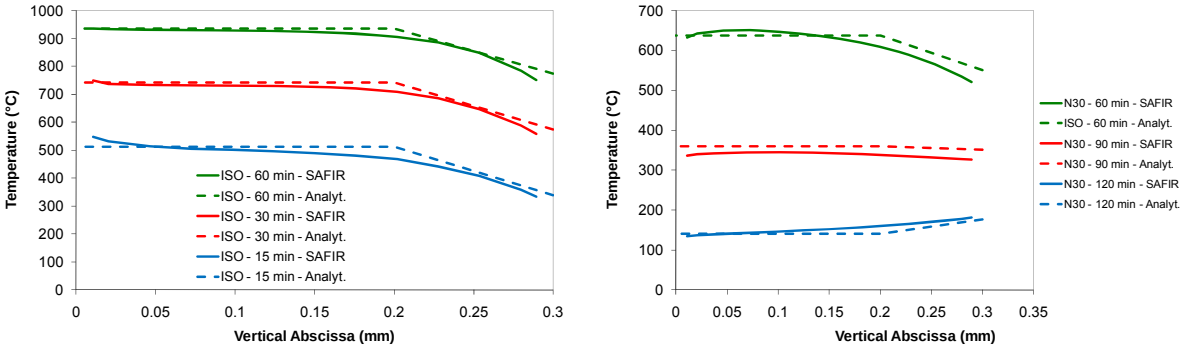

Figure 2-57 : Temperature profiles in the IPE 300 joint zone under ISO fire and parametric fire curves

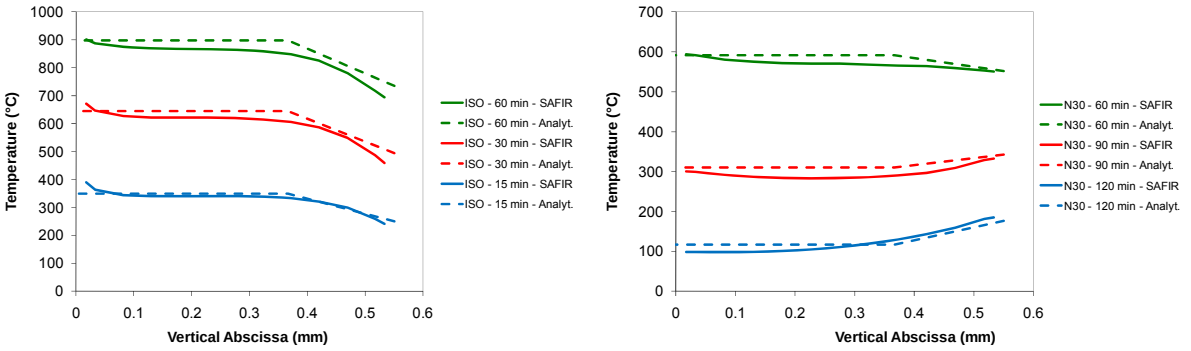

Figure 2-58 : Temperature profiles in the IPE 550 joint zone under ISO fire and parametric fire curves

2.5.6 Simple connections

As mentioned previously, the major part of the present chapter is focused on flush end-plate connections where the end-plate is in contact with the beam flanges and the column flange. Some finite elements analyses have been built in SAFIR program with fin plate, web cleats and header plate connections (Figure 2-59). As an output of these numerical analyses performed on the IPE 300 configuration, significant differences have been observed between the extremity of the beam flanges

and the sections of the column flange situated at the same level (Figure 2-60). This is due to the fact that the radiation between steel surfaces can not be taken into account in 3-D thermal analysed realised with this numerical tool and that the gap between the beam and column flanges avoids or limits transfers by conduction. Figure 2-61 shows that the type of connection has no influence on temperatures at the level of beam flanges and that the temperature of the flanges on the beam side is almost equal to the temperature obtained with the 2-D model of the beam.

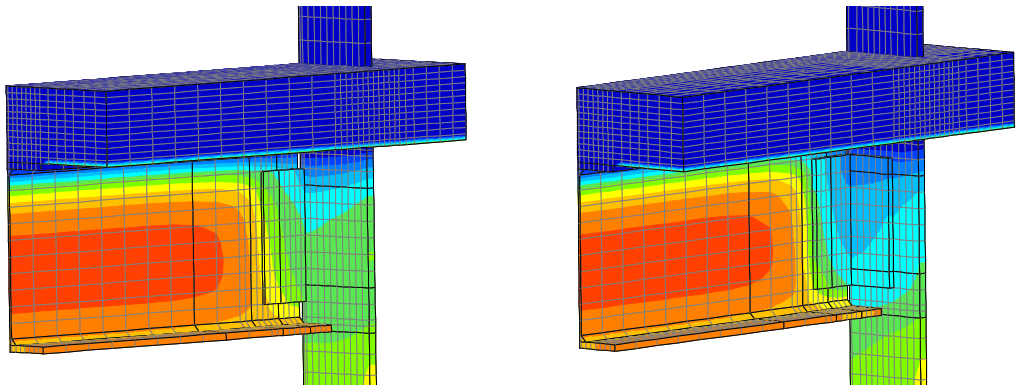

Figure 2-59 : Finite element models with fin plate connections (left) and web cleats connections (right)

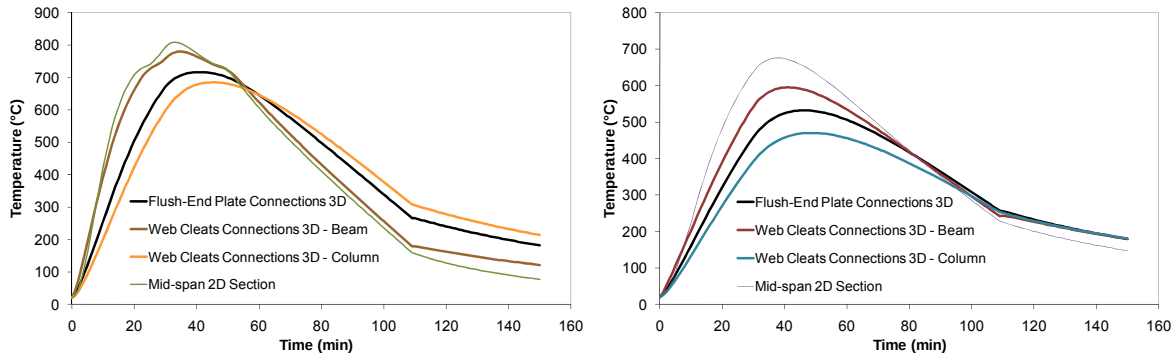

Figure 2-60 : Temperatures in the joint zone (SAFIR) - Levels of bottom (left) and top (right) flanges

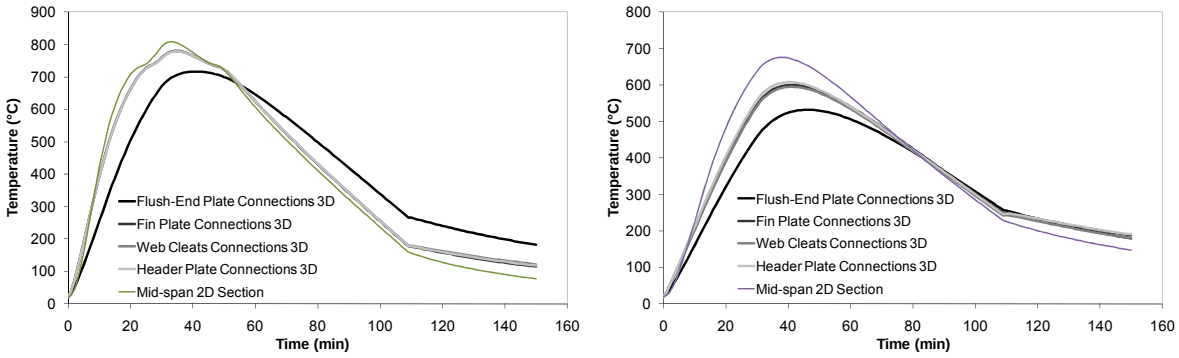

Figure 2-61 : Temperatures in the joint zone (SAFIR) - Levels of bottom (left) and top (right) flanges

The integration of radiation between the beam and column surfaces would produce a reduction of the gap of temperature observed here between the beam and column sides. However, it is not possible to quantify the importance of these radiative fluxes and of the real gap of temperature. More investigations would be needed to check if the assumption of a uniform temperature in the beam and column sides at the levels of beam flanges is still valid in simple connections.

2.6 Conclusions

After a review of existing methods and recommendations for the evaluation of temperature profiles in beam sections and joint zones, this chapter contains improvements to existing rules and proposals for new methods. The new methods differ by the degree of simplicity, the field of applicability and the accuracy of the predicted results. Comparisons with numerical simulations performed in the finite element program SAFIR have been described for the validation of these new methods. It is assumed in these numerical models that the contact between the steel profile and the concrete slab is perfect.

The “original” Lumped Capacity Method gives good predictions of temperature in steel and composite beams but the main drawback of this method is the fact that the temperature is assumed to be uniform on the section or the zone considered. This method has been applied separately to obtain the temperature at the levels of top and bottom flanges. The evaluation of shadow factors has been adapted to evaluate temperature in the two flanges. For the top flange, a shadow factor based on the Hottel rule has been defined for 2-D beam flanges and this concept has been extended to 3-D joint zones. The application of this method is relatively simple and gives good results for short fires with no cooling phase. After more than 40 minutes of standard ISO fire or during the cooling phase of a parametric fire curve, the differences with numerical results become significant.

In the adapted version of the Lumped Capacity Method mentioned in the previous paragraph, the interface between the top flange of the steel beam and the concrete slab is supposed to be adiabatic. In order to account for heat transfers between the steel elements and the concrete slab, the Composite Section Method has been proposed. This method consists in the integration of a part of the concrete slab in the heated surface or volume considered in the Lumped Capacitance Method. This method leads to a good correlation with numerical results during the heating phase of standard ISO fire but not during the cooling phase of parametric fire curves.

The main drawbacks of the two previously-mentioned methods are linked to the fact that some heat transfers between the zone considered and the other zones are ignored. In order to take all the heat transfers into consideration, they have been listed and analysed independently which led to the development of the Heat Exchange Method. The results obtained by use of this method correlates very

well with the numerical results during both heating and cooling phases of parametric fire curves defined in the Annex A of the EN 1991-1-2. However, the application becomes more fastidious and is limited to a certain range of parametric fire curves. Indeed, the expression of the flux between the top flange of the beam and the slab is given as a function of the parameter Γ used in parametric fire curves defined in the Annex A of the EN 1991-1-2. More investigations would be necessary to extend the field of application of the Heat Exchange Method to any fire curve.

The investigations are mainly focused on the temperatures at the levels of the top and bottom flanges, considered separately. A bilinear temperature profile has been proposed to interpolate the analytically-calculated temperatures on the beam height. This procedure is simple and shows a good agreement with the numerical results in 2-D beam sections and 3-D joint zones during the heating and cooling phases of parametric fire curves.

The influence of the type of connections on the results has been analysed. The results obtained numerically can be divided into two groups depending on the existence of a contact or not between the beam flanges and the column flange. This is due to the fact that the heat transfers by radiation between two surfaces of the joint are not taken into account in the numerical model. In reality, these transfers will reduce the gap of temperature obtained numerically between the beam and column sides but this effect has not been quantified. In absence of reliable data about thermal distribution in simple connections (no contact between the beam flanges and the column flange), it is assumed that a unique value of the temperature is sufficient at one level, as currently recommended in the current Eurocode recommendations for composite joints. This assumption should be validated by experimental tests or more complex numerical models would be necessary.

3 Evaluation of the internal forces in axially and rotationally restrained beams under natural fire

3.1 Introduction

When an unprotected steel structure is subjected to a natural fire, the distribution of internal forces in the elements of this structure varies quickly and extensively. The distribution of internal forces is quite difficult to predict because a lot of parameters have an influence: longitudinal and transversal distributions of temperature through the heated elements, stiffness and resistance of the joints, mechanical loading, axial and rotational stiffnesses of the surrounding structure, etc.

Under a uniform elevation of a temperature ΔT, an element tends to elongate freely (Figure 3-1a) and the elongation ΔL_t is given by Eq. 3-1, where α and L are respectively the coefficient of thermal elongation and L the length of the element. If the longitudinal displacements of this element are avoided (Figure 3-1b), the elevation of temperature will create an axial thrust F_T in the element (Eq. 3-2) that depends on the extensional stiffness EA of the element.

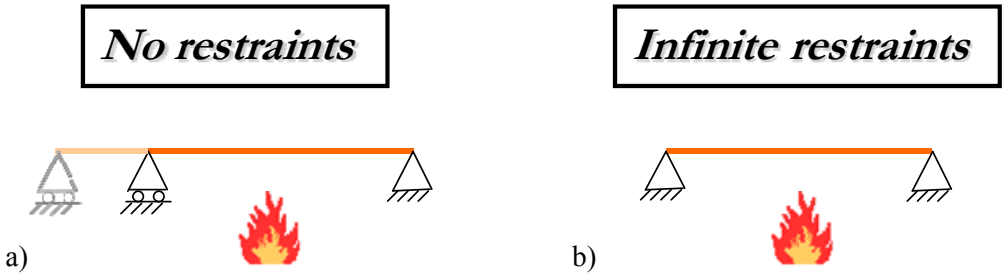

Figure 3-1 : Free and restrained beams submitted to a uniform elevation of temperature

$\Delta L_t = \alpha \, \Delta T \, L$	**3-1**
$F_T = EA \, \alpha \, \Delta T$	**3-2**

These two situations are extreme boundaries: heated elements are usually partially restrained and the flexibility of the surrounding structure can be represented by a spring with an extensional stiffness K_A (Figure 3-2). The equilibrium is obtained by stating that i) the cumulated elongations of the beam and the spring are equal to 0 and that ii) the axial force is equivalent in the beam and the spring (Eqs 3-3 to 3-5). In Eq. 3-5, $K_{A,beam}$ is defined as the axial stiffness of the beam.

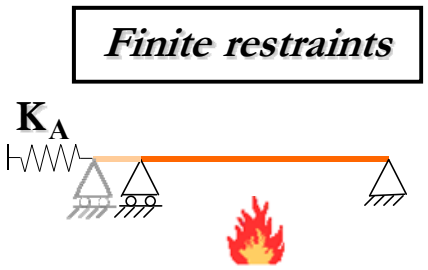

Figure 3-2 : Partially-restrained beam submitted to a uniform elevation of temperature

$\Delta L_{beam} = \Delta L_{t,beam} + \Delta L_{m,beam} = \alpha\ \Delta T\ L + \frac{F_T\ L}{EA}$	**3-3**
$\Delta L_{spring} = \frac{F_T}{K}$	**3-4**
$F_T = \frac{\alpha\ \Delta T\ L}{\left(\frac{1}{K_A} + \frac{L}{EA}\right)} = \frac{\alpha\ \Delta T\ L}{\left(\frac{1}{K_A} + \frac{1}{K_{A,beam}}\right)}$	**3-5**

A similar approach can be followed for the evaluation of the bending moment M_t induced by a uniform gradient of temperature in a beam that is partially or completely restrained in rotation at its extremities. Considering a beam submitted to a linear distribution of temperature accross his height h, between the top temperature T_1 and the bottom temperature T_2, the curvature χ_t is given by Eq. 3-6. In case of simply-supported beams, the rotation at the beam extremity θ_t and the vertical deflection at the mid-span of the beam δ_t are given by Eqs 3-6 to 3-8. On the opposite, a beam with two extremities fixed in rotation will be subjected to a thermally-induced bending moment M_t (Eq. 3-9).

$\chi_t = \alpha \frac{(T_2 - T_1)}{h}$	**3-6**
$\theta_t = \chi_t \frac{L}{2}$	**3-7**
$\delta_t = \chi_t \frac{L^2}{8}$	**3-8**
$M_t = EI\ \alpha \frac{(T_2 - T_1)}{h}$	**3-9**

In intermediate cases, the effect of the surrounding structure is represented by rotational springs with a rotational stiffness K_R. The equation of compatibility states the equilibrium between the rotation θ_t induced by the thermal gradient and the rotations caused by the bending moment M_t in the rotational spring and the beam (Eqs 3-10 and 3-11).

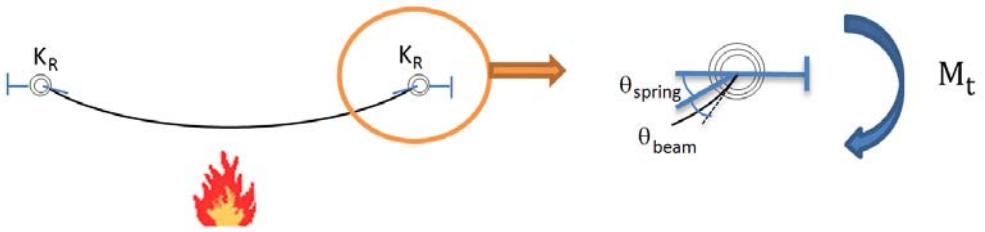

Figure 3-3 : Rotation of the extremity of a rotationally-restrained beam under thermal gradient

$\theta_t = \frac{\chi_t L}{2} = \theta_{beam} + \theta_{spring} = \frac{M_t L}{2\,EI} + \frac{M_t}{K_R}$	**3-10**
$M_t = \frac{\frac{\chi_t L}{2}}{\frac{1}{K_R} + \frac{L}{2\,EI}}$	**3-11**

In real cases, beams are simultaneously subjected to axial forces and bending moments induced by the non-uniform elevation of temperature. The two effects can not be considered independently because:

- Vertical deflections of the beam implies a beam shortening and a variation of the axial force;
- Excentrated compressive (or tensile) forces cause an increase (or decrease) of bending moment in the beam.

Consequently, the structural analysis of a single beam under mechanical and thermal loadings requires considering the equilibrium equation in the deformed configuration in order to account for second order effects.

It should be noted that catenary action allows resisting to vertical loads without developing high bending moments that the beam could not withstand. This type of action is usually avoided at room temperature because it necessitates large vertical deflections and the serviceability criteria are not fulfilled. However, serviceability criteria are inexistent or less severe for the design of elements under accidental load cases, like fire situation. Experimental tests and analytical developments have demonstrated that the fire resistance could be improved by accounting for the catenary action in the design of steel [Liu, 2002] and composite structures [Bailey, 2000] if specific requirements are respected (design of connections and surrounding structure, design of reinforcement bars in composite beams, etc).

A method has recently been developed to evaluate the vertical deflection and internal forces in axially and rotationally restrained steel beams (and in joints, by extension) subjected to uniform or punctual vertical loads at elevated temperatures [Yin, 2005a & 2005b]. In this method, the field of

displacements is expressed as a function of the mid-span deflection and this value is obtained after the resolution of the equilibrium equation in the mid-span section. This method is presented and discussed within this chapter and several improvements are proposed in order to get good predictions of the bending moments in joints during both the heating and cooling phases of a natural fire. This method has been implemented and validated against numerical simulations realised with SAFIR software.

3.2 Description of the Yin method [Yin, 2005a & 2005b]

3.2.1 Equilibrium equation

An isolated steel beam, axially and rotationally restrained, is submitted to symmetrical mechanical and thermal loading (Figure 3-4).

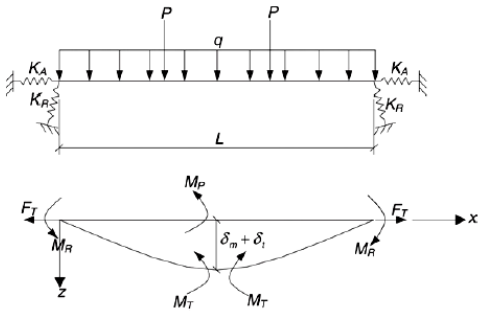

Figure 3-4 : Beam deflection and equilibrium diagrams (Wang, 2005a)

The equilibrium equation is:

$F_T\left(\delta_m + \delta_t\right) + M_T + M_R + M_P = 0$	**3-12**

- F_T is the axial load, supposed constant along the beam length ;
- δ_m is the maximum mechanical deflection due to load ;
- δ_t is the maximum thermal bowing deflection ;
- M_T is the beam's mid-span bending moment ;
- M_R is the restraint bending moment ;
- M_P is the externally applied free bending moment ;

Each term can be expressed as a function of the deflection in the mid-span section of the beam. The complete deflection profile of the beam is expressed as a function of the mid-span deflection. In case of pinned connections, the boundary conditions are:

$$z\big|_{\substack{x=0\\x=L}} = 0 \qquad z\big|_{x=\frac{L}{2}} = \delta_{m,\max} \qquad \left.\frac{d^2 z}{dx^2}\right|_{\substack{x=0\\x=L}} = 0$$

and these conditions are fulfilled for the fourth order of Eq. 3-13.

$$z_{pinned} = \frac{16\,\delta_{m,\max}}{5\,L}\left(\frac{x^4}{L^3} + \frac{2\,x^3}{L^2} + x\right) \qquad \textbf{3-13}$$

3.2.2 Axial force F_T

Assuming that the beam deflection is z(x), the beam shortening due to lateral deflection is:

$$\Delta L = \int_0^L \left[1 + \left(\frac{dz}{dx}\right)^2\right]^{1/2} dx - L \qquad \textbf{3-14}$$

The beam thermal expansion is:

$$\Delta L_t = \varepsilon_{th}\, L \qquad \textbf{3-15}$$

Thus, the axial force is determined by:

$$F_T = K_A^{'}\,\Delta L_m = K_A^{'}\left(\Delta L - \Delta L_t\right) \qquad \textbf{3-16}$$

where ΔL_m is the change of the beam length if it was not axially restrained and K'_A is the global axial restraint stiffness defined as:

$$\frac{1}{K_A^{'}} = \frac{1}{K_A} + \frac{L}{E_T\,A} + \frac{1}{K_A} \qquad \textbf{3-17}$$

3.2.3 Mid-span bending moment M_T

The bending moment in the mid-span section is:

$$M_T = E_T\,I\,\chi_m\big|_{x=\frac{L}{2}} = E_T\,I\left.\frac{d^2 z_m}{dx^2}\right|_{x=\frac{L}{2}} \qquad \textbf{3-18}$$

3.2.4 Support bending moment M_R

The bending moment at the beam extremity is:

$M_R = K_R \theta\big\|_{x=0} = K_R \left.\frac{dz_m}{dx}\right\|_{x=0}$	**3-19**

3.2.5 Inelastic interaction between axial load and bending moment

Eqs 3-16, 3-18 and 3-19 are only valid in the elastic domain. In order to extend this method to inelastic problems without applying iterative processes, an incremental approach has been proposed. In this approach, the axial force F_T is calculated with Eq. 3-16 and compared to the plastic axial force F_{pl}. If the axial force F_T is higher than F_{pl}, the axial force is reduced to F_{pl} and the resistant bending moment is equal to 0. If not, the residual bending moment $M_{interaction}$ is calculated with an interaction curve M-F. The bending moment M in a cross-section is the minimal value between, on one side, the bending moment $M_{elastic}$ calculated by Eq. 3-18 or 3-19 and, on the other side, the residual bending moment by interaction with axial forces $M_{interaction}$ (Figure 3-5).

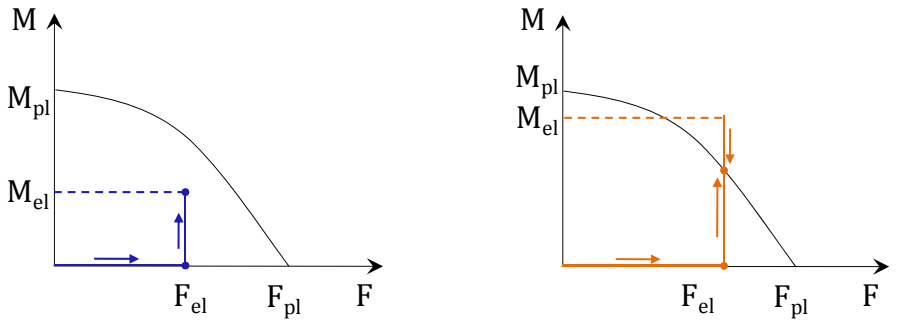

Figure 3-5 : Elastic (left) and inelastic (right) interactions between axial load and bending moment

This interaction can be expressed as an analytical formula that only depends on geometrical and mechanical properties of the beam.

3.2.6 Rotational restraints at the beam extremities

The presence of rotational restraints implies a modification of the deflection profile. In the case of fully restrained rotations, the boundary conditions are:

$$z\big|_{\substack{x=0\\x=L}} = 0 \qquad z\big|_{x=\frac{L}{2}} = \delta_{m,\max} \qquad \left.\frac{dz}{dx}\right|_{\substack{x=0\\x=L}} = 0$$

and the fourth order polynomial equation that satisfies to these condition is:

$z_{rigid} = \frac{16\,\delta_{m,\max}}{L^2}\left(\frac{x^4}{L^2} - \frac{2\,x^3}{L} + x^2\right)$	**3-20**

For flexible rotational restraints, a linear interpolation between pinned and fully rigid cases is proposed. The deflection profile of the beam is:

$z = \left(1 - c_f\right) z_{pinned} + c_f \, z_{rigid}$	**3-21**

where:

$c_f = \frac{K_R^{'} L}{EI} \leq 1$	**3-22**
$\frac{1}{K_R^{'}} = \frac{1}{K_R} + \frac{L}{E_T I} + \frac{1}{K_R}$	**3-23**

3.2.7 Non-uniform distributions of temperature

Under a non-uniform distribution of temperature, a simply-supported beam will bow under the thermal gradient, so that the total beam deflection is the sum of mechanical and thermal deflections:

$z = z_m + z_t$	**3-24**

Assuming a constant curvature

$$\chi_t = -\frac{\alpha \Delta T}{h}$$

where ΔT is the temperature difference between the top and bottom of the beam cross-section, h the height of the cross-section and α the coefficient of thermal expansion for steel. The boundary conditions for the thermal deflection profile are

$$z\big|_{\substack{x=0 \\ x=L}} = 0 \qquad z\big|_{x=\frac{L}{2}} = \delta_{t,\max} \qquad \chi_t = \frac{d^2 z}{dx^2} = -\frac{\alpha \Delta T}{h}$$

This equation can be used to fit a parabolic function (Eq. 3-25).

$z_t = -\frac{\alpha \, \Delta T}{2 \, h}\left(x^2 - L \, x\right)$	**3-25**

and the maximal thermal bowing deflection $\delta_{t,max}$ at the beam centre can be calculated as:

$\delta_{t,\max} = \frac{\alpha \, \Delta T \, L^2}{8 \, h}$	**3-26**

For a fully rigid beam under non-uniform temperature distribution, $z_t = 0$. The restrained thermal curvature will be converted into a hogging bending moment M_t at the beam ends.

$M_t = \frac{E_T I_y \alpha \Delta T}{h}$	**3-27**

in which E_T is the Young's modulus at temperature T, that of the support point.

For intermediate cases between pinned connections ($K_R = 0$) and rigid connections ($K_R = \infty$), an interpolation is made between these extreme cases (Eqs 3-28 & 3-29).

$M_T = c_s M_{T,s} + c_f M_{T,f}$	**3-28**
$M_R = c_f M_{R,f}$	**3-29**

where $M_{T,s}$, $M_{R,s}$ and $M_{T,f}$ are respectively the mid-span bending moment with pinned connections, the bending moment at the beam extremity and at mid-span with rigid connections (Eqs 3-30 to 3-32).

$M_{T,s} = E_T I_y \frac{9.6\,\delta_{m,\max}}{L^2}$	**3-30**
$M_{T,f} = E_T I_y \frac{9.6\,\delta_{m,\max}}{L^2} - E_T I_y \frac{\alpha \Delta T}{h}$	**3-31**
$M_{T,f} = E_T I_y \frac{32\,\delta_{m,\max}}{L^2} - E_T I_y \frac{\alpha \Delta T}{h}$	**3-32**

3.3 Modifications to the Yin method

3.3.1 Evaluation of the Axial Force F_T

3.3.1.1 Origin and nature of the modification

In the Yin method, the axial force F_T of the beam is evaluated elastically (Eq. 3-16) and reduced to the plastic axial force F_{pl} by an interaction criteria (Figure 3-5). The elasto-plastic domain between the proportional limit $f_{p,\theta}$ and the effective yield strength $f_{y,\theta}$ in the stress-strain diagram of carbon steel at elevated temperatures (Figure 3-6) is neglected in this procedure. At room temperature, these parameters are equivalent but the ratio $f_{p,\theta}/f_{y,\theta}$ becomes equal to 0.42 at 400°C so that neglecting plastic strains is, at elevated temperatures, a substancial assumption.

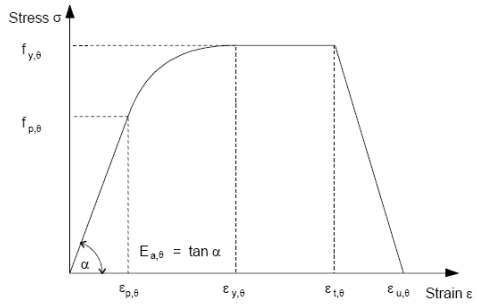

Figure 3-6 : Stress-strain diagram of carbon steel at high temperatures [CEN, 2004a]

Consequently, the axial forces are over-estimated if the mechanical strain $\varepsilon_{m,beam}$ of the beam under axial forces satisfies to Eq. 3-33.

$\varepsilon_{m,beam} = \frac{\Delta L_{m,beam}}{L} \in \left[\varepsilon_{p,\theta} ; \varepsilon_{y,\theta} \right]$	**3-33**

To Yin, the over-estimation of axial forces is on the safe side. However, it should be considered that this assumption also causes an under-estimation of the vertical deflections. Indeed, this approach is not always safe because the beam and the joints may be subjected to higher tensile forces than predicted during both the heating and cooling phases of a natural fire. The risk of failure in the joint zone, especially brittle failures of bolts and welds, is still amplified in presence of tensile forces.

The main difficulty for considering the elasto-plastic branch of the material law defined in the EN 1993-1-2 is the fact that the secant extensional stiffness $(EA)_{beam}$ varies with the mechanical strain ε_m and that this induces an iterative process (Eq. 3-35).

$\Delta L_m = \Delta L_{m,beam} + \Delta L_{m,spring} = \frac{F_T L}{(EA)_{beam}} + \frac{2F_T}{K_A}$	**3-34**
$\varepsilon_{m,beam} = \frac{F_T}{(EA)_{beam}} = \frac{\Delta L_m}{L + \frac{2(EA)_{beam}}{K_A}}$	**3-35**

The modification is aimed at integrating a more accurate method to evaluate the axial force F_T that is induced in the beam by a variation of length ΔL_m.

3.3.1.2 Description of the modification

The accurate evaluation of the $\varepsilon_{m,beam}$ and $(EA)_{beam}$ necessitates an iterative process. This is avoided by evaluating F_{propor}, $\Delta L_{m,propor}$, F_{pl} and $\Delta L_{m,pl}$ analytically and using interpolations between these points of the (F_T ; ΔL_m) diagram. The analytical expressions of $\Delta L_{m,propor}$ and $\Delta L_{m,pl}$ (Eqs 3-36 & 3-37) are

obtained under the assumption that the stiffness of the surronding frame K_A remains constant and that the yield strain $\varepsilon_{y,\theta}$ of carbon steel is 0.02 (according to the EN 1993-1-2 recommendations).

$\Delta L_{m,propor} = A f_y k_{p,\theta} \left(\frac{L}{EA} + \frac{2}{K_A} \right)$	**3-36**
$\Delta L_{m,pl} = 0.02 L + \frac{2 A f_y k_{y,\theta}}{K_A}$	**3-37**

An elliptic interpolation between (F_{propor} ; $\Delta L_{m,propor}$) and (F_{pl} ; $\Delta L_{m,pl}$) is more adapted than a linear interpolation because no sudden variation of the slope is induced in the (F_T ; ΔL_m) diagram when F_T reaches F_{propor} (Eq. 3-42). This type of interpolation improves the convergence of the routine. In the branch of ellipsa, the axial force is calculated as follows:

$K_A^{'} = \left(\left(L/EA \right) + 2/K_A \right)^{-1}$	**3-38**
$c = \frac{\left(F_{pl} - F_{propor} \right)^2}{\left(\Delta L_{m,pl} - \Delta L_{m,propor} \right) K_A^{'} - 2\left(F_{pl} - F_{propor} \right)}$	**3-39**
$b^2 = c\left(\Delta L_{m,pl} - \Delta L_{m,propor} \right) K_A^{'} + c^2$	**3-40**
$a^2 = \left(\Delta L_{m,pl} - \Delta L_{m,propor} \right)\left(\Delta L_{m,pl} - \Delta L_{m,propor} + c/K_A^{'} \right)$	**3-41**
$F_T = F_{propor} - c + \left(b/a \right)\left[a^2 - \left(\Delta L_{m,pl} - \Delta L_m \right)^2 \right]^{(1/2)}$	**3-42**

However, for few cases, the denominator of c is negative and the term of the square root in Eq. 3-42 is negative for some values of ΔL_m. It is advised to adopt linear interpolations between (F_{propor} ; $\Delta L_{m,propor}$) and (F_{pl} ; $\Delta L_{m,pl}$) when c is negative.

3.3.2 Evaluation of the Bending Moments M_R and M_T

3.3.2.1 Origin of the modification

Up to now, the support bending moment M_R and mid-span bending moment M_T are calculated by assuming an elastic behaviour (Eqs 3-18 and 3-19) and then, are limited by the interaction criteria between axial force and bending moment (Figure 3-5). Again, the effect of the elliptic branch of the stress-strain diagram of carbon steel at high temperatures is not taken into account. A procedure is described in § 3.3.2.2 to evaluate the diagram (M ; χ) of an I-shape beam subjected to an axial force F_T and a non-uniform distribution of temperature. The bending moment at the beam extremity M_R is also limited to the resisting bending moment of the joint $M_{Rd,joint}$.

3.3.2.2 Description of the modification

3.3.2.2.1 $F_T = 0$, $T = 20°C$

Evaluation of the elastic bending moment M_{el}

At room temperature, the proportionality limit f_p and the effective yield strength f_y of carbon steel are identical. Consequently, the moment-curvature diagram of a section is linear until the effective yield strength is reached in the extreme fibres. The elastic moment M_{el} is the elastic modulus W_{el} multiplied by the effective yield strength of steel f_y (Eq. 3-43). The elastic curvature χ_{el} is the ratio between the elastic moment M_{el} and the beam rotational stiffness EI (Eq. 3-44).

$M_{el} = W_{el} \cdot f_y$	**3-43**
$\chi_{el} = M_{el} / EI$	**3-44**

Evaluation of the plastic bending moment M_{pl}

The plastic moment M_{pl} is the plastic modulus W_{pl} multiplied by the effective yield strength of steel f_y (Eq. 3-45). Theoretically, the plastic moment M_{pl} can only be mobilised if the curvature χ is infinite (Figure 3-7). However, it is observed that the slope of the curvature-moment diagram is almost horizontal when $\chi_{pl} = 0.02$ rad/m at room temperature (Eq. 3-46 and Figure 3-8).

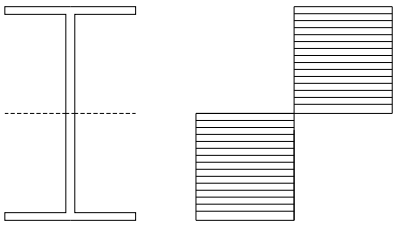

Figure 3-7 : Distribution of stresses in an I-profile under pure bending

$M_{pl} = W_{pl} \cdot f_y$	**3-45**
$\chi_{pl} = 0.02 \qquad [rad/m]$	**3-46**

Global Moment – Curvature diagram

Under pure bending, the ultimate curvature χ_u is characterised by strains equal to $\varepsilon_t = 0.15$ (end of the yield plateau in the stress-strain diagram) at the top and bottom extremities (Eq. 3-47).

$\chi_u = \dfrac{\varepsilon_t}{h/2}$	**3-47**

Between χ_{el} and χ_{pl}, the curvature-moment diagram is represented by the branch of an ellipse respecting the following conditions (Eqs 3-48 to 3-50):

$M\left(\chi=\chi_{el}\right)=M_{el}$	**3-48**
$\frac{dM}{d\chi}\left(\chi=\chi_{el}\right)=EI$	**3-49**
$M\left(\chi=\chi_{pl}\right)=M_{pl}$	**3-50**

For any curvature χ comprised between χ_{el} and χ_{pl}, the bending moment M is given by Eq. 3-51.

$M\left(\chi\right)=M_{el}-c+\left(b/a\right)\left[a^2-\left(M_{pl}-M\right)^2\right]^{0.5}$	**3-51**
$c=\frac{\left(M_{pl}-M_{el}\right)^2}{\left(\chi_{pl}-\chi_{el}\right)EI-2\left(M_{pl}-M_{el}\right)}$	**3-52**
$b^2=c\left(\chi_{pl}-\chi_{el}\right)EI+c^2$	**3-53**
$a^2=\left(\chi_{pl}-\chi_{el}\right)\left(\chi_{pl}-\chi_{el}+c/EI\right)$	**3-54**

This analytical method correlates very well with the numerical results (Figure 3-8). The complete yield plateau is not represented in order to get a good view of the elastic and elasto-plastic domains.

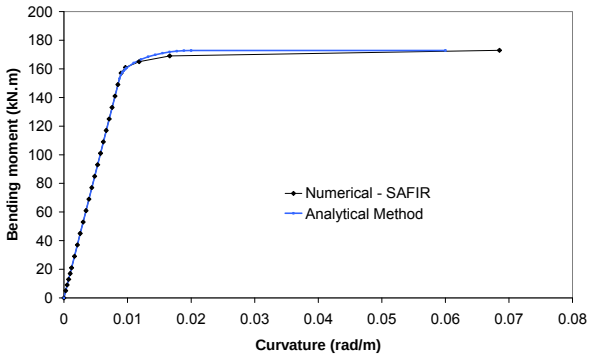

Figure 3-8 : Numerical and analytical curvature -moment diagrams of a IPE 300 section (F_T=0 and T=20°C)

3.3.2.2.2 F_T constant, T = 20°C

Evaluation of the elastic bending moment M_{el}

Under axial forces, the gravity centre of an IPE section is not the horizontal axis of symmetry. Plastic deformations are produced as soon as one of the flanges reaches the proportional limit.

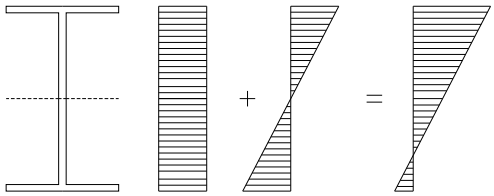

Figure 3-9 : Distribution of stresses in an I-profile under bending and axial forces

Thus, the elastic moment is obtained as follows:

$\sigma = \sigma_F + \sigma_M = \frac{F_T}{A} + \frac{M\,h}{2\,I} = f_y$	**3-55**
$M_{el} = \frac{2\left(f_y - \sigma_F\right) I}{h}$	**3-56**

Evaluation of the plastic bending moment M_{pl}

Under low axial forces, the plastic neutral axis remains in the beam web (Figure 3-10a). For higher loads, the plastic neutral axis is in a flange (Figure 3-10b). The axial forces are equilibrated by the stresses in the white zone and the plastic bending moment, taking the M-F interaction into account, is mobilised by the stresses in the hatched zone.

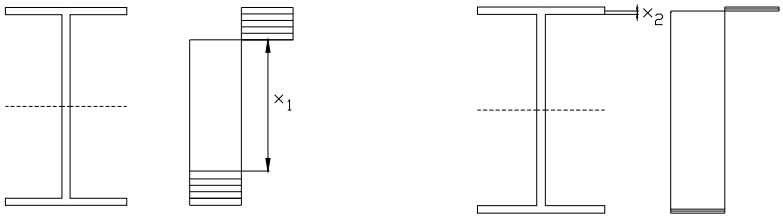

Figure 3-10 : Distribution of stresses in an IPE section submitted to axial forces and bending moment

The plastic neutral axis is situated in the web if Eq. 3-57 is satisfied and the plastic bending moment is $M_{pl,1}$ (Eq. 3-59), where b, h, t_f and t_w are respectively the flange width, the total height, the flange thickness and web thickness of the beam profile. The length l_{rc} is a fictive length expressed as the ratio between the area of the root radius and the web thickness (Eq. 3-58). When the plastic neutral axis is situated in a flange, the plastic bending moment M_{pl} is given by Eqs 3-60 and 3-61.

$x_1 = \frac{F_T}{f_y\,t_w} \leq\ h - 2\,t_f + 2\,l_{rc}$	**3-57**
$l_{rc} = \left(2 - \frac{\pi}{2}\right)\frac{r_c^2}{t_w}$	**3-58**

$M_{pl,1} = f_y \left(b t_f \left(h - t_f \right) + t_w \left(\frac{h}{2} - t_f - \frac{x_1}{2} \right) \left(\frac{h - 2t_f - x_1}{2} \right) + l_{rc} t_w \left(h - 2t_f - \frac{2r_c}{3} \right) \right)$	**3-59**
$x_2 = \frac{F_T - \left(A - 2bt_f \right) f_y}{2b f_y}$	**3-60**
$M_{pl,2} = f_y b \left(t_f - x_2 \right) \left(h - \left(t_f - x_2 \right) \right)$	**3-61**

Global Moment – Curvature diagram

Figure 3-11 shows the comparison between the curvature-moment diagrams obtained analytically and numerically in case of a IPE 300 steel section under F_T = 250 kN (plastic neutral axis in the web) and F_T = 700 kN (plastic neutral axis in a flange).

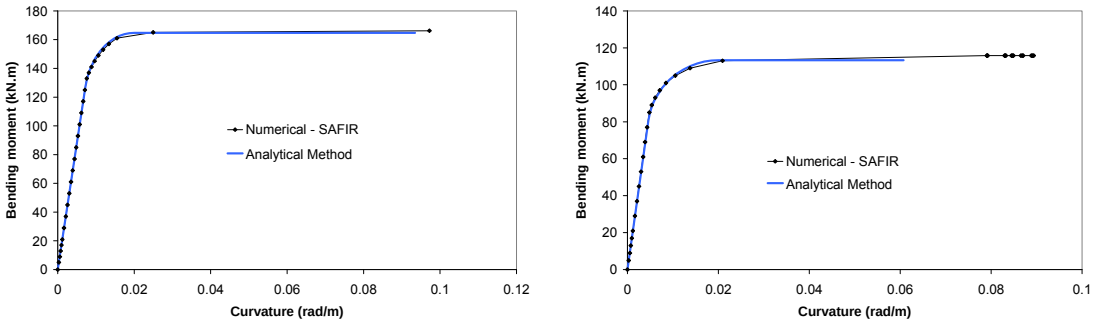

Figure 3-11 : Curvature -moment diagrams of a IPE 300 section at 20°C: (a) F_T=250 kN – (b) F_T=700 kN

3.3.2.2.3 $F_T = 0$, T uniform

Evaluation of the proportional bending moment M_{propor}

At elevated temperatures, the proportional and effective yield strengths of steel are different. Thus, the elastic curvature χ_{el} and the elastic moment M_{el} defining the end of the linear part of the curvature-moment diagram are substituted by the proportional curvature χ_{propor} and the proportional moment M_{propor}. The slope of this linear range EI is reduced by the reduction factor k_E defined in the EN 1993-1-8.

Evaluation of the plastic bending moment M_{pl}

Higher temperatures induce larger deformations and higher values of the plastic curvature χ_{pl}. In order to get a good agreement with the numerical results, the following values of χ_{pl} have been used:

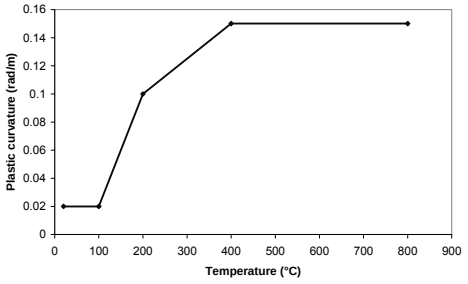

T (°C)	χ_{pl} (rad/m)
20	0.02
100	0.02
200	0.1
400	0.15
800	0.15

Figure 3-12 : Plastic curvature of a steel beam at elevated temperatures

Global Moment – Curvature diagram

The plastic bending moment M_{pl} is obtained by multiplication between the plastic bending moment at room temperature $M_{pl,20°C}$ and the reduction factor for effective yield strength k_y. Figure 3-13 shows the comparison between the curvature-moment diagrams obtained analytically and numerically for of an IPE 300 steel section under pure bending at different temperatures (200°C, 400°C, 600°C and 800°C).

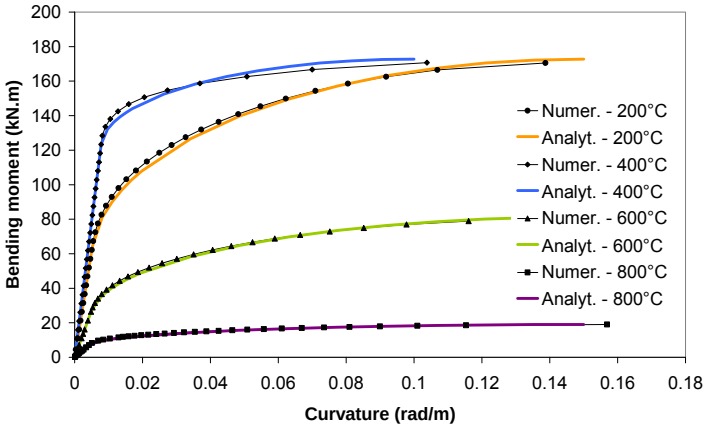

Figure 3-13 : Curvature-moment diagrams of an IPE 300 section (No axial forces)

3.3.2.2.4 F_T constant, T uniform

The developments of the § 3.3.2.2.2 and § 3.3.2.2.3 have been coupled to predict the curvature-moment diagrams of steel beams simultaneously subjected to an axial force and a uniform elevation of temperature. However, an adaptation of the plastic curvature χ_{pl} is necessary. Due to the fact that the proportional limit of carbon steel is different from the effective yield strength at elevated temperature, the axial load may cause higher stresses than the proportionality limit and large strains ε_F. Thus, the plastic strains are reached earlier and the plastic moment with smaller curvatures. An interaction coefficient k_χ is defined to take the M-F interaction into account for the evaluation of the plastic curvature χ_{pl} under a uniform elevation of temperature (Eq. 3-62 and 3-63).

$k_\chi = \left(1 - \sqrt{\frac{\varepsilon_F}{\varepsilon_y}}\right)^2$	**3-62**
$\chi_{pl,F_T \neq 0} = k_\chi \ \chi_{pl,F_T=0}$	**3-63**

At room temperature, the factor k_χ implies a negligible reduction of the plastic curvature because deformations due to the axial forces ε_N are very small with respect to the plastic strain ε_y. Figure 3-14 shows comparisons between the curvature-moment diagrams obtained analytically and numerically for an IPE 300 steel section for various combinations of axial forces and temperatures.

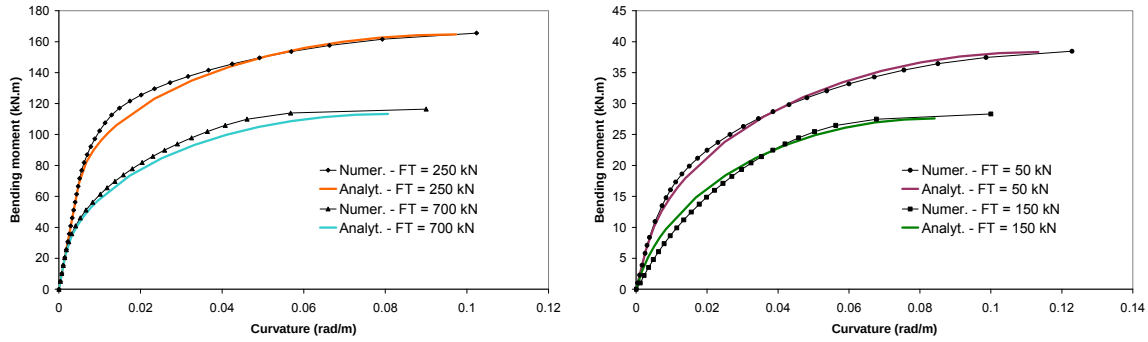

Figure 3-14 : Curvature -moment diagrams of an IPE 300 section: a) T = 300°C – b) T = 700°C

3.3.2.2.5 $F_T = 0$, T not uniform

In real steel beams, top flanges are partially or totally shielded by a concrete slab and the temperature is not uniform on the section. Non-uniform distributions of temperature necessitate some adaptations.

Evaluation of the proportional bending moment M_{propor}

Under a uniform distribution of temperature and without axial forces, the centre of gravity of the beam section is situated on the horizontal axis of symmetry of the beam. When the distribution of temperature is not symmetric, the position of the centre of the gravity $z_{C.G.}$ and the elastic rotational stiffness EI under a uniform distribution of temperature can be calculated as follows (Eqs 3-64 and 3-65), where $k_{E,1}$, $k_{E,2}$ and $k_{E,3}$ are respectively the reduction factors for the slope of the linear elastic range k_E of the top flange, the web and the bottom flange.

$z_{C.G.} = \frac{b t_f \left(\frac{h}{2} - \frac{t_f}{2}\right)\left(k_{E,1} - k_{E,3}\right)}{b t_f \left(k_{E,1} + k_{E,3}\right) - \left(A - 2 b t_f\right) k_{E,2}}$	**3-64**

$$EI = E\left(b t_f \left(k_{E,1}\left(\frac{h}{2} - \frac{t_f}{2} - z_{C.G.}^2 \right) + k_{E,3}\left(\frac{h}{2} - \frac{t_f}{2} + z_{C.G.}^2 \right) \right) + k_{E,2}\left(A - 2 b t_f \right) z_{C.G.}^2 \right) + E\left(\left(k_{E,1} + k_{E,3} \right) \frac{b t_f^3}{12} + k_{E,2} \frac{t_w}{12} \left(h - t_f \right)^3 \right)$$	**3-65**

As the temperature is not uniform, the proportionality limit can be reached in the flanges or the web because the cold parts are stiffer and submitted to higher stresses. The proportional bending moment M_{propor} under a non-uniform distribution of temperature can be calculated as follows:

$$\varepsilon_{propor,i} = \frac{k_{p,i} f_y}{k_{E,i} E}$$	**3-66**
$$M_{propor} = \min_{i=1}^{3} \left(\frac{k_{p,i} f_y \left(EI \right)}{\left(z_i - z_{C.G.} \right) k_{E,i} E} \right)$$	**3-67**

where z_i is the distance between the C.G. of the flange or web and the C.G. of the section.

The difference between thermal strains in the top flange $\varepsilon_{t,top}$ and the bottom flange $\varepsilon_{t,bottom}$ causes a thermal curvature χ_t in asymmetrically heated sections (Eq. 3-69) and the proportional curvature χ_{propor} is given by Eq. 3-69.

$$\chi_t = \frac{\varepsilon_{t,top} - \varepsilon_{t,bottom}}{h}$$	**3-68**
$$\chi_{propor} = \chi_t + \frac{M_{propor}}{EI}$$	**3-69**

Evaluation of the plastic bending moment M_{pl}

The plastic neutral axis can be situated either in the beam web or in the colder flange (Figure 3-15).

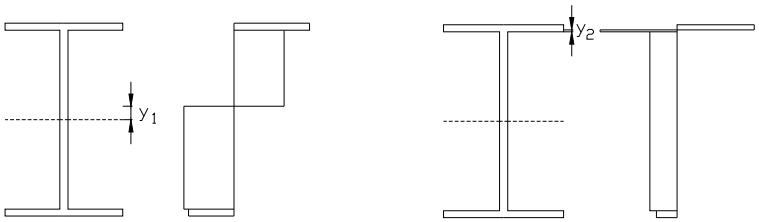

Figure 3-15 : Position of the plastic neutral axis in non-uniformly heated sections

Under non-uniform distributions of temperature and pure bending, the plastic curvature $\chi_{pl,FT=0}$ is calculated with Figure 3-12, considering an average temperature T_m of the two flanges. The thermal curvature is added to that value (Eq. 3-70).

$\chi_{pl,FT=0,T_1 \neq T_3} = \chi_t + \chi_{pl,FT=0,T=(T_1+T_3)/2}$	**3-70**

The plastic bending moment M_{pl} without under a uniform distribution of temperature any axial force can be calculated easily for the two configurations plotted on Figure 3-15 (Eqs 3-71 and 3-72).

$M_{pl,1} = f_y \left(b t_f \left(k_{y,1} \left(\frac{h}{2} - \frac{t_f}{2} - y_1 \right) + k_{y,3} \left(\frac{h}{2} - \frac{t_f}{2} + y_1 \right) \right) + \frac{t_w k_{y,2}}{2} \left(\frac{h}{2} - \frac{t_f}{2} - y_1 \right)^2 \right)$ $+ f_y \left(\frac{t_w k_{y,2}}{2} \left(\frac{h}{2} - \frac{t_f}{2} + y_1 \right)^2 + l_{rc} k_{y,2} \left(h - 2t_f - \frac{2r_c}{3} \right) \right)$	**3-71**
$M_{pl,2} = f_y \left(b \frac{y_2^2}{2} k_{y,1} + b t_f k_{y,3} \left(\frac{h}{2} - \frac{t_f}{2} - y_2 \right) + \left(A - 2 b t_f \right) k_{y,2} \left(\frac{h}{2} - y_2 \right) \right)$ $+ f_y b \frac{\left(t_f - y_2 \right)^2}{2} k_{y,1}$	**3-72**

Global Moment – Curvature diagram

In the present work, several thermal distributions have been considered (Table 3-1). These distributions result from a thermal analysis performed on an IPE 300 profile heated on three faces by a parametrical curve of the EN 1993-1-2 - Annex A and covered by a flat concrete slab. T_1, T_2 and T_3 are representative of the same analysis after 10, 20 and 30 minutes. No cooling phase has been considered.

	Top flange	Web	Bott. Flange
T_1 (°C)	244.5	552.1	487.3
T_2 (°C)	358.9	570	571.9
T_3 (°C)	429.6	679.8	669.7

Table 3-1 : Distribution of temperature in the three chosen scenarios

Figure 3-16 shows a comparison between the curvature-moment diagrams obtained analytically and numerically in case of an IPE 300 steel section with no axial force and different distributions of temperature. The plastic neutral axis is situated in one flange for $T = T_3$. In that case, the elliptic branch is more conservative than for the two other distributions of temperature.

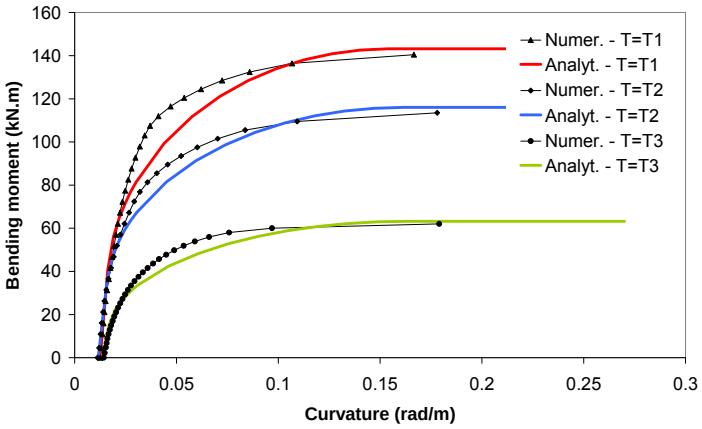

Figure 3-16 : Curvature -moment diagrams of a IPE 300 section (F_T= 0)

3.3.2.2.6 M = 0, T not uniform, $F_T = F_{T,1}$

The position of the centre of gravity $z_{C.G.}$, the elastic rotational stiffness EI and the position of the plastic neutral axis y_P are independent of the level of axial forces but parasitic moments develop due to the fact that the centre of gravity and the plastic neutral axis are not the horizontal axis of symmetry. As a consequence of this, the axial force F_{pl} leading to a complete plasticization of a steel section under a non-uniform distribution of temperature is not the sum of the plastic resistances of each part. In reality, F_{pl} is the axial force for which the parasitic moment created by the lever arm between the neutral plastic axis and the horizontal axis of symmetry is equal to the residual plastic moment under $F_T = F_{pl}$. The methodology for the evaluation of the residual plastic moment $M_{pl,FT}$ in a steel section submitted to axial forces and a non-uniform distribution of temperature is given in § 3.3.2.2.7.

3.3.2.2.7 F_T constant, T not uniform

Evaluation of the proportional bending moment M_{propor}

The effect of the stresses $\sigma_{F,i}$ produced by the applied axial force F_T (Eq. 3-73) on the proportional bending moment M_{propor} is taken into consideration by deducting the ratio $\sigma_{F,i}/f_y$ of the reduction factors for proportional limit $k_{p,i}$ (Eq. 3-75). It must be underlined that the stresses $\sigma_{F,i}$ are different in the three parts of the beam because the values of $k_{E,i}$, $f_{p,i}$ and $f_{y,i}$ in these parts are different. The position of the centre of gravity $z_{C.G.}$ also has an influence on the proportional bending moment because a lever arm is created between the applied force and the internal distribution of forces and a parasitical bending moment $M_{t,propor}$ is applied to the section (Eq. 3-74). The proportional bending moment M_{propor} is increased or decreased by this parasitical bending moment $M_{t,propor}$, depending on the sign of the applied bending moment. Finally, if proportional bending moment M_{propor} is negative, it

means that the applied axial forces cause plastic deformations in at least one part of the beam. In that case, M_{propor} is reduced to 0.

$\sigma_{N,i} = \frac{F_T \, k_{E,i}}{\sum_i k_{E,i} \, A_i}$	**3-73**
$M_{t,propor} = \left\| F_T \, z_{C.G.} \right\|$	**3-74**
$M_{propor} = \frac{f_y (EI)}{E_{20°C}} \min_i \left(\frac{k_{p,i} - \sigma_{N,i} / f_y}{y_i \, k_{E,i}} \right) \pm M_{t,propor} \geq 0$	**3-75**
$\chi_0 = \chi_{th} \pm \frac{M_{t,propor}}{EI}$	**3-76**
$\chi_{propor} = \chi_0 + \frac{M_{propor}}{EI}$	**3-77**

where A_i, EI, $E_{20°C}$, χ_0, χ_{propor} are respectively the cross-section area of the zone i, the the rotational stiffness of the beam (Eq. 3-65), the Young's modulus at room temperature, the beam curvature under the axial force F_T and the beam curvature under the combination of the axial force F_T and M_{propor}.

If plastic deformations exist in at least one part of the section (web and/or flange), Eq. 3-73 is not valid anymore. However, this will have a minor influence on the proportional bending moment because M_{propor} will be very low or 0. Moreover, the ratio between $k_{p,\theta}$ and $k_{E,\theta}$ is almost constant at elevated temperatures ($k_{p,\theta}/k_{E,\theta}$ is comprised between 55% and 60% for temperatures going from 400°C to 1200°C). As the stiffer parts are also the parts that have higher proportional limits, this implies that the proportionality limit will approximately be reached in all the parts at the same axial load F_T. This last statement is not true if the steel grade is not uniform on the section.

Evaluation of the plastic bending moment M_{pl}

The plastic bending moment M_{pl} of an I-profile subjected to an axial force F_T and an asymmetric distribution of temperature is calculated after evaluation of the position of the plastic neutral axis and equilibrium between the applied axial force and the resistant axial force. Parasitical bending moments $M_{t,pl}$ are created by the existence of a lever arm y_P between the center of the section and the position of the plastic neutral axis (Eq. 3-78). This parasitic moment is favourable or not, depending on the sign of the applied bending moment, of the axial force F_T and of the thermal gradient χ_t.

$M_{t,pl} = \left\| F_T \, y_P \right\|$	**3-78**

Under a uniform elevation of temperature, the plastic curvature χ_{pl} accounting for the effect of axial forces is given by Eq. 3-63. Under non-uniform distributions of temperature, the strains ε_F produced

by an axial force F_T vary linearly on the profile height and the stress-strain diagrams are different in the three zones. As a simplified approach, the term ε_F is calculated as the strain created by the average stress σ_F (Eq. 3-79) in the stress-strain diagram of carbon steel at the average temperature T_m (Eq. 3-80). The stress-strain diagram of carbon steel is linear-elliptic (EN 1993-1-2).

$\sigma_F = F_T / A$	**3-79**
$T_m = \dfrac{(T_1 + T_3) b t_f + T_2 (A - 2 b t_f)}{A}$	**3-80**

The analytical expressions of M_{pl} and $M_{t,pl}$ are given in Appendix A for six possible configurations.

Application to sections under pure axial force

The evaluation of the plastic axial force F_{pl} of a steel section under a non-uniform distribution of temperature consists in the calculation of the axial force F_T inducing a parasitical plastic moment $M_{t,pl}$ equilibrated by the residual bending moment of the section M_{pl} (see § 3.3.2.2.6). Under the distribution of temperature T_2 (see Table 3-1), a slight difference is observed between the plastic axial forces calculated analytically and numerically (Table 3-2). This difference is due to low vertical displacements of the beam in the numerical simulation that reduces the effect of parasitical moments by second order effects. In absence of parasitical moments, the axial resistance would have been equal to 1023.4 kN. Under thermal distribution T_3, the analytical method gives a very good prediction of the plastic axial force F_T. In that case, the plastic neutral axis is situated in a flange and the modification of the lever arm of the applied axial forces by beam deflections is negligible. Here, the sum of the resistances of the flanges and the web considered separately is equal to 712.5 kN and this shows that the reduction of the plastic axial force due to thermal gradient is 37%.

kN	$T = T_2$	$T = T_3$
$F_{pl,Analyt.}$	833.2	446.3
$F_{pl,SAFIR}$	849.1	447.5

Table 3-2 : Comparison between plastic axial forces under non-uniform distributions of temperature predicted analytically and numerically

Application to sections under axial force and bending moment

Figures 3-17 and 3-18 show that the correlations between the results obtained analytically and those given by the finite element program SAFIR are very good. It can be noted that the effect of compressive forces on the reduction of the plastic bending moment is much more severe for sagging. For distribution of temperature T_3, the plastic hogging moment is even higher under F_T = 200 kN than under F_T = 80 kN (Figure 3-18). The reasons to this have already been mentioned previously.

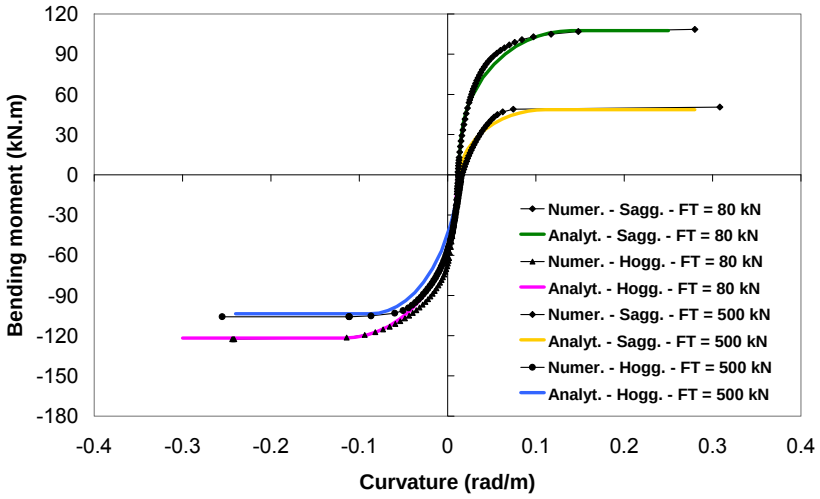

Figure 3-17 : Curvature-moment diagrams of a IPE 300 section under $T=T_2$

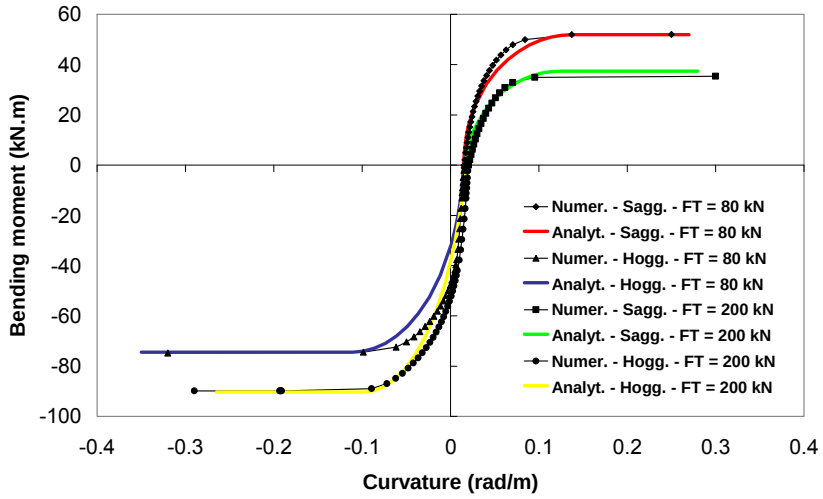

Figure 3-18 : Curvature-moment diagrams of a IPE 300 section under $T=T_3$

In most of the cases analysed here, the proportional bending moment M_{propor} is lower than the half of the plastic bending moment M_{pl}. The approximation of the resisting bending moment under a given curvature χ is largely overestimated with the elastic-plastic method used by Yin. Figure 3-19 shows a comparison between the results given by the elastic-plastic method and those given by the non-linear methods ($T = T_3$, $F_T = 200$ kN, Sagging moment).

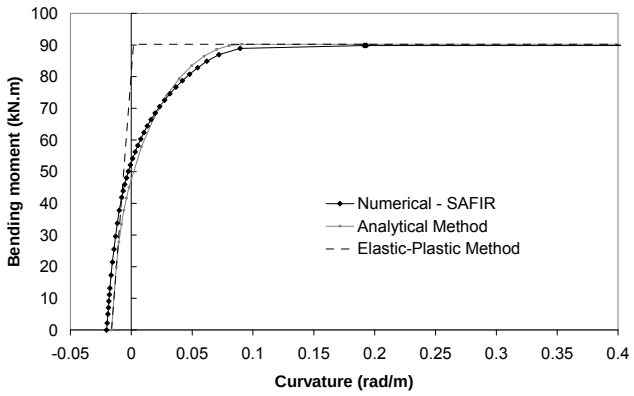

Figure 3-19 : Comparison between the elastic-plastic method and the non-linear methods

3.3.2.3 General Procedure to obtain the bending moment M in a I-section under axial force F_T, non-uniform distribution of temperature (T_1,T_2,T_3) and curvature χ

1) a) Storage of the geometrical and mechanical properties of the steel beam.

b) Evaluation of the fictive length l_{rc} (see Eq. 3-58).

2) a) Storage of the temperatures of the flanges and the web.

b) Calculation of the average temperature between the two flanges T_m.

c) Calculation of the reduction factors k_y, k_p and k_E (EN 1993-1-2) for T_1, T_2, T_3 and T_m.

d) Calculation of the plastic curvature without considering the effect of axial forces $\chi_{pl,FT=0}$ under $T = T_m$ (Figure 3-12).

e) Calculation of the thermal elongations $\varepsilon_{t,top}$, $\varepsilon_{t,bottom}$ and curvature χ_t (EN 1993-1-2 and Eq. 3-68).

3) a) Calculation of the centre of gravity $z_{C.G.}$ and rotational stiffness EI (Eqs 3-64 and 3-65).

b) Calculation of parasitical moment $M_{t,propor}$ and the initial curvature χ_0 (Eqs 3-74 and 3-76).

c) Calculation of the proportional moment M_{propor} and proportional curvature χ_{propor} (Eqs 3-75 and 3-77).

4) a) Calculation of the strain ε_F (Eqs 3-79, 3-80 and EN 1993-1-2)

b) Calculation of the plastic curvature without axial forces χ_{pl} (Figure 3-12).

c) Calculation of the plastic curvature χ_{pl} accounting for axial forces (Eqs 3-62 and 3-63).

d) Calculation of the parasitical bending moment $M_{t,pl}$ (Eq. 3-78).

e) Calculation of the plastic bending moment M_{pl} (Appendix A)

5) a) Calculation of the parameters a, b and c of the ellipse equation (Eq. 3-52 to 3-54)

b) Calculation of the moment M under the given curvature χ (Eq. 3-51).

3.3.3 Evaluation of thermal deflections d_t and thermally-induced moments M_t

3.3.3.1 Origin of the modifications

The thermal deflections δ_t due to a non-uniform distribution of temperature are given by Eq. 3-8 for pinned connections and are equal to zero for rigid connections. In the latter case, thermally-induced bending moments M_t develop at the beam extremities (Eq. 3-9). Between these two configurations, it is recommended by Yin to interpolate with the coefficient c_f (Eqs. 3-21 and 3-29). Another expression of the thermally-induced moments that does not require any interpolation is given here and a method is proposed to extend it to cases where the bending moment at the beam extremity is limited by the resisting moment of the joint.

3.3.3.2 Description of the modifications

Expression of the thermally-induced bending moment M_t

In rotationally-restrained beams, the rotation of the beam extremity that would have appeared without any restraints is counteracted by the rotation of the rotational spring and the curvature of the beam under the thermally-induced bending moment M_t.

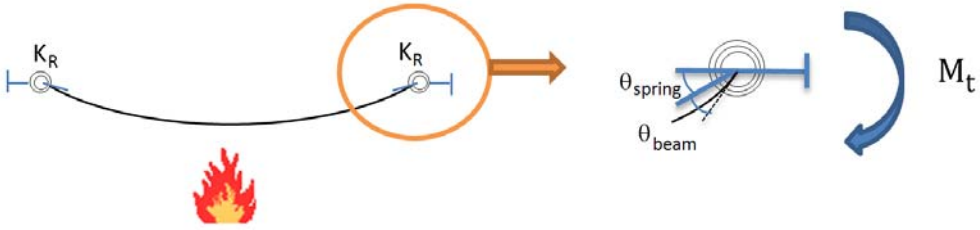

Figure 3-20 : Rotation of the extremity of a rotationally-restrained beam under thermal gradient

The equilibrium between the thermally-induced rotation and the rotation caused by restraints is stated by Eq. 3-81, allowing the evaluation of the thermally-induced moment M_t (Eq. 3-82).

$\theta_t = \frac{\chi_t L}{2} = \theta_{beam} + \theta_{spring} = \frac{M_t L}{2EI} + \frac{M_t}{K_R}$	**3-81**

$$M_t = \frac{\frac{\chi_t L}{2}}{\frac{L}{2EI} + \frac{1}{K_R}}$$	**3-82**

Extension to cases with a limited resisting moment of the joint $M_{Rd,joint}$

In the algorithm developed by the author on the basis of Yin Method and including the modifications mentioned described in this work, the bending moment M_R at the beam extremity is limited by the resisting moment of the joint. When the bending moment M_R, calculated as a function of the curvature (see § 3.3.2), is higher than the joint resistance $M_{Rd,joint}$, M_R is reduced to $M_{Rd,joint}$. Consequently, the curvature at the beam extremity is overestimated in the beam and underestimated in the rotational spring. The real mechanical curvature of the beam is calculated from the (M ; χ) relationship and the secant rotational stiffness EI of the beam near the joint is the ratio between the bending moment and the real curvature.

The expression of the thermally-induced bending moment M_t is given in Eq. 3-82. The increase of the bending moment at the beam extremity and the decrease of the bending moment at the beam mid-span imply a variation of stiffness in both section and a redistribution of internal forces. In order to account for this, Eq. 3-82 has been substituted in the algorithm by Eq. 3-83. The correction factor 0.8 has been calibrated on numerical simulations presented in § 3.5. Additional investigations would be necessary to evaluate accurately this correction coefficient but 0.8 give satisfactory results for the numerous combinations tested within this work.

$$M_t = \frac{0.8\,\frac{\chi_t L}{2}}{\frac{L}{2EI} + \frac{1}{K_R}}$$	**3-83**

Thus, the thermally-induced bending moment M_t is added to the bending moment at the beam extremity obtained from the extremity curvature $\chi_{m,x=0}$ and limited to the plastic bending moments of the beam and the joint (Eq. 3-84). The thermal deflection δ_t is given by Eq. 3-85.

$$M_{R,restr} = \min\left(M_R + M_t \,;\, M_{pl,joint} \,;\, M_{pl,beam}\right)$$	**3-84**
$$\delta_t = \frac{\chi_t L^2}{8} - \frac{\left(M_{R,restr} - M_R\right)L^2}{8\left(EI\right)}$$	**3-85**

3.3.4 Extensional stiffness of the beam

3.3.4.1 Origin of the modifications

The extensional stiffness K_A of a beam is equal to EA/L when the Young's modulus E and cross-section area A are constant along the beam span L. When a beam undergoes large deflections, this formula is not valid anymore because of second-order effects. The beam deflections are increased by the bending moments and the horizontal distance between the beam extremities is reduced. This means that the axial stiffness of the beam is reduced.

3.3.4.2 Description of the modifications

A more accurate expression of the axial stiffness has been calculated in case of simply-supported beams and fully fixed beams deflection profiles. In both cases, the axial stiffness has been evaluated as the ratio between the unitary horizontal loads applied at the beam extremities and the variation of the distance between these extremities (Figure 3-21). It has been considered that the length reduction is very low in comparison with the beam length ($\delta << L$).

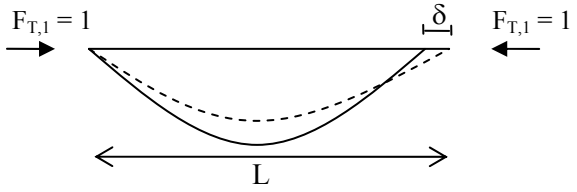

Figure 3-21 : Influence of second order effects on a beam axial stiffness

The complete developments of the calculation of axial stiffness taking second-order effects into account are described in Appendix B. The variation of the distance between the beam extremities is obtained by use of the virtual work principle for a deformable body (Bernoulli) applied to beams with no consideration of the shear forces contribution. Under a unitary force $F_{T,1} = 1$, the virtual work is the reduction of horizontal distance between the beam extremities d (Eq. 3-86). The axial stiffness $K_{A,beam}$ of the beam is the ratio between the applied force F_T and the beam shortening d (Eq. 3-87).

$$d = \int_0^L \frac{M.M_1}{EI} dx + \int_0^L \frac{F_T.F_{T,1}}{EA} dx$$	**3-86**
$$K_{A,beam} = \frac{F}{d} = \frac{1}{\left(\int_0^L \frac{M.M_1}{EI} dx + \int_0^L \frac{F_T.F_{T,1}}{EA} dx \right)}$$	**3-87**

The beam shortening under a unitary force has been evaluated in case of simply-supported beams (Eq. 3-88) and fully-fixed beams (Eq. 3-89).

$\int_0^L \frac{M.M_1}{EI}dx + \int_0^L \frac{F_T.F_{T,1}}{EA}dx = \frac{L}{EA} + \frac{3968\,\delta_{m,\max}^2\,L}{7875\,EI} - \frac{4352\,\delta_{m,\max}^2}{875\,EA\,L}$	**3-88**
$\int_0^L \frac{M.M_1}{EI}dx + \int_0^L \frac{F_T.F_{T,1}}{EA}dx = \frac{L}{EA} + \frac{128\,\delta_{m,\max}^2\,L}{315\,EI} - \frac{512\,\delta_{m,\max}^2}{105\,EA\,L}$	**3-89**

The evolution of the extensional stiffness $K_{A,beam}$ is given as a function of the vertical deflection in the mid-span section $\delta_{m,max}$ in Tables 3-3 and 3-4 for simply-supported and fully-fixed beams (IPE 300 section – L = 5 m). These tables show that vertical deflections have a significant influence on the extensional stiffness of the beam.

Deflection	Extensional Stiffness	Relative Extensional Stiffness
0 mm	226.0 kN/mm	1.000
50 mm	209.5 kN/mm	0.927
200 mm	100.1 kN/mm	0.443
500 mm	25.5 kN/mm	0.113

Table 3-3 : Extensional stiffness of a IPE 300 including second-order effects (simply-supported)

Deflection	Extensional Stiffness	Relative Extensional Stiffness
0 mm	226.0 kN/mm	1.000
50 mm	212.6 kN/mm	0.941
200 mm	112.6 kN/mm	0.498
500 mm	31.0 kN/mm	0.137

Table 3-4 : Extensional stiffness of a IPE 300 including second-order effects (fully-fixed)

3.3.5 Coefficient of interpolation c_f between pinned and rigid cases

3.3.5.1 Origin of the modifications

For simply-supported and fully-rigid beams, the deflection profile is given as a function of the mid-span deflection in Eqs 3-13 and 3-20. Between these two extreme cases, Yin interpolates the deflection profile using the coefficient c_f defined in Eq. 3-22, where K'_R is calculated similarly to K'_A and is called "effective end rotational restraint". This expression has no physical meaning for rotational springs. An approach stating the equilibrium between the bending moment in the rotational spring and the beam extremity is proposed by the author to calculate the coefficient $c_{f,new}$ for interpolations between pinned and rigid deflection profiles.

3.3.5.2 *Description of the modifications*

The coefficient of interpolation c_f is aimed at calculating the displacements, rotations and curvatures of the beam for any value of the stiffness of the rotational springs K_R (Eqs 3-90 to 3-92).

$z(x) = (1 - c_f)\, z_{pinned} + c_f\, z_{rigid}$	**3-90**
$\theta(x) = (1 - c_f)\dfrac{dz_{pinned}}{dx} + c_f \dfrac{dz_{rigid}}{dx}$	**3-91**
$\chi(x) = (1 - c_f)\dfrac{d^2 z_{pinned}}{dx^2} + c_f \dfrac{d^2 z_{rigid}}{dx^2}$	**3-92**

The equilibrium between the bending moment in the rotational spring and the beam extremity is stated in Eq. 3-95 to obtain $c_{f,new}$. The deflection profiles obtained with the values of $c_{f,Yin}$ and $c_{f,new}$ are plotted on Figure 3-22 for one case at room temperature. A 5 metre-long IPE 300 beam is submitted to a vertical loading w = 10 kN/m and the stiffness of the rotational springs is 10,000 kN.m/rad.

$\theta(x=0) = (1 - c_{f,new})\left.\dfrac{dz_{pinned}}{dx}\right\|_{x=0} = (1 - c_{f,new})\dfrac{16\,\delta_{m,\max}}{5}$	**3-93**
$\chi(x=0) = c_{f,new}\left.\dfrac{d^2 z_{rigid}}{dx^2}\right\|_{x=0} = c_{f,new}\, 32\,\delta_{m,\max}$	**3-94**
$K_R\,\theta(x=0) = EI\,\chi(x=0) \quad \Rightarrow \quad c_{f,new} = \dfrac{K_R}{\dfrac{10\,EI}{L} + K_R}$	**3-95**

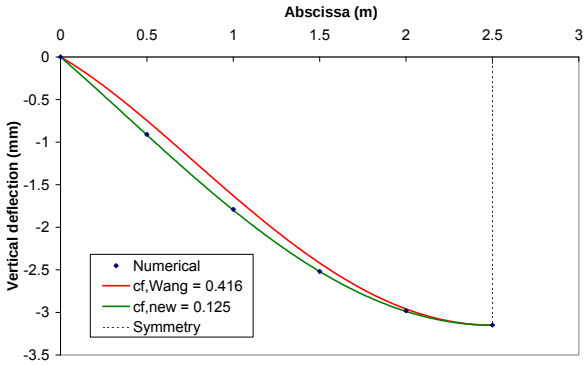

Figure 3-22 : Comparisons of deflection profiles obtained with $c_{f,Wang}$ and $c_{f,new}$

3.4 Validation of the numerical model in SAFIR

3.4.1 Brief description of SAFIR program - Mechanical module [Franssen, 2005]

SAFIR program has been briefly introduced for thermal applications in § 2.4.1. The mechanical module works with truss elements, shell elements and (2-D and 3-D) beam elements. For applications at elevated temperatures, the temperature history is read from the files created during the thermal analysis. The use of 3-D beam elements is preceded by a torsional analysis. Large displacements are considered in all the types of element and the effect of thermal strains can be accounted for. In the present work, structures and sub-structures are modelled with beam elements. The cross-section of beam elements, defined in the thermal module, is meshed in 2-D finite elements. The extrusion of this 2-D section creates a 3-D beam element where the plane finite elements become fibre elements. The global propoerties of the 2-D section are calculated assuming that the area of one finite element is concentrated at the centre of gravity of that element.

3.4.2 Preliminary Discussion

The software SAFIR will be used as a reference to validate the analytical method after modifications. The choice of a numerical model implies that some assumptions are made and some physical phenomena are neglected. For that reason, some experimental tests have been simulated with the numerical model that will be used later for the validation of the analytical method.

In its analytical work, Yin justified that the different types of instabilities can be neglected:

- local buckling is rarely a problem in hot-rolled steel universal beam sections (and by extension in European I-shape beams);

- the yielding of the lower flange near its supports under combined action of restrained thermal expansion and hogging bending moment (observed in Cardington fire tests) is not a failure mode and does not reduce the local bending moment capacity of the beam;

- the beam's bending moment capacity has a minor contribution to the beam's load carrying capacity within the catenary action stage so that discounting the complex issue of local buckling/yielding would not compromise the accuracy of the obtained results;

- lateral torsional buckling has very little effect because a laterally buckled steel beam will be pulled back by catenary action;

- it is demonstrated that the flexural buckling stress of a beam about its major axis in compression is very close to its yield stress.

On the basis of these statements, the numerical model build in SAFIR is a two-dimensional model with 2-D beam elements. The description of the tests simulated to validate the model and the comparisons between numerical and experimental results are given in § 3.4.3 and 3.4.4.

3.4.3 Description of the tests performed at the University of Manchester

Liu has performed experimental tests on simply-supported beams and sub-structures similar to a rugby goal post (Figure 3-23) to investigate in detail the role of connections and axial restraints on catenary action and its ability to prevent beam deflections from running away at high temperatures [Liu, 1999a]. During the first few preliminary tests carried out on beams with end-plate connections, beams failed prematurely with extensive diagonal web buckling between the end-plates and the loading jack positions. As the shear failure was not a primary object of this investigation, horizontal stiffeners were welded at the centre of the beam web near its ends to avoid further failure by shear. After elimination of the unusable data, the experimental programme consists in the following tests:

- 2 tests on simply-supported beams
- 3 tests on sub-structures with web cleats connections
- 10 tests on sub-structures with flush end-plate connections

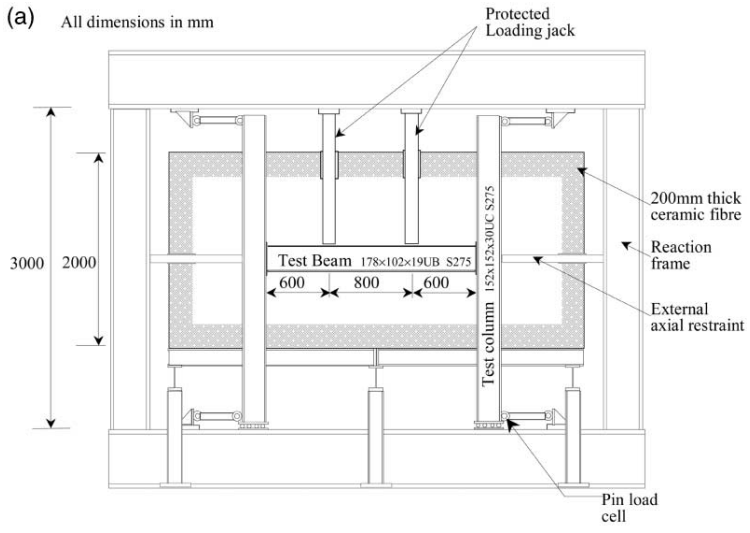

Figure 3-23 : Schematic drawing of the test arrangement of Liu [1999a]

The beams, with a section 178x102x19UB (S275), were mainly unprotected but top flanges were wrapped with 15 mm thick ceramic fibre blanket in order to simulate the heat-sink effect due to the

concrete slab. The columns, with a section 152x152x30UC (S275), together with the connections were fire-protected by the use of a 50 mm thickness of ceramic fibre blanket.

Two types of connections were selected as being typical of those commonly used in practice, namely double web cleats and flush end-plates (Figure 3-24). The web-cleat connection, which is assumed to have no significant moment capacity, was designed for shear only using angle sections 75x75x8 and M16 Grade 8.8 bolts. A 10 mm thick flush end-plate with M16 Grade 8.8 bolts was used as an alternative connection.

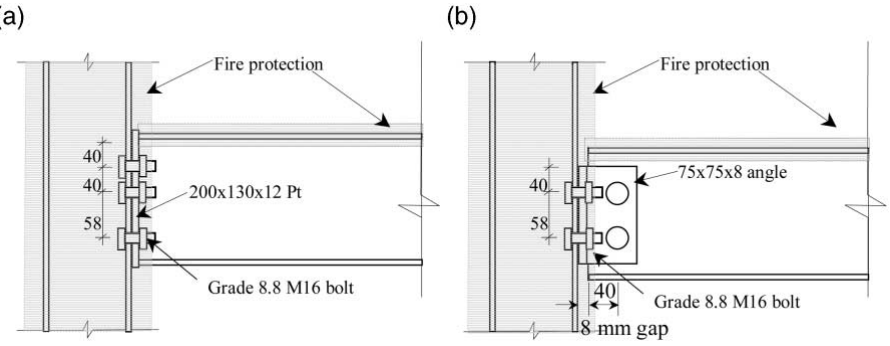

Figure 3-24 : (a) Flush end-plate connection and (b) Web cleats connection [T.C.H. Liu., 1999a]

The beam specimen was subjected to a constant vertical load and the furnace was programmed to follow the ISO 834 standard temperature-time curve. Three main levels of loading (load ratios of 0.3, 0.5 and 0.7) were tested. The Load Ratio is defined as the ratio of the applied load under fire conditions to the design load-carrying capacity at room temperature of the beam considered as simply-supported.

The 3 metre 152x152x30UC (S275) fire-protected column alone provided an axial restraint equivalent to a stiffness of 8 kN/mm to the test beam. The possible in-plane restraint imposed by its neighbouring sub-frames has been estimated to a range between 10 and about 70 kN/mm. With the use of additional struts spanning between the column of the test frame and the column of the reaction frame (Figure 3-23), two other overall stiffnesses of 35 and 62 kN/mm were achieved.

In the majority of tests performed on flush end-plate connections, the formation of plastic hinges was observed in the sections where the loading is applied. An exception is the test where the load ratio is equal to 0.9 and the axial restraint is 8 kN/mm: the excessive material degradation near the connection probably led to local flange buckling causing an almost immediate failure of the specimen.

In tests with web-cleat connections, critical temperatures of the beams are 20°C smaller than those obtained with flush end-plate connections. No local buckling was observed closed near to the extremities of the lower flanges. Although usually considered as pinned, web-cleat connections

resisted a minimal amount of moment (around 7 kN.m) and the transferred moment still increased after the 8-mm thick gap between the bottom flange of the beam and the column flange was closed.

3.4.4 Numerical simulation of the tests performed at the University of Manchester

3.4.4.1 Thermal Analyses

The distribution of temperature in the beam has been calculated with SAFIR assuming that the boundary conditions are adiabatic on the upper flange. In fact, the insulating material avoids any heat flux during a limited period of time but the precision is sufficient to use this distribution of temperature in the mechanical analysis (Figure 3-25). The test temperature is the typical temperature measured during one test.

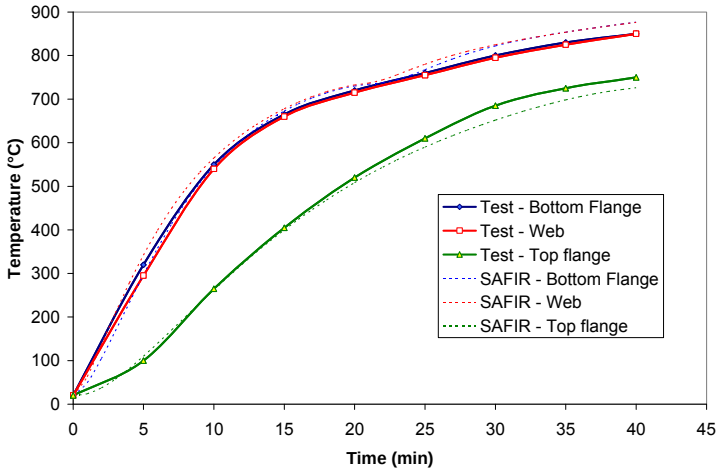

Figure 3-25 : Comparison between numerical and measured temperatures in the mid-span cross-section

3.4.4.2 Mechanical Analyses

3.4.4.2.1 Simply-supported beams

The failure of a simply-supported beam is reached when the first plastic hinge is formed in the most critical cross-section or zone. The analytical calculation of the beam fire resistance consists in evaluating the time at which the reduction of the resisting bending moment due to the elevation of temperature is equal to the load ratio. In the present cases, the actual load ratios are lower than the design load ratios because the actual yield strength of steel at room temperature, measured on coupon tests, is higher than 275 MPa. Assuming that the temperature is constant on the complete beam cross-section, the critical temperature calculated analytically is given in (Table 3-5).

Design Load Ratio	Actual Load Ratio	Critical Temperature
0.5	0.42	620°C
0.7	0.58	565°C

Table 3-5 : Critical temperature of tested simply-supported beams

The comparisons between the mid-span deflections measured experimentally and obtained numerically are plotted on Figure 3-26. The failure of the beam is reached in the numerical simulations for slightly lower temperatures than observed experimentally. The bottom flange temperature at the failure in the test is about 35°C higher than the one leading to the failure in the numerical model. The mid-span deflection increases more quickly in the numerical simulations.

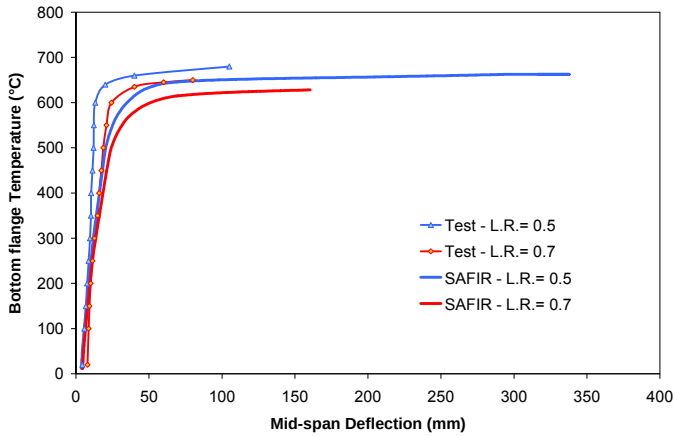

Figure 3-26 : Comparison of numerical and analytical deflections in simply-supported beams

Comparing the numerical and experimental results with the analytical solution is not simple because of the non-uniform distribution of temperature in the beam cross-section. Figure 3-27 shows the distribution of temperature at failure time for two values of the design load ratio.

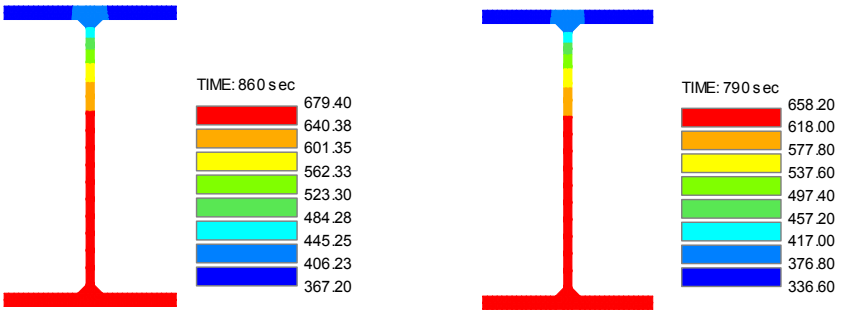

Figure 3-27 : Distribution of temperature in UB 178x102x19 at failure time

(a) Design L. R. = 0.5 - Time = 860 sec (b) Design L. R. = 0.7 - Time = 790 sec

3.4.4.3 Substructures with flush end-plate connections – BEAM elements

The three tests performed on web cleats connections have not been modelled in the FE software SAFIR because the models representing the action of flush end-plate connections are simpler than the one of web cleats connections. The present validation is focused on the prediction of internal forces in beams under fire conditions. The modelling of the action of simple connections under fire conditions will be treated in Chapters 5 and 6.

In tests with axial restraints equal to 35 kN/mm and 62 kN/mm, the axial stiffness of the end restraint is low. This is due to the fact that the restraining system is not fully effective at the beginning of the tests. In the numerical simulations of these tests, "Translated BILIN_COMP" material laws (Figure 3-28) have been allocated to the elements representing the axial restraints. The values of the initial strain before the contact is effective ε_{ini} have been adjusted so that the "numerical gap" is closed when the experimental axial thrust starts to increase significantly.

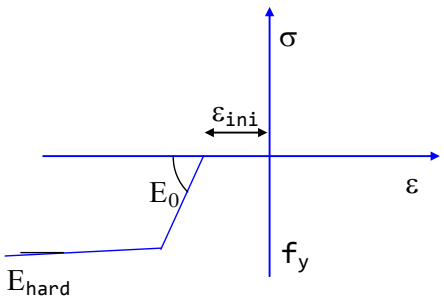

Figure 3-28 : 'Translated BILIN_COMP' material law

Globally, the correlation between the vertical deflections, beam axial forces and hogging bending moments measured during the tests and those given by numerical models are very good (Figures 3-34 to 3-38). Slight differences are obtained for hogging bending moments but it should be noted that some experimental results are inconsistent: in tests with K_A = 62 kN/mm, the hogging bending moment is almost equivalent at the beginning of the tests for load ratios equal to 0.3 and 0.5 and the bending moments are lower for the higher load ratio during a large part of the fire (Figure 3-33). These comparisons show that the 2-D model used in SAFIR with beam elements provide reliable predictions of the displacements and internal forces in axially and rotationally restrained beams under fire.

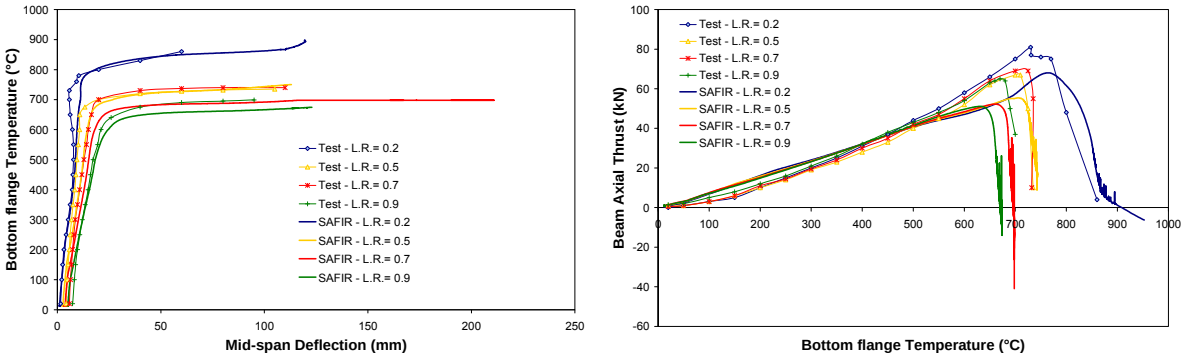

Figure 3-29 : Tests with K_A = 8 kN/mm - Mid-span deflection (left) and Beam axial thrust (right)

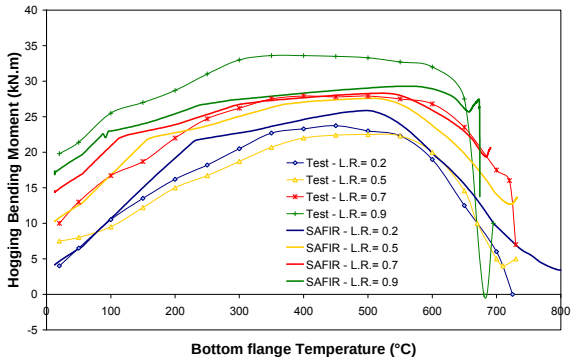

Figure 3-30 : Tests with K_A = 8 kN/mm – Hogging bending moment

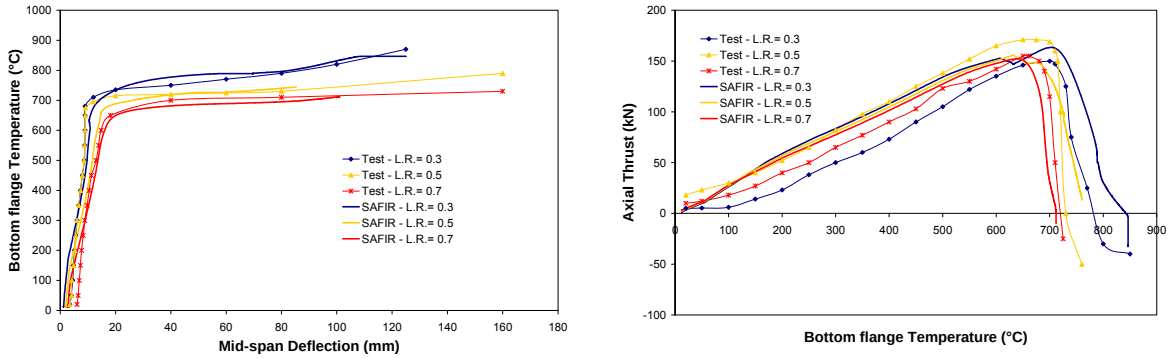

Figure 3-31 : Tests with K_A = 35 kN/mm - Mid-span deflection (left) and Beam axial thrust (right)

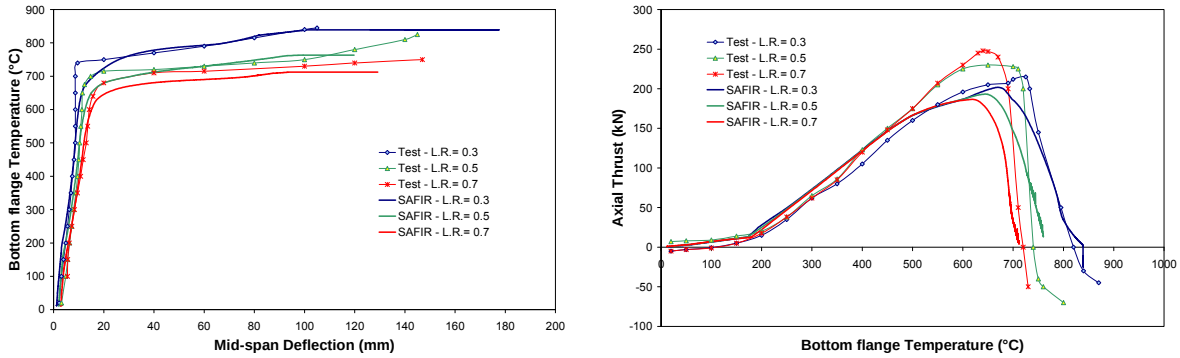

Figure 3-32 : Tests with K_A = 62 kN/mm - Mid-span deflection (left) and Beam axial thrust (right)

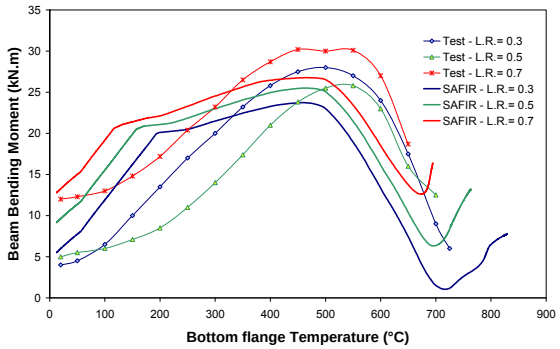

Figure 3-33 : Tests with K_A = 62 kN/mm – Hogging bending moment

3.5 Validation of the Modified Method under heating phase

3.5.1 Simply-supported beam – Non-uniform distribution of temperature

The Modified Method has been tested for a 6-meter long simply-supported beam with no rotational restraints. The cross-section of the beam is IPE 300 and the steel grade is S275. The load ratio w is defined as the ratio between the uniformly-distributed vertical loading and plastic vertical loading of the beam. The level of axial restraints K is the ratio between the stiffness of the axial spring representing the behaviour of the surrounding frame and the extensional stiffness of the beam at room temperature. The temperature is assumed to be uniform and to increase linearly in the beam web, the top flange and the bottom flange until failure. Initially, the temperature is equal to 20°C in the three parts. At the failure, the variation of temperature (with regard to 20°C) in the top and bottom flanges are respectively equal to the variation of temperature in the web multiplied by 0.8 and 1.2. The values of the mid-span deflections, the axial forces and the mid-span bending moments obtained by the Modified Method and by numerical simulation are compared on Figures 6-33 to 6-36 for two different cases. The average temperature of these graphs is the temperature of the web.

The difference between the results given by the Modified Method and SAFIR are mainly due to the approximation of the beam deflection profile in the Modified Method, as explained hereafter. When the bending moment at mid-span is equal to the proportional bending moment M_{propor}, large variations of the curvature are necessary to increase the bending moment at mid-span. In real cases and numerical simulations, curvature varies more near the mid-span section than in the other sections of the beam. Consequently, reaching the proportional bending moment does not induce sudden variations of the mid-span vertical displacement in numerical simulations. In the analytical method, the curvature is a function of the vertical deflection and it is necessary to reach large deflections to obtain a large curvature in the mid-span section. This explains why, by example, a sudden variation of vertical displacement occurs at around 400°C in Figure 3-36. This over-estimation of the vertical displacement implies an under-estimation of the axial force.

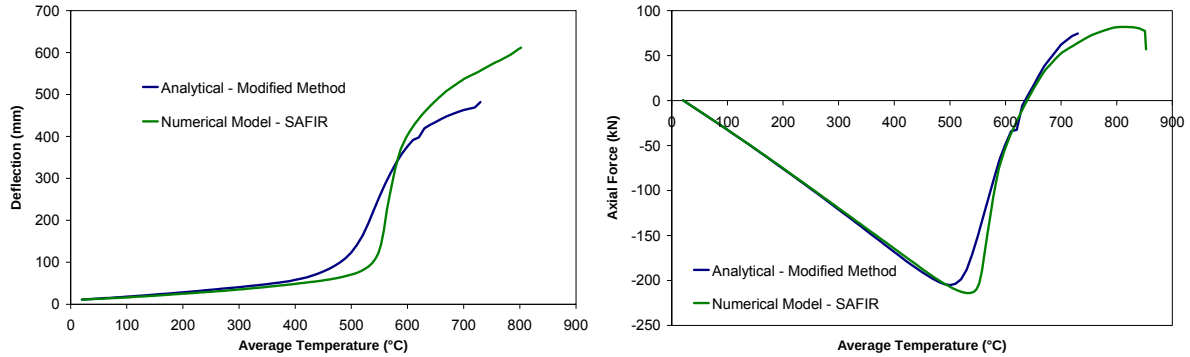

Figure 3-34 : Deflection (left) and Axial force (right) in IPE 300 beam – w = 0.3 – K = 3%

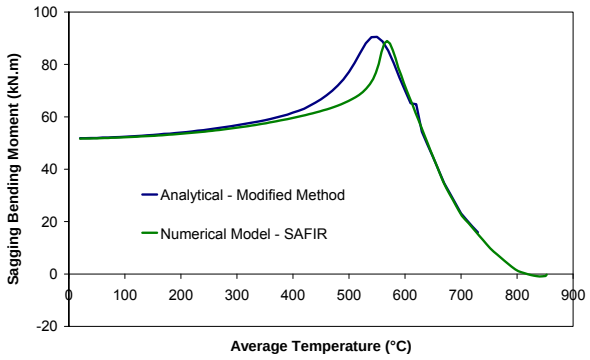

Figure 3-35 : Sagging bending moment in IPE 300 beam – w = 0.3 – K = 3%

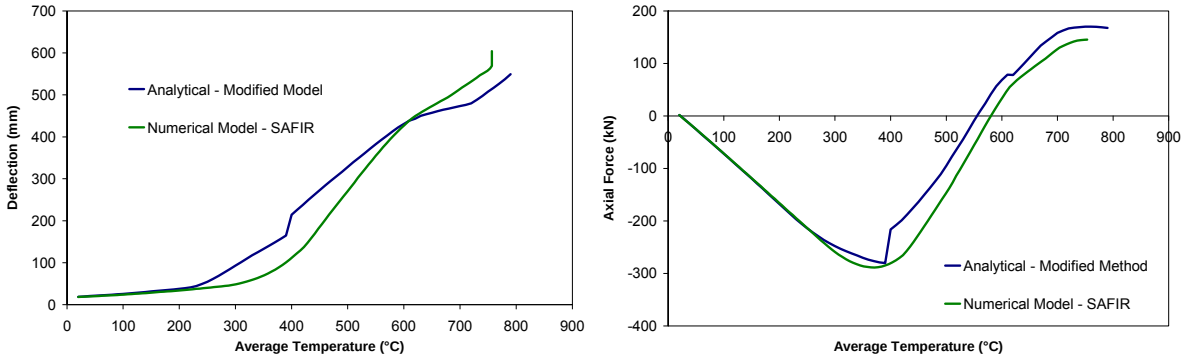

Figure 3-36 : Deflection (left) and Axial force (right) in IPE 300 beam – w = 0.5 – K = 7%

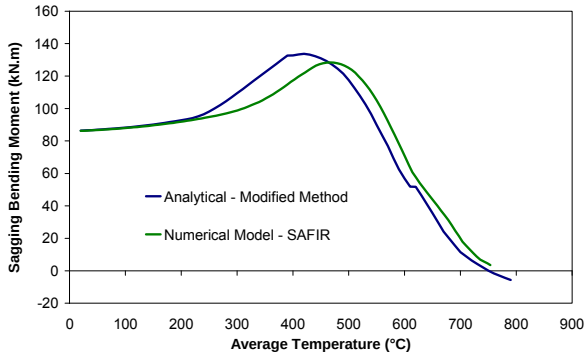

Figure 3-37 : Sagging bending moment in IPE 300 beam – w = 0.5 – K = 7%

3.5.2 Rotational restraints (elastic) – Non-uniform distribution of temperature

The geometrical properties, mechanical properties and evolution of the distribution of temperature of the beam tested here are the same as those described in § 3.5.1. Rotational restraints are modelled by an elastic spring with a rotational stiffness of 3,000 kN.m/rad.

The numerical simulations have been performed with two material laws for steel: a) the material law of carbon steel defined in the EN 1993-1-2 including the descending branch for strains higher than 0.15 and b) the material law of carbon steel defined in EN 1993-1-2 with an infinite yield plateau, ignoring the descending branch. When rotations of the beam extremities are limited by restraints, the presence of the descending branch causes failures for small vertical deflections. By ignoring the descending branch of the material law for carbon steel, the analytical method over-estimates the fire resistance of a beam. In the design of structures under fire, the mid-span deflections are often limited to L/20 and such a rule avoids over-estimating significantly the fire resistance of a beam. Figures 3-38 to 3-41 show that the prediction of the displacements and internal forces given by analytical and numerical methods for two configurations.

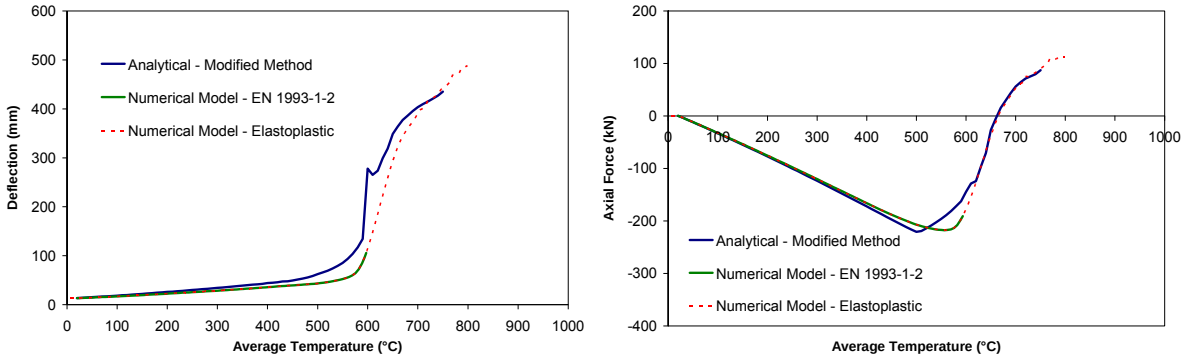

Figure 3-38 : Deflection (left) and Axial force (right) in IPE 300 beam – w = 0.5 – K = 3%

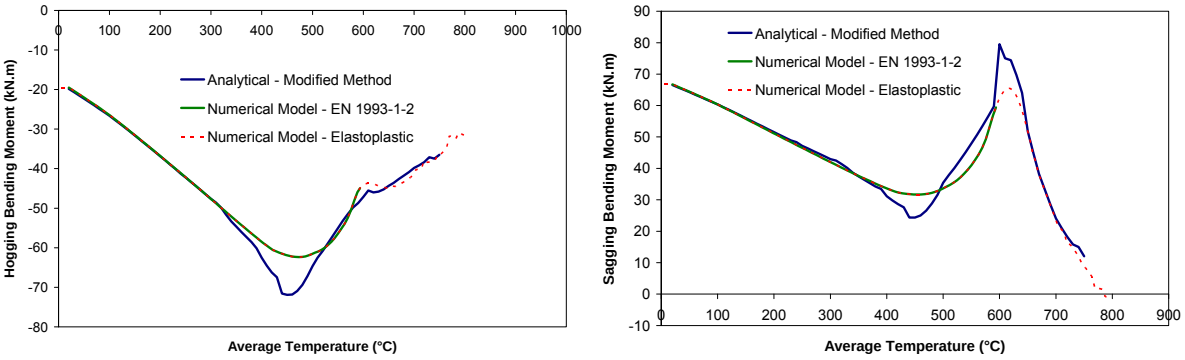

Figure 3-39 : Hogging (left) and Sagging (right) bending moment in IPE 300 beam – w = 0.5 – K = 3%

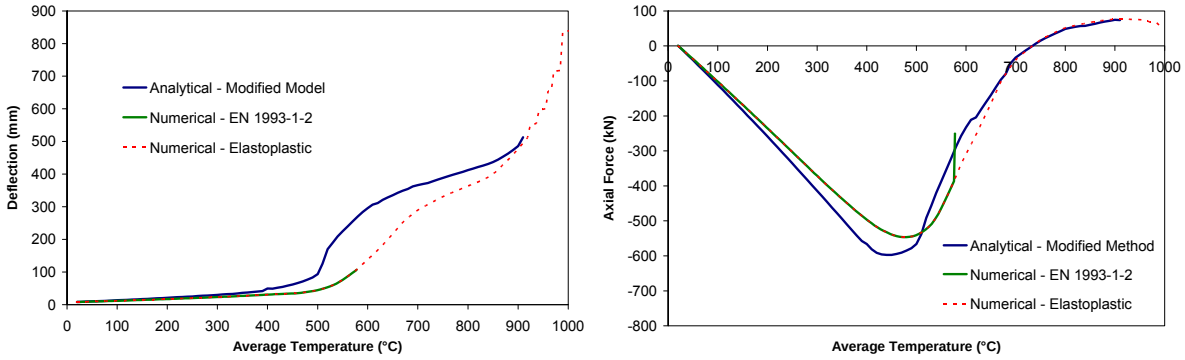

Figure 3-40 : Deflection (left) and Axial force (right) in IPE 300 beam – w = 0.3 – K = 10%

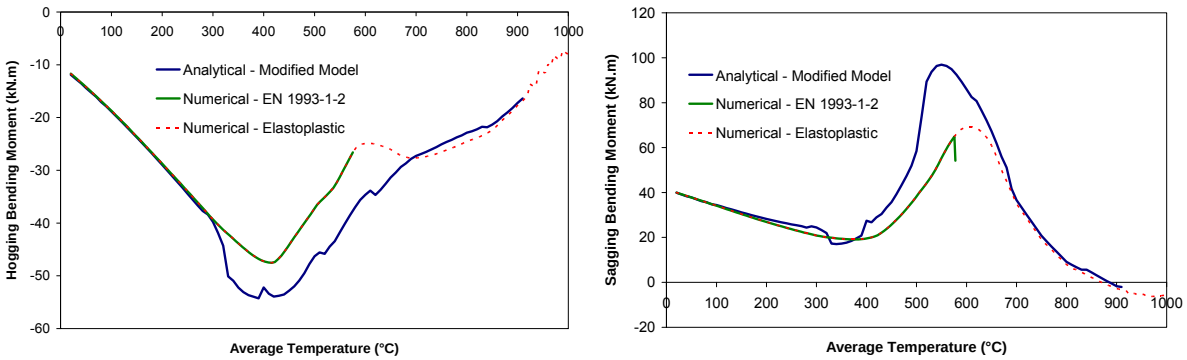

Figure 3-41 : Hogging (left) and Sagging (right) bending moment in IPE 300 beam – w = 0.3 – K = 10%

3.5.3 Rotational restraints (bilinear) – Non-uniform distribution of temperature

The validity of the Modified Method in case of semi-rigid joints with bilinear behaviour has been tested on a similar configuration to the one described in § 3.5.1 (geometrical properties, mechanical properties and evolution of the distribution of temperature). The rotational restraints are modelled by a bilinear rotational spring with an initial stiffness of 3,000 kN.m/rad and a maximal bending moment of 20 kN. The comparisons of the numerical and analytical results are given in Figures 3-47 to 3-50. The yield plateau in the M-χ diagram of the joint allows large rotations at the beam extremities. Consequently, the beam failure occurs after large deflections have been developed in the numerical simulations performed with the material law of carbon steel including the descending branch.

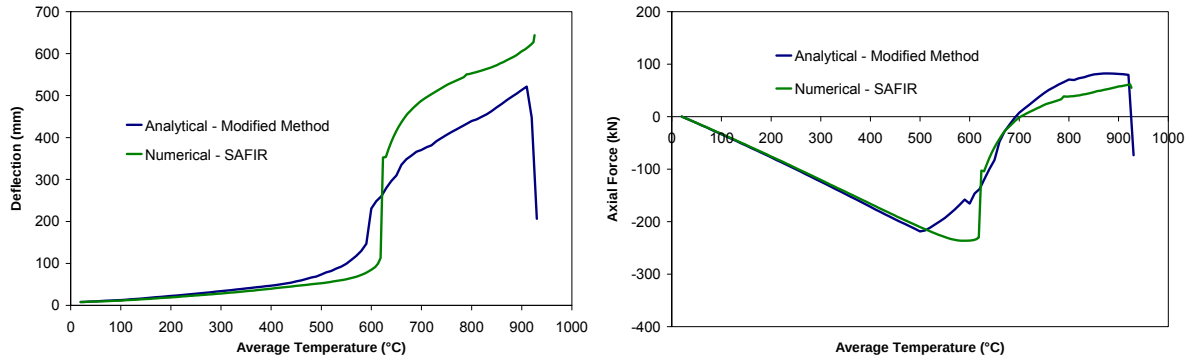

Figure 3-42 : Deflection (left) and Axial force (right) in IPE 300 beam – w = 0.3 – K = 3%

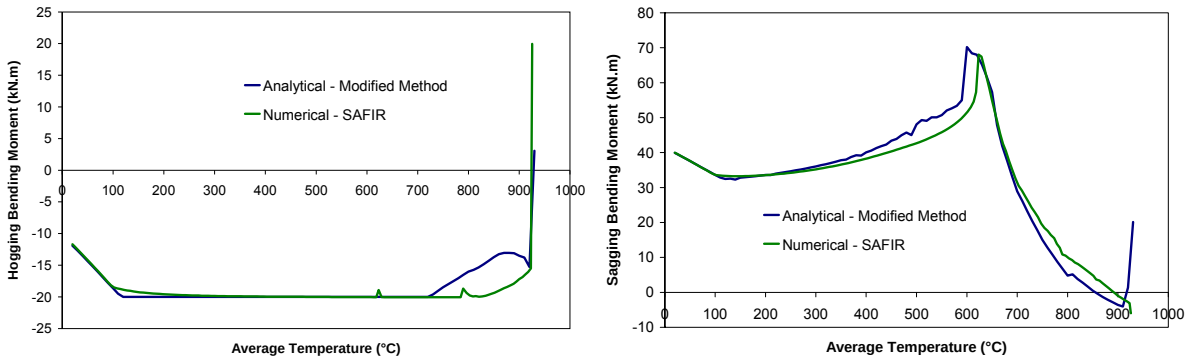

Figure 3-43 : Hogging (left) and Sagging (right) bending moment in IPE 300 beam – w = 0.3 – K = 3%

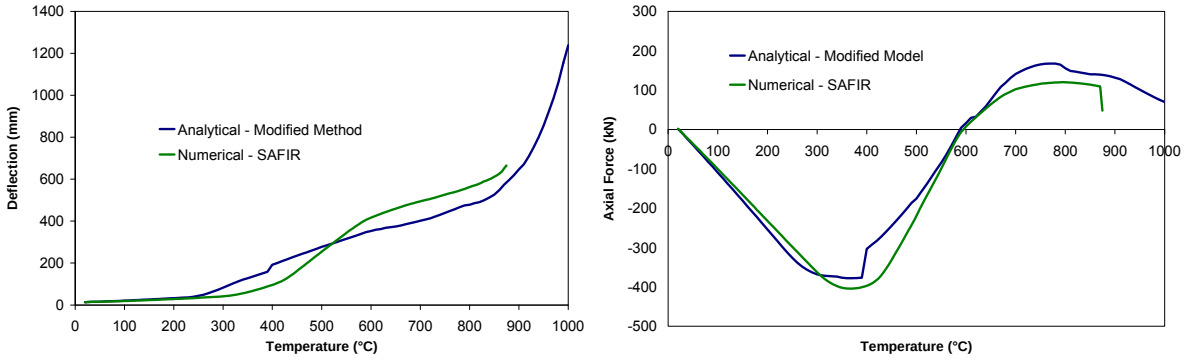

Figure 3-44 : Deflection (left) and Axial force (right) in IPE 300 beam – w = 0.5 – K = 10%

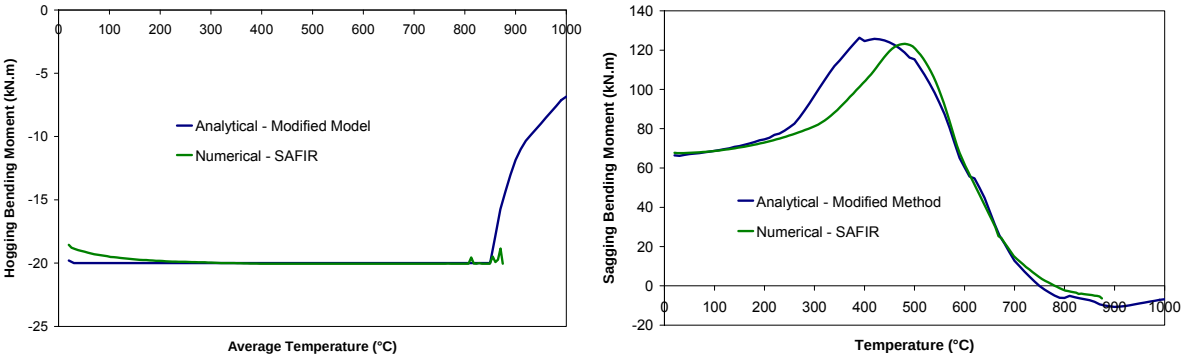

Figure 3-45 : Hogging (left) and Sagging (right) bending moment in IPE 300 beam – w = 0.5 – K = 10%

3.5.4 Influence of the modifications proposed by the author

3.5.4.1.1 Introduction

The influence of the modifications described in § 3.3.1 to § 3.3.5 has been analysed by comparisons between the results obtained with and without these modifications. The study case is the 6-meter long IPE 300 (S275 Grade) heated uniformly. The axial rotational restraints are elastic ($K_A/K_{A,beam}$ = 3% ;

K_R = 3,000 kN.m/rad) and the load ratio is 0.5. This study case has been solved with the Modified Method including all the modifications, considered as the reference analytical method and the influence of the modifications have been analysed separately. Modifications n°1 and n°2 are considered as two steps of a unique modification that consists in translating the bilinear (F_T , ΔL_m) and (M , χ_m) diagrams into non-linear (F_T , ΔL_m) and (M , χ_m) diagrams. Modification n°3 is an improvement aimed at extending the field of application of the method (account of the resisting moment of joint $M_{Rd,joint}$). So, no comparison can be made for this modification. Modifications n°4 and n°5 are respectively related to the deflection profile ($c_{f,new}$ vs $c_{f,Yin}$) and the evaluation of the beam axial stiffness $K_{A,beam}$ with and without second-order effects.

3.5.4.1.2 Modifications n°1 & n°2: (F_T , ΔL_m) and (M , χ_m) diagrams

Figures 6-45 and 6-46 show that the correlation between analytical and numerical results is significantly improved by the inclusion of modifications n°1 and n°2 in the temperature domain where plastic strains are developed in the beam. Moreover, the convergence of the routine built to solve the General Equation (Eq. 3-12) is not obtained with the original method at the transition between "bending behaviour" and "catenary behaviour". Adopting non-linear laws for the axial force-elongation and moment-curvature diagrams allows a more progressive transition between the two types of behaviours where bilinear laws necessitates robust algorithms.

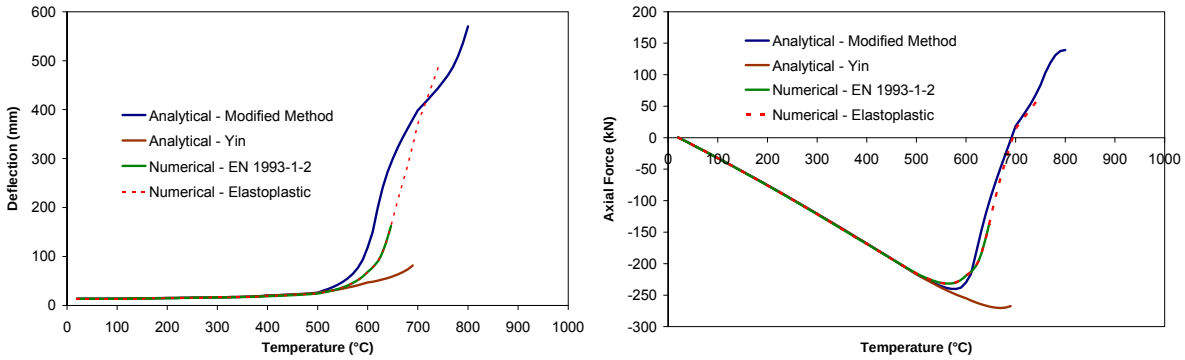

Figure 3-46 : Deflection (left) and Axial force (right) in IPE 300 beam – w = 0.5 – K = 3%

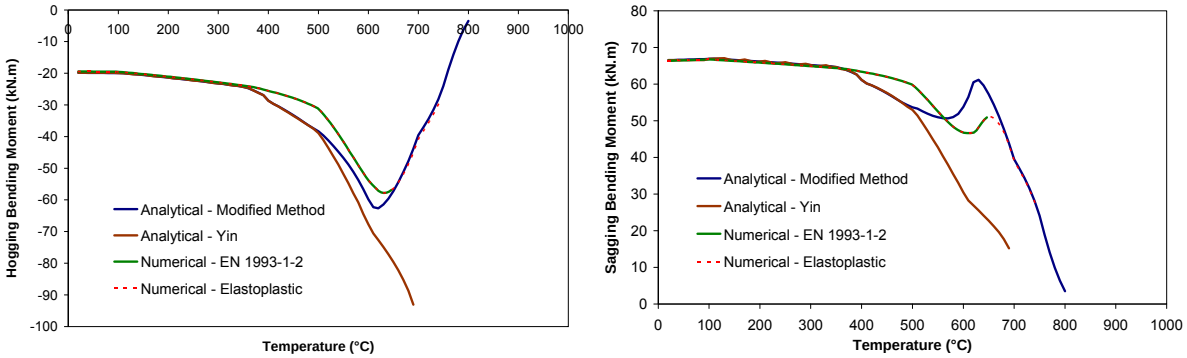

Figure 3-47 : Hogging (left) and Sagging (right) bending moment in IPE 300 beam – w = 0.5 – K = 3%

3.5.4.1.3 Modifications n°4: Axial stiffness of the beam $K_{A,beam}$

The influence of second-order effects on the deflections of the beam and the distribution of internal forces is negligible. The results obtained with and without second-order effects are superposed and can not be distinguished. In fact, the axial deformability of the surrounding structure is much higher than the deformability of the beam, especially in the present case (K = 3%). In addition, the reduction of the beam stiffness is significant for large deflections. When this condition is fulfilled, the axial force F_T in the beam is between F_{propor} and F_{pl} so the elastic stiffness of beam has a low influence on the results.

3.5.4.1.4 Modifications n°5: Coefficient of interpolation for deflection profile c_f

The coefficient of interpolation c_f for the beam deflection profile has a very low influence on the vertical deflections and the evolution of axial forces (Figure 3-43) but influences significantly the distribution of bending moments in case of semi-rigid joints, especially at low temperatures where the behaviour of the beam is elastic (Figure 3-49). In the present case, the coefficients of interpolation calculation by the original expression $c_{f,Yin}$ (Eq. 3-22) and the new expression $c_{f,new}$ (Eq. 3-95) are respectively 0.416 and 0.125. At low temperatures, the use of $c_{f,Yin}$ leads to an over-estimation of the hogging bending moment at the beam extremity and an under-estimation of the sagging bending moment at the beam mid-span.

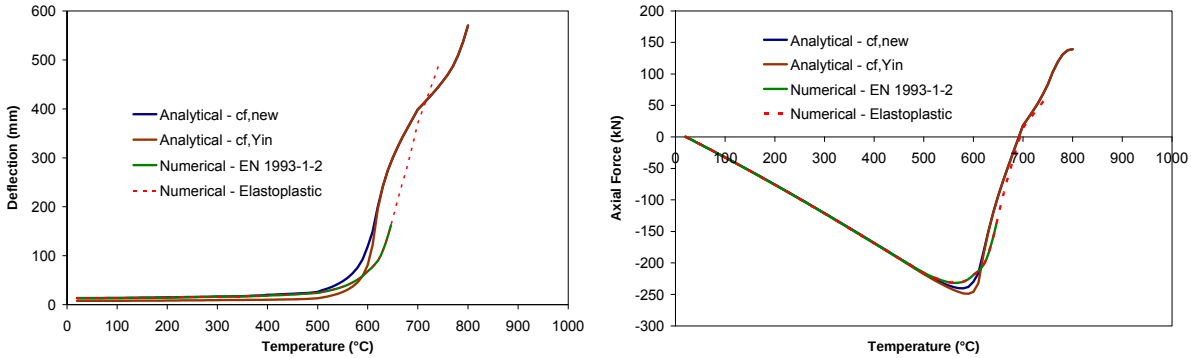

Figure 3-48 : Deflection (left) and Axial force (right) in IPE 300 beam – w = 0.5 – K = 3%

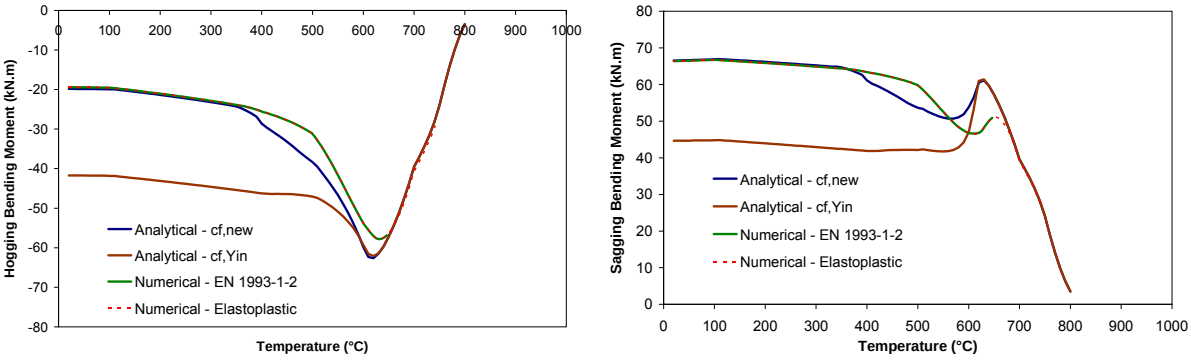

Figure 3-49 : Hogging (left) and Sagging (right) bending moment in IPE 300 beam – w = 0.5 – K = 3%

3.6 Extension of the Yin method to cooling phase [Li, 2006]

The performance of restrained steel beams during the cooling phase of a fire has been investigated and an incremental method has been proposed to predict the evolution of deflections and axial forces in a restrained steel beam during both the heating and cooling phases. The stress-strain relation of steel when unloading is assumed to be elastic. When temperature decreases from an initial temperature T_1 to a final temperature T_2, the stress-strain diagram is supposed to change so that the plastic strain at T_1 and T_2 are the same, based on the Massing rule [Franssen, 1990 & El-Rimawi, 1996].

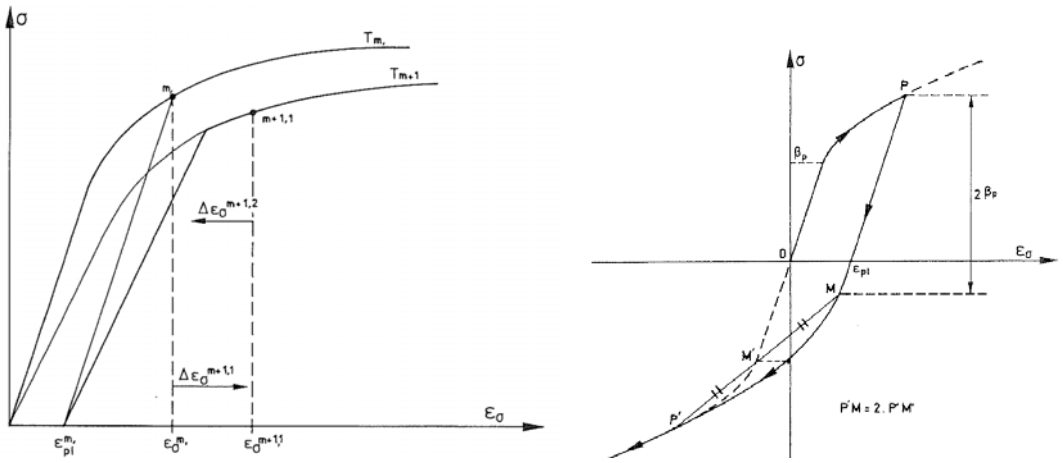

Figure 3-50 : Stress-strain diagram of carbon steel after variation of temperature (left) and unloading (right) according to Franssen [1990]

This extension of Yin Method has been compared to results given by ANSYS software for an axially and rotationally-restrained beam subjected to uniform distributions of temperature. The deflections and axial forces are good but, similarly to the validations of the Yin Method, no comparisons are made for the bending moments obtained at mid-span and at the beam extremity.

3.7 Extension of the Modified Method to cooling phase

3.7.1 Introduction

The Yin Method, developed for the heating phase only, is aimed at evaluating the deflections and distribution of internal forces by a unique resolution of the General Equation. The procedure proposed by Li to extend this method to the cooling phase of a fire is based on a step-by-step procedure and necessitates that the General Equation is solved many times. In the present work, the evaluation of the deflections and the distribution of internal forces at a time t of the cooling phase only depends on the results obtained at the end of the heating phase t_{ref} and the distribution of temperature at time t (Eq. 3-96). This means that calculating the displacements and the distribution of internal forces in an axially and rotationally-restrained beam after a complete heating-cooling cycle only necessitates two resolutions of the General Equation.

$z = z_{ref} + \Delta z$	**3-96**

where z, z_{ref} and Δz are the vertical deflection at time t, the vertical deflection at the reference time t_{ref} and the variation of deflection during the phase considered. The reference time is 0 for the heating phase and the duration of the heating phase for the cooling phase.

In real cases, the cooling down of the top and bottom flanges of a beam under natural fire start at two distinct times and the definition of the reference time representing the end of the heating phase is based on an assumption. When such an analysis is realised in a F.E. model (e.g.: SAFIR), the beam finite elements are divided into fibers and the simultaneous heating in top fibers and cooling in bottom fibers can be taken into account. This can not be realised with the presented simplified methods.

3.7.2 Evaluation of the Axial Force F_T during the cooling phase

The calculation of axial forces during the cooling phase of a fire is obtained by application of the Massing rule and the rule of conservation of the plastic deformations during the cooling phase. The plastic mechanical variation of length (including contributions of the beam and the spring) at the end of the heating phase $\Delta L_{m,pl}$ is given by Eq. 3-97, where $\Delta L_{m,ref}$, $F_{T,ref}$ and $K'_{A,ref}$ are respectively the variation of length, the axial force and the global axial restraint stiffness at the reference time t_{ref}. The translated (F_T ; ΔL_m) diagram at a time t of the cooling phase is represented on Figure 3-51 (bold green line).

$$\Delta L_{m,pl} = \Delta L_{m,ref} - \frac{F_{T,ref}}{K'_{A,ref}} \qquad \textbf{3-97}$$

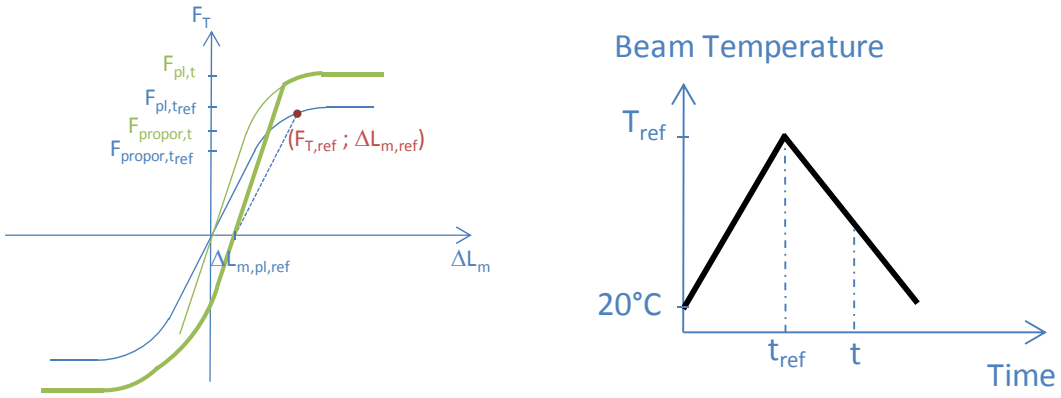

Figure 3-51 : (F_T ; ΔL_m) diagram at time t of the cooling phase of a fire

3.7.3 Evaluation of the Bending Moments M_R and M_T during the cooling phase

The procedure for the determination of the axial force F_T in the beam during the cooling phase (§ 3.7.2) is reproduced for the (M_T ; $\chi_{x=L/2}$) and (M_R ; $\chi_{x=0}$) diagrams to calculate the bending moment in the mid-span section of the beam M_T (Figure 3-54) and at the beam extremity (Figure 3-53). For the bending moment at the beam extremity M_R, an adaptation is necessary if the bending moment M_R has been limited to the joint resistance $M_{Rd,joint}$ at the reference time. If the rotation of the beam extremity decreases, the bending moment M_R reduces because the joint recover its elastic stiffness. The two

different procedures proposed to evaluate the plastic curvature at the beam extremity $\chi_{pl,x=0}$ are given in Eqs 3-99 and 3-100, depending on the comparison between the bending moment at the reference time $M_{R,ref}$ and the joint resistance.

$\chi_{pl,x=L/2} = \chi_{x=L/2,ref} - \frac{M_{T,ref}}{EI_{el,ref}}$	**3-98**

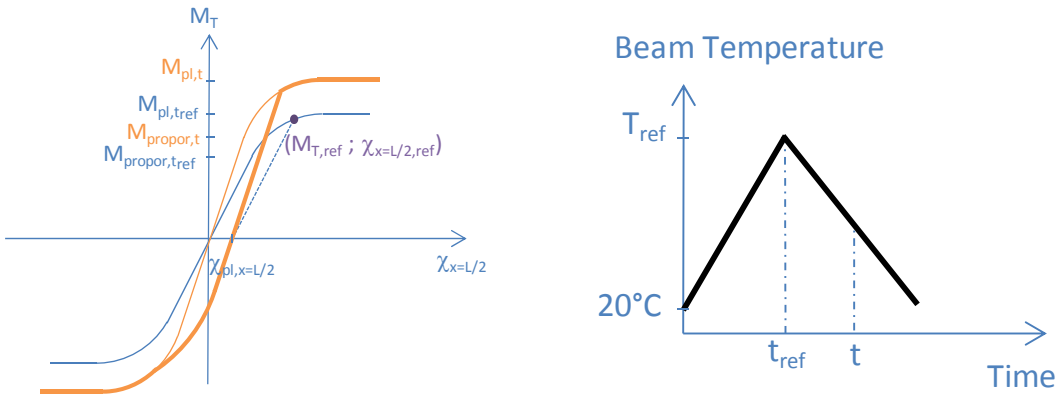

Figure 3-52 : (M_T ; $\chi_{x=L/2}$) diagram at time t of the cooling phase of a fire

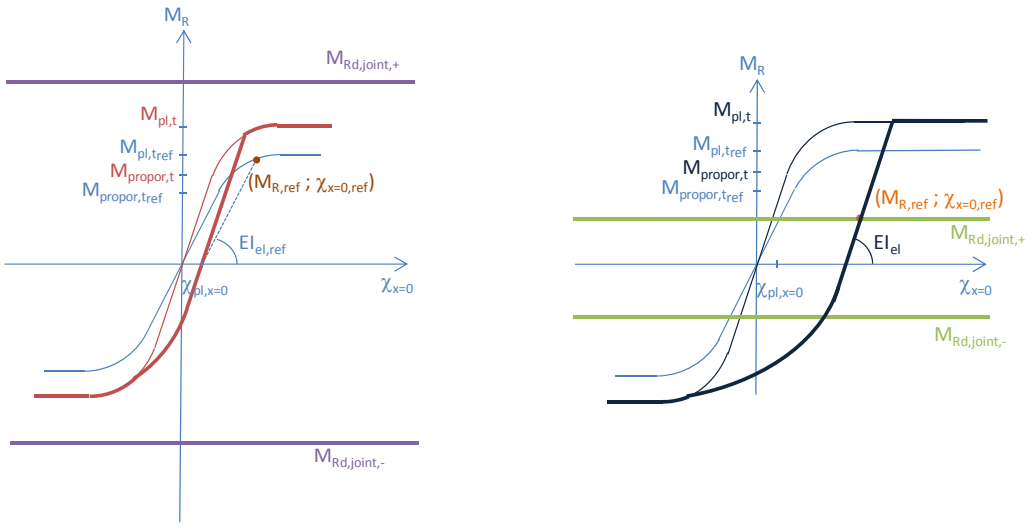

Figure 3-53: (M_R ; $\chi_{x=0}$) diagram at time t of the cooling phase of a fire

$\chi_{pl,x=0} = \chi_{x=0,ref} - \frac{M_{R,ref}}{EI_{el,ref}} \quad if \quad \lvert M_R \rvert \geq \lvert M_{Rd,joint} \rvert$	**3-99**
$\chi_{pl,x=0} = \chi_{x=0,ref} - \frac{M_{Rd,joint}}{EI_{el}} \quad if \quad \lvert M_R \rvert < \lvert M_{Rd,joint} \rvert$	**3-100**

$EI_{el,ref}$ and EI_{el} are the beam rotational stiffness at the reference time and at the time t considered.

3.8 Validation of the Modified Method under cooling phase

3.8.1 Simply-supported beam – Non-uniform distribution of temperature

Figures 3-54 to 3-57 show comparisons between deflections, axial forces and mid-span bending moments obtained analytically and numerically. The 6-meter long IPE 300 beam is heated up linearly to an average temperature of 650°C and cooled down linearly. At the end of the heating phase, the temperatures in the top flange, the web and the bottom flange are 600°C, 650°C and 700°C. The prediction of deflections and internal forces is good during both the heating and cooling phases, especially for axial forces F_T.

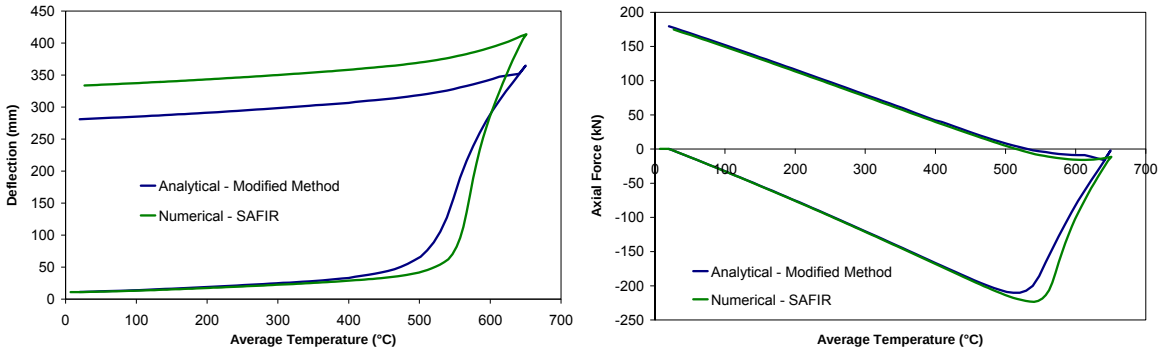

Figure 3-54 : Deflection (left) and Axial force (right) in IPE 300 beam – w = 0.3 – K = 3%

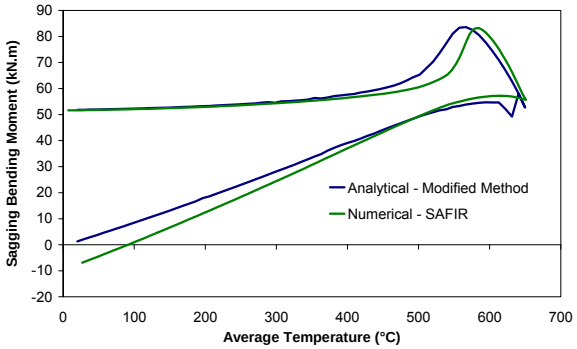

Figure 3-55 : Sagging bending moment in IPE 300 beam – w = 0.3 – K = 3%

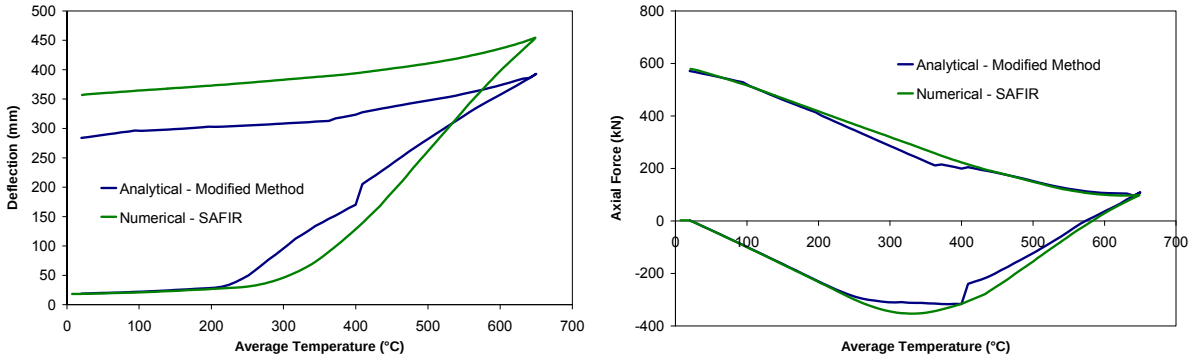

Figure 3-56 : Deflection (left) and Axial force (right) in IPE 300 beam – w = 0.5 – K = 10%

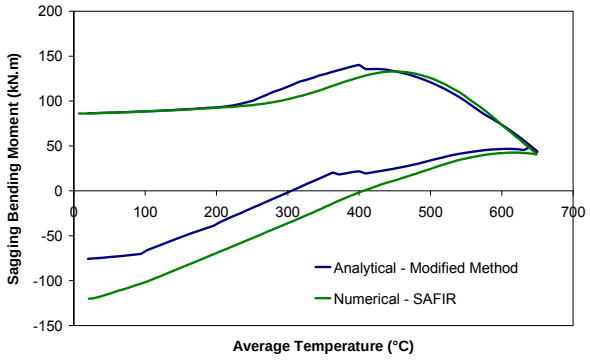

Figure 3-57 : Sagging bending moment in IPE 300 beam – w = 0.5 – K = 10%

3.8.2 Rotationally-restrained beam – Uniform distribution of temperature

Finally, the results given by the Modified Method for a rotationally-restrained beam (K_R = 3,000 kN.m/rad ; $M_{Rd,joint}$ = 20 kN.m) show a good agreement with numerical results (Figures 3-58 to 3-61). As already observed previously, the results during the heating phase are better for a lower level of axial restraints. This is due to the fact that the complete deflection profile of the beam is deduced from the mid-span deflection and the boundary conditions (via c_f). When the mid-span bending moment reaches the proportional moment of the section, the curvature $\chi_{m,x=L/2}$ and the mid-span deflection must increase much in order to mobilize higher bending moments while the curvature increase locally in real cases. For high levels of axials restraints, the over-estimation of the mid-span deflection induces large second-order bending moments. However, this imprecision (and limitation of the method) is softened at higher temperatures and during the cooling phase.

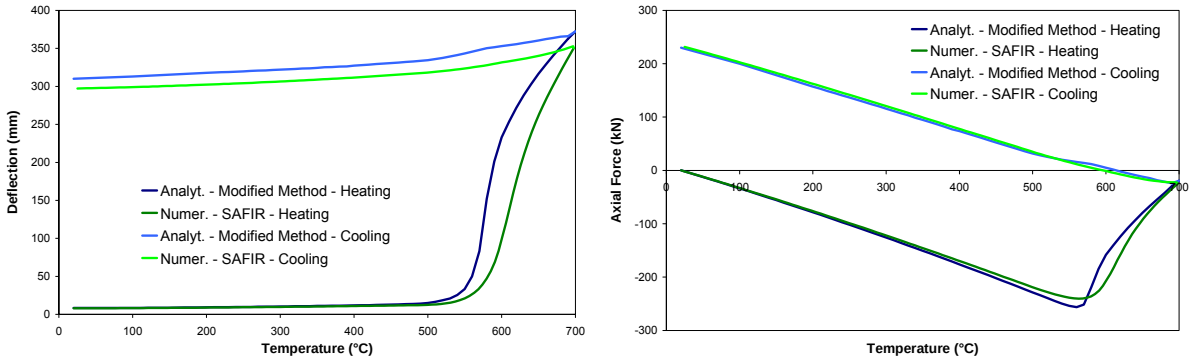

Figure 3-58 : Deflection (left) and Axial force (right) in IPE 300 beam – w = 0.3 – K = 3%

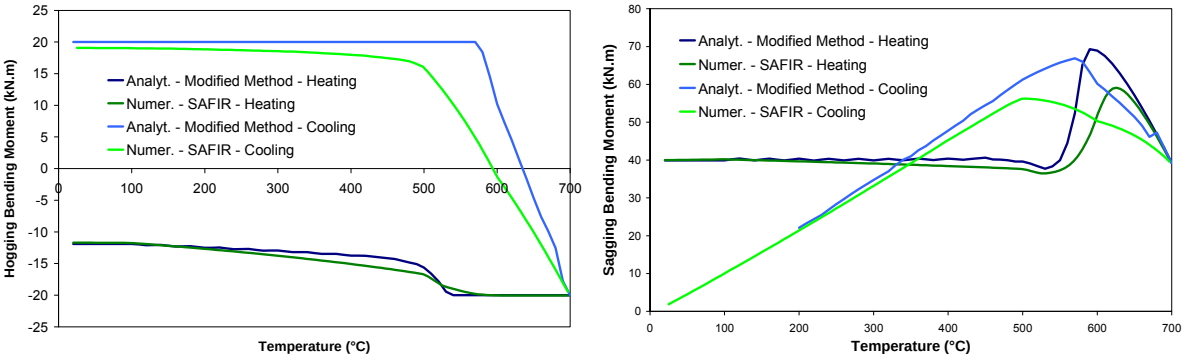

Figure 3-59 : Hogging (left) and Sagging (right) bending moment in IPE 300 beam – w = 0.3 – K = 3%

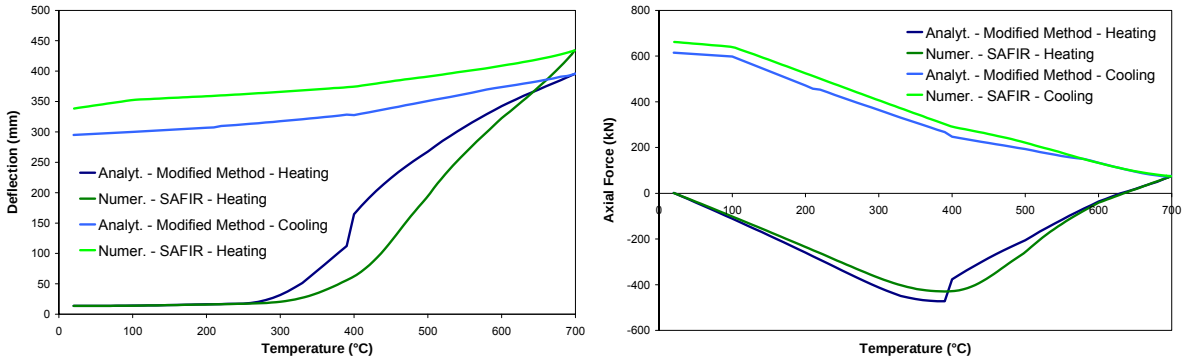

Figure 3-60 : Deflection (left) and Axial force (right) in IPE 300 beam – w = 0.5 – K = 10%

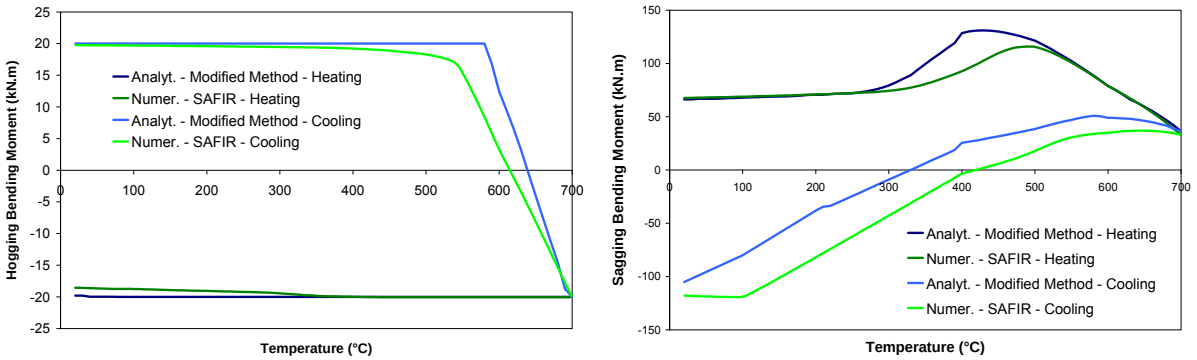

Figure 3-61 : Hogging (left) and Sagging (right) bending moment in IPE 300 beam – w = 0.5 – K = 10%

3.9 Conclusions

The method developed by Yin is a simplified method aimed at predicting the deflections and axial forces in axially and rotationally-restrained beams under uniform or non-uniform distributions of temperature [Yin, 2005a and 2005b]. Li has extended this method to the cooling phase of a natural fire [Li, 2006]: the unloading in the stress-strain diagrams of steel is realised following the Masing's rule and plastic strains are assumed to be constant for an incremental variation of temperature. The analytical developments of these two works have been validated by comparisons with the results obtained from numerical simulations performed with Abaqus software. However, this validation is only focused on the evolutions of vertical deflections and axial forces in the beam.

The author proposed several modifications and improvements to the calculation of the distribution of bending moments in the simplified method of Yin and Li. The limitation of bending moments at the beam extremities to the resistance of joints has also been taken into account. The comparisons between the deflections and internal forces predicted by the Modified Method and a numerical model in SAFIR showed a good agreement. The ability of SAFIR to predict the evolution of deflections and internal forces in restrained beams has been shown by the numerical simulations of a series of tests realised at the University of Manchester on 'rugby goal post' sub-structures [Liu, 2002].

Five modifications have been proposed by the author to improve the simplified method developed by Yin and Li. The objective of the first two modifications is to take into account the elliptic branch of the stress-strain diagram of carbon steel at elevated temperatures when evaluating axial forces and bending moments from the elongations and curvatures in the beam. An analytical method has been developed that gives the moment-curvature diagram of a beam section subjected to an axial force and a non-uniform elevation of temperature, taking into account the elliptic branch. The third modification ensures the compatibility of rotations at the extremity of the beam and in the rotational spring

representing the joint and the surrounding structure. This compatibility allows the evaluation of thermally-induced bending moments applied to the beam extremity, this evaluation being adapted to account for the resisting moments of joints. The fourth modification is proposed to take into consideration the variation of the beam axial stiffness with mid-span vertical deflections. Finally, the last modification is based on the equilibrium between the bending moment in extremity beam section and in the rotational spring. This leads to the definition a new coefficient of interpolation for the deflection profile. The influence of these five modifications on the predictions of deflections and internal forces has been analysed and it is demonstrated that, except for the fourth one, all the modifications have a significant and favourable influence on the results predicted by this analytical method.

However, this simplified method still includes several sources of imprecision or limitations:

- The deflection profile of the beam is function of the mid-span deflection and of the stiffness of the rotational springs. The shape of the profile is based on an elastic assumption so that some discrepancies can be obtained after plastic deformations appear in the beam mid-span section. These discrepancies become more evident for high levels of axial restraints.

- Uniformly-distributed loads and symmetrical boundary conditions have been considered in the present work. The deflection profiles for beams subjected to a point load at mid-span have been calculated by Yin and could be used with the Modified Method. For other load cases, new deflection profiles should be defined and tested.

- The moment-rotation diagrams of joints are usually not bilinear and vary with temperatures. In the present work, the characteristics of the joint do not vary with the heating and the cooling of the beam.

As a conclusion of Chapter 3, several enhancements have been added to the simplified analytical method proposed by Yin. Step by step, the modifications have made the algorithm of resolution heavier and some approximations still remain. This tends to demonstrate that this simplified method should only be used for axially-restrained beams, simply-supported or connected to protected joints that can be represented by a bilinear law. The extension of this method to joints with bilinear moment-curvature laws has necessitated a heavy work and several approximations to evaluate the thermally-induced bending moments. The analysis of the distribution of internal forces in beams or sub-structures subjected to natural fire integrating the real behaviour of typical simple connections (fin plate connections, double web cleats connections, header plate connections, etc) by simple method becomes beyond practical reach. The behaviour of these types of connections will be treated in detail in Chapters 5 and 6 by use of F.E. models.

4 Characterisation of the mechanical behaviour of bolts and welds under natural fire

4.1 Introduction

A study realised by British Steel and focused on the remaining strength of different carbon steel grades after heating up to 800°C and cooling demonstrated i) that no decrease in strength or notch toughness occurred after heating to temperatures up to 600°C and ii) that deterioration of properties was observed for other cases but that the strength levels are still well in excess of the maximum allowable design stresses [Lapwood, 1980]. As a consequence of this, the behaviour of carbon steel is usually assumed to be reversible in usual fire design applications. Due to the manufacturing process of bolts, composed of a quenching phase from an austenitising temperature slightly higher than 800°C until around 500°C and a tempering phase, the mechanical behaviour of bolts at elevated temperatures differs noticeably from the mechanical behaviour of carbon steel. Up to now, the investigations about the mechanical behaviour of bolts and welds have essentially been funded on the results of isothermal tests performed on specimens heated up to different temperatures. The reversibility of the mechanical properties of bolts and welds after they have been subjected to high temperatures has never been studied previously. On the basis of the present level of knowledge, new tests have been performed at the Centro Sviluppo Materiali (Italy). These tests on bolts and welds are described within Chapter 4.

Due to the brittle behaviour of bolts, the design of bolted connections at room temperature is usually realised so that the resistance of bolts is higher than the resistance of the connected elements. This type of design implies that the elastic limit of the bolt is not reached before the elastic resistance of ductile components. During the heating and cooling phases of a natural fire, the reduction of bolts resistance is more significant than the reduction of resistance of carbon steel elements. In these conditions, the risk of bolt failures exists and the ductility of bolts has a predominant role on the behaviour of the connection. The author developed appropriate mathematical models for representing the behaviour of the “bolt in tension” and “bolt in shear” components under fire conditions, including both heating and cooling phases of a fire. A brief review of the previous experimental investigations on bolts and welds at elevated temperatures is established hereafter.

The first series of tests performed on bolts are displacement-controlled tensile and shear tests realised at temperatures between 20°C and 700°C and showing a descending branch before the full breaking of bolts [Riaux, 1980]. The influence of creep was particularly analysed in that work. The strength

reduction factors mentioned in the EN 1993-1-2 have been determined on the basis of the experimental work carried out at British Steel on Grade 8.8 M20 hexagonal head bolts. Series of tests on bolts in tension and double shear were realised at temperatures up to 800°C [Kirby, 1995]. Tests in tension have highlighted that problems of premature failure by thread stripping are controlled by the lack of fit between the nut and the bolt rather than the insufficient capacity of one component. The measured reductions of resistance due to the elevation of temperature showed similar patterns in tension and shear. The comparison between the performance of high-strength bolts and the prescriptions of Eurocode for hot rolled structural steel showed that the bolts are far more sensitive because of the heat treatment methods used in their manufacture. The difference is marked in the range of temperature between 300°C and 700°C. A new and unique strength reduction factor was defined for bolts acting in shear and tension. By modifying the heating rate and the soaking time before the application of the mechanical loading in some tests, it was demonstrated that the influence of these parameters on the results was small. However, in recent researches, tests performed on Grade 10.9 bolts have underlined the significant effect of creep on the behaviour of bolt material at high temperatures [Gonzalez, 2008].

To the knowledge of the author, the unique available data about the evolution of welds resistance at elevated temperatures is the series of tests performed by British Steel that lead to the reduction factors defined in the EN 1993-1-2 [Latham, 1993]. The evolution of the resistance of welds as a function of temperature is intermediary between the curves obtained for carbon steel and bolts (Figure 4-1).

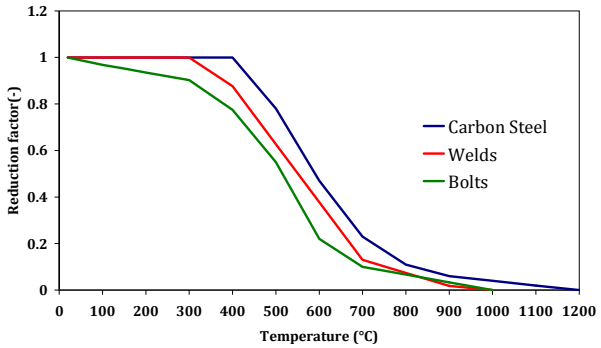

Figure 4-1 : Reduction factors for carbon steel, welds and bolts according to EN 1993-1-2 [CEN, 2004a]

4.2 Test methodology

The experimental programme undertaken on bolts and welds at the Centro Sviluppo Materiali includes three different types of isothermal tests:

a) Room temperature tests performed to get reference strengths.

b) Steady-state tests performed at elevated temperatures in order to obtain the strength evolution of bolts and welds during the heating phase.

c) "Natural fire tests" or steady-state tests performed at various failure temperatures T_f after heating to an up temperature T_u, in order to investigate the strength behaviour of bolts and welds during the cooling phase.

In steady-state tests performed after heating only, the procedure is similar to the one followed by British Steel. The tested specimens were heated unloaded at a speed of 10-30°C/min until the desired temperature. The load was applied after a stabilisation period of 15 minutes that ensures a uniform distribution of temperature in the specimen (Figure 4-2a). In the "natural fire tests", the temperature was stabilised at an up value of temperature T_u during 15 minutes and was decreased until the failure temperature T_f at a speed of 10-30°C/min. The mechanical loading was applied after the temperature is T_f (Figure 4-2b). Temperatures of the furnace are measured by a thermocouple.

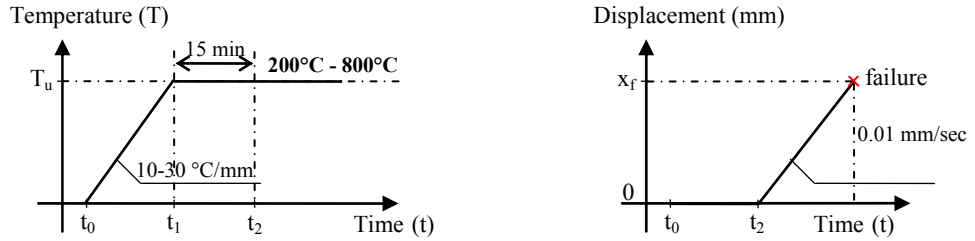

(a)

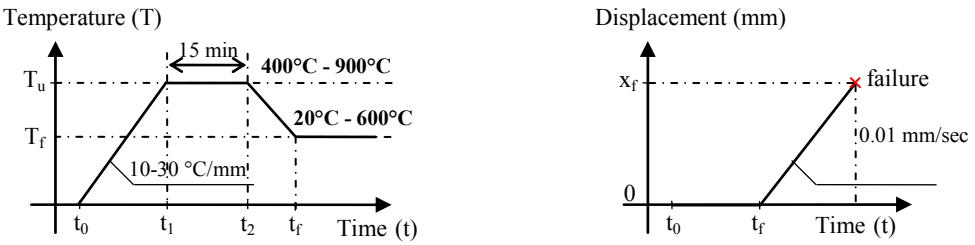

(b)

Figure 4-2 : Test procedures for bolts experiments after heating (a) or heating and subsequent cooling (b)

From the steady-state tests after heating only, the strength of bolts and welds can be plotted in terms of reduction factor (the ratio of the bolt/weld resistance after heating to the bolt/weld resistance at room temperature) as a function of the temperature, see thick line on Figure 4-3. This procedure will allow drawing a comparison with the results obtained by British Steel. The objective of the "natural fire tests" is to obtain the evolution of the bolt/weld strength as a function of the up temperature T_u and the failure temperature T_f (see dotted lines on Figure 4-3).

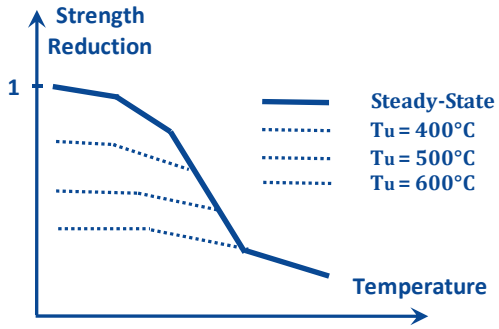

Figure 4-3 : Schematic presentation of the results given by the tests

4.3 Experimental tests performed on Grade 8.8 bolts

4.3.1 Test set-up

The furnace used for testing is an electrical furnace with manual adjustment of power. Tests are performed imposing a furnace power that resulted in a heating rate in the range of 10°-30°C/min. During the cooling phase the furnace is switched off and ventilated. The cooling rate is approximately in the same range of 10°-30°C/min.

Design codes (e.g.: EN 1993-1-2) give separate values for the resistance of bolts in tension and shear. Consequently, two different test set-ups have been designed to investigate separately the mechanical behaviour of bolts in tension and in shear at elevated temperature. Due to the limited loading capacity of test equipment, it has been decided to use size M12 bolts which are smaller than those used in building structures (minimum M16). Special investigation has been undertaken to check the consequences of this decision. Clamps for both tensile and shear tests have been fabricated using the NIMONIC 115 heat resistant alloy so that the behaviour of clamps remains elastic during the complete test and prying actions due to clamps deformation are limited. The configurations and the NIMONIC pieces used for the two types of tests are given on Figures 4-4 & 4-5.

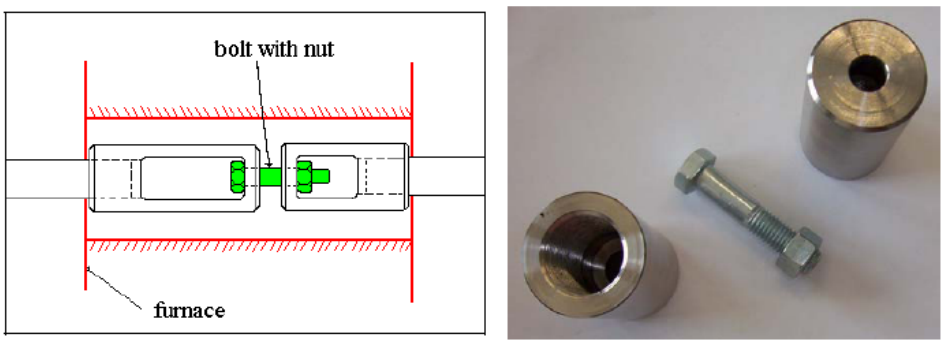

Figure 4-4 : Bolt-nut assembly and clamps for tensile tests at elevated temperatures

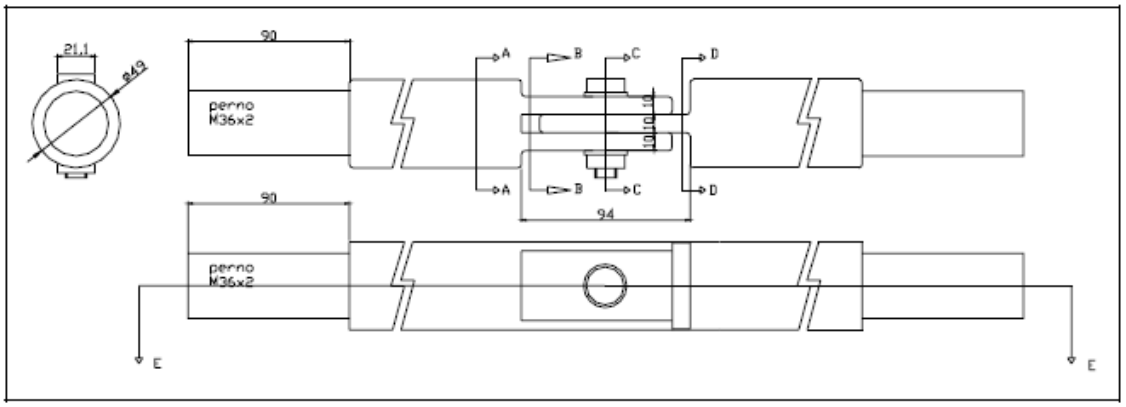

Figure 4-5 : Bolted connection design for shear tests at elevated temperatures

4.3.2 Characterization of the tested Grade 8.8 bolts

4.3.2.1 Mechanical properties

The tested M12x50 bolts are hexagonal-head and half-threaded bolts in accordance with the requirements of DIN 931 Norm. The value of the bolt strength f_{ub} has been roughly evaluated by hardness tests on two bolt shank sections. Analysed points are located in the center of the shank section. The mean value of the Rockwell Hardness A is 64.5 RHA and it suggests an approximate value of the ultimate tensile stress of 930 MPa. The ultimate tensile strength has also been estimated by a more accurate procedure: tensile tests have been performed on specimens machined from bolts according to the UNI EN ISO 898-1 standard (Figure 4-6). The results of these tensile tests are listed on Table 4-2.

Specimen ID	Location ID	Rockwell Hardness (RHA 60 kg)
P1	Close to the surface	64
	Center	64
	Close to the surface	65
P2	Close to the surface	65
	Center	64
	Close to the surface	65
Mean value		64.5

Table 4-1 : Results of the hardness tests performed on bolts

Figure 4-6 : Intact bolt and machined specimens tested to characterise the bolt material

Test ID	YS [MPa]	UTS [MPa]
T1	914	952
T2	912	953
T3	882	956
T4	916	962
Mean values	906	956

Table 4-2 : Results of the tensile tests performed on machined specimens

4.3.2.2 *Chemical composition*

The chemical composition of the tested Grade 8.8 bolts is given in Table 4-3.

Element	C	Si	Mn	P	S	B	Cr
Content (%)	0.200	0.015	0.980	0.013	0.015	0.0028	0.210
Element	Mo	Ni	Cu	N	Al	Ti	
Content (%)	0.003	0.025	0.026	0.004	0.038	0.028	

Table 4-3 : Chemical composition of tested bolts

4.3.3 Test schedule

The summary of the different tests performed on bolts is listed in Tables 4-4 & 4-5. It includes:

- 2 tests on bolts at room temperature ;
- 4 steady-state tests performed to compare the results obtained on M12 bolts with the values of Eurocode 3 that have been derived from tests performed on M20 bolts;
- 18 “natural fire tests” in tension and 15 “natural fire tests” in shear. In fact, the tensile tests have shown that the mechanical behaviour of bolts (see § 4.3.4) was reversible when the temperature has not been higher than 400°C during the heating phase. The natural fire tests on bolts in shear with $T_f = 400°C$ have not been performed.

Steady-state Tests		Natural fire tests		
$T_u = T_f$ [°C]	n. tests	T_u [°C]	T_f [°C]	n. tests
20	2	400	200	2
200	1		100	1
400	1		20	1
600	1	600	400	1
800	1		300	1
			200	2
			100	1
			20	1
		800	600	1
			400	1
			300	1
			200	2
			100	1
			20	1
		900	20	1

Table 4-4 : Detailed programme of tensile tests performed on bolts

Steady-state Tests		Natural fire tests		
$T_u = T_f$ [°C]	n. tests	T_u [°C]	T_f [°C]	n. tests
20	2	600	400	1
200	1		300	1
400	1		200	2
600	1		100	1
800	1		20	1
		800	600	1
			400	1
			300	1
			200	2
			100	1
			20	1
		900	20	1

Table 4-5 : Detailed programme of shear tests performed on bolts

4.3.4 Test results

4.3.4.1 Experimental observations

Figure 4-7 shows the bolts tested in tension after heated up to T_u = 600°C and cooled down to different T_f before the mechanical load was applied. One of the two tests in which T_f = 200°C has been missed and that bolt is not shown. Bolts are positioned in function of the test temperature T_u (from 20°C on the left to 400°C on the right).

Figure 4-7 : Bolts tested in tension after natural fire at different T_f temperatures after reaching T_u = 600°C

Out of 24 tensile tests performed on bolts, the failure by striction of the bolt has been obtained in 21 tests. In the other three tests, threads of the bolt and the nut are deformed but the thread stripping is only observed on a limited height of the two elements. The presence of a partial nut stripping could be explained by i) a lack of fit between the bolt and the nut or ii) by the fact that the nut has been submitted to bending deformations during the test and that the contact between the bolt and the nut was localised on a limited height of the nut. In this situation, the nut stripping should be observed in the contact zone (red zone on Figure 4-8b) and the other part of the nut (green zone on Figure 4-8b) should have remained intact.

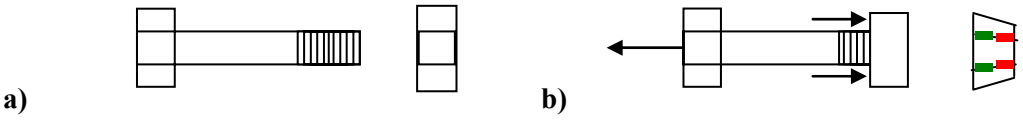

Figure 4-8 : Initial (a) and final (b) configurations of the bolt and the nut in presence of bending deformations

One of the three specimens that failed by partial nut stripping has been cut longitudinally at the University of Liege to observe the mode of failure. The fitting between cut elements is obtained in the position shown on Figure 4-9a. The deformations in the nut are situated in the internal part what is in contradiction with the two assumptions mentioned. It demonstrates that the nut was not completely screwed when the failure occurred, probably because the nut lost some turns during the test performance.

a) 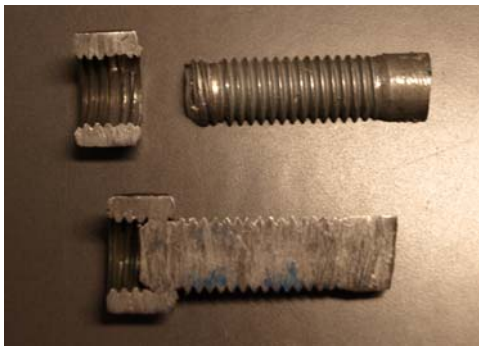 b) 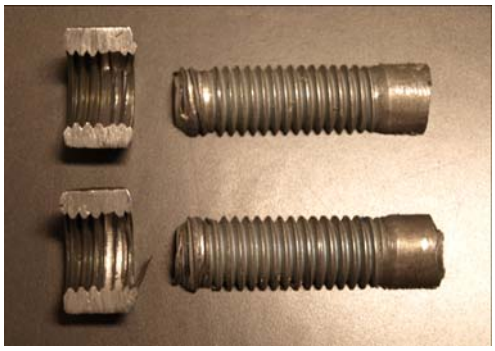

Figure 4-9 : Specimens cut longitudinally after a failure by nut stripping

These tests have consequently been rejected and the results have not been considered in the subsequent analytical work.

In shear tests, all the bolts failed according to the expected mode of failure and no test results have been rejected.

4.3.4.2 Interpretation of the basic measurements

Gross test results have required a pre-treatment in order to account for two types of out of control phenomena:

- For low load levels, disclosing of connection clearance in the test rig induces some spurious displacements and the force-displacement graph is not linear whereas the behaviour of the material is still elastic.
- The components of the test rig develop their own elongation during loading. Because the elongation was measured between two referential points located outside the furnace, this elongation of the test rig must be evaluated in order to measure correctly the elongation of the bolt.

The first operation of the data pre-treatment is a horizontal displacement of the origin of the force-displacement graph in order to eliminate the parasitic displacements due to the initial adjustments of the rig. The origin shift *s* is evaluated by calculating the slope of the straight line joining the points related to $N = 1/4\ N_{max}$ and $N = 3/4\ N_{max}$ and the new origin of the graph is the intersection between this line and the axis of displacements (Figure 4-10). For few cases, especially at high temperatures, the non-linear part of the diagram start before $3/4\ N_{max}$. Consequently, the same procedure has been used with the two points $N = 1/4\ N_{max}$ and $N = 1/2\ N_{max}$.

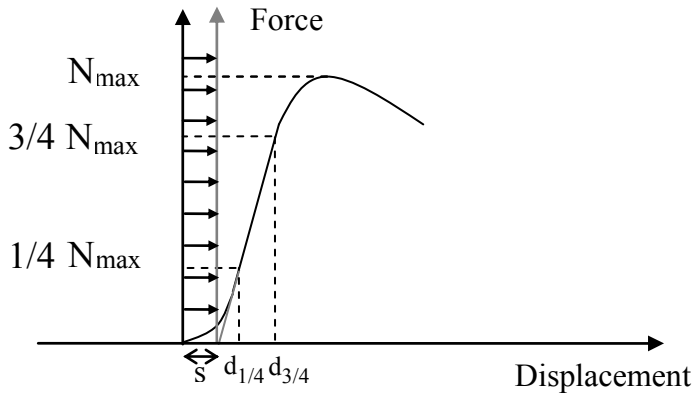

Figure 4-10 : Horizontal shift of the origin of the Force-displacement diagram

The second operation of the data pre-treatment consists in removing the spurious displacements caused by the deformations of the test rig during the test. For tensile tests, the variation of length has been measured between two points situated outside the furnace. Consequently, the measured values include the deformation of the bolt and the deformation of the test rig. The deformations of the tested bolt have been obtained under the assumptions, afterwards experimentally confirmed, that the Young's modulus of bolts at elevated temperature is equivalent to the one of carbon steel and that the test rig remains elastic during the complete mechanical test. Thus, the difference between the total measured deformations and the elastic deformations of the bolt predicted mathematically allows deriving the elastic stiffness of the test rig. According to the EN 1993-1-8, the stiffness coefficient of the component "bolt in tension" is given by Eq. 4-1 for two bolts, where A_s and L_b are respectively the reduced section area of the bolt and the bolt elongation length. For one bolt, the stiffness $S_{b,t}$ of the force-displacement diagram is deduced in Eq 4-2.

$k_{b,t} = 1.6\ A_s / L_b$	**4-1**
$S_{b,t} = 0.8\ E A_s / L_b$	**4-2**

The Young's modulus of bolts E is taken as equal to 210,000 MPa and the reduction of this modulus at elevated temperatures is supposed to follow recommendations of the EN 1993-1-2 for carbon steel. Graphically, elastic deformations of the test rig are subtracted from the complete experimental curve as illustrated on Figure 4-11.

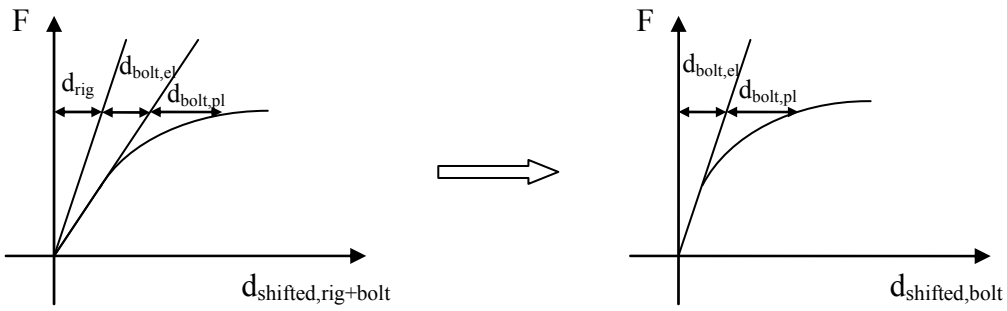

Figure 4-11 : Elimination of the spurious displacements due to the deformations of the test rig

A specific additional steady-state test has been performed at 400°C ($T_u = T_f = 400°C$) in order to verify the validity of this procedure for tensile tests. In this additional test, both the variation of the bolt length by use of an extensometer dedicated to high temperature tests and the variation of the distance between the external points of reference (same procedure as for all the other tests) have been measured. Figure 4-12 shows that the elongation measured by extensometers inside the furnace during the additional test ("Test 2 - Furnace Extensometers") compares very well with the corrected elongation from measures at the external points of reference ("Test 2 - Ext. Points of Reference"). The third curve ("Test 1 - Ext. Points of Reference Test 1 corrected") represents the force-displacement diagram of the previous steady-state test performed at 400°C, after corrections based on elastic assumptions.

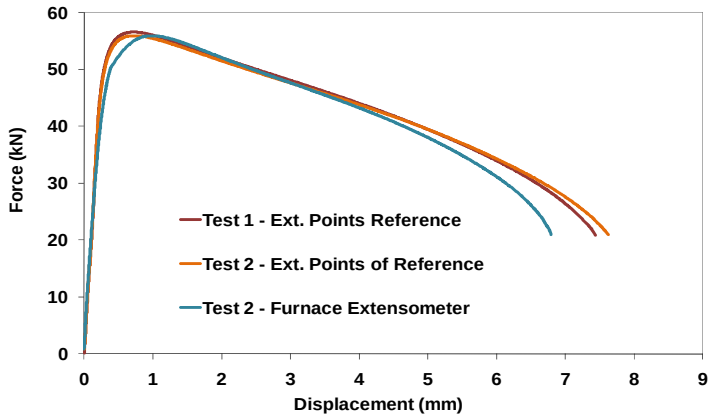

Figure 4-12 : Force-displacement diagram of bolts at $T_u = T_f = 400°C$

A completely similar procedure has been applied to the gross data obtained from the measurement of the shear tests. The method has been adapted for the evaluation of the initial stiffness of the bolt. The initial stiffness of the bolt in shear is taken from the recommendations of the EN 1993-1-8. The expression of the stiffness coefficient of bolts in shear $k_{b,s}$ (Eq. 4-3) is based on the assumption of the presence of two bolts. So, the initial stiffness of a unique bolt in single shear is given Eq. 4-4.

$k_{b,s} = \frac{16 n_b d^2 f_{ub}}{E d_{M16}} \quad [mm]$	**4-3**
$S_{b,s} = \frac{8 d^2 f_{ub}}{d_{M16}} \quad [kN/mm]$	**4-4**

In these expressions, d and d_{M16} are respectively the diameter of the bolt and the diameter of a reference M16 bolt, n_b is the number of shear planes, f_{ub} and E are the ultimate strength and the Young's modulus of the bolt.

4.3.5 Results obtained after pre-treatment of the gross data

4.3.5.1 Reduction factors for the bolt strength k_b obtained experimentally

In Eurocodes, the reduction factor k_b is defined as the ratio between the bolt ultimate strength at elevated temperature $f_{ub,Tu=Tf}$ and the bolt ultimate strength at room temperature $f_{ub,20°C}$. The values of this parameter obtained by the steady-state tests performed on M12 bolts are plotted on Figure 4-13. Even if slight differences are observed at 200°C, the comparison with the values of strength reduction factor k_b proposed in the EN 1993-1-2 and developed on the basis of M20 bolt tests (Figure 4-12) indicates that the diameter of the bolt has a limited influence on tests results.

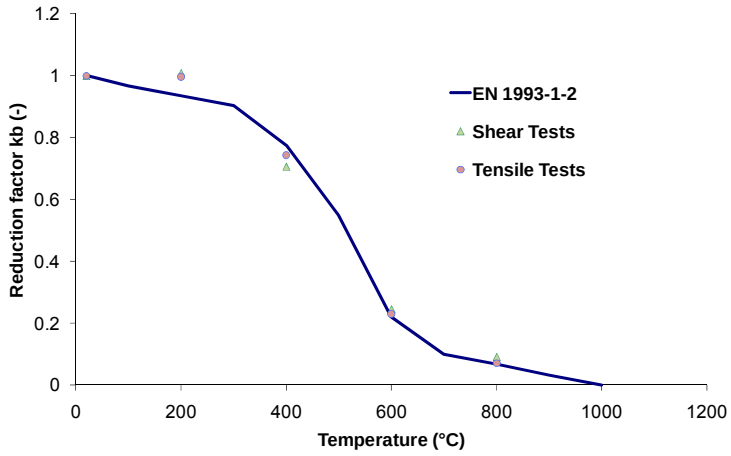

Figure 4-13 : Values of k_b given by steady-state tests (M12 bolts) and EN 1993-1-2 (M20 bolts)

The total reduction factors for bolt strength k_b obtained experimentally in the natural fire tests for three different maximum temperatures (T_u = 400°C, 600°C and 800°C) are plotted on Figures 4-14 & 4-15. The heating phase is represented by a test at room temperature and four steady-state tests realised at four different temperatures. The other three curves, representing the behaviour of bolts during the cooling phase, have been obtained by the so-called "natural fire tests" performed at different temperatures T_f after a same maximal temperature T_u has been reached (T_u = 400°C, 600°C or 800°C).

When two tests are performed under the same conditions (see Table 4-4) the average value of these results are used.

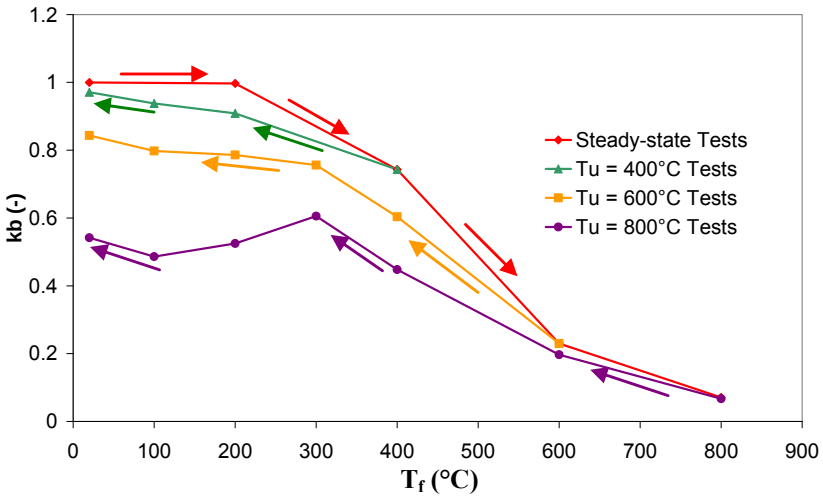

Figure 4-14 : Tensile tests - Reduction factor for bolt strength k_b

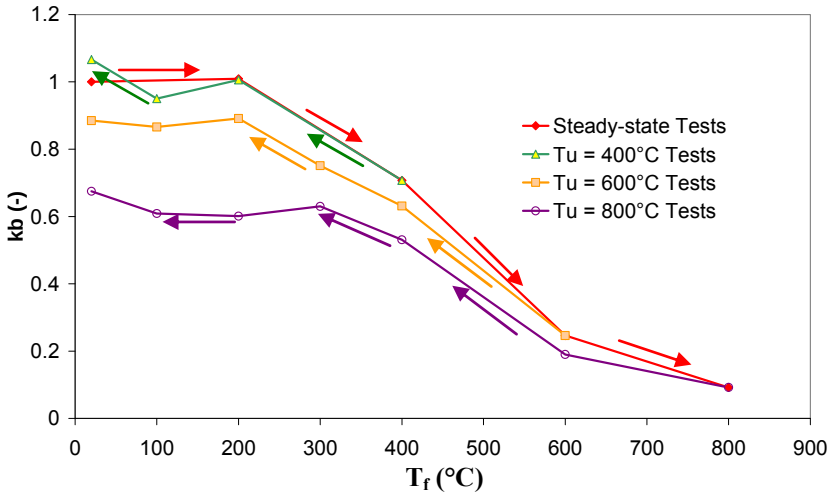

Figure 4-15 : Shear tests – Reduction factor for bolt strength k_b

4.3.5.2 Force-displacement diagrams obtained experimentally for bolts in tension

The results of tensile tests are not presented in the form of stress-strain diagrams because i) the cross-section of the bolt shank situated between the head and the nut is not constant and ii) additional deformations may develop in the nut zone when the force is transferred between the bolt and the shank. However, stress-strain expressions would be needed by engineers that would like, for example, to perform numerical simulations by representing bolts with brick elements. For the information of the reader, the distance between the bolt head and the nut is 50 mm and the bolt is half-threaded.

Figures 4-16 to 4-22 give an overview of the force-displacement relationships obtained from several tensile tests performed at the same temperature (Figures 4-16 to 4-19) or after reaching a same up

temperature T_u at the end of the heating phase (Figures 4-20 to 4-22). The brittle curves are related to the tests where a partial nut stripping occurred (Figure 4-18). No explication is given to the fact that these three tests are characterised by a same test temperature T_u = 200°C and it is supposed to be a coincidence during the test procedure. Bolts have a more ductile behaviour when the maximal temperature of the heating phase T_u is 800°C than for lower values of T_u. For values of T_u equal to 600°C or lower, the ultimate force is obtained for a 1-mm displacement and there is no horizontal yield plateau in the force-displacement diagram. This plateau exists in tests performed at higher temperatures and the measured forces only decreases after the displacement has reached 8 or 10 mm.

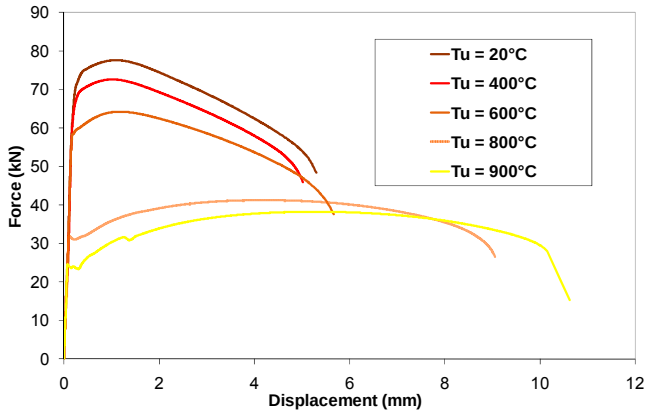

Figure 4-16 : Force-displacement diagrams obtained experimentally (tension) – T_f = 20°C

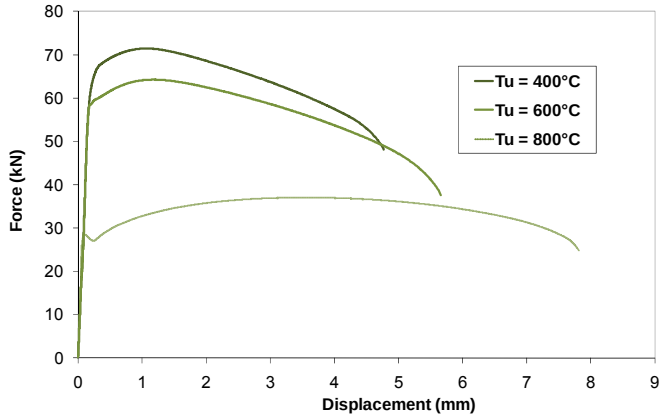

Figure 4-17 : Force-displacement diagrams obtained experimentally (tension) – T_f = 100°C

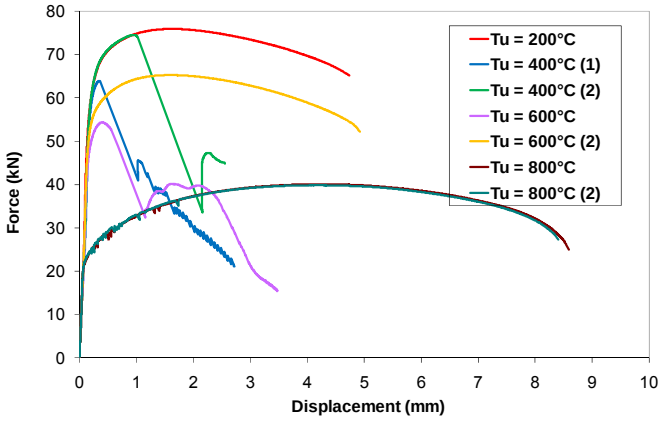

Figure 4-18 : Force-displacement diagrams obtained experimentally (tension) – T_f = 200°C

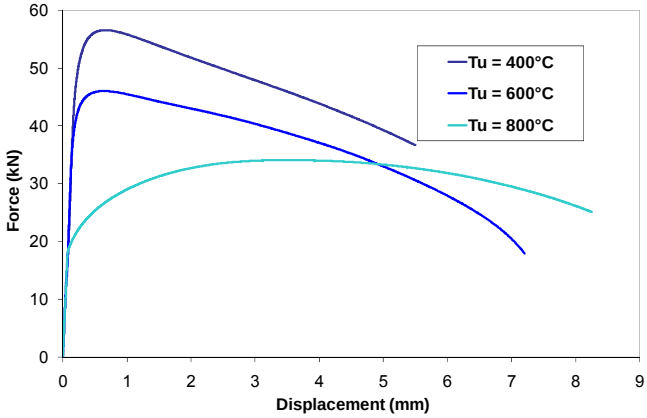

Figure 4-19 : Force-displacement diagrams obtained experimentally (tension) – T_f = 400°C

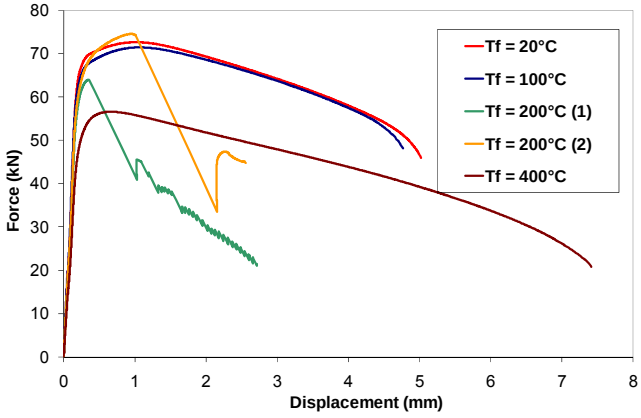

Figure 4-20 : Force-displacement diagrams obtained experimentally (tension) – T_u = 400°C

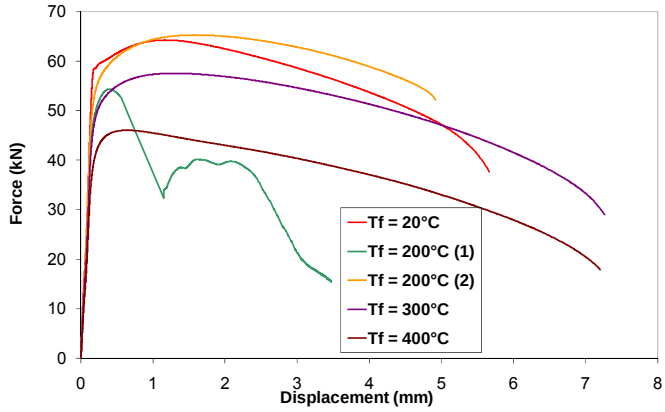

Figure 4-21 : Force-displacement diagrams obtained experimentally (tension) – T_u = 600°C

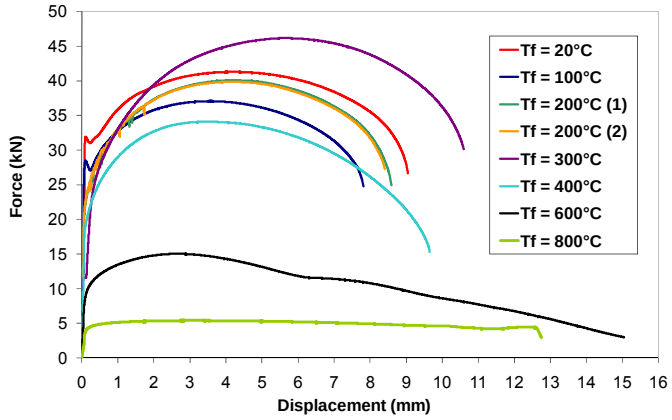

Figure 4-22 : Force-displacement diagrams obtained experimentally (tension) – T_u = 800°C

4.3.5.3 Force-displacement diagrams obtained experimentally for bolts in shear

The results of shear tests are presented through force-displacement diagrams. On Figures 4-23 to 4-25, each diagram gathers the post-treatment results obtained from all the shear tests performed at a same failure temperature T_f (20°C, 100°C and 200°C). The curves plotted on Figures 4-26 & 4-27 represents the results of tests where temperature has respectively reached 600°C and 800°C at the end of the cooling phase.

Similarly to what was demonstrated by tensile tests, bolts have a more ductile behaviour for high values of the up temperature T_u and/or the failure temperature T_f but the variation of the ductility under different thermal conditions is not so marked in shear tests. The large yield plateau observed in several tensile tests does not exist in shear tests except for one case (T_u = 800°C, T_f = 600°C). In two tests, the measurements have unwillingly been stopped before the unloading (Figure 4-24).

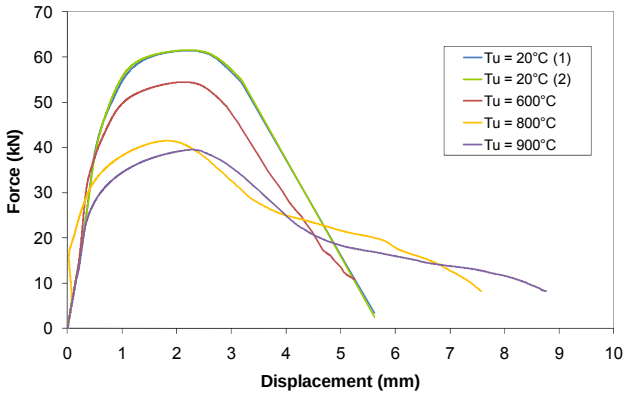

Figure 4-23 : Force-displacement diagrams obtained experimentally (shear) – T_f = 20°C

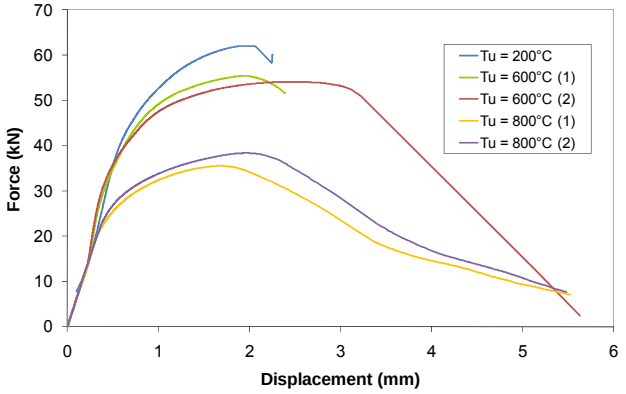

Figure 4-24 : Force-displacement diagrams obtained experimentally (shear) – T_f = 200°C

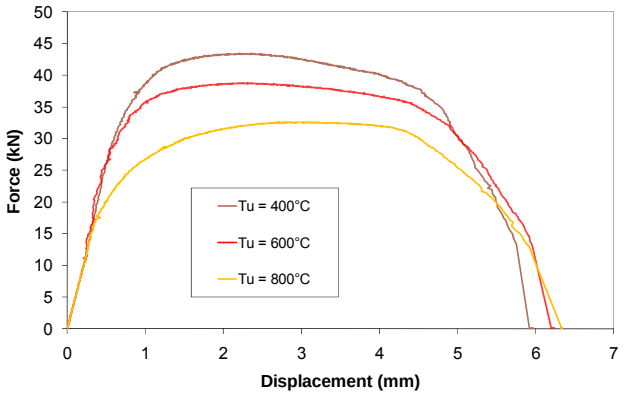

Figure 4-25 : Force-displacement diagrams obtained experimentally (shear) – T_f = 400°C

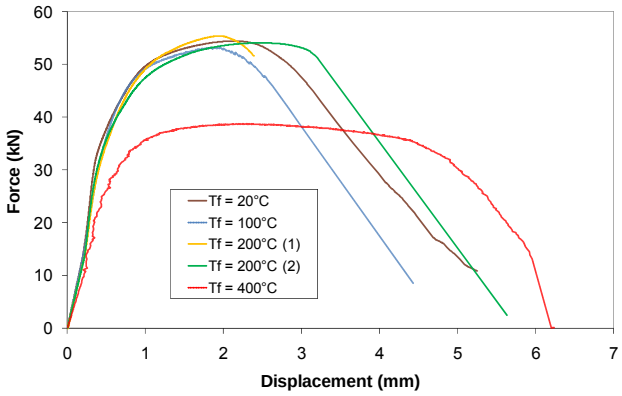

Figure 4-26 : Force-displacement diagrams obtained experimentally (shear) – T_u = 600°C

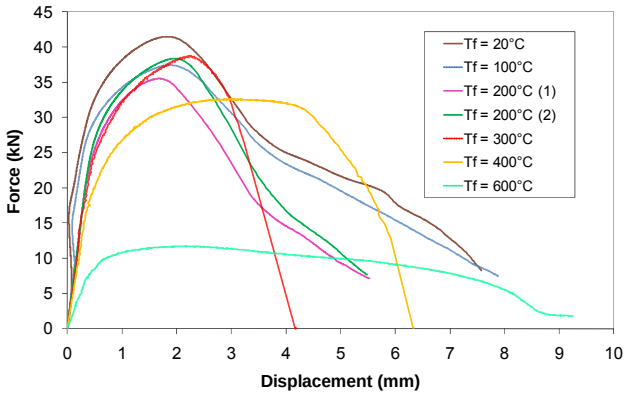

Figure 4-27 : Force-displacement diagrams obtained experimentally (shear) – T_u = 800°C

4.4 Analytical models for bolts under heating and subsequent cooling

In order to integrate the force-displacement relationship of bolts submitted to tensile or shear forces during a natural fire into models based on the Component Method, it is necessary to define simple mathematical models established on the experimental results presented previously. Firstly, a method will be given to calculate the reduction of the bolt strength as a function of the up temperature T_u and the failure temperature T_f. This step consists in extending the field of application of the reduction factor for the bolt strength k_b, given in the current Eurocodes, to the cooling phase of a natural fire. A unique method has been developed for the resistance of bolts in tension and shear. Secondly, separate force-displacement models have been proposed for bolts under tensile or shear forces.

4.4.1 Evolution of the ultimate bolt strength f_{ub} during cooling

A reduction factor for the non-reversibility of the bolt strength k_{nr} is defined as the ratio between the bolt ultimate strength f_{ub} in steady-state tests (direct heating until the temperature $T_u = T_f$) and the bolt ultimate strength f_{ub} at the same temperature T_f during cooling. This ratio has been plotted as individual points for each test on Figure 4-28. The following observations can be made:

- For T_f below 500°C, k_{nr} remains constant whatever the maximal temperature T_u. This means that the permanent loss of strength induced by cooling has fully developed when the temperature comes back to 500°C.
- When the temperature at the end of the heating phase T_u is not higher than 500°C, k_{nr} is approximately equal to 1. This means that no permanent loss of strength occurs if the temperature does not exceed 500°C.
- Shear tests seem to give slightly higher k_{nr} values than tensile tests.

Based on the experimental results, the residual bolt ultimate strength $f_{ub}\left(T_f, T_u\right)$ during the cooling phase should be calculated according to the following method:

a) EN 1993-1-2 gives the reduction of the bolt strength $k_b\ (T_f)$ without considering the effect of cooling;
b) The additional effect of cooling, k_{nr}, is calculated from Eqs 4-5 and 4-6:

$k_{nr} = 1$	$for \quad T_u \le 500°C$	**4-5**
$k_{nr} = 1 - \frac{0.4}{300}\left(T_u - \max\left(T_f\ ; 500°C\right)\right)$	$for \quad 500°C \le T_u \le 800°C$	**4-6**

c) Finally, the value of the ultimate bolt strength accounting for the non-reversible behaviour of steel is given by Eq. 4-7. :

$f_{ub,T_t,T_u} = k_{b,T_t}\, k_{nr,T_t,T_u}\, f_{ub,20°C}$	**4-7**

The analytical expressions of k_{nr} are given below for the three particular values of T_u for which experimental results are available (Eqs 4-8 to 4-10). It has been decided to use the same expressions for tension and shear, even if the experimental values are slightly higher for shear. These expressions are compared with the values obtained from tensile and shear tests on Figure 4-28.

$k_{nr} = 1$	$for \quad T_u = 400°C$	**4-8**

$k_{nr} = \max\left(0.83\,;\,0.83 + 0.17\left(\frac{T_f - 500}{100}\right)\right) \quad for \quad T_u = 600°C$	**4-9**
$k_{nr} = \max\left(0.6\,;\,0.6 + 0.4\left(\frac{T_f - 500}{300}\right)\right) \quad for \quad T_u = 800°C$	**4-10**

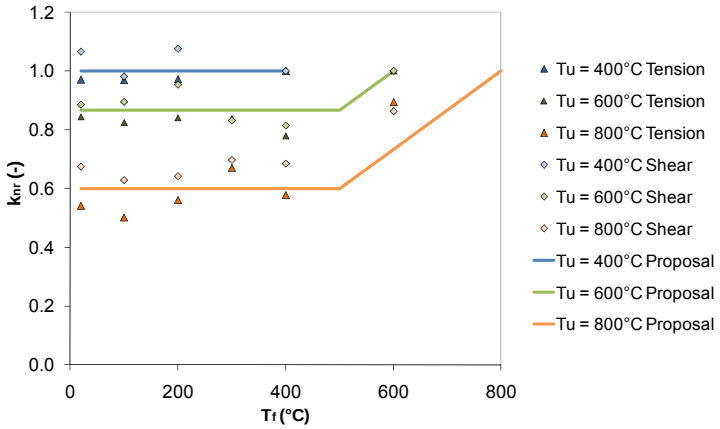

Figure 4-28 : Tensile and Shear tests – Reduction factor for yield strength due to non-reversible

The comparison between the reduction factors for bolt strength k_b during the cooling phase obtained experimentally and evaluated analytically are plotted on Figures 4-29 (tensile tests) and 4-30 (shear tests). In the latter one, the analytical expression seems to be a little bit too conservative but lower values would be unsafe in the case of tensile tests.

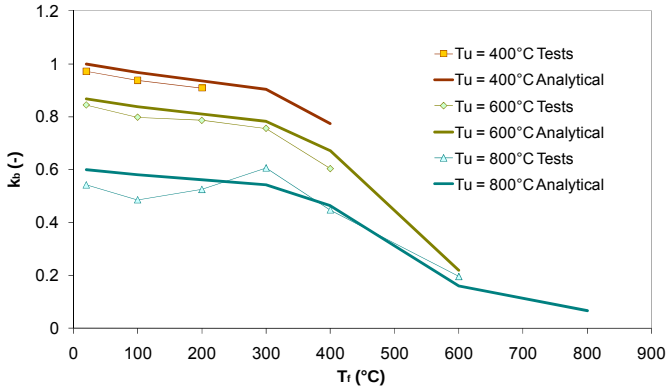

Figure 4-29 : Tensile Tests – Comparison between experimental and analytical values of the reduction factor for bolt strength k_b

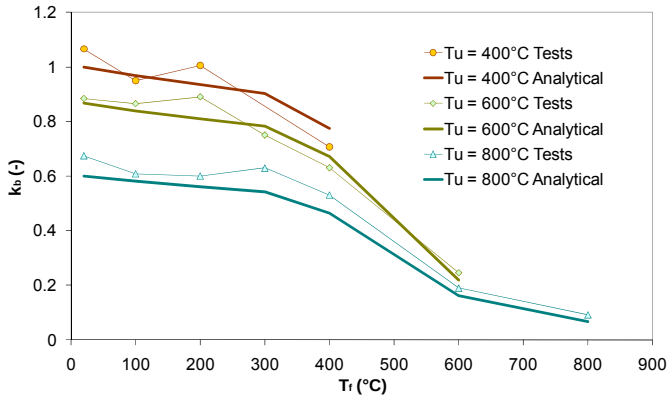

Figure 4-30 : Shear Tests – Comparison between experimental and analytical values of the reduction factor for bolt strength k_b

4.4.2 Force-displacement diagram in tension during heating and cooling phases

4.4.2.1 Shape and evaluation of the parameters of the force-displacement diagram

A mathematical model for the stress-strain diagram of bolts has been recently proposed and calibrated by use of the experimental results reported from the tests performed by Riaux on bolts at elevated temperatures [RFCS, 2008]. This mechanical model is composed of an elastic branch, a branch of ellipsa, a yield plateau and a bilinear descending branch (Figure 4-31). The differences with this diagram and the one given in the En 1993-1-2 for carbon steel are i) the yield plateau is shorter for bolts than for carbon steel, ii) the descending branch is bilinear and iii) the failure strain ε_u is equal to 0.35 for bolts, instead of 0.2 for carbon steel.

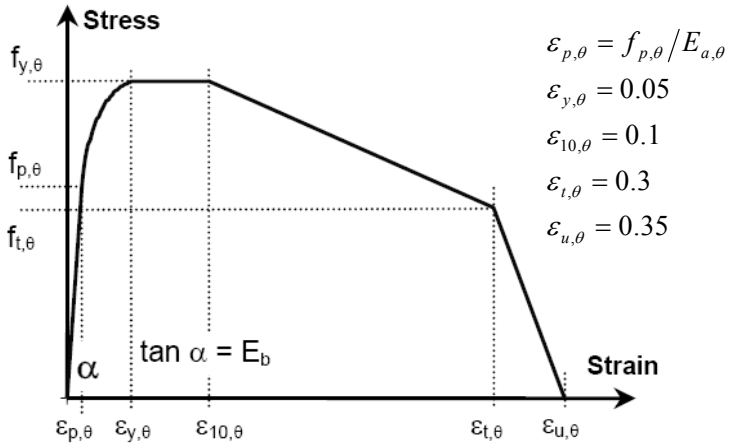

Figure 4-31 : Mathematical model proposed on the basis of results obtained from Riaux tests

This model has been translated into a force-displacement diagram and the horizontal plateau has been deleted so that $\varepsilon_{y,\theta}$ and $\varepsilon_{10,\theta}$ would be equivalent in the stress-strain form. The parameters of the stress-strain diagram $f_{y,\theta}$, $f_{p,\theta}$, $f_{t,\theta}$, $\varepsilon_{y,\theta}$, $\varepsilon_{t,\theta}$ and $\varepsilon_{u,\theta}$ have been translated into $F_{ub,\theta}$, $F_{pb,\theta}$, $F_{tb,\theta}$, $d_{pb,\theta}$, $d_{yb,\theta}$, $d_{tb,\theta}$ and

$d_{ub,\theta}$. Analytical expressions of these new parameters have been calibrated with the experimental tests performed at the Centro Sviluppo Materiali during both the heating and cooling phases.

- **Ultimate tensile resistance $F_{ub,\theta}$**

The calculation of the bolt ultimate strength $f_{ub,\theta}$ has been exposed in detail in § 4.4.1. The ultimate tensile force that a bolt can resist to is equal to this strength multiplied by the reduced cross-section of the bolt (Eq. 4-11).

$$F_{ub,T_u,T_f} = k_{nr,T_u,T_f}\, k_{b,T_f}\, f_{ub,20°C}\, A_s \qquad \textbf{4-11}$$

- **Proportional tensile resistance $F_{pb,\theta}$**

At elevated temperatures, the proportional limit $f_{p,\theta}$ and the yield limit $f_{y,\theta}$ of carbon steel are distinguished in the EN 1993-1-2 and the ratio between these two values $k_{pc,\theta} = f_{p,\theta}/f_{y,\theta}$ is given in Table 4-6. It should be noted that the ratio $k_{p,\theta}$ given in the Eurocodes for carbon steel is the ratio $f_{p,\theta}/f_{y,20°C}$ and must not be merged with $k_{pc,\theta}$.

For bolts, the ratio $k_{pb,\theta}$ is defined as the ratio between the proportional tensile force $F_{pb,\theta,}$ and the ultimate tensile force $F_{ub,\theta}$. In the proposed model, the ratio $k_{pb,\theta}$ only depends on the maximal temperature of the heating phase T_u. Table 4-6 gives the value of this ratio for different values of T_u. For intermediate values, no test results or few of them are available. As a simple assumption, linear interpolations will be drawed between the points of the proposed table.

T (°C)	$k_{pc,\theta,EN\ 1993\text{-}1\text{-}2}$
20	1
200	0.807
400	0.420
600	0.383
800	0.454
900	0.625

T_u (°C)	$k_{pb,\theta}$
20	0.9
200	0.8
400	0.75
600	0.75
800	0.6
900	0.6

Table 4-6 : Values of $k_{pc,\theta}$ (carbon steel) and $k_{pb,\theta}$ (bolts)

At room temperature, k_{pb} is equivalent to the coefficient k_2 used in the EN 1993-1-8 to evaluate the resistance of bolts in tension $F_{t,Rd}$ (Eq. 4-12). The recommended value of this coefficient is 0.9 except for countersank bolts, where the recommended value is 0.63.

$$F_{t,Rd} = k_2\, f_{ub}\, A_s \qquad \textbf{4-12}$$

The initial stiffness $S_{b,t}$ of the bolt in tension is given in Eq. 4-2. The proportional displacement $d_{pb,\theta}$ is the ratio between the proportional tensile force $F_{pb,\theta}$ and the initial stiffness $S_{b,t}$.

● **Proportional displacement $d_{pb,\theta}$**

The reduction factor for bolt strength k_b is given in the EN 1993-1-2 but no specific reduction factor for the Young's modulus of bolts exists in the Eurocode. Similarly to what has been assumed during the operation of data pre-treatment, the evolution of the Young's modulus of bolts is supposed be the same as the one defined in the EN 1993-1-2 for carbon steel.

● **Yield displacement $d_{yb,\theta}$**

The yield displacement $d_{yb,\theta}$ is the variation of the bolt length when the applied force reaches the ultimate tensile force $N_{ub,\theta}$. The value of this displacement is fixed equal to 1 mm.

● **Point of inflexion ($F_{tb,\theta}$; $d_{tb,\theta}$)**

By analysing the force-displacement curves obtained experimentally (after treatment of the data), it can be observed that all the curves pass by the point ($F_{tb,\theta}$ = 40 kN ; $d_{tb,\theta}$ = 5 mm) or ($F_{tb,\theta} = F_{ub,\theta}$; $d_{tb,\theta}$ = 5 mm) when the ultimate tensile resistance $F_{ub,\theta}$ is smaller than 40 kN. In the latter case, the force-displacement relationship includes a horizontal plateau.

● **Ultimate displacement $d_{ub,\theta}$**

In good approximation, the ultimate displacement $d_{ub,\theta}$ is 12.5 mm in the tests performed after temperature reached 800°C at the end of the heating phase. In other cases ($T_u \leq 600$°C), the ultimate displacement $d_{ub,\theta}$ is around 7.5 mm.

4.4.2.2 Comparison between the proposed model and experimental results

In the tests performed for characterising the bolt material, the ultimate tensile stress was 956 MPa. However, the two tensile tests on bolts at 20°C have given lower values of the ultimate tensile strength f_{ub} than expected. After dividing the maximal applied force by the reduced cross-section area (A_s = 84.3 mm²), the ultimate tensile stresses measured are 886 MPa and 921 MPa. For the following comparisons, the ultimate tensile stress has been taken as the average value 903 MPa.

Approached curves resulting from the application of the proposed mathematical model are confronted to the experimental curves on Figures 4-32 to 4-38. Figures 4-32 and 4.33 are focused on the force-displacement diagrams of bolts at elevated temperatures with no cooling phase. The others figures show that the proposed model also gives good predictions of the force-displacement diagrams of bolts

in tension during the cooling phase. On Figure 4-38, the correlation is slightly less good than for other cases; this is due to the disparity of the coefficient for non reversibility k_{nr} obtained from tests on bolts heated to T_u = 800°C before cooling (Figure 4-28).

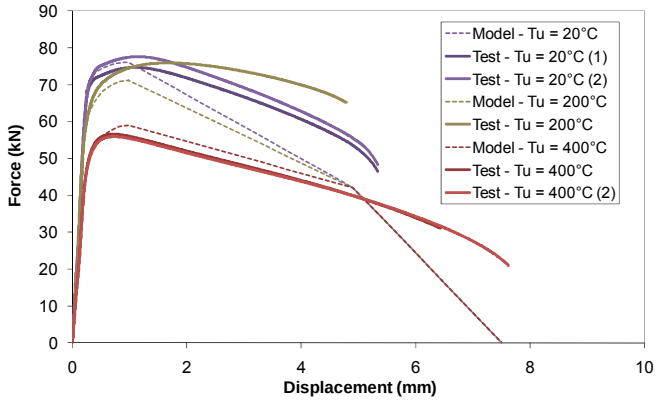

Figure 4-32 : Comparison between analytical model for tension and experimental results – Steady-state tests with no cooling phase ($T_f = T_u \leq 400°C$)

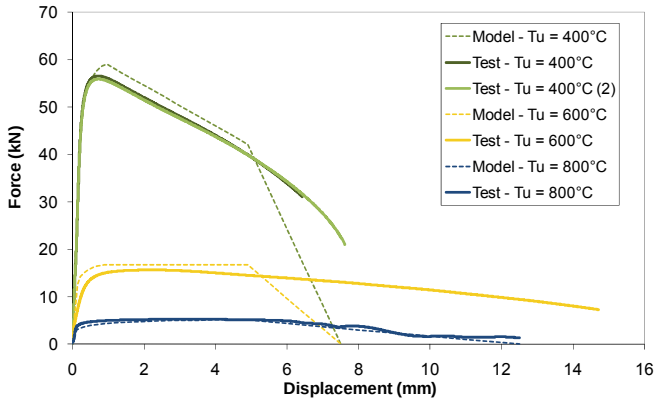

Figure 4-33 : Comparison between analytical model for tension and experimental results – Steady-state tests with no cooling phase ($T_f = T_u \geq 400°C$)

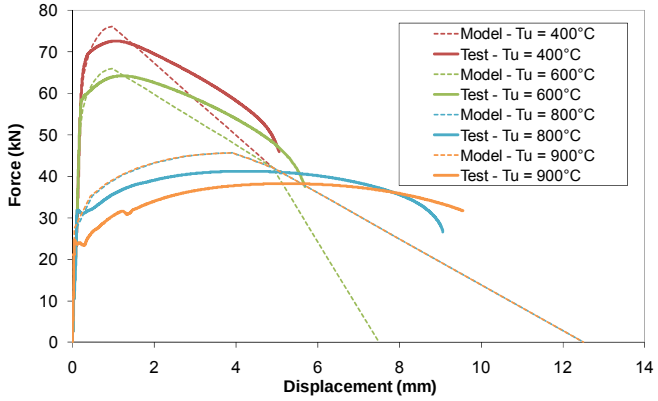

Figure 4-34 : Comparison between analytical model for tension and experimental results – T_f = 20°C

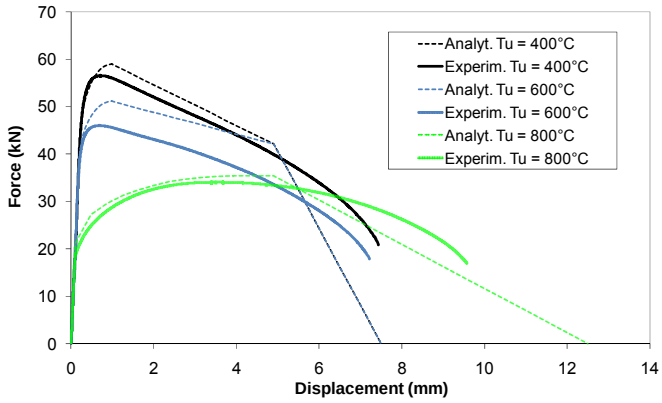

Figure 4-35 : Comparison between analytical model for tension and experimental results – T_f = 400°C

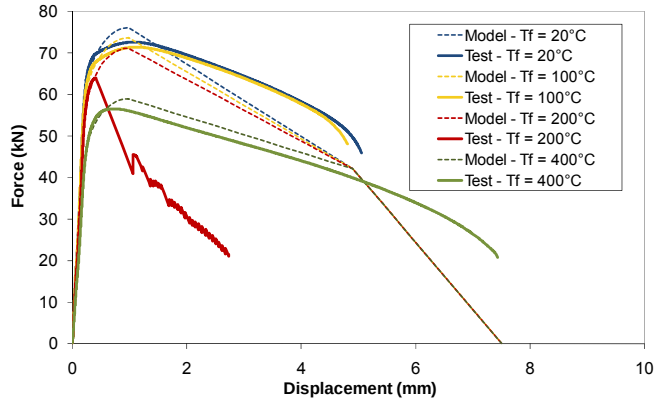

Figure 4-36 : Comparison between analytical model for tension and experimental results – T_u = 400°C

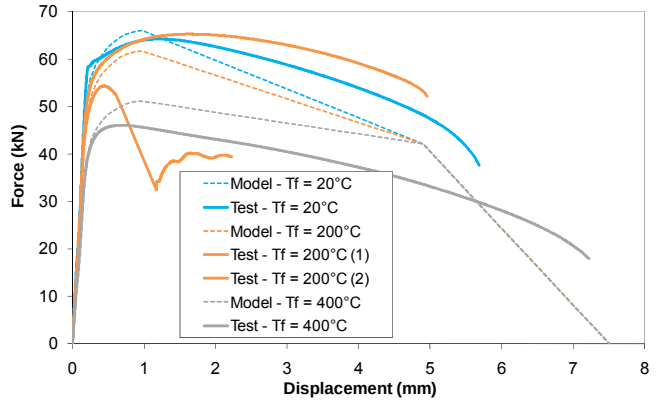

Figure 4-37 : Comparison between analytical model for tension and experimental results – T_u = 600°C

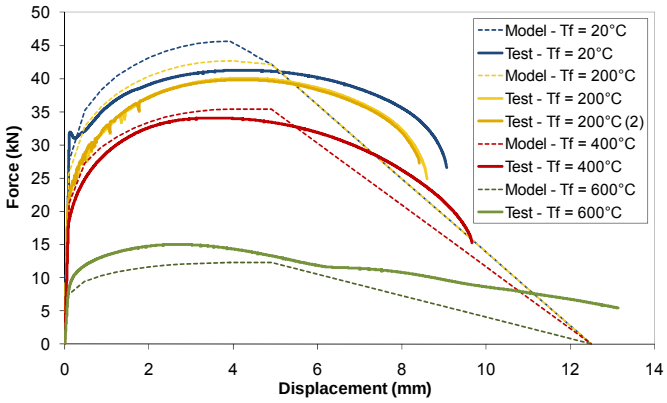

Figure 4-38 : Comparison between analytical model for tension and experimental results – T_u = 800°C

4.4.3 Force-displacement diagram in shear during heating and cooling phases

4.4.3.1 Existing model at room temperature [Henriques, 2007]

The response of bolts subjected to shear forces at room temperature has been investigated and a model has recently been proposed by Henriques on the basis of experimental double-shear tests performed on bolts of different grades (5.8, 8.8 and high-strength bolts) and different diameters (M16, M20 and M24 bolts) in Moscow [Karmalin, 1989]. This mechanical model is trilinear and the different parameters of this law have been expressed as a function of the grade and the diameter of the bolt. The EN 1993-1-8 only allows calculating the elastic branch of this model. The procedure for evaluating all the parameters of this force-displacement model is described hereafter. In order to avoid any confusion with the parameters of the model for bolts in tension, the parameters proposed by Henriques will be kept similar in the present work.

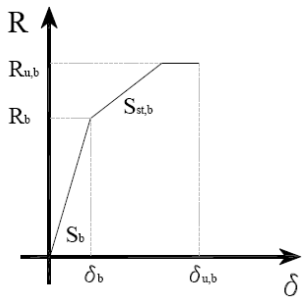

Figure 4-39 : Tri-linear law applied to bolt in shear at room temperature [Henriques, 2007]

● **Initial Stiffness S_b**

The expression of the initial stiffness S_b mentioned in the EN 1993-1-8 has already been used for the pre-treatment of the experimental results (called $S_{b,v}$ in Eq. 4-4).

● **Elastic Resistance R_b**

In the EN 1993-1-8, the design resistance of bolts in shear $F_{v,Rd}$ is equal to the elastic resistance R_b.

$R_b = F_{v,Rd} = \alpha_v \, f_{ub} \, A$	**4-13**

In this equation, A is the tensile stress area of the bolt A_s if the shear plane passes through the threaded portion of the bolt and the gross cross-section of the bolt if the shear plane passes through the unthreaded portion of the bolt. For bolt classes 4.6, 5.6 and 8.8 with shear plane in the threaded part of the bolt, the coefficient α_v is 0.5. In all other cases, α_v is 0.6. The elastic deformation δ_b may be derived by division of the elastic resistance by the initial stiffness S_b (Eq. 4-14)

$\delta_b = \dfrac{R_b}{S_b}$	**4-14**

● **Strain-Hardening Stiffness $S_{st,b}$**

The strain-hardening stiffness $S_{st,b}$ is defined as a percentage of the initial S_b (Eq. 4-15), where the factor β is dependant of the bolt grade. For grade 8.8 bolts, the proposed value of β is 7.

$S_{st,b} = \dfrac{S_b}{\beta}$	**4-15**

● **Ultimate Resistance $R_{u,b}$**

Under pure shear, the maximum allowed stress τ_{ub} is 0.7 f_{ub} so that the ultimate resistance of a bolt in shear is given by Eq. 4-16. The ratio between the elastic resistance R_b and the ultimate resistance $R_{b,u}$ depends on the value of α_v used in Eq. 4-13. Under the assumption that the shear plane passes through the threaded part of the shank, this ratio depends on the bolt grade (Eqs 4-17 & 4-18).

$R_{u,b} = 0.7 \, f_{ub} \, A$		**4-16**
$R_{u,b} = 1.15 \, R_b$	*for bolt grades* 4.6, 5.6 *and* 8.8	**4-17**
$R_{u,b} = 1.4 \, R_b$	*for bolt grades* 5.8 *and* 10.9	**4-18**

However, these equations do not correlate well with experimental tests of Moscow. For grade 8.8 bolts, a new ratio has been determined (Eq. 4-19) for M16, M20 and M24 bolts.

$R_{u,b} / R_b = 1.05$	**4-19**

● **Ultimate Deformation $\delta_{u,b}$**

The ultimate deformation $\delta_{u,b}$ has been defined as a function of the elastic resistance R_b and the initial stiffness S_b (Eq. 4-20) and the coefficient η has been calibrated on the results of the Moscow tests [Karmalin, 1989]. This coefficient varies with the bolt diameter (Table 4-7).

$$\delta_{u,b} = \eta \frac{R_b}{S_b} \qquad \textbf{4-20}$$

Bolt Diameter	η
M16	3.0
M20	3.5
M24	4.2

Table 4-7 : Values of the factor η as a function of the bolt diameter

Finally, the comparison between the experimental measurement and the Henriques model is given in Figure 4-40. In his work, the author underlines that, for 8.8 bolts, the curves are very close to the maxima of the experimental results and expresses the idea that it is due to an incorrection in the plotting of the experimental results. The orange line represents the level of the ultimate resistance $R_{u,b}$ of an M24 bolt calculated by Eq. 4-16 and the expected values of the parameters R_b, δ_b and $R_{u,b}$ are given in Table 4-8.

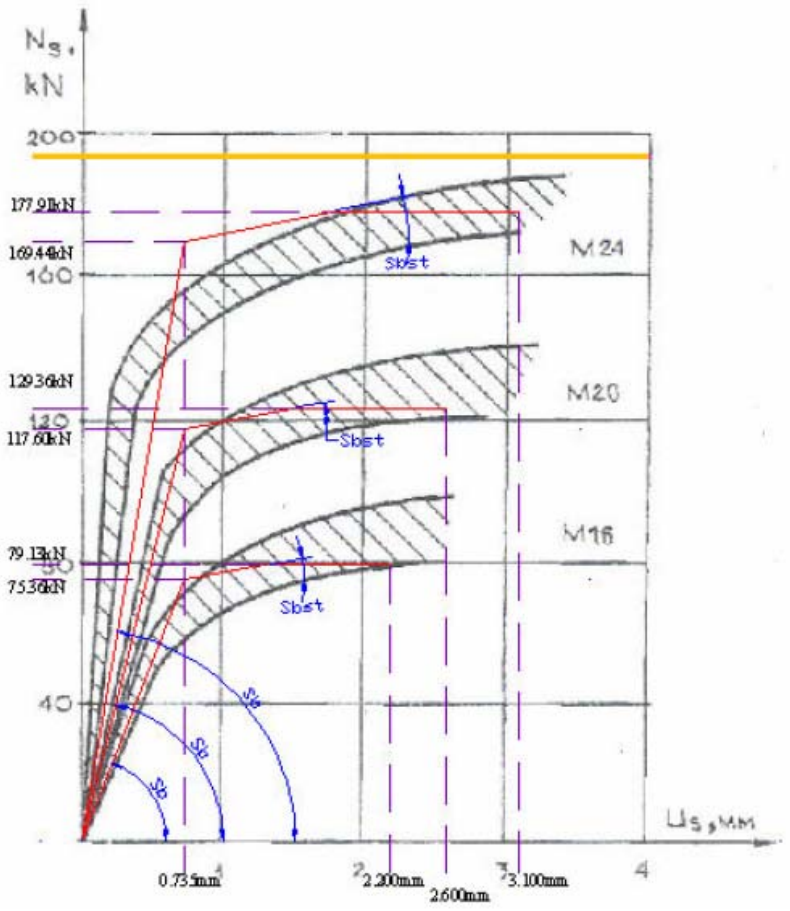

Figure 4-40 : Experimental and derived curves given by the Henriques model [Henriques, 2007]

Bolt Diameter	M16	M20	M24
R_b (kN)	75.36	117.6	169.44
δ_b (mm)	0.735	0.735	0.735
$R_{u,b}$ (kN)	86.66	135.24	194.86

Table 4-8 : Expected values of R_b, d_b and $R_{u,b}$ for grade 8.8 bolts

4.4.3.2 Modifications to the Henriques model for M12 grade 8.8 bolts

First of all, it should be mentioned that the work of Henriques is focused on M16, M20 and M24 bolts. The model could be easily translated to M12 bolts except for the ultimate deformation $\delta_{u,b}$ that, via the factor η, varies significantly with the bolt diameter (Table 4-8). However, some parameters of the Henriques model will be slightly modified, even at room temperature. The explanations of these modifications are given here and are linked to the observation of the Figure 4-40.

- The ratio between the values of the elastic resistance R_b and the ultimate resistance $R_{u,b}$ obtained experimentally seems to be higher than the proposed ratio 1.05. The value of 1.05

seems to be a consequence of the difference observed between the values elastic resistances experimentally and predicted with the Eurocode recommendations. For grade 5.8 bolts and high-strength bolts, the proposed ratios are respectively 1.58 and 1.44. To the author, the real ultimate strength f_{ub} of the tested grade 8.8 bolts has probably been over-estimated.

- The factor β has probably been over-estimated for the same reason. The proposed value of β is only 2.5 for grade 5.8 bolts and 1.5 for high-strength bolts, instead of 7 for grade 8.8 bolts.

- Finally, the ultimate deformation $\delta_{u,b}$ of the model is smaller than the experimental values of $\delta_{u,b}$ and the factor elastic deformation δ_b is slightly over-estimated.

In order to obtain a good correlation with the results of the tests performed at the Centro Sviluppo Materiali on M12 bolts, the adapted values considered are given in Table 4-9. In the future, the ratio $R_{u,b}/R_{u,b}$ will be represented by the factor κ.

β	5
κ	1.2
η	4

Table 4-9 : Adapted values of factors β, κ and η at 20°C

In the model proposed by the author, the force-displacement curve includes a branch of ellipsa between the elastic resistance R_b and the ultimate resistance $R_{b,u}$, and a linear descending branch is added at the end of the yield plateau (Figure 4-41). The failure displacement $\delta_{f,b}$ is defined as the displacement at which the resistance come back to 0.

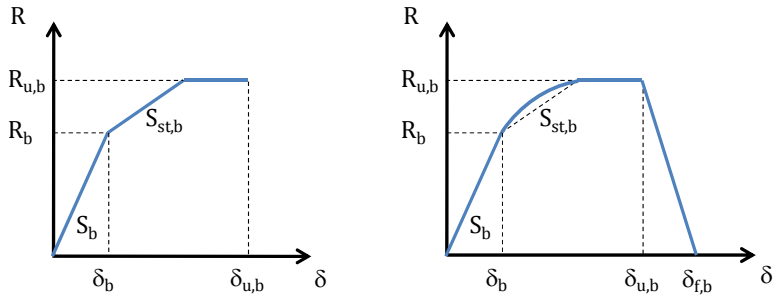

Figure 4-41 : Henriques tri-linear law (left) and non-linear law proposed by the author (right)

At room temperature, the failure displacement of a M12 grade 8.8 bolt is 6 mm. The two models are compared with the results of the two shear tests performed at the Centro Sviluppo Materiali on bolts at room temperature (Figures 4-42 and 4-43). The horizontal plateau of the Henriques model is not drawn because the factor η is not determined for M12 bolts. The under-estimation of the ultimate

resistance $R_{b,u}$ by the Henriques model is clear for these two tests. Finally, the denomination of the characteristic deformations is translated into characteristic displacements to avoid any confusion because the signification of the French word “déformation” is “strain”.

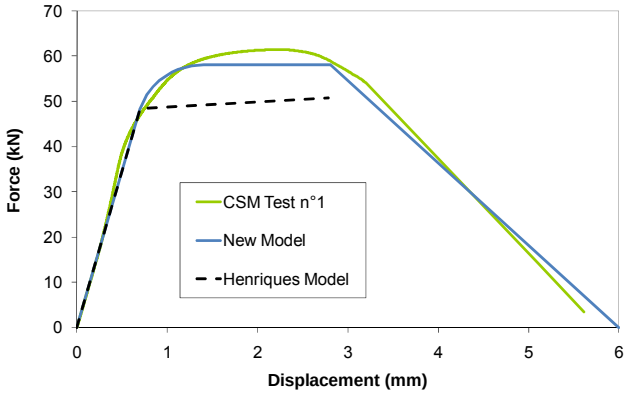

Figure 4-42 : Comparison of the mathematical models for shear with CSM test n°1 on M12 bolts

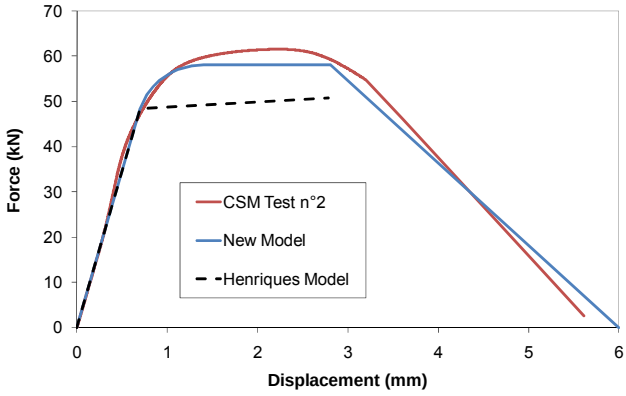

Figure 4-43 : Comparison of the mathematical models for shear with CSM test n°2 on M12 bolts

4.4.3.3 Extension of the Henriques model to the heating and cooling phases of a fire for M12 grade 8.8 bolts

The new model based on the Henriques work has been adapted to represent the force-displacement diagrams of bolts in shear at elevated temperatures, including both the heating and cooling phases of a fire. The procedure to evaluate the characteristic points of the diagrams is described hereafter.

● **Initial Stiffness $S_{b,\theta}$**

The initial stiffness of a bolt in shear S_b is multiplied by the reduction factor of the Young’s modulus k_E defined the EN 1993-1-2 to obtain the initial stiffness of the bolt in shear at elevated temperature $S_{b,\theta}$ (Eq. 4-21). The evolution of the initial stiffness is supposed to be reversible.

$S_{b,T_f} = k_E \, S_{b,20°C}$	**4-21**

● **Elastic Resistance $R_{b,\theta}$**

At elevated temperatures, the elastic resistance $R_{b,20°C}$ is multiplied by the reduction factor for bolts k_b (EN 1993-1-8) and the reduction factor for the non-reversible behaviour k_{nr} (Eq. 4-22). The value of k_{nr} depends on the test temperature T_f and the maximal temperature the bolt has been heated to T_u (Eqs 4-5 & 4-6). For grade 8.8 bolts, the coefficient α_v is kept equal to 0.6. The elastic displacement $d_{b,\theta}$ is obtained by coupling the two previous equations (Eq. 4-23).

$R_{b,T_u,T_f} = k_{b,T_f} \, k_{nr,T_u,T_f} \, R_{b,20°C}$	**4-22**
$\delta_{b,T_u,T_f} = \dfrac{R_{b,T_u,T_f}}{S_{b,T_f}} = \dfrac{k_{b,T_f} \, k_{nr,T_u,T_f}}{k_{E,T_f}} \dfrac{R_{b,20°C}}{S_{b,20°C}}$	**4-23**

● **Strain-Hardening Stiffness $S_{st,b,\theta}$**

At elevated temperatures, the factor β is expressed in Eq. 4-25 as the product of one term β_f that depends on the test temperature T_f (Table 4-11a) and one term β_u that depends on the maximal temperature of the heating phase T_u (Table 4-11b).

$\beta_{T_u,T_f} = S_{b,T_u,T_f} \big/ S_{st,b,T_u,T_f} = \beta_f \, . \, \beta_u$	**4-24**

a)

T_f (°C)	β_f
20	5
200	5
400	5
600	4
800	3
900	-

b)

T_u (°C)	β_u
20	1
200	1
400	1
600	1
800	2
900	2

Table 4-10 : Values of the factors β_f (a) and β_u (b) at elevated temperatures

● **Ultimate Resistance $R_{u,b,\theta}$**

The ratio κ between the values of the elastic resistance R_b and the ultimate resistance $R_{u,b}$ of grade 8.8 bolts is under-estimated by Henriques and the value of 1.2 has been proposed at 20°C, instead of 1.05 previously. At elevated temperatures, this ratio is expressed in Eq. 4-25 as the product of one term κ_f that depends on the test temperature T_f (Table 4-11a) and one term κ_u that depends on the maximal temperature of the heating phase T_u (Table 4-11b).

$\kappa_{T_u,T_f} = R_{u,b,T_u,T_f} \big/ R_{b,T_u,T_f} = \kappa_f \, . \, \kappa_u$	**4-25**

a)

T_f (°C)	κ_f
20	1.2
200	1.2
400	1.2
600	1.4
800	1.75
900	-

b)

T_u (°C)	κ_u
20	1
200	1
400	1
600	1
800	1.1
900	1.1

Table 4-11 : Values of the factors κ_f (a) and κ_u (b) at elevated temperatures

● **Ultimate Displacement $\delta_{u,b,\theta}$**

The factor η of Eq. 4-20 is also defined as the product between one term η_f that depends on the test temperature T_f (Table 4-12a) and one term η_u that depends on the maximal temperature of the heating phase T_u (Table 4-12b).

$$\eta = \frac{\delta_{b,T_u,T_f}}{\delta_{u,b,T_u,T_f}} = \eta_f \ \eta_u \qquad \textbf{4-26}$$

a)

T_f (°C)	η_f
20	4
200	5
400	6
600	6
800	6
900	-

b)

T_u (°C)	η_u
20	1
200	1
400	1
600	1
800	1.25
900	1.25

Table 4-12 : Values of the factors κ_f (a) and κ_u (b) at elevated temperatures

● **Failure Displacement $\delta_{f,b,\theta}$**

Finally, the failure displacement $\delta_{f,b,\theta}$ only depends on the maximal temperature of the heating phase T_f (Table 4-13).

T_u (°C)	$\delta_{f,b,Tu}$ (mm)
20	6
200	6
400	7
600	11
800	15
900	-

Table 4-13 : Values of the failure displacement as a function of T_u

4.4.3.4 Comparison between the proposed model and experimental results

The curves obtained by use of the proposed mathematical model are compared with experimental curves on Figures 4-44 to 4-48. Figures 4.44 to 4.46 show plots of analytical and experimental results of several tests performed at the same failure temperature T_f. In the next two figures, all the curves of one diagram are comparisons of the results from several tests performed on bolts after the same up temperature T_u has been reached at the end of the heating phase.

Globally, the proposed model leads to good correlations with experimental tests but this is a consequence of the fact that the model has been built to fit with the results of these tests. In the majority of the comparisons, the predicted force-displacement diagram is on the safe side except for few cases with $T_f = 400°C$ (Figure 4-46) but it is considered that the over-estimation of the resistance remains acceptable.

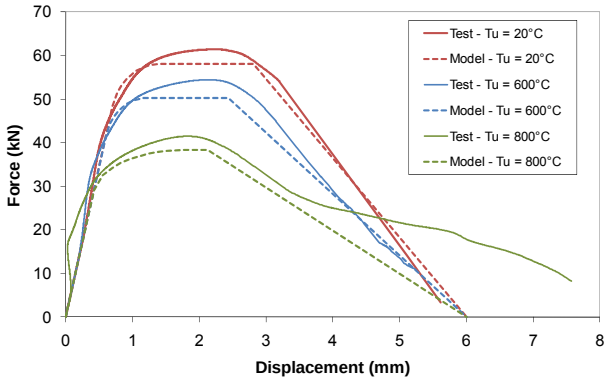

Figure 4-44 : Comparison between analytical model for shear and experimental results – $T_f = 20°C$

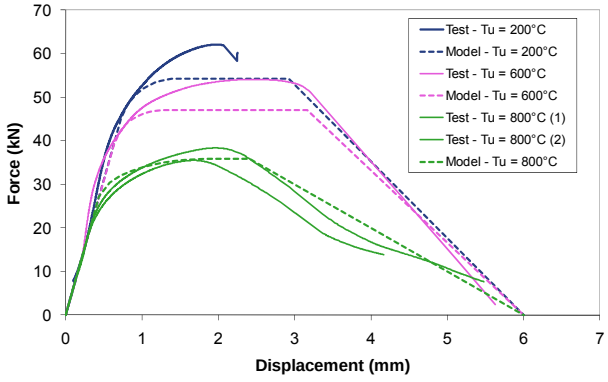

Figure 4-45 : Comparison between analytical model for shear and experimental results – $T_f = 200°C$

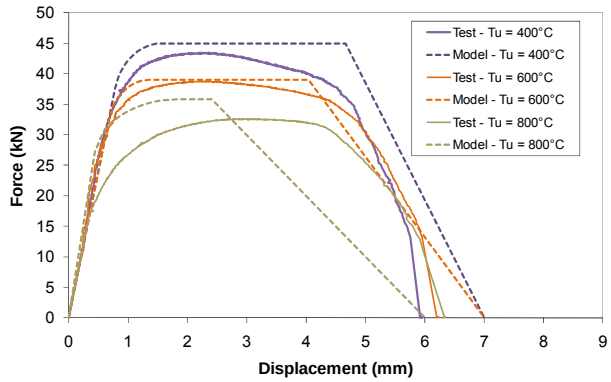

Figure 4-46 : Comparison between analytical model for shear and experimental results – T_f = 400°C

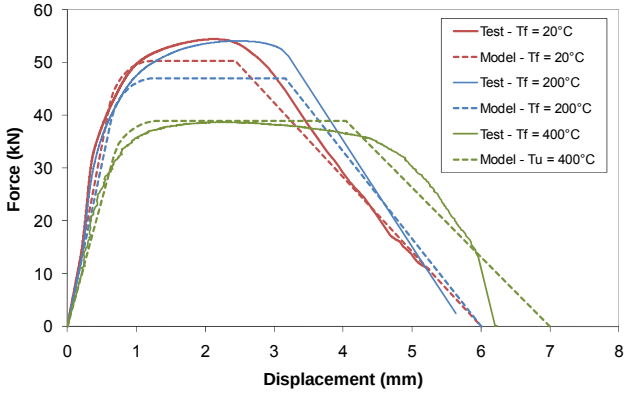

Figure 4-47 : Comparison between analytical model for shear and experimental results – T_u = 600°C

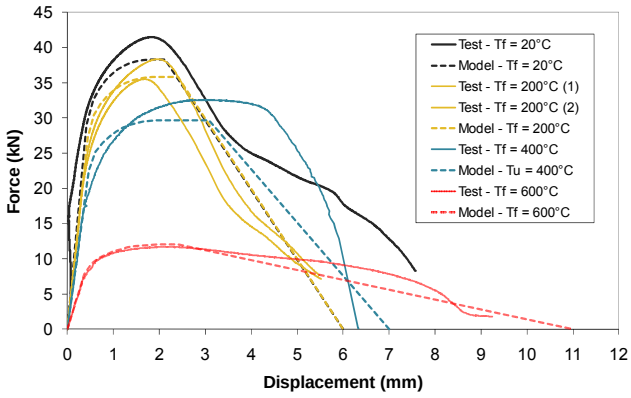

Figure 4-48 : Comparison between analytical model for shear and experimental results – T_u = 800°C

4.5 Experimental tests performed on welds

4.5.1 Introduction

Welds only work in shear even when they are used to connect elements subjected to tensile, compressive and shear stresses. The two types of weld connections are fillet welds and butt welds. Fillet welds are used in tee or lap configurations where the connection does not need to develop the full strength of the connected components. The reasons for the wider use of fillet welds (80% of welded connections) are the large tolerances allowed and the lower price. This process is less expensive because plates do not need any preparation, less weld metal is deposited and inspection is usually less exptensive than for butt welds [Corus & Kumar]. Full penetration butt welds are used in highly stressed connections. Partial penetration butt welds are used in intermediate cases.

At room temperature, the design resistance of a fillet weld at room temperature is sufficient if Eqs 4-27 & 4-28 are verified, where f_u, β_w and γ_{M2} are the nominal ultimate tensile strength of the weaker part joined, the appropriate correlation factor (Table 4-14) and the partial safety coefficient used for connections. The stresses $\sigma_\perp, \sigma_{//}, \tau_{//}$ and $\tau_\perp$ are represented on Figure 4-49. Consequently, the resistance $F_{w,Rd}$ of a fillet weld submitted to shear forces is given by Eq. 4-29.

$\left[\sigma_\perp^2 + 3\left(\tau_\perp^2 + \tau_{//}^2\right)\right]^{0.5} \le f_u / \left(\beta_w \gamma_{M2}\right)$	**4-27**
$\sigma_\perp \le f_u / \gamma_{M2}$	**4-28**
$F_{w,Rd} = \dfrac{a\, f_u}{\sqrt{3}\,\beta_w \gamma_{M2}}$	**4-29**

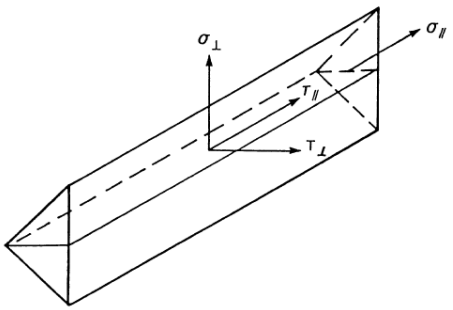

Figure 4-49 : Stresses on the throat section of a fillet weld

Standard and steel grade			Correlation factor β_w
EN 10025	**EN 10210**	**EN 10219**	
S 235 S 235 W	S 235 H	S 235 H	0,8
S 275 S 275 N/NL S 275 M/ML	S 275 H S 275 NH/NLH	S 275 H S 275 NH/NLH S 275 MH/MLH	0,85
S 355 S 355 N/NL S 355 M/ML S 355 W	S 355 H S 355 NH/NLH	S 355 H S 355 NH/NLH S 355 MH/MLH	0,9
S 420 N/NL S 420 M/ML		S 420 MH/MLH	1,0
S 460 N/NL S 460 M/ML S 460 Q/QL/QL1	S 460 NH/NLH	S 460 NH/NLH S 460 MH/MLH	1,0

Table 4-14 : Correlation factor β_w for fillet welds

4.5.2 Test set-up

The tests on welds have been performed on a unique configuration: a reduced transversal butt weld joint. The welding technique was Manual Metal Arc welding and the specimens were machined from butt welded 4 mm thick S355JR plates.

The welded joints have been checked by visual and X-Ray inspections: stop-start positions were present but no defects were found in the weld so as it is in accordance with the general quality level of constructional purposes for the specific welding technique.

Figure 4-50 : Butt welded joints used for the tests on welds under natural fire

4.5.3 Test schedule

The summary of the tests performed on welds is listed in Table 4-15. It includes:

- 2 tests on welds at room temperature ;
- 4 steady-state tests performed to make comparisons with the values of Eurocode 3 for welds ;
- 13 “natural fire tests” but 2 of them have been missed.

Steady-state Tests		Natural fire tests		
$T_u = T_f$ [°C]	n. tests	T_u [°C]	T_f [°C]	n. tests
20	1	400	200	1
200	1		100	1
400	1		20	1
600	1	600	400	++
800	1		200	++
			20	1
		800	600	1
			400	1
			200	1
			20	1
		900	400	1
			200	1
			20	1

Table 4-15 : Detailed programme of tensile tests performed on welds

4.5.4 Test results

The behaviour of welds is brittle: the deformations measured before the failure of that component are small. The main output of the tests performed on welded specimens is the evolution of the welds strength after the different thermal conditions. As a first step, the reduction factors obtained from steady-state tests have been compared to the reduction factors for welds defined in the Annex D of the EN 1993-1-2. The correlation is good at 800°C but for lower temperatures, the values of current Eurocode seems to overestimate the strength reduction factors for welds (Figure 4-51).

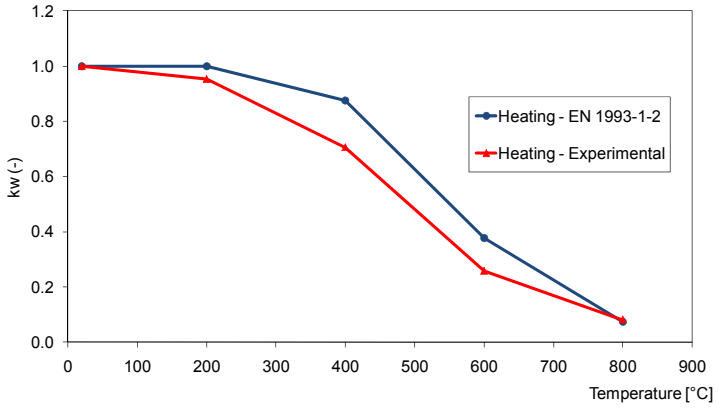

Figure 4-51 : Strength reduction factor for welds k_w from steady-state tests

The strength reduction factors k_w extracted from the results of experimental tests are plotted on Figure 4-52 and the numeric values are listed in Table 4-16. The reduction of welds resistance during the heating phase is given by the red curve. The other curves represent the reduction of welds resistance after heating until different up temperatures T_u and subsequent cooling. The resistance of welds is

reversible for heating-cooling cycles where temperature remains lower or equal to 600°C. For tests where the temperature T_u reached at the end of the heating phase is 800°C or 900°C, there is a permanent reduction of the welds resistance after cooling. The impact of the thermal cycle on the weld strength between 20°C and 400°C is similar for these two values of T_u.

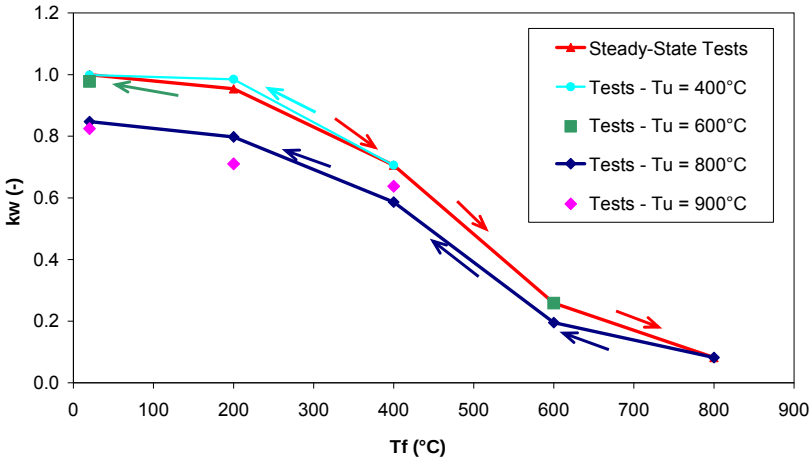

Figure 4-52 : Strength reduction factor for welds k_w from "natural fire" tests

T_f	EC 1993-1-2	Steady-State	T_u = 400°C	T_u = 600°C	T_u = 800°C	T_u = 900°C
20°C	1	1.000	0.998	0.978	0.848	0.825
200°C	1	0.954	0.985		0.798	0.711
400°C	0.876	0.706	0.706		0.586	0.638
600°C	0.378	0.258		0.258	0.195	
800°C	0.074	0.082			0.082	

Table 4-16 : Experimental values of k_w

No photographs of the tested specimens have been obtained from the Laboratory in charge of these tests. It has consequently not been possible to identify the failure mode and to ensure that the resistance of welds was weaker than the one of the connected plates. For such a specimen with a butt weld, the failure under tensile forces may occur i) in the plate, far away from the weld, ii) in the plate, in the thermally-affected zone or iii) in the weld. However, the evolution of the weld resistance during the heating phase obtained experimentally (through so-called "stready-state tests") tends to demonstrate that the failure occurred in the weld zone. Indeed, the resistance of the specimens at elevated temperature (before cooling) measured experimentally decreases more than what is predicted by the EN 1993-1-2 (reduction factor for welds k_w). As the reduction factor for the yield strength of carbon steel k_y is still higher than the reduction factor for welds k_w, the difference between the experimental measurements and the results predicted by Eurocodes would still be higher. This tendancy is confirmed by the results of the tests performed after cooling because the loss of resistance due to non-reversible behaviour goes until 20% of the initial resistance where previous tests performed

on carbon steel specimens demonstrated that the loss of resistance after a heating-cooling cycle was situated between 5 and 10% for peak temperatures of 600°C to 800°C [Lapwood, 1980].

4.6 Resistance of welds under heating and subsequent cooling

Based on the experimental results, the residual welds ultimate strength $f_{uw}\left(T_f, T_u\right)$ during the cooling phase should be calculated according to the following method:

a) EN 1993-1-2 gives the reduction of the bolt strength $k_w\ (T_f)$ without considering the effect of cooling;

b) The additional effect of cooling, k_{nr}, is calculated from Eqs 4-30 to 4-32:

$k_{nr} = 1$	$for \quad T_u \le 600°C$	**4-30**
$k_{nr} = 1 - \frac{0.2}{200}\left(T_u - \max\left(T_f\ ; 600°C\right)\right)$	$for \quad 600°C \le T_u \le 800°C$	**4-31**
$k_{nr} = 1 - \frac{0.2}{200}\left(800°C - \max\left(T_f\ ; 600°C\right)\right)$	$for \quad 800°C \le T_u \le 900°C$	**4-32**

c) Finally, the value of the ultimate weld strength accounting for the non-reversible behaviour of steel is given by Eq. 4-33 :

$f_{uw,T_t,T_u} = k_{w,T_t}\, k_{nr,T_t,T_u}\, f_{uw,20°C}$	**4-33**

The analytical expressions of k_{nr} are given below for the particular values of T_u for which experimental results are available (Eqs 4-34 and 4-35). These expressions are compared with the values obtained from tensile and shear tests on Figure 4-53. Figure 4-54 shows the comparison between the reduction factors for the weld strength during the cooling phase obtained with experimental and analytical results. The analytical expression overestimates the weld ultimate strength, especially for T_f equal to 400°C and 600°C. These differences derive from the variations between the experimental and recommended reduction factors for weld strength during the heating phase (see Figure 4-51).

$k_{nr} = 1$	$for \quad T_u = 400°C \quad and \quad T_u = 600°C$	**4-34**
$k_{nr} = \max\left(0.8\ ; 0.8 + 0.2\left(\frac{T_f - 600}{200}\right)\right)$	$for \quad T_u = 800°C \quad and \quad T_u = 900°C$	**4-35**

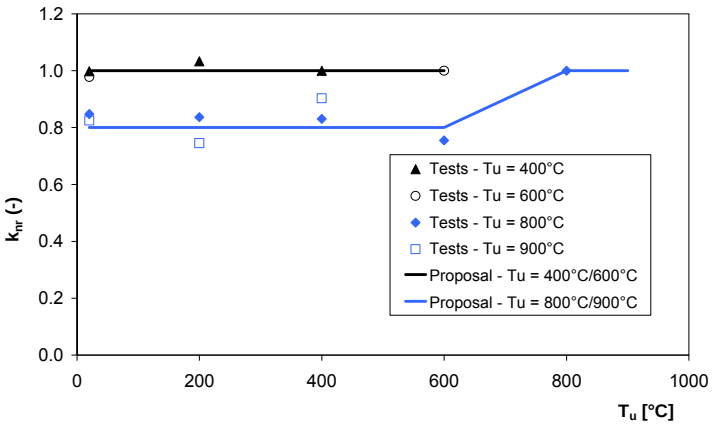

Figure 4-53 : Reduction factor for non-reversible behaviour of weld strength

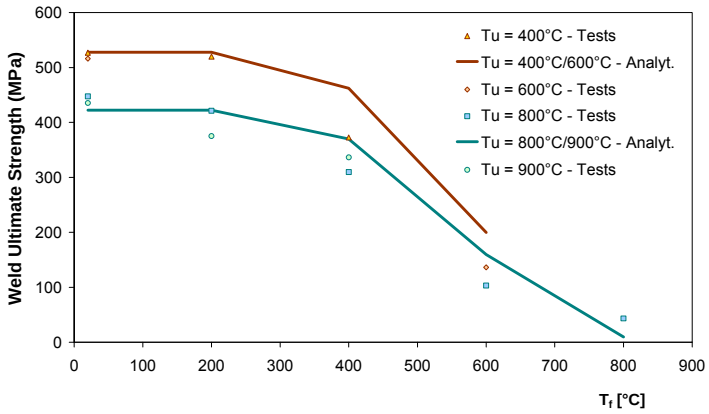

Figure 4-54 : Reduction factor for non-reversible behaviour of weld strength

4.7 Conclusions

The tensile and shear tests performed on bolts within the present experimental programme at the Centro Sviluppo Materiali show that a heating-cooling cycle has a significant effect on the mechanical characteristics of Grade 8.8 bolts. For maximal temperatures of 500°C or higher, the resistance of bolts has lower values during cooling than it had during heating. The ratio of both values reaching 60% in some cases. The increase of ductility for bolts in tension and shear after heating above 500°C has already been observed previously in Kirby tests. The present tests have shown that this increase of ductility is maintained during the cooling phase if the temperature is higher than 500°C at the end of the heating phase.

Calibrated on the experimental results, force-displacement models have been proposed for bolts in tension and in shear during the heating and cooling phases of a fire. These force-displacements models

contain an elastic branch, an elliptic or elasto-platic branch, a plateau and a linear or bilinear descending branch. It can be introduced into components-based models or finite element models (see Chapters 5 and 6). The non-reversible behaviour of bolts at elevated temperatures has been quantified by the definition of a new coefficient k_{nr} that depends on the temperature reached at the end of the heating phase T_u and the temperature of the test T_f. Similar values of the coefficient k_{nr} have been obtained for bolts in tension and in shear.

The results of the experimental work carried out at the Centro Sviluppo Materiali on welded specimens are focused on the evolution of resistance of welds during the heating and cooling phases of a natural fire. This series of test tends to demonstrate that the resistance of weld is reversible until 600°C. For higher temperatures, the additional loss of resistance during cooling cycle is can reach 20% of the resistance during heating. Similarly to what was done for bolts, the evolution of welds under heating and subsequent cooling has led to the definition of a coefficient for the non-reversible behaviour of welds k_{nr}. The values given to this coefficient are valid on the condition that the failure of the welded specimens in the experimental tests was really by insufficient resistance of the welds. This still needs to be demonstrated, as no tested specimens or photographs of the tested specimens have been made available to the author. The analysis of the obtained results nevertheless tends to show that the hypothesis of a failure in the weld is the most likely failure mode.

5 Models of beam-to-column joints under fire loading

5.1 Definition and classifications of joints

The two different English words “joints” and “connections” are distinguished in the EN 1993-1-8 [CEN, 2005a]. A connection is a location where two or more elements meet and the most common types of connections are web cleats, flange-cleats, end-plate, fin plate and welded connections. For design purposes, the connection is the assembly of the basic components required to represent the transfer of the relevant internal forces and moment between two connected elements. The joint is the zone where the members are interconnected (Figure 5-1). The most common joint configurations are single-sided and double-sided beam-to-column joints, beam and columns splices and column bases (Figure 5-2). For design purposes, the joint is the assembly of all the basic components required to represent the behaviour during the transfer of the relevant internal forces and moments between the connected members. For example, a beam-to-column joint includes a web panel and one connection or two connections.

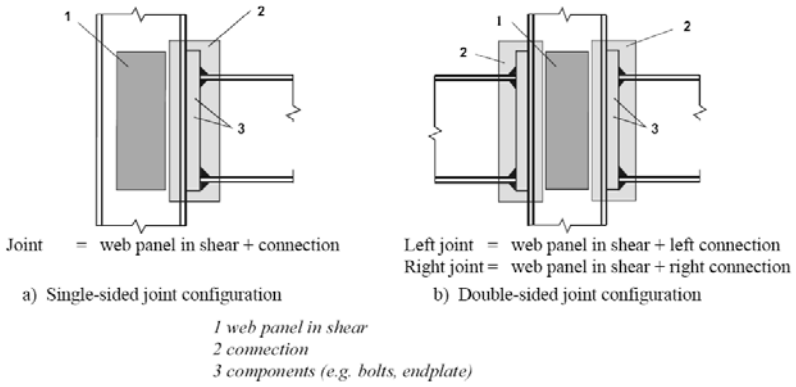

Figure 5-1 : Parts of a beam-to-column joint [CEN, 2005a]

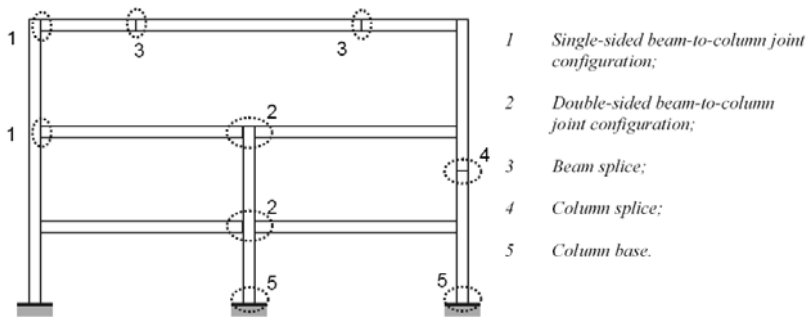

Figure 5-2 : Joint configurations [CEN, 2005a]

Joints may be classified by their stiffness, their strength or their capacity of rotation.

5.1.1 Classification of joints by stiffness

A joint may be classified as rigid, nominally pinned or semi-rigid according to its rotational stiffness by comparing its initial rotational stiffness $S_{j,ini}$ with the classification boundaries defined in Figure 5-3. The rotational stiffness of a joint is the moment required to produce a unit rotation in that joint.

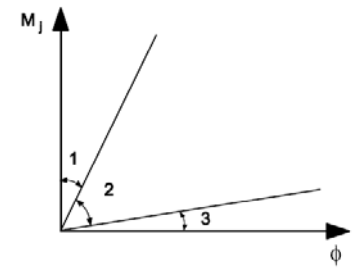

Zone 1: rigid, if $S_{j,ini} \geq k_b EI_b / L_b$

where
$k_b = 8$ for frames where the bracing system reduces the horizontal displacement by at least 80 %
$k_b = 25$ for other frames, provided that in every storey $K_b/K_c \geq 0,1$ *)

Zone 2: semi-rigid

All joints in zone 2 should be classified as semi-rigid. Joints in zones 1 or 3 may optionally also be treated as semi-rigid.

Zone 3: nominally pinned, if $S_{j,ini} \leq 0,5\, EI_b / L_b$

*) For frames where $K_b/K_c < 0,1$ the joints should be classified as semi-rigid.

Key:

K_b	is	the mean value of I_b/L_b for all the beams at the top of that storey;
K_c	is	the mean value of I_c/L_c for all the columns in that storey;
I_b	is	the second moment of area of a beam;
I_c	is	the second moment of area of a column;
L_b	is	the span of a beam (centre-to-centre of columns);
L_c	is	the storey height of a column.

Figure 5-3 : Classification of joints by stiffness [CEN, 2005a]

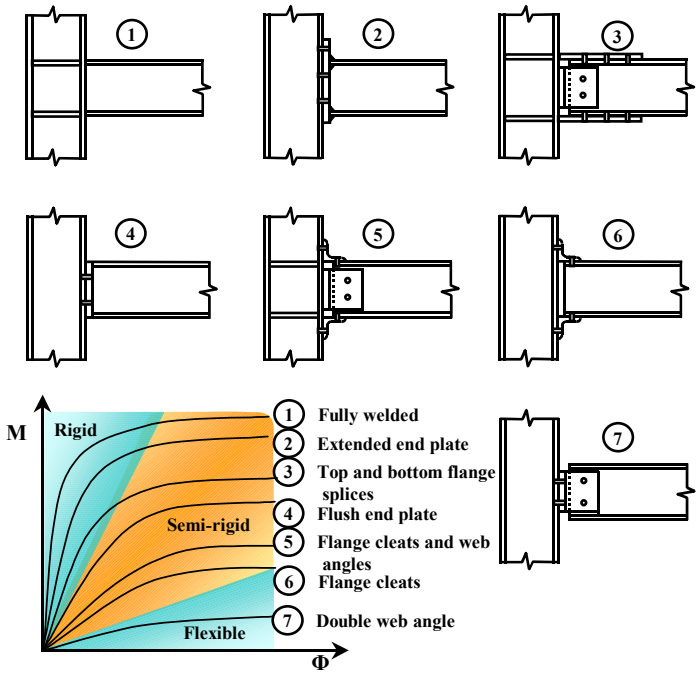

Figure 5-4 : Typical beam-to-column joints and stiffness classification [Spyrou, 2002]

A nominally pinned joint (in the stiffness classification) shall be capable of transmitting the internal forces, without developing significant moments which might adversely affect the members or the structure as a whole and shall be capable of accepting the resulting rotations under the design loads. Joints classified as rigid may be assumed to have sufficient rotational stiffness to justify analysis based on full continuity. A joint which does not meet the criteria for a rigid joint or a nominally pinned joint should be classified as a semi-rigid joint.

5.1.2 Classification of joints by strength

A joint may be classified as full-strength, nominally pinned or partial strength by comparing its design moment resistance $M_{j,Rd}$ with the design moment resistances of the members that it connects. When classifying joints, the design resistance of a member should be taken as that member adjacent to the joint.

The design resistance of a full-strength joint shall not be less than that of the connected members. A joint may be classified as full-strength if it meets one of the criteria given in Figure 5-5. A nominally pinned joint (according to the strength classification) shall be capable of transmitting the internal forces, without developing significant moments which might adversely affect the members or the structure as a whole. It shall be classified as nominally pinned if its design moment resistance $M_{j,Rd}$ is not greater than 0.25 times the design moment resistance required for a full-strength joint, provided that it also has sufficient rotation capacity to accept the resulting rotations under the design loads. A joint which does not meet the criteria for a full-strength joint or a nominally pinned joint should be classified as a partial-strength joint.

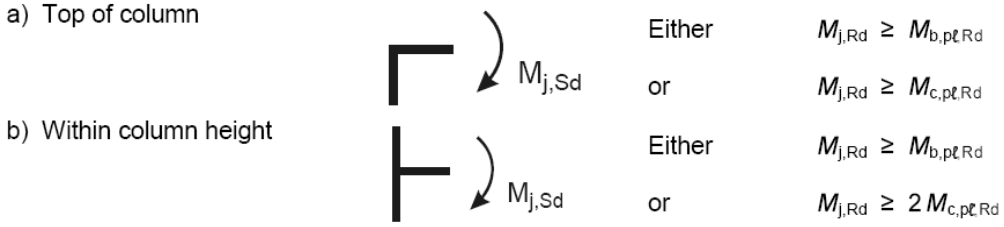

Figure 5-5 : Criteria for full-strength joints

where $M_{b,pl,Rd}$ and $M_{c,pl,Rd}$ are the design bending resistance of the beam and the column.

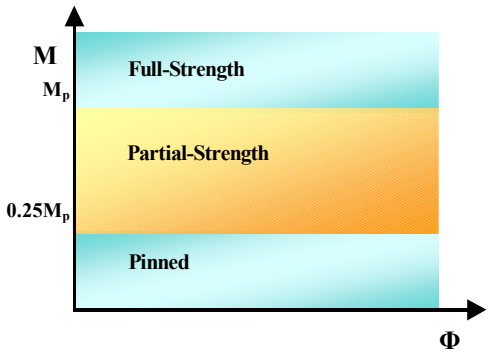

Figure 5-6 : Classification of joints by strength according to EN 1993-1-8 [Spyrou, 2002]

5.1.3 Classification of joints by capacity of rotation and ductility

The ductility of a joint is characterised by the ability of this joint to maintain its plastic moment over a sufficient rotation. A sufficient degree of ductility allows the redistribution of internal forces without brittle failure. Jaspart introduced the concept of ductility classes to deal with the rotation capacity of moment resistant joints [Jaspart, 1997] and to adapt the frame analyses and joints design. Some recommendations on usual simple joints have also been proposed by the same author to ensure the safe character of the "hinge assumption" in global analyses [Jaspart, 2008]. These rules consist in verifying that the bending moment induced in the joints remains low, even for large rotations, and that no brittle failures occur under the combination of shear forces and bending moments in the joint zone. In addition to this work, a thesis has led to ductility requirements for bolted connections loaded in shear [Henriques, 2007]. By use of the Component Method, described in detail later, investigations focused on the ductility and rotation capacity of semi-rigid joints have been realised in the early 2000's [Girão Coelho, 2001], [Beg, 2004] and [Girão Coelho, 2004].

In the EN 1993-1-8, the issue of the rotation capacity of joints is presently covered by means of approximate inequations for bolted and welded joints.

5.2 Models of semi-rigid joints

5.2.1 Curve-fit Models

Curve-fit models are mathematical equations fitted to represent the relationship between bending moments and rotations in joints on the basis of experimental results. The most recent developments on curve-fit models for joints are based on the Ramberg-Osgood equation [Ramberg and Osgood, 1943] that was initially dedicated to metallic materials under uni-axial stresses (Eq. 5-1).

$\varepsilon = \frac{\sigma}{E} + K\left(\frac{\sigma}{E}\right)^n$	**5-1**

where ε, σ are the strain and the stress and K, n are constant coefficients that depend on the material being considered.

This equation has been adapted to joints (Eq. 5-2) at room temperature [Ang, 1984] and then, extended to joints at elevated temperatures [El-Rimawi, 1989]. An additional parameter λ, function of the lever arm D between internal tensile and compressive forces, has been introduced [El-Rimawi, 1997] to account for dimensions of the joint (Eqs 5-3 & 5-4) on the basis of experimental tests [Lawson, 1990].

$\phi = \frac{M}{A} + 0.01\left(\frac{M}{B}\right)^n$	**5-2**
$\lambda = \frac{D - 50}{303.8 - 50}$	**5-3**
$\phi = \frac{M}{\lambda^2 A} + 0.01\left(\frac{M}{\lambda B}\right)^n$	**5-4**

where the parameters A, B and n are depending on the type of joint and on the distribution of temperature.

The implementation of this type of model into a frame analysis is quite easy but necessitates that the parameters have been calibrated by use of experimental results. Due to the existence of a large number of connection configurations and the necessity to consider the influences of axial forces and temperature, curve-fit models are rarely used in practice.

5.2.2 Mechanical Models

The global action of a joint is represented in a mechanical model by a combination of individual components activated under mechanical loading. Each component is substituted by a spring that is characterised by a force-displacement diagram. The strength and the initial stiffness of the main components are given in the EN 1993-1-8 and are the Component Method is commonly used for the design of joints at room temperature. The mechanism of the Component Method is described in more detail in § 5-3.

At room temperature, the European Work Group COST C1 has standardised the use of the Component Method and this one was integrated in the Eurocode 3, as an Annex and then as a part of the final version. These rules can be implemented into softwares, as it has been done in CoP by Jaspart and Weynand [CoP]. At elevated temperatures, the use of this method is much more complex for two reasons. Firstly, the strength and the stiffness of the components are continuously modified. Secondly,

the joint is subjected to time-depending internal forces during the fire because of thermally-induced forces and the effect of plasticity. Consequently, the use of the Component Method is not yet common for applications at elevated temperatures (§ 5.4).

5.2.3 Finite Element Models

In finite element models, the real geometry of joints is meshed in shell, beam or solid elements and the action of the joint is reproduced after solving numerically equations of equilibrium under fire loading, mechanical loading and boundary conditions. These types of analyses predict very well the response of joints but finite element models also contains several drawbacks. Firstly, such analyses are time-consuming (definition of the input data, running of the FE program, extraction of the results). Secondly, the knowledge of assumptions made by the FE program is sometimes incomplete when using commercial software where no access is given to the sources. Finally, the degree of complexity for building a finite element program and defining the data is linked to the degree of precision targeted. The risk of making a mistake in one of these two operations is usually higher in finite element models than in the other models described here.

At room temperature, finite element models have been commonly used to represent the behaviour of joints. Fewer models have been developed to describe the simultaneous action of thermal and mechanical loadings on the resistance and the deformations of joints. The first three-dimensional program capable of analysing the detailed behaviour of connections is FEAST, developed at the University of Manchester [Liu, 1996 and 1999b]. The non-uniform thermal expansion and the non-linear material properties at high temperature were taken into consideration. The action of bolts and the contact between the column and the end-plate were modelled by beam elements. Comparisons with tests results [Lawson, 1990; Leston-Jones, 1997 and Al-Jabri, 1999] provided a validation of this program.

El-Houssieny developed a three-dimensional finite element model to simulate the behaviour of semi-rigid extended end-plate connection [El-Houssieny, 1998]. The validation of this model against experimental tests was followed by an extensive parametric study aimed at understanding the behaviour of different connection components at elevated temperature and this lead to equations for the design of different typical connections at elevated temperatures.

The use of 3D solid elements and contact elements in commercial finite element packages ABAQUS and ANSYS has also been validated for the modelling of commonly used connections at elevated temperatures. A model for flush end-plate connections realised in the ABAQUS package [Al-Jabri, 2005] has been validated by modelling tests performed previously by the same author [Al-Jabri, 1999]. Sarraj built a three-dimensional FE model of a fin plate connection at elevated temperature in

ABAQUS [Sarraj, 2006]. He validated this model against lap joint tests at room temperature [Richard, 1980] and a beam test performed by Wald and Ticha at the Czech Technical University. Yu also used ABAQUS package to model tests he performed on isolated joints with web cleats connections under different combinations of shear and tying forces at elevated temperatures [Yu, 2009a]. Lou performed, in ANSYS program, thermal analyses followed by structural analyses of two tests that he realised on extended end-plate connections at elevated temperatures [Lou, 2006].

Finally, tests performed on sub-frames with various types of steel joints (fin plate connections, extended end-plate connections, header plate connections and welded connections) under natural fire [Santiago, 2008a and 2008b] have been modelled in the finite element code LUSAS by use of shell, solid and spring elements [Santiago, 2008c]. The test on welded connections has also been modelled in SAFIR software. The global behaviour of the frame and the joint failure modes obtained within this numerical work are in agreement with the experimental observations.

5.2.4 Macro-element Models

Macro-elements models are usually based on mechanical models and enable to account for the effects of interaction between frames and connections without requiring the modelling of the connections geometry with finite elements. Several “connection finite elements” have been built on the basis of the Component Method for applications at room temperature. The reader should refer to literature for macro-models developed at room temperature [Poggi, 1988; Atamaz-Sibai, 1993; Li, 1995 and Bayo, 2005]. Step-by-step, the influence of axial forces and shear forces on the moment-rotation relationship of connections has been integrated in these macro-elements models. However, all the elements are not aimed at simulating the behaviour of a connection exposed to natural fire i) because the degradation of the stiffnesses and resistances as a function of time are not integrated and ii) because of the necessity to predict the behaviour of the joint under cooling and unloading.

Recently, a two-noded spring element developed in Vulcan on the basis of curve-fit models has been extended to the use of the Component Method [Block, 2006]. This 3D finite spring element with zero length has been validated against experimental tests at room temperature and at high temperatures, although several limitations exist: the automatic consideration of group effects between bolt rows, shear deformations in column web and buckling of the beam bottom flange are not possible.

5.3 Component Method at room temperature

5.3.1 General principle of the Component Method

The Component Method is a versatile approach for calculating rotational stiffness, axial stiffness and the capacity of joints. The original feature of this method is to consider any joint as a set of individual basic spring-like components (Figure 5-7). For each component, the force-displacement relationship is computed and assembled to form a spring model, which represent the global behaviour of the joint.

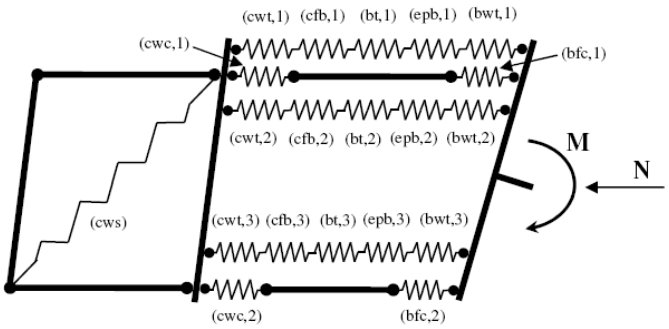

Figure 5-7 : Spring model of an extended end-plate joint for moment and axial force [Cerfontaine, 2004]

The application of this method requires the following three steps:

- Identification of the active components in the considered joint;
- Evaluation of the stiffness and/or resistance characteristics for each individual basic component;
- Assembly of all components and evaluation of the whole joint stiffness and/or resistance characteristic.

A number of words in relationship with the Component Method will be used extensively within the present and next chapters. In order to make the use of these terms clear, they are defined below.

Line of bolts: Group of bolts located at the same level in a connection. A line of bolts commonly comprises two bolts.

Component: Specific part of a joint that contributes to the mechanical behaviour (resistance and stiffness) of that joint. Components are activated under tensile forces only, under compressive forces only or under both of them. For example, “bolts in tension”, “column flange in bending” and “column flange in compression” are components activated in usual connections. In the Component Method, each component is modelled by a spring.

Row (of components): Group of components situated at a same level. When a row transfers a tensile or compressive force, all the components of that row are submitted to this tensile or compressive force. Consequently, the global resistance $F_{i,Rd}$ and the global stiffness K_i of a row i containing n_{comp} components are given in Eqs 5-5 and 5-6.

$F_{i,Rd} = \min_{j=1}^{n_{comp}} \left(F_{i,j,Rd} \right)$	**5-5**
$K_i = \left(\sum_{j=1}^{n_{comp}} K_{i,j}^{-1} \right)^{-1}$	**5-6**

where $F_{i,j,Rd}$ and $K_{i,j}$ are respectively the resistance and the stiffness of the component j of the row i.

Bolt row: Row located at the level of one line of bolts and representing the components activated when tensile forces are transferred with this line of bolts.

Compression row: Row of components allowing the transfer of compressive forces. The most typical compression row in beam-to-column joints represents the transmission of forces by contact from the beam flange to an end-plate or directly to the column flange.

5.3.2 Active components in usual beam-to-column joints

The principles and the first developments of the Component Method are due to the analytical and experimental investigations at the University of Delft [Zoetemeijer, 1983]. The work realised by Tschermmernegg contributed to the development of this method. He focused on the component "panel in shear" [Tschermmernegg, 1988] and applied the principles of the Component Method to composite joints [Tschemmernegg, 1994]. Jaspart proposed several mechanical models for the representation of beam-to-column joints and column splices [Jaspart, 1997]. The resistance and the stiffness coefficient of the components activated in the common steel joints and given in the EN 1993-1-8 are listed in Table 5-1. These expressions will be detailed in the § 6.4.3.

Component	Resistance	Stiffness Coefficient
Column web panel in shear	$V_{wp,Rd} = \frac{0.9 f_{y,wc} A_{vc}}{\sqrt{3} \gamma_{M0}}$	$k_{cws} = \frac{0.38 A_{vc}}{\beta z}$
Column web in tension	$F_{c,wc,Rd} = \frac{\omega b_{eff,t,wc} t_{wc} f_{y,wc}}{\gamma_{M0}}$	$k_{cwt} = \frac{0.7 b_{eff,t,wc} t_{wc} f_{y,wc}}{d_c}$

Column web in compression	$F_{c,wc,Rd} = \frac{\omega b_{eff,c,wc} t_{wc} f_{y,wc}}{\gamma_{M0}} \leq \frac{\omega \rho b_{eff,c,wc} t_{wc} f_{y,wc}}{\gamma_{M0}}$	$k_{cwc} = \frac{0.7 b_{eff,c,wc} t_{wc} f_{y,wc}}{d_c}$
Column flange in bending	T-stub Model [EN 1993-1-8]	$k_{cfb} = \frac{0.85 l_{eff} t_{fc}^3}{m^3}$
End-plate in bending	T-stub Model [EN 1993-1-8]	$k_{epb} = \frac{0.85 l_{eff} t_{fc}^3}{m^3}$
Beam flange and web in compression	$F_{c,fb,Rd} = \frac{M_{c,Rd}}{h - t_{fb}}$	$k_{bfc} = \infty$
Bolts in tension	$F_{t,Rd} = \frac{0.9 f_{ub} A_s}{\gamma_{M2}}$	$k_{bt} = \frac{1.6 A_s}{L_b}$
Bolts in shear	$F_{v,Rd} = \frac{\alpha_v f_{ub} A_s}{\gamma_{M2}}$	$k_{bs} = \frac{16 n_b d^2 f_{ub}}{E_b d_{M16}}$
Bolts in bearing	$F_{b,Rd} = \frac{\alpha_b k_1 f_u d t_p}{\gamma_{M2}}$	$k_{bs} = \frac{24 n_b k_b k_t f_u}{E}$
Welds	$F_{w,Rd} = a \frac{f_{uw}/\sqrt{3}}{\beta_w \gamma_{M2}}$	$k_w = \infty$

Table 5-1 : Resistance and stiffness coefficient of components in common joints

In this table, $f_{y,wc}$ is the yield stress, f_u is the ultimate stress of the plate, f_{ub} is the ultimate stress of bolt, f_{uw} is the ultimate stress of weld, E is the Young's modulus of the plate, E_b is the Young's modulus of bolts, γ_{M0}, γ_{M1} and γ_{M2} are partial safety factors, A_{vc} is the shear area of the column profile, b is the transformation parameter, z is the lever arm between the compressive resistance and the tensile resistance, t_{wc} is the thickness of the column web, $b_{eff,t,wc}$ and $b_{eff,c,wc}$ are the effective widths of the column in the compression and tension zone, ω and ρ are the reduction factors for interaction with shear forces and for plate buckling, d_c is the clear depth of the column web, l_{eff} is the smallest value of the effective lengths calculated for a bolt row (considered individually or as a part of a group of bolt rows), t_{fc} is the thickness of the column flange, m is the distance between the bolt centre-line and the weld connecting the beam web to the end-plate, $M_{c,Rd}$ is the design moment resistance of the beam cross-section, h is the height of the connected beam, t_{fb} is the thickness of the beam flange, A_s is the tensile stress area of the bolt, L_b is the elongation length of the bolt, α_v is an empirical value derived from experiments accounting for secondary bending actions on bolts in shear, n_b is the number of shear planes in the bolt, d is the bolt diameter, d_{M16} is the nominal diameter of an M16 bolt, t_p is the

plate thickness, k_1, k_b and k_t are coefficients depending on the geometrical data, a is the throat thickness of the weld fillet and β_w is the correlation factor for welds.

5.3.3 Bending moment resistance of the joint

Under pure bending, the moment resistance of the joint $M_{j,Rd}$ is evaluated by resolution of the mechanical model (Figure 5-8), as described in the EN 1993-1-8. The resistance of all the components are calculated as mentioned previously and the bending moment resistance $M_{j,Rd}$ is obtained by Eq. 5-7 where h_r is the distance from bolt-row r to the centre of compression and $F_{tr,Rd}$ is the effective design tension resistance of bolt-row r. The design tension resistance of one bolt row $F_{tr,Rd}$ is the minimal value between the resistances of the components of that row ; in addition, the sum of the tensile forces in all the bolt rows must not be higher than i) the resistance of the flange in compression and ii) the resistance of the web panel in shear. Consequently, the maximal resistant moment is obtained by considering bolt rows in sequence, starting from the bolt row farthest from the centre of compression and progressing to the closest one.

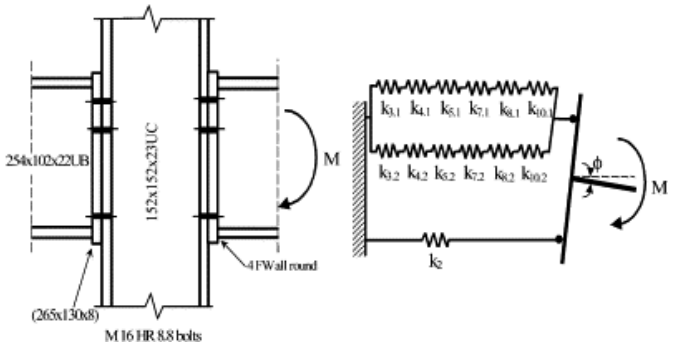

Figure 5-8 : Geometry and model of a cruciform joint with end-plate connections under pure bending (Simões da Silva, 2001a)

$M_{j,Rd} = \sum_r h_r F_{tr,Rd}$	**5-7**

The evaluation of the bending moment resistance also necessitates considering failure mechanisms including two or more bolt rows. The procedure suggested in the Eurocode 3 to account for group effects is to consider a bolt row individually as a first step and then to limit the tensile force in that row so that the resistance of the groups formed with bolts situated above the considered row (in case of hogging moment) is higher than the resultant force in these groups. This procedure is summarised hereafter for a fictive case with three bolts rows, starting from the farthest bolt row 1 to the closest bolt row 3:

- The resistance of the bolt row 1 considered individually $F_{t1,Rd}$ is the minimal value between the resistances of all the components included in bolt row 1. The resistance of bolt row 1 is $F_{t1,Rd}$.

- The resistance of the bolt row 2 considered individually $F_{t2,Rd}$ is the minimal value between the resistances of all the components included in bolt row 2. The resistance of the group 1-2 formed by the bolt rows 1 and 2, $F_{t,1\text{-}2,Rd,}$ is the minimal value between the resistances of all the components of the group 1-2. The resistance of bolt row 2 is given by Eq. 5-8:

$F_{t,1-2,Rd} = \min\left(F_{t2,Rd}\,;\, F_{t,1-2,Rd} - F_{t1,Rd}\right)$	**5-8**

- The resistance of the bolt row 3 considered individually $F_{t3,Rd}$ is the minimal value between the resistances of all the components included in bolt row 3. The resistance of the group 2-3 formed by the bolt rows 2 and 3, $F_{t,2\text{-}3,Rd,}$ is the minimal value between the resistances of all the components of the group 2-3. The resistance of the group 1-3 formed by the bolt rows 1, 2 and 3, $F_{t,1\text{-}3,Rd,}$ is the minimal value between the resistances of all the components of the group 1-3.The resistance of bolt row 3 is given by Eq. 5-9:

$F_{t,1-3,Rd} = \min\left(F_{t3,Rd}\,;\, F_{t,2-3,Rd} - F_{t2,Rd}\,;\, F_{t,1-3,Rd} - F_{t1,Rd} - F_{t2,Rd}\right)$	**5-9**

5.3.4 Rotational stiffness of the joint

The initial rotational stiffness of a joint $S_{j,ini}$ is evaluated by resolution of the mechanical model on the basis of the stiffness coefficients $k_{i,j}$ of the components included in the joint represented by a mechanical model. This resolution is simplified step-by-step as follows. Firstly, an equivalent spring with a stiffness coefficient $k_{eq,i}$ is defined for each bolt row and for the compression row (Step 1). Then, the equivalent springs of the $n_{rows,t}$ bolt rows are substituted by a unique spring for the tension zone with a stiffness coefficient $k_{eq,t}$ (Step 2). Finally, the initial rotational stiffness of the joint is given by Eq. 5-13.

$k_{eq,i} = \left(\sum_{j=1}^{n_{comp}} k_{i,j}^{-1}\right)^{-1}$	**5-10**
$k_{eq,t} = \dfrac{\sum_{i=1}^{n_{rows,t}} k_{eq,i}\, z_i}{z_{eq}}$	**5-11**
$z_{eq} = \dfrac{\sum_{i=1}^{n_{rows,t}} k_{eq,i}\, z_i^2}{\sum_{i=1}^{n_{rows,t}} k_{eq,i}\, z_i}$	**5-12**

$S_{j,ini} = \dfrac{E\, z_{eq}^2}{\left(\dfrac{1}{k_{eq,t}} + \dfrac{1}{k_{eq,c}} \right)}$	**5-13**

In this formulae, z_i is the distance between the bolt row i and the centre of compression assumed to be situated at the centre of the beam flange in compression, z_{eq} is the equivalent lever arm (Eq. 5-12), $k_{eq,t}$ and $k_{eq,c}$ are the stiffness coefficients for the tension zone and the compression zone.

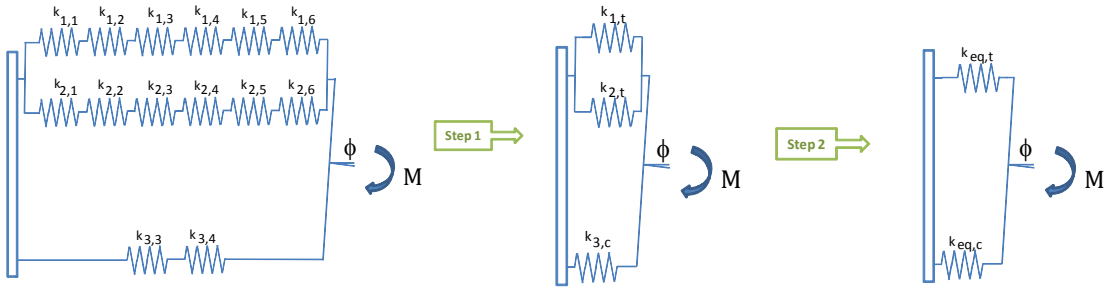

Figure 5-9 : Steps for the evaluation of the rotational stiffness of a joint based on the Component Method

5.3.5 Moment-rotation diagram

The actual moment-rotation response of a joint is non-linear. In the recommendations of the European Working Group COST C1 [Jaspart, 1999], three different M-ϕ relationships are suggested for the characterization of the semi-rigid behaviour of connections at room temperature (Figure 5-10). This curves are extrapolated from the bending moment resistance $M_{j,Rd}$ and the rotational stiffness $S_{j,ini}$. The non-linear curve is composed of an elastic branch until 2/3 $M_{j,Rd}$, a non-linear branch and a plateau until the capacity of rotation ϕ_{Cd} (Figure 5-10c). The rotational stiffness S_j of a beam-to-column joint for a moment $M_{j,Ed}$ less than the design moment resistance $M_{j,Rd}$ of the joint may be obtained with sufficient accuracy from Eqs 5-14 and 5-15, where Ψ is a coefficient given in Table 5-2.

$S_j = S_{j,ini}$	$if \quad M_{j,Ed} \le 2/3\, M_{j,Rd}$	**5-14**
$S_j = \dfrac{S_{j,ini}}{\left(1.5\, M_{j,Ed} / M_{j,Rd}\right)^{\Psi}}$	$if \quad 2/3\, M_{j,Rd} \le M_{j,Ed} \le M_{j,Rd}$	**5-15**

The simplest curve is bilinear (Figure 5-10a). Comparative studies were performed to calibrate an idealised joint stiffness $S_{j,ini}/\eta$ [Jaspart, 1997] where the stiffness modification factor η depends on the type of joint and the joint configuration (Table 5-3). In an elastic analysis considering the idealised joint stiffness, the moment $M_{j,Ed}$ should remain lower than the design moment resistance $M_{j,Rd}$.

As a conservative assumption, each curve lying under the non-linear curve may be used in a frame analysis. The tri-linear curve respects this statement (Figure 5-10b). However, if an elastic analysis is realised with the initial joint stiffness $S_{j,ini}$, the moment $M_{j,Ed}$ should remain lower than 2/3 $M_{j,Rd}$.

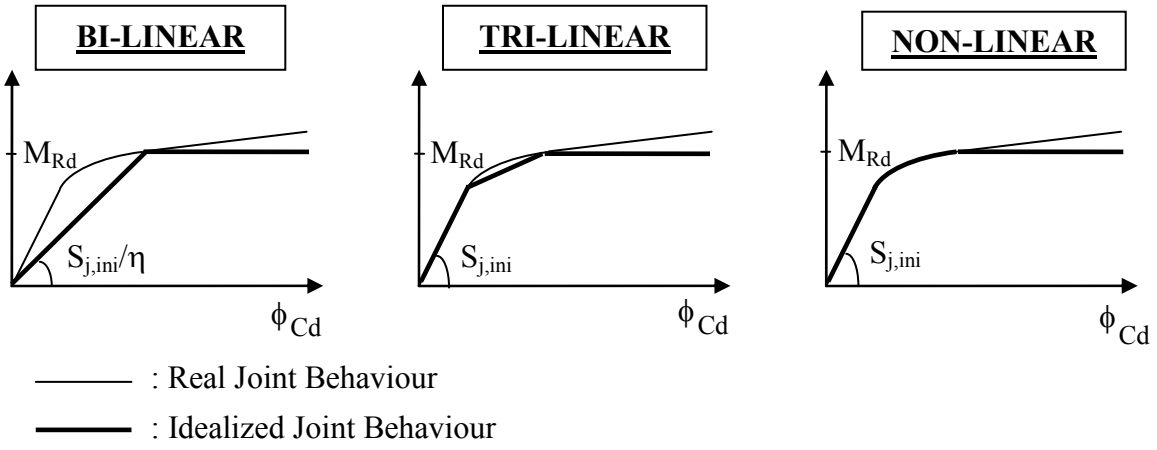

Figure 5-10 : Possibilities of curve idealisation [Jaspart,1999]

Type of connection	ψ
Welded	2,7
Bolted end-plate	2,7
Bolted angle flange cleats	3,1
Base plate connections	2,7

Table 5-2 : Values of the coefficient Ψ for different types of connections [CEN, 2005a]

Type of connection	Beam-to-column joints	Other types of joints (beam-to-beam joints, beam splices, column base joints)
Welded	2	3
Bolted end-plate	2	3
Bolted flange cleats	2	3,5
Base plates	-	3

Table 5-3 : Stiffness modification coefficient η [CEN, 2005a]

Jaspart has proposed a method to evaluate a post-critical stiffness of a joint and to deduce the rotation reached at the ultimate bending moment [Jaspart, 1991].

5.3.6 Interaction between axial force and bending moment

The general principle of the Component is to consider a joint as a set of individual basic spring-like components. This principle applies to any combination of bending moment and axial forces. However, the procedures deduced from this principle to evaluate the bending moment resistance $M_{j,Rd}$ and the rotational stiffness $S_{j,ini}$ are not valid anymore in presence of significant axial forces. It is mentioned in the EN 1993-1-8 that the validity of the Component Method, as described in this norm, is limited to cases where the axial force in the connected beam does not exceed 5% of design resistance $N_{pl,Rd}$ of the beam cross-section (instead of 10% in the Annex J included in the previous version of the Eurocode 3). If the axial force N_{Ed} in the connected beam exceeds 5% of this design resistance, a conservative method may be used to deal with the M-N interaction in the joint (Eq. 5-16).

$\frac{M_{j,Ed}}{M_{j,Rd}} + \frac{N_{j,Ed}}{N_{j,Rd}} \leq 1$	**5-16**

where $M_{j,Ed}$, $N_{j,Ed}$ are the internal forces applied to the joint and $M_{j,Rd}$, $N_{j,Rd}$ are respectively the design moment resistance and the axial design resistance of the joint.

The analytical development realised in the 1990's to extend the Component Method to beam-to-column joints with bolted connected submitted to a combination of bending moment and axial force has not lead to satisfactory results [Hoffmann, 1993; Hermann, 1997 and Guisse, 1997] because i) the application of the proposed methods is restrictive and/or ii) the influence of axial forces on the rotational stiffness and the capacity of rotation is not considered. In consequence, iterative methods have been developed mainly at the University of Liège. As a result of these investigations [Finet, 1994; Jaspart, 1997 and Cerfontaine, 2004], the ASCON software is a tool dedicated to the determination of M-N interaction diagram for different joints, accounting for group effects. The rotational stiffness and the capacity of rotation of joints have also been considered. A similar calculation procedure has been developed at the University of Coimbra [Simões da Silva, 2001b].

These analytical procedures have been compared to the few existing experimental results on the mechanical behaviour of joints subjected to a combination of axial force and bending moment. The first series of tests have been performed by Wald at the University of Prague on eccentrically loaded beam-to-column joints and beam-to-beam splices [Wald, 2001]. The second experimental study has been conducted on single-sided major-axis joints with flush and extended end-plate connections at the University of Coimbra [Simões da Silva, 2004 and De Lima, 2004].

5.4 Use of the Component Method under natural fire

5.4.1 Effects of natural fire on the Component Method

Thanks to the numerous research projects focused on the development of the rules of the Component Method at room temperature, especially in Europe, engineers have gained confidence in this approach and it has been included in the Eurocode recommendations for the design of common joints after the last questions have been dealt with. The investigations about the use of the Component Method under fire conditions are more recent. The difficulties to extend the field of application to fire are given hereafter:

- The number of fire tests performed on joints is small and this makes the validation of the models difficult. This limitation is related to two main reasons: the cost of fire tests performed on joints and the existence of few real cases where fire has induced a failure in joints.

- The difficulty to reproduce experimentally and numerically the real thermal conditions and internal forces in the joint of a frame subjected to fire. The continuous change of stress distribution is combined to spatial and temporal variations of mechanical properties.

A state-of-the-art of available experimental results obtained from tests focused on the behaviour of steel joints at elevated temperature is realised in § 5.4.2 and a review of the existing mechanical models based on the Component Method for joints at elevated temperature is given in § 5.4.3.

5.4.2 Experimental tests performed on isolated joints under fire conditions

The first experimental tests on connections have been undertaken at CTICM under standard fire conditions [Kruppa, 1976]. This study showed that the failure of bolts was preceded by significant deformations in other elements of the joint. British Steel conducted two fire tests on rigid joints [B.S., 1982]. It was observed that considerable deformations are developed in the joint during the fire and that the assumption of a rigid behaviour at high temperatures is consequently not valid anymore.

Later, some tests realised to investigate the global behaviour of joints have been performed by the Steel Construction Institute on three common types of connections: extended end-plate, flush end-plate and double web cleats connections [Lawson, 1990]. He found that the bolts and welds remained intact in spite of the large deformations in the connection. These tests also highlighted the benefits of rotational restraints on the behaviour of steel and steel-concrete composite beams and the significant difference of temperature between the joint zone and the beam bottom flange.

A series of eleven tests performed at the University of Sheffield was aimed at deriving a set of moment-rotation curves of a unique joint configuration (flush end-plate connections) submitted to five different load ratios at elevated temperature [Leston-Jones, 1997]. This experimental programme led the definition of simplified models based on curve-fit procedures. In continuation of this work, twenty similar tests on flush and header plate connections have been realised to analyse the influence of the size of members, the type of connection and the failure modes [Al-Jabri, 1999]. The components of the tension zone and compression zone within a steel joint at elevated temperature have also been studied experimentally at the University of Sheffield. Successively, tests have been performed at elevated temperatures on column webs under transversal compression forces [Spyrou, 2004a] and equivalent T-stubs submitted to tensile forces [Spyrou, 2004b].

Two unrestrained cruciform joints with extended end-plate connections have been tested in China [Lou, 2006]. The connection failed by two different failure modes at room temperature and ambient temperature. Although temperature measured during the fire test near the bolts was lower than the one measured in the column web, the connections failed by buckling of the column web at ambient temperature and by failure of bolts during the fire test.

Recently, a research programme has been conducted at the Universities of Sheffield and Manchester with the aim of investigating the capacity and ductility of steel connections at elevated temperatures. This project has involved a series of tests (Figure 5-11) on common steel connections: web cleats connections [Yu, 2009a], fin plate connections [Yu, 2009c] and flush end-plate connections [Yu, 2008]. The inclination of the applied forces allows an adjustment of the ratio between tensile forces and bending moments in the joint.

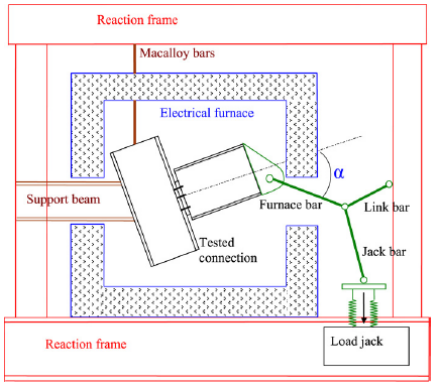

Figure 5-11 : Test set-up and detail of the tested web-cleat connections (Yu, 2009b)

As mentioned previously, one of the main difficulties encountered to reproduce the real conditions of a joint subjected to fire is due to the interaction with the surrounding structure. The effect of axial restraints and thermally-induced thrusts during both the heating and cooling phases of a fire have to be

considered in order to understand the behaviour of joints and connected elements in real cases. Plastic deformations and instability phenomena may also cause a redistribution of internal forces between members and a variation of bending moments in joints. A new design method based on membrane effects and consisting in fire-protecting a part of the beams that composes steel frames with composite floors [Bailey, 2000] is another example of the fact that the distribution of internal forces can completely differ at room temperature and under fire conditions due to the interaction between the elements of a structure. Tests performed on sub-structures and full-scale buildings will be described in Chapter 6.

5.4.3 Existing models based on the Component Method under fire loading

The application of the Component Method under fire loading has been adapted to elevated temperatures by reducing the resistance and stiffness of the components identified in the joint according to the recommendations of EN 1993-1-8 at room temperature. The reduction factors for effective yield strength k_y and for the slope of the linear elastic range k_E defined in the EN 1993-1-2 for structural elements have been used for individual components and the methodology for calculating the moment resistance and the rotational stiffness of a joint at elevated temperature is kept similar to the one developed at room temperature.

This approach has been firstly used for a flush end-plate connection with two bolt rows [Leston-Jones, 1997]. In this model, the two bolt rows have been replaced by an equivalent bolt row and the basic components identified are the column flange in bending, the bolts in tension, the end-plate in bending and the column web in compression. The model has been validated against of elevated-temperature tests realised by Leston-Jones.

The same procedure has been extended to all the components of the EN 1993-1-8 with the extension of the post limit component stiffness [Simões da Silva, 2000 and 2001a]. Under anisothermal conditions, the moment-rotation response of the steel joint is supposed to be constant on a short time step and the approach is reiterated at each time step. Good predictions of the mechanical behaviour of flush end-plate connections have been obtained under isothermal and anisothermal conditions.

Another component-based model based on the work of Leston-Jones has been proposed to predict the behaviour of steel and composite header plate connections at high temperatures [Al-Jabri, 2004]. This model has been compared with test data obtained previously by the same author [Al-Jabri, 1999].

Based on the experimental tests he performed independently on the tension and compression zones, Spyrou has defined joints as two rigid elements connected by two non-linear springs representing the action of the two zones [Spyrou, 2004c] so that i) the effect of axial forces is integrated in the model

and ii) moment-rotation curves are automatically calculated in the global analysis. Shear forces are not taken into account in this model. A more complete version of this model has been proposed by Block and incorporated into Vulcan software [Block, 2007]. The effect of cooling is also considered by use of the Masing rule. The web shear component has been added to this model for end-plate connections [Qian, 2009].

The integration of models based on the Component Method into ADAPTIC has been realised for flush end-plate connections, extended end-plate connections, double web cleats connections, top and seat angles connections and fin plate connections [Ramli Sulong, 2005]. Tri-linear force-displacement relationships have been defined for all components.

Santiago developed a general model divided in four partial models for flush end-plate and extended end-plate connections [Santiago, 2008d]. Each partial model is valid for a combination of axial force (tension or compression) and bending moment (hogging or bending). When the axial force passes from compression to tension or the bending moment passes from hogging to sagging, the partial model used for the joint is modified. The classic Masing rule has also been implemented for the unloading and reloading of active rows.

Finally, component-based models have been recently developed by Yu for web cleats connections [Yu, 2009b], fin plate connections [Yu, 2009c] and flush end-plate connections [Yu, 2009d] and validated against experimental results performed under isothermal conditions.

6 Experimental and numerical investigations on the behaviour of simple connections under natural fire

6.1 Introduction and scope of Chapter 6

Investigations on the behaviour of connections in steel structures subjected to fire can not be dissociated from the behaviour of the connected members. Chapter 3 has underlined that the evolution of internal forces in joints during a fire is intimately related to the behaviour of the beam and to the axial and rotational stiffnesses provided by the rest of the structure. The combination of axial forces, shear forces and bending moments transmitted by connections varies incessantly while the resistance and stiffness of the connection components are also function of the evolution of temperature.

This explains why tests have recently been performed on steel sub-structures by Efectis Netherlands under heating and subsequent cooling. Similarly to the tests performed at the University of Coimbra [Santiago, 2008b], the present tests are intermediary between fire tests performed on isolated joints (e.g.: tests performed at the University of Sheffield, see § 5.4.2) and real scale fire tests (e.g.: Cardington test, see Santiago, 2008d). A brief review of existing experimental tests on global structures is realised before the description of the new tests perfomed in Metz and Delft.

This chapter also presents mechanical models developed for fin plate, web cleats and header plate connection under fire and the results obtained from the numerical investigations using these models. These models have been validated against experimental tests performed by Efectis Netherland and numerical results given by other numerical models. Additional parametrical analyses have been run with these simple models and a design procedure has been proposed on the basis of this numerical work.

A special attention is paid to the behaviour of fin plate connections and an additional model, more complicated to build, has been developed for the prediction of bolt failures in this type of connections. This model is validated against very recent isothermal tests performed by Yu [2009c] on isolated joints subjected to a variable combination of tensile forces and bending moment.

6.2 Fire tests on steel sub-structures and real-scale structures: State-of the art

The fire tests performed on rugby goal-post by Liu at the University of Manchester have been presented in § 3.4.3. These tests were aimed at analysing the influence of axial restraints, the type of connections and the load level on the behaviour of beams under fire. The beam section used was quite small but these tests demonstrated that, with regard to pinned connections, stiff and resistant connections could enhance the fire resistance of steel beams by the reduction of the mid-span moment and by the development of catenary action.

Several large-scale tests have been performed in the late 1990's at the Cardington Laboratory. The 7th test was conducted on a 8-storey steel framed building subjected to a compartmental fire. This test allowed the examination of temperature development and distribution of internal forces in the structure during the fire. The description of the tests, measurements and behaviour of the components of the structure are reported in detail in [Wald, 2003].

In continuation to the 7th Cardington test, a series of six fire tests have been performed on steel sub-structures at the University of Coimbra. The thermal conditions of the 7th Cardington test have been reproduced and the influence of connection typologies on the behaviour of steel structures under natural fire has been investigated. Three flush end-plate connections, one extended end-plate connection, one welded connection and one header plate connection have successively been tested. The test performed with header plate connections will be discussed in § 6.4.7.2.

6.3 Description of the new experimental tests performed in Metz and Delft

6.3.1 Tests performed in Metz

The two tests performed in Metz consist of bare-steel sub-structures with a double-sided beam-to-column joint composed of flush end-plate connections. Axial restraints are applied to the beam in order to represent the action of a surrounding frame. The test set-up is described in Figure 6-1 and was identical for the two tests. On the left, a schematic drawing of the test set-up is given. The analysed beam-to-column joint is enclosed in a blue circle on the schematic drawing of the Figure 6-1. The geometrical characteristics of the connections are given in Figure 6-2. The 5.5 metre-long IPE 300 beam is submitted to a punctual load and a part of that beam (1.7 m) is situated outside the furnace.

The HEA 220 column is thermally protected, except near the joint. The extremity of the beam is connected to a sub-structure that provides axial restraints. This sub-structure is a rigid column that is pinned at its bottom extremity and connected to the mid-span section of a flexible beam at its top extremity. The column and the flexible beam of the restraining system are shown on Figure 6-1 (right). In order to get an accurate value of the restrained effect, a specific test was carried out. A restrained effect of around 2 kN/mm (representing 1 % of the beam axial stiffness) has been derived.

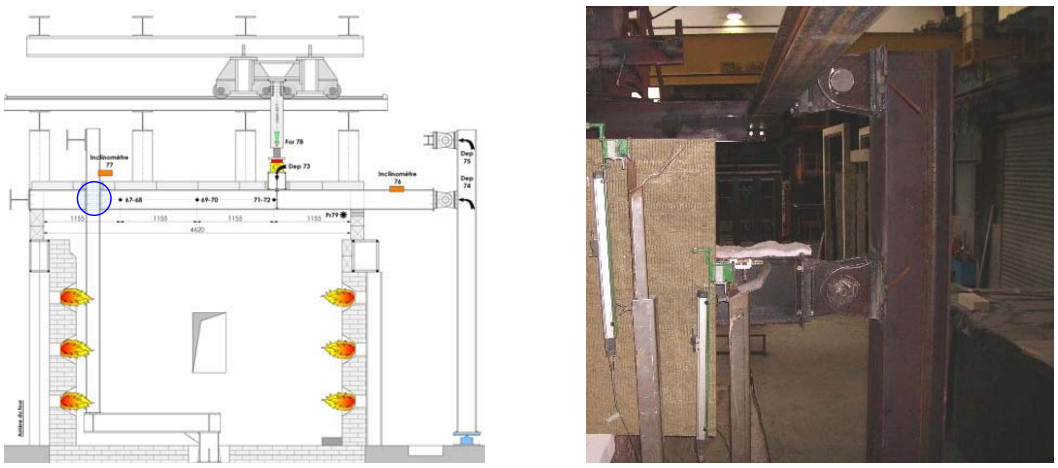

Figure 6-1 : Schematic drawing of the test set-up (left) and view of the restraining sub-structure (right) [Efectis France, 2007a]

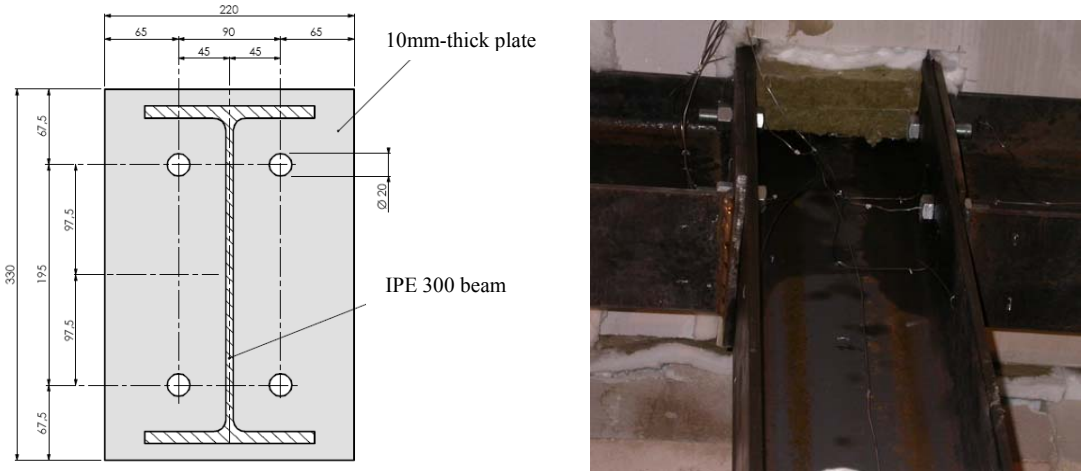

Figure 6-2 : Geometry of the double-sided joint with flush end-plate connections [Efectis France, 2007a]

The punctual loading applied during the two tests is approximately equal to 35 kN. In fire tests, the mechanical loading is usually characterised by the load ratio, defined as the ratio between the maximal bending moment in the beam and the plastic moment of the section. The steel grade is S235 for the beam. Considering a yield stress f_y equal to 235 MPa, the load ratio w is equal to 0.3 but the real yield stress is usually significantly underestimated, especially for the S235 steel grade. Unfortunately, no

coupon tests have been realised before or after the fire tests. The load ratio w is probably situated between 0.2 and 0.25 is these two tests.

These tests are aimed at investigating the behaviour of joints during both heating and cooling phases. During the first test, the specimen was heated increasingly until the steel beam can no longer bear the applied load. A speed of heating equal to 10°C/min has been followed. The test has been stopped after the ambient temperature of the furnace has reached 840°C. No failure of the bolts or other connection components occurred but the vertical displacement was higher than 220 mm when the burners have been stopped.

For the second test, the specimen was heated up to 700°C with a 10°C/min speed of heating. The heating phase was followed by a plateau lasting for 20 minutes and a cooling phase corresponding to the natural cooling conditions of the furnace. No failures have been observed in the joint zone. The vertical displacement was 58 mm at the end of the heating phase and remained constant during the temperature plateau and cooling phase.

6.3.2 Tests performed in Delft

The series of tests realised in Delft include two tests on bare-steel sub-structures (fin plate and web cleats connections) and four tests on steel-concrete composite sub-structures (fin plate, web cleats, header plate and extended end-plate connections). The main difference between the tests performed in Metz and Delft is the level of axial restraints and the type of connections. A specific test on the restraining frame used for Delft tests has shown that the spring stiffness is equal to 17 kN/mm (K = 6.6 %). Simple connections are used for the tests performed on bare-steel sub-structures in Delft while flush end-plate connections have been used for the tests in Metz.

The loaded beam is a 4.4 metre-long IPE 300 profile and a short section (0.5 m) is situated outside the furnace. The HEB 300 column is thermally-protected, except near the joint. The punctual loading used for bare-steel sub-structures is equal to 60 kN. The results of coupon tests on the components of the tested sub-structures are given in Table 6-1. An average value of 345 N/mm² is obtained for the yield strength of the beam steel. Consequently, the load ratio w was equal to 0.3 in the tests on bare-steel structures.

Identification	Re 0.2% N/mm^2	Rm N/mm^2	A %
Fin plate	323	467	32.4
Web angle	320	440	34.9
End plate	323	467	33.7
Column test 1	232	382	37.1
Column test 2	224	381	39.0
Column test 3	230	380	36.4
Column test 4	255	379	37.3
Column test 5	220	380	35.3
Column test 6	238	381	39.4
Beam test 1	342	471	29.8
Beam test 2	340	474	28.0
Beam test 3	358	473	27.8
Beam test 4	336	471	28.8
Beam test 5	342	473	29.8
Beam test 6	354	475	24.2

Table 6-1 : Results of coupon tests performed on tested elements of Delft fire tests [Efectis NL, 2009]

During the tests, it was predicted to control the furnace so that the evolution of temperature given in Figure 6-3 was applied to the steel beam. It was intended to switch off the furnace after a short plateau at 600°C. However, the heating has been continued slowly in the two tests on steel sub-structures until significant deflections were obtained (around 200 mm). This procedure is an “optimization” of the risk of connection failure during the cooling phase. Indeed, the heating phase is stopped on the verge of the beam failure so that significant plastic strains are developed and high tensile forces will appear during the cooling phase. As a result of such a test, it can be concluded that:

- If no failure in the connection is observed during the cooling phase of a test, the risk of failure is inexistent for all the cases with the same joint configuration, the same mechanical loading and the same speed of heating. In case of shorter durations of the cooling phase, no more failures would have occurred in the connection components during the cooling phase. In case of a longer heating phase, the beam (or the connection) would have failed before the cooling phase takes place.

- If a failure is observed during the cooling phase, no conclusion can be drawn for the cases where the heating would have been stopped earlier.

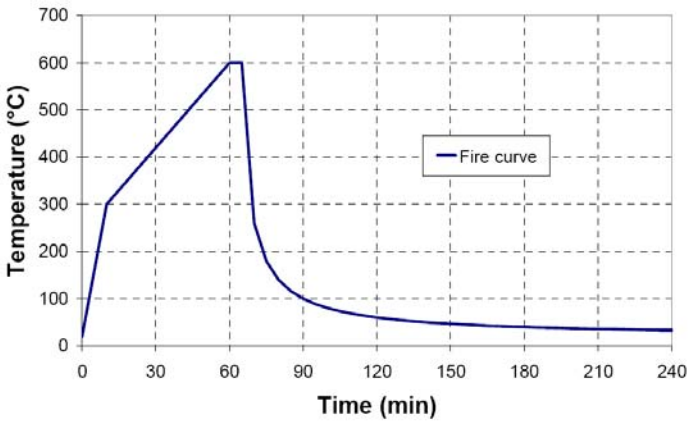

Figure 6-3 : Predicted evolution of temperature in the steel beam (before adaptation)

The geometry of the fin plate connections was the same for the test performed on steel and composite sub-structures (Figure 6-4). The connection is composed of a 230 x 100 x 10 fin plate and three M20 Grade 8.8 bolts. In the test with a steel sub-structure, the average furnace temperature reached 650°C. As the speed of heating was quite low at the end of the heating phase (5-10°C/min), the temperature has approximately reached 650°C in the beam bottom flange at mid-span. Near the joint, the temperature of the beam bottom flange reached 600°C.

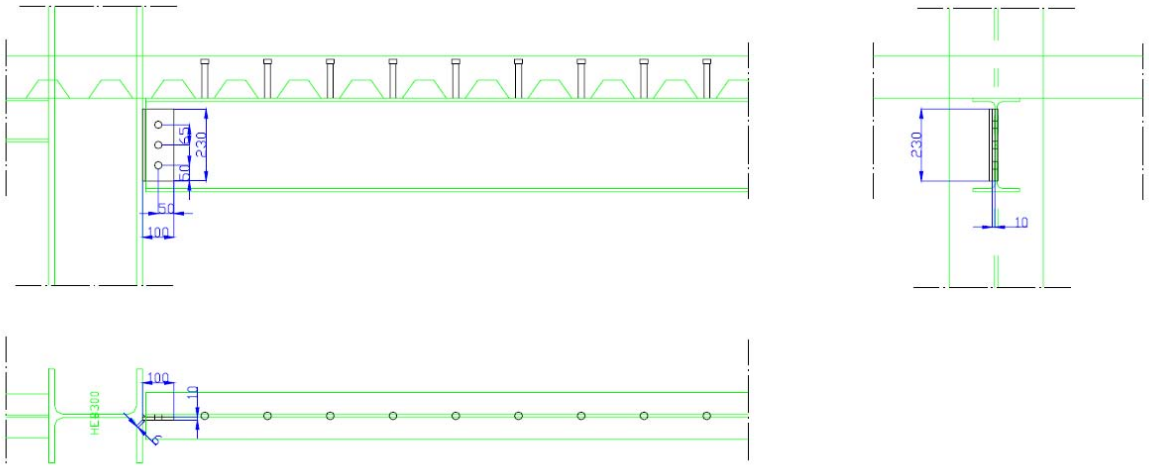

Figure 6-4 : Geometrical properties of the fin plate connection (Test n°1)

The three bolts broke in shear after 127 minutes (Figure 6-5) but a short discontinuity is observed after 108 minutes in the measurements of horizontal elongation in the restraining system. This tends to demonstrate that one bolt has probably failed at that moment. The connection failure has not caused a fall down of the beam because the beam top flange was still supported by the fin plate after the failure of all the bolts.

Figure 6-5 : Fin plate connection after failure of the connection

The geometry of the double web cleats connections used for the two tests performed on steel and composite sub-structures is plotted on Figure 6-6. The connection is composed of two 240 x 90 x 9 web cleats and nine M20 Grade 8.8 bolts. In the test with a steel sub-structure, the average furnace temperature and the temperature of the beam bottom flange at mid-span reached 670°C after 70 minutes before cooling down. In the joint zone, the temperature of the beam bottom flange has not been higher than 600°C.

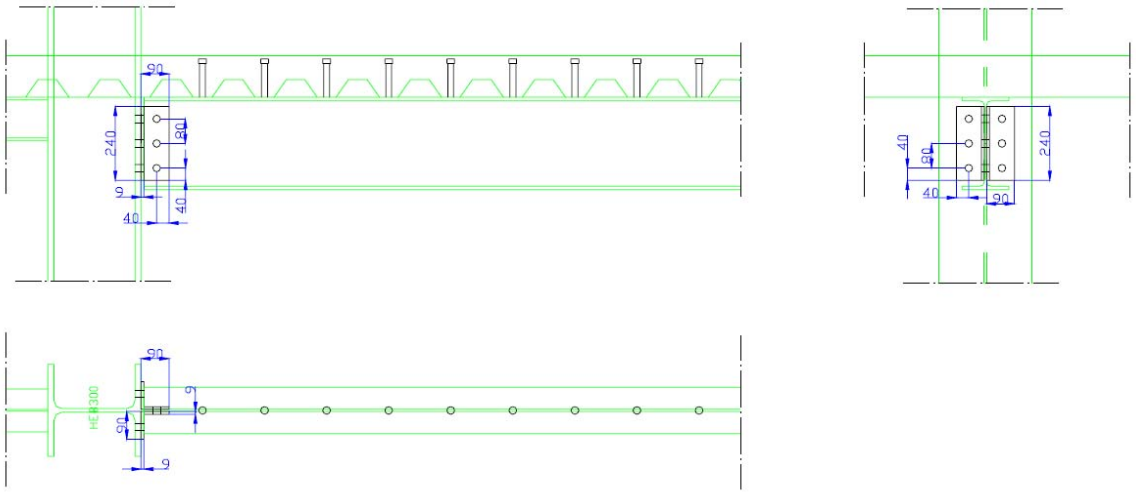

Figure 6-6 : Geometrical properties of the double web cleats connection (Test n°2)

After seven hours of test, no failure of the connection had occurred. Minor deformations of the web cleats have been observed.

Figure 6-7 : Double web cleats connection after the test

6.4 Model for connections under natural fire: Bilinear Fibres

6.4.1 Introduction

The modelling of the mechanical behaviour of steel joints under fire by use of simple models is a quite recent and complicated discipline (see § 5.4.3), especially for the types of connections analysed here. The interaction between axial forces, shear forces and bending moments, the existence of failure modes with 2 or more bolt rows, the different reductions factors for bolts, welds and carbon steel components at elevated temperatures, the influence of a heating-cooling cycle on the resistance of bolts and welds, the contact between the beam and column flange under large rotations, the local buckling of the beam web or beam bottom flange are a non-exhaustive list of phenomena that should be taken into account when modelling the behaviour of common simple connections under natural fire conditions.

In the Bilinear Fibres Model, the action of joints in a structure or a sub-structure is represented by a beam element including one fibre per (compressive or bolt) row. A fibre is defined as a sectional area in the cross-section of a beam element that has no dimension in the plane of the section: the area is concentrated at the position of the fibre (in this work, all figures will represent the fibres with a section, for illustration purposes). The sectional area of the section is equal to the sum of the area of all fibres of the section. The second moment of area of the section depends on the area and the vertical position of all fibres:

$EI_{section} = \sum_{i=1}^{n_{fibres}} E_i A_i d_i^2$	**6-1**

In this equation, E_i, A_i and d_i are respectively the Young's modulus of the fibre i, the cross-section area of the fibre i and the vertical distance between the position of the fibre i and the position of the centre of gravity of the cross-section.

In the present model, the resistance $F_{Rd,row}$ and the initial stiffness $K_{ini,row}$ of one row is calculated by Eqs 6-2 and 6-3.

$F_{Rd,row} = \min_{j=1}^{n_{comp}} \left(F_{Rd,j} \right)$	**6-2**
$K_{ini,row} = \left(\sum_{j=1}^{n_{comp}} K_{ini,j}^{-1} \right)^{-1}$	**6-3**

where $F_{Rd,j}$, $K_{ini,j}$ and n_{comp} are respectively the resistance of the component j, the axial stiffness of the component j and the number of components of that row.

The length of the beam element representing the action of the joint L_j is usually determined as the distance between the symmetry axis of the column and the section where the internal forces are transfered from the beam to the connection or directly from the beam to the column. For example, this section is passing by the center of bolts in fin plate connections. The cross-section area A_i of each fibre is chosen arbitraly. In this section of the work, the material laws assigned to the fibres are bilinear and work in tension, in compression or in the two domains. They are characterised by a fictive Young's modulus E_i and yield strength $f_{y,i}$ obtained by Eq. 6-4 and 6-5.

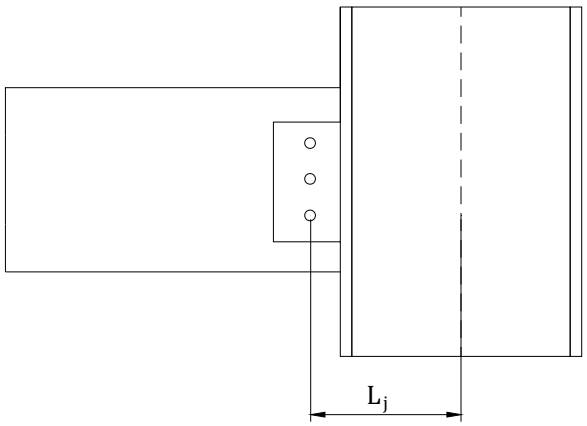

Figure 6-8 : Length of the beam element representing the action of the joint for a fin plate connection

$f_{y,i} = \frac{F_{Rd,i}}{A_i}$	**6-4**

$E_i = \frac{K_{ini,i} L_j}{A_i}$	**6-5**

The existing material laws defined in SAFIR are not adapted to asymmetric constitutive laws. New laws and adaptations have been implemented for joint applications (see the description in § 6.4.2).

6.4.2 New material laws and adaptations to SAFIR for the Bilinear Fibres Model

6.4.2.1 'BILIN' material law

The 'BILIN' material law has already been defined in SAFIR for applications at room temperature. This law is symmetric in tension and compression. The behaviour is elastic until a yield limit f_y and the slope is equal to the hardening modulus E_{hard} for higher strains. If a hardening branch is reached (for example, $\sigma = \sigma_1$), the unloading is elastic from σ_1 to $\sigma_1 - 2f_y$ before the other hardening branch is reached (Figure 6-9).

As a first step, the 'BILIN' material law has been extended to elevated temperatures on the basis of the law defined in the EN 1993-1-2 for carbon steel at elevated temperatures. At each time step, the reduction factors for yield strength k_y and for the slope of the linear elastic range k_E are calculated for each fibre as a function of the temperature of this fibre. However, the temperature measured or calculated in one row is not a sufficient indication for applications based on the Component Method because:

- The resistance of one row of components is the minimal value of all the components of that row. As the resistance of bolts and welds decreases faster than carbon steel, the reduction of resistance in one row does not follow the curves of bolts, welds or carbon steel.

- The evolution of the resistance is not reversible for bolts and welds components[*] so that, in a real application, the resistance at two instants characterised by a same temperature is different.

[*] It is assumed in the present work that the behaviour of carbon steel components can be regarded as reversible for the domain of temperature considered ($20°C \leq T \leq 700°C$).

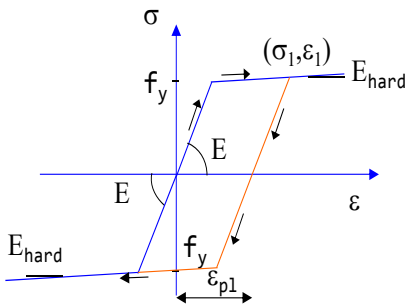

Figure 6-9 : Elasto-plastic behaviour of the 'BILIN' material law

Consequently, the use of the reduction factors defined for carbon steel necessitates calculating, at each time step and for each row of components, the ratio between the resistance of the row at this time step and the resistance of the row at room temperature. Then, a fictive temperature characterised by a reduction factor k_y equal to the calculated ratio is allocated to the fibre representing the row of components considered.

However, this method still has two drawbacks:

- The procedure for evaluating the fictive temperature is quite long.
- The reduction of stiffness of a row of components due to the elevation of temperature depends on the fictive temperature and is probably not good.

An adaptation has been realised in the SAFIR software to allow the user to choose between i) an automatic evaluation of the reduction factors k_y and k_E as a function of the temperature of the fibre and ii) a direct definition of the reduction of resistance and stiffness in the fibres. This option is also available for the new material laws defined in § 6.4.2.2 to § 6.4.2.4.

6.4.2.2 'BILIN_COMP' and 'Translated BILIN_COMP' material laws

'BILIN_COMP' is a material law that only resists to compressive stresses. In compression, the behaviour is elastic until a yield limit f_y and the slope is equal to the hardening modulus E_{hard} for higher strains (Figure 6-10a). The unloading is elastic and the plastic strain ε_{pl} remains constant. In tension, this material has no resistance and no stiffness (Figure 6-10b).

If we consider a 'BILIN_COMP' fibre subjected to a loading-unloading cycle where the maximal compressive stress σ_{max} is higher than f_y, the plastic strain ε_{pl} remains constant during the unloading. After this cycle, the fibre strain ε can reduce freely with no variation of the stress σ but the plastic

strain ε_{pl} remains unchanged and the stresses will be 0 for the $\varepsilon < \varepsilon_{pl}$. To sum up, the plastic strain ε_{pl} can not decrease.

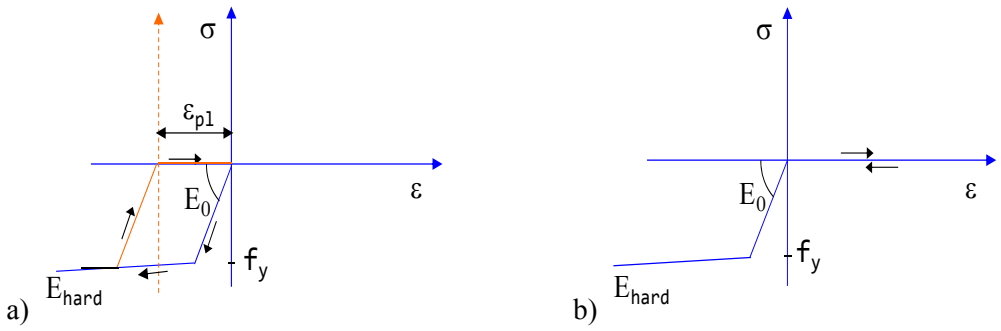

Figure 6-10 : 'BILIN_COMP' material law subjected to negative (left) and positive strains (right)

The 'BILIN_COMP' law is used to model the transfer of forces by contact between beam and column flanges (with or without intermediary end-plate). The definition of an initial translation to the left ε_{ini} is allowed in this material law (Figure 6-11) so that the contact is obtained after the closing of an initial gap (Eq. 6-6). This law is called 'Translated BILIN_COMP' and is used for the contact between beam and column flanges in simple connections (fin plate, double web cleat or header plate).

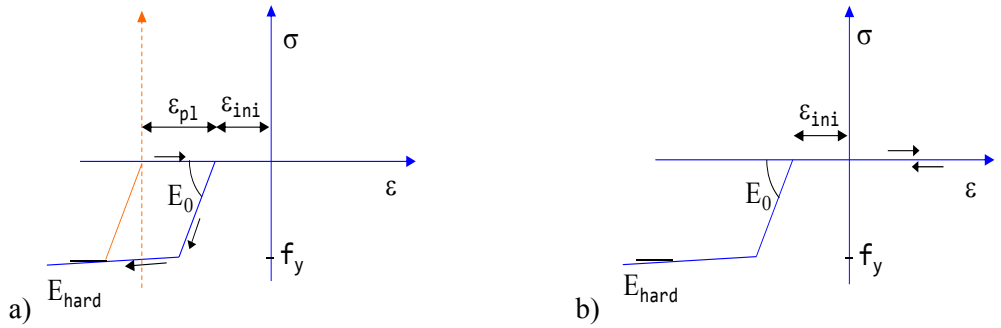

Figure 6-11 : 'Translated BILIN_COMP' law subjected to negative (left) and positive strains (right)

$\varepsilon_{ini} = \frac{L_{gap}}{L_j}$	**6-6**

where L_{gap} and L_j are the dimension of the gap and the length of the finite element representing the action of the joint.

6.4.2.3 'BILIN_TENS'and 'BILIN_BOLTS' material laws

The 'BILIN_TENS' material law is symmetric to the 'BILIN_COMP' one (resisting to tensile stresses instead of compressive stresses) but this law has only been used in the present work for modelling the bolt rows of flush end-plate connections. The 'BILIN_BOLTS' law has been defined for the

modelling of bolt rows in header plate connections. The unique difference between these two laws is the fact that the plastic strain ε_{pl} can decrease in the 'BILIN_BOLTS' law when the fibre strain ε decreases with no variation of the associated stress σ (the (σ ; ε) point moves on the horizontal axis)

The reason why the material law 'BILIN_BOLTS' has been used for bolt rows of header plate connections and the conditions that must be fulfilled to use it will be described in § 6.4.3.3.

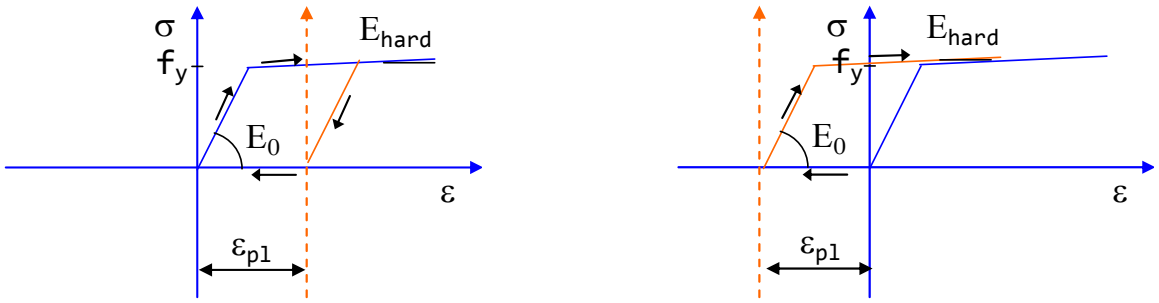

Figure 6-12 : BILIN_BOLTS material law subjected to positive (left) and negative strains (right)

6.4.2.4 "BILIN_ASYM" material law

Finally, a 'BILIN_ASYM' material law has been defined for rows of components that work differently under compressive and tensile stresses. In this law, the elastic limit f_y and the Young's modulus E are different in tension and compression. In both domains, the unloading is realised following a parallel to the elastic branch until reaching the horizontal axis (Figure 6-13).

This material law is dedicated to the bolt rows of double web cleat connections (see § 6.4.3.4) and flush end-plate connections (see § 6.4.3.1).

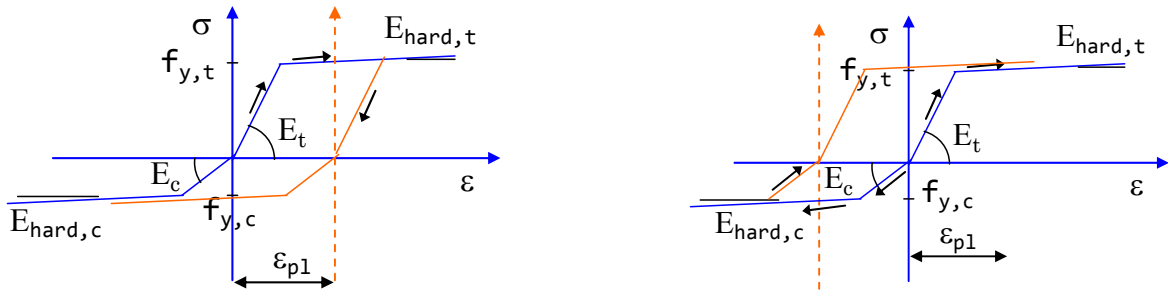

Figure 6-13 : BILIN_ASYM material law subjected to positive (left) and negative strains (right)

6.4.3 Application of the Bilinear Fibres Models to several types of connections

6.4.3.1 Flush end-plate connections

6.4.3.1.1 Bilinear Fibre Model for flush end-plate connections

In flush end-plate connections, the internal forces (axial and shear forces, bending moments) are transferred by the bolt rows, weld fillets and by contact between the beam flange and the end-plate. In the transmission of compressive forces at the level of beam flanges, the activated components are "beam flange in compression" and the "column web in compression". In presence of bending moments, the component "column web in shear" should also been considered. The transfer of tensile forces at the level of bolt rows activates four components: bolts in tension, end-plate in bending, column flange in bending and column web in tension.

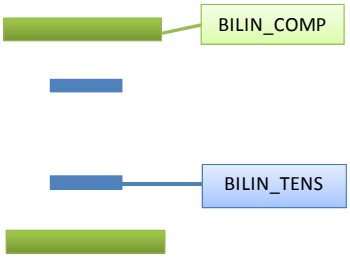

Figure 6-14 : Four-fibre model for flush end-plate connections with two bolt rows

6.4.3.1.2 Transfer of compressive forces at room temperature

The expressions of the resistance $F_{c,wc,Rd}$ and the stiffness $k_{c,wc}$ of the column web in compression defined in the EN 1993-1-8 are reported in Eqs 6-7 and 6-8. The reduction factor for buckling ρ depends on the plate slenderness λ_p (Eqs 6-9 and 6-10) and the effective width of the column web in compression $b_{eff,c,wc}$ is given, for a flush end-plate connection and a rolled H section column, by Eq. 6-11. The reduction factor ω for interaction with shear is given in Table 6-2 where the transformation parameter β is 1 in single-sided joints. Finally, the factor k_{wc} reduces the resistance of the column web in compression when the maximum longitudinal stress $\sigma_{com,Ed}$ due to axial force and bending moment in the column exceeds 0.7 $f_{y,wc}$ in the web (Eq. 6-12).

$F_{c,wc,Rd} = \frac{\omega b_{eff,c,wc} t_{wc} f_{y,wc}}{\gamma_{M0}} \leq \frac{\omega \rho b_{eff,c,wc} t_{wc} f_{y,wc}}{\gamma_{M1}}$	**6-7**
$k_{cwc} = \frac{0.7 b_{eff,c,wc} t_{wc} f_{y,wc}}{d_c}$	**6-8**

$\rho = \min\left(\left(\overline{\lambda}_p - 0.2\right)\Big/\overline{\lambda}_p^2 ; 1\right)$	**6-9**
$\overline{\lambda}_p = 0.932\sqrt{\dfrac{b_{eff,c,wc}\, d_{wc}\, f_{y,wc}}{E\, t_{wc}^2}}$	**6-10**
$b_{eff,c,wc}\, t_{wc} = t_{fb} + 2\sqrt{2}\, a_p + 5\left(t_{fb} + r_c\right) + 2\, t_p$	**6-11**
$k_{wc} = \min\left(1.7 - \sigma_{com,Ed}\,/\,f_{y,wc}\right)$	**6-12**

Transformation parameter β	Reduction factor ω
$0 \le \beta \le 0{,}5$	$\omega = 1$
$0{,}5 < \beta < 1$	$\omega = \omega_1 + 2\,(1-\beta)\,(1-\omega_1)$
$\beta = 1$	$\omega = \omega_1$
$1 < \beta < 2$	$\omega = \omega_1 + (\beta - 1)\,(\omega_2 - \omega_1)$
$\beta = 2$	$\omega = \omega_2$
$\omega_1 = \dfrac{1}{\sqrt{1 + 1{,}3(b_{eff,c,wc}\, t_{wc}\,/\,A_{vc})^2}}$	$\omega_2 = \dfrac{1}{\sqrt{1 + 5{,}2(b_{eff,c,wc}\, t_{wc}\,/\,A_{vc})^2}}$

Table 6-2 : Reduction factor for interaction with shear [CEN, 2005a]

In Eqs 6-7 to 6-12, t_{fb}, t_{wc}, t_p, r_c, d_c, $f_{y,wc}$, E, γ_{M0} and γ_{M1} are the beam flange thickness, the column web thickness, the plate thickness, the column radius fillet, the clear depth of the column web, the yield strength of the column web, the Young's modulus of the column web and partial safety factors.

The resistance of a beam flange and the adjacent compression zone of the beam web in compression $F_{c,fb,Rd}$ is given in Eq. 6-13. In flush end-plate connections, this force is assumed to act at the level of the centre of compression. This component is supposed to be sufficiently rigid so that its flexibility is neglected in the models based on the Component Method.

$F_{c,fb,Rd} = M_{c,Rd}\Big/\left(h - t_{fb}\right)$	**6-13**

where h is the depth of the connected beam, t_{fb} is the flange thickness and $M_{c,Rd}$ is the design moment resistance of the beam cross-section.

The resistance of an unstiffened column web panel is obtained by Eq. 6-14 provided the column web slenderness satisfies the condition in Eq. 6-15.

$V_{wp,Rd} = \dfrac{0.9\, f_{y,wc}\, A_{vc}}{\sqrt{3}\,\gamma_{M0}}$	**6-14**
$d_c\,/\,t_{wc} \le 69\,\varepsilon$	**6-15**

$\varepsilon = \sqrt{235/f_{y,wc}}$	**6-16**
$k_{cws} = \dfrac{0.38\,A_{vc}}{\beta\, z}$	**6-17**

A_{vc} is the shear area of the column and z is the lever arm between the centre of compression and the centre of gravity of the tension zone (Figure 6-15).

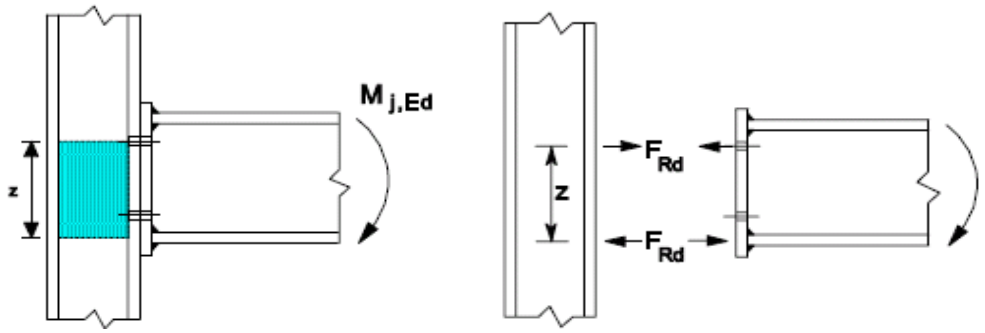

Figure 6-15 : Lever arm in a flush end-plate connection under pure bending [CEN, 2005a]

6.4.3.1.3 Transfer of tensile forces at room temperature

The transfer of tensile forces at the level of bolt rows activates four components: bolts in tension, end-plate in bending, column flange in bending and column web in tension. The component "bolts in tension" has been analysed in detail in Chapter 4. The resistance of the end-plate and the column flange in bending is calculated by evaluation of the three failure modes of the T-stub in tension (complete yielding of the flange – Eq. 6-18, bolt failure with column yielding – Eq. 6-19 or bolt failure – Eq. 6-20). These three failure modes are represented on Figure 6-16.

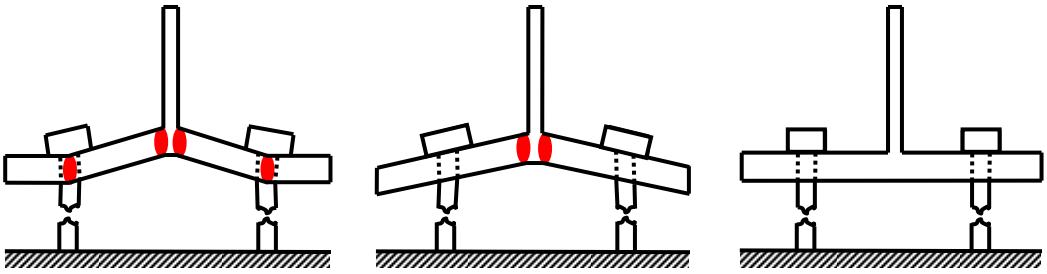

Figure 6-16 : Failure Modes 1, 2 and 3 of T-stub in tension

$F_{T,1,Rd} = \dfrac{(8n - 2e_w)\, M_{pl,1,Rd}}{2mn - e_w(m+n)}$	**6-18**
$F_{T,2,Rd} = \dfrac{2\,M_{pl,2,Rd} + n\sum F_{t,Rd}}{m+n}$	**6-19**

$F_{T,3,Rd} = \sum F_{t,Rd}$	**6-20**
$M_{pl,1-2,Rd} = 0.25 \sum l_{eff,1-2}\, t_{fc}^2\, f_{y,fc} / \gamma_{M0}$	**6-21**
$n = \min(e_{\min}; 1.25m)$	**6-22**
$e_w = d_w / 4$	**6-23**

where t_{fc}, $f_{y,fc}$, $F_{t,Rd}$ and γ_{M0} are the thickness of the column flange, the yield strength of the column flange, the design resistance of bolts and the partial safety coefficient. The effective lengths $l_{eff,1}$ and $l_{eff,2}$ for an unstiffened column flange are evaluated by use of Table 6-3 for individual bolt rows and groups of bolt-rows. The geometric parameters m, e, e_{min}, n and d_w are defined on Figure 6-17. For end-plates, the effective lengths are given in Table 6-4.

Bolt-row Location	Bolt-row considered individually		Bolt-row considered as part of a group of bolt-rows	
	Circular patterns $\ell_{eff,cp}$	Non-circular patterns $\ell_{eff,nc}$	Circular patterns $\ell_{eff,cp}$	Non-circular patterns $\ell_{eff,nc}$
Inner bolt-row	$2\pi m$	$4m + 1{,}25e$	$2p$	p
End bolt-row	The smaller of: $2\pi m$ $\pi m + 2e_1$	The smaller of: $4m + 1{,}25e$ $2m + 0{,}625e + e_1$	The smaller of: $\pi m + p$ $2e_1 + p$	The smaller of: $2m + 0{,}625e + 0{,}5p$ $e_1 + 0{,}5p$
Mode 1:	$\ell_{eff,1} = \ell_{eff,nc}$ but $\ell_{eff,1} \le \ell_{eff,cp}$		$\sum \ell_{eff,1} = \sum \ell_{eff,nc}$ but $\sum \ell_{eff,1} \le \sum \ell_{eff,cp}$	
Mode 2:	$\ell_{eff,2} = \ell_{eff,nc}$		$\sum \ell_{eff,2} = \sum \ell_{eff,nc}$	

Table 6-3 : Effective lengths for an unstiffened column flange [CEN, 2005a]

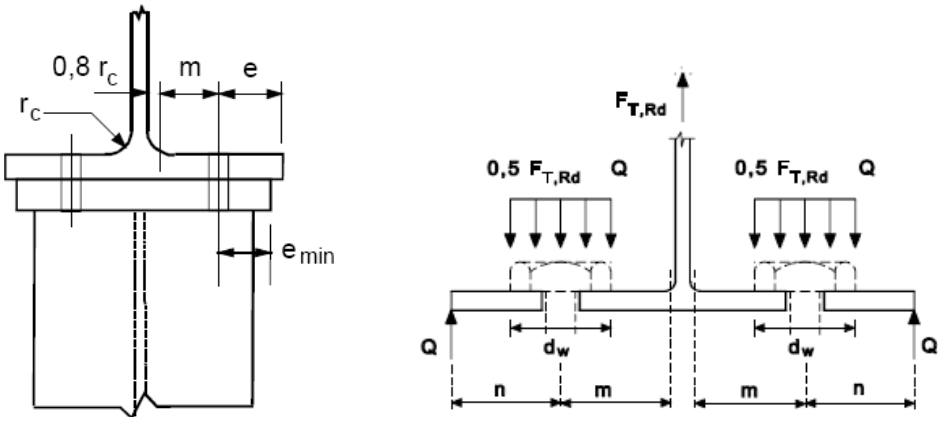

Figure 6-17 : Geometrical parameters for the evaluation of the effective lengths of unstiffened column

Bolt-row location	Bolt-row considered individually		Bolt-row considered as part of a group of bolt-rows	
	Circular patterns $\ell_{eff,cp}$	Non-circular patterns $\ell_{eff,nc}$	Circular patterns $\ell_{eff,cp}$	Non-circular patterns $\ell_{eff,nc}$
Other inner bolt-row	$2\pi m$	$4m + 1{,}25\,e$	$2p$	p
Other end bolt-row	$2\pi m$	$4m + 1{,}25\,e$	$\pi m + p$	$2m+0{,}625e+0{,}5p$
Mode 1:	$\ell_{eff,1} = \ell_{eff,nc}$ but $\ell_{eff,1} \le \ell_{eff,cp}$		$\sum\ell_{eff,1} = \sum\ell_{eff,nc}$ but $\sum\ell_{eff,1} \le \sum\ell_{eff,cp}$	
Mode 2:	$\ell_{eff,2} = \ell_{eff,nc}$		$\sum\ell_{eff,2} = \sum\ell_{eff,nc}$	

Table 6-4 : Effective lengths for an end-plate [CEN, 2005a]

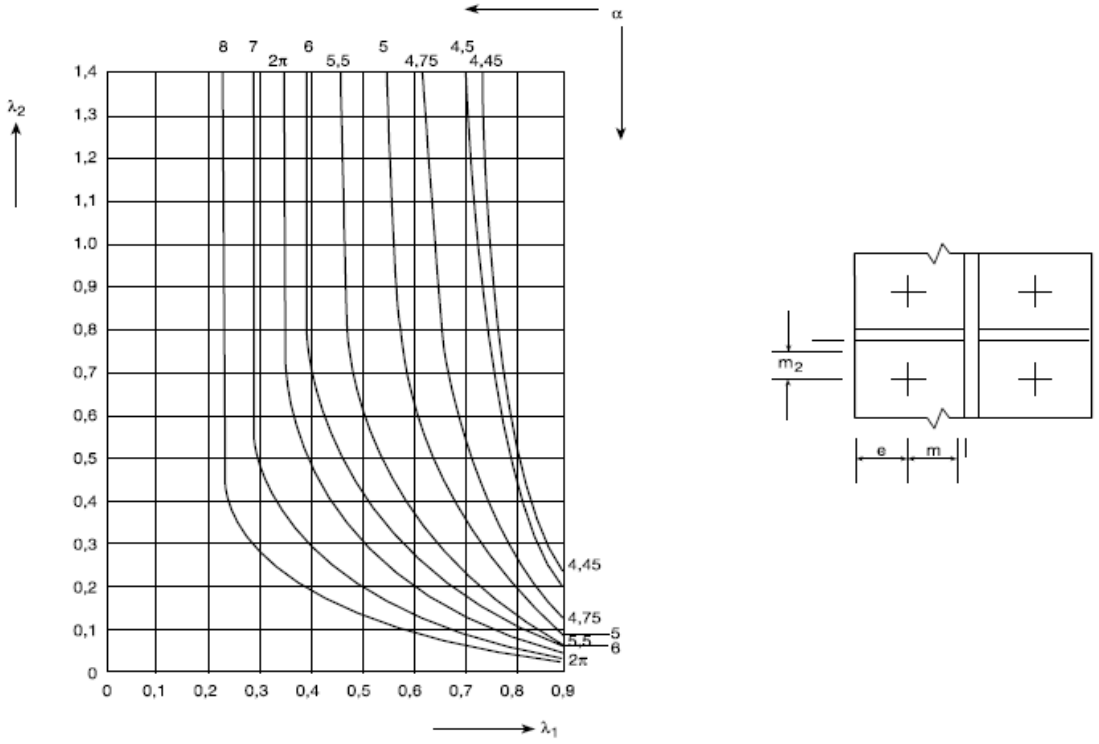

Figure 6-18 : Values of α for the effective length of the first bolt row situated below the tension flange of beam (component "end-plate in bending") [CEN, 2005a]

Finally, the design resistance of an unstiffened column web subject to transverse tension $F_{t,wc,Rd}$ should be determined from Eq. 6-24 where ω is a reduction factor to allow for the interaction with shear in the column web panel (see Table 6-2). For bolted connections, the recommended value of the effective width $b_{eff,t,wc}$ is the effective length of the equivalent T-stub representing the column flange (Table 6-3).

$$F_{t,wc,Rd} = \frac{\omega b_{eff,t,wc} t_{wc} f_{y,wc}}{\gamma_{M0}} \qquad \textbf{6-24}$$

6.4.3.1.4 *Assumptions in the Bilinear Fibres Model at high temperatures*

The resistance and the stiffness of the four fibres are calculated at an elevated number of time steps. That procedure has been automated in an Excel file but several assumptions or simplifications have been made:

- The stiffness of the bolt, weld and carbon steel components is obtained by multiplication of the stiffness calculated at room temperature by the reduction factor for the slope of the linear range k_E, defined in the EN 1993-1-2, during both the heating and cooling phases. This also applies to the other types of connections of § 6.4.3.

- Under fire conditions, all the partial safety coefficients γ_{M0}, γ_{M1} and γ_{M2} are taken equal to 1. This also applies to the other types of connections of § 6.4.3.

- The reduction factor k_{wc} should be adapted in function of the internal forces in the beam but, in this work, this coefficient has been kept equal to 1 under fire conditions.

6.4.3.2 *Fin plate connections*

6.4.3.2.1 *Bilinear Fibre Model for fin plate connections*

The beam elements used to model the action of fin plate connections include one fibre per bolt row and two fibres for the contact between the beam and column flanges (Figure 6-19). Bolt rows are represented by a 'BILIN' fibre including seven components: beam web in bearing, fin plate in bearing, bolt in shear, fin plate in tension/compression, the beam web in tension/compression and the column (beam and web) in tension/compression. However, the influence of the last four components on the resistance and the stiffness of one bolt row is negligible compared to the influence of the three first components mentioned. For the contact between the beam and column flanges, the components "beam flange in compression", "column flange in bending" and "column web in compression" are activated after the gap between the flanges are activated. The material law allocated to these fibers is 'Translated BILIN_COMP'.

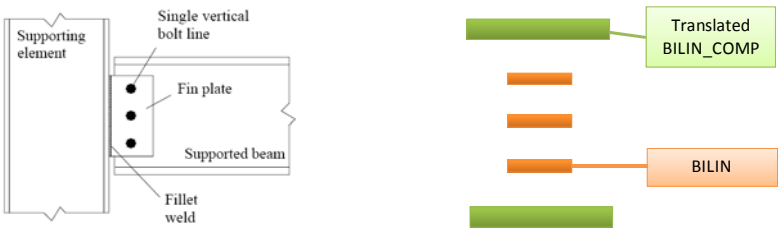

Figure 6-19 : Fin plate connection (left) and Bilinear Fibre Model (right)

6.4.3.2.2 Transfer of compressive forces by contact between flanges at room temperature

The components activated by the contact between beam and column flanges have already been presented in flush end-plate connections (Eqs 6-7 to 6-17). The evaluation of the effective width of the column web in compression $b_{eff,c,wc}$ is given must be slightly modified due to the absence of end-plate and welding (Eq. 6-25). The initial translation ε_{ini} is given by Eq. 6-6.

$b_{eff,c,wc} = t_{fb} + 2\sqrt{2}\,a + 5\left(t_{fb} + r_c\right)$	**6-25**

6.4.3.2.3 Transfer of tensile and compressive forces by bolt shearing at room temperature

The components identified by the Component Method for a bolt row of a fin plate connection are: beam web in bearing, fin plate in bearing, bolt in shear, fin plate in tension/compression, the beam web in tension/compression and the column (beam and web) in tension/compression. The component "bolts in shear" has been analysed in detail in Chapter 4. The resistance and the stiffness of a plate in bearing is given by Eq. 6-26 to Eq. 6-32.

$F_{b,Rd} = \dfrac{\alpha_b\, k_1\, f_u\, d\, t}{\gamma_{M2}}$	**6-26**
$\alpha_b = \min\left(\dfrac{e_1}{3d_0}; \dfrac{f_{ub}}{f_u}; 1\right)$	**6-27**
$k_1 = \min\left(2.8\dfrac{e_2}{d_0} - 1.7\,; 2.5\right) \qquad \left(for\ edge\ bolt\ rows\right)$	**6-28**
$k_1 = \min\left(1.4\dfrac{p_2}{d_0} - 1.7\,; 2.5\right) \qquad \left(for\ intermediary\ bolt\ rows\right)$	**6-29**
$S_{b,ini} = 12\, n_b\, k_b\, k_t\, f_u\, d$	**6-30**
$k_b = \min\left(\dfrac{e_1}{4d} + 0.5; \dfrac{p_1}{4d} + 0.375; 1.25\right)$	**6-31**
$k_t = \min\left(1.5\dfrac{t_{wb}}{d_{M16}}; 2.5\right)$	**6-32**

where t_{wb}, f_{ub}, f_u, d_0, d, d_{M16}, n_b, γ_{M2} are the thickness of the beam web, the ultimate strength of bolts, the ultimate strength of the plate, the nominal bolt diameter, the hole diameter, the nominal diameter of a M16 bolt, the number of bolts of that row and the partial safety coefficient. The other geometrical parameters are represented on Figure 6-20 for a horizontal applied force.

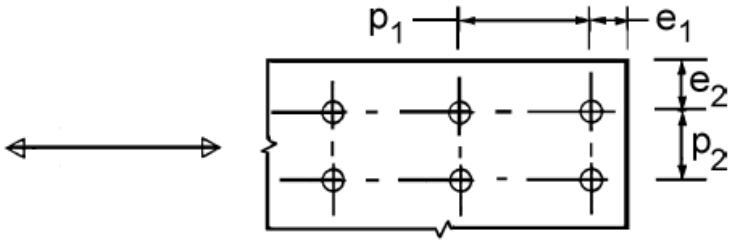

Figure 6-20 : Parameters for spacing of fasteners [CEN, 2005a]

The resistances in section of the beam web and the fin plate are usually calculated on the respective complete heights. In order to take the resistance in section into account in the Bilinear Fibres Model, the complete heights of the fin plate and the beam are divided into zones characterised by an individual resistance and an individual stiffnesses (Figure 6-21).

$F_{sect,i,Rd} = \frac{l_{eff,i}\, t\, f_y}{\gamma_{M0}}$	**6-33**
$S_{sect,i,ini} = \frac{l_{eff,i}\, t\, E}{L_p}$	**6-34**

where t is the thickness of the plate, f_y and E are the yield strength and the Young's modulus of the plate and L_p is the length of the plate in tension or compression and included in the joint zone.

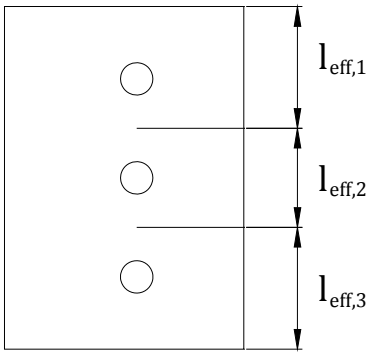

Figure 6-21 : Division of a plate into sections for the resistance in section

The resistance and the stiffness of the components "column flange in bending" and "column web in tension", activated when tensile forces are transferred, have already been mentioned for fin plate connections (§ 6.4.3.1).

6.4.3.2.4 Assumptions in the Bilinear Fibres Model at high temperatures

- The resistance and the stiffness of the column is assumed to be sufficient so that the neglection of the modes of failure related to these components and their flexibility can be neglected in the analyses.

- The resistance in section of the beam and the fin plate and the flexibitlity of these two components are supposed to have an insignificant influence on the mechanical behaviour of the fin plate connection.

- The resistance and the stiffness of the beam web and the fin plate in bearing is different under tensile and compression forces because the spacings are different. In presence of shear forces, this is still different because the reaction in one bolt row is oblique. In the simulations with the Bilinear Fibres Model, the resistance and the stiffness of these two components have been calculated under horizontal tensile forces. This is a safe approach because i) this leads to the lower resistance of the beam web and ii) the thickness of the beam web is smaller than the thickness of the fin plate in all the cases analysed.

6.4.3.3 Header plate connections

All the components activated in header plate connections have been described in the paragraph dedicated to flush end-plate connections. The unique difference is that, initially, there is no contact between the column and beam flanges in header plate connections. The transmission of compression at the level(s) of beam flanges necessitates that the initial gap is closed.

If the Bilinear Fibres Model presented for flush end-plate connections is simply adapted by substitution of the two 'BILIN_COMP' fibres in two 'Translated BILIN_COMP' fibres, no compressive forces and bending moments can be transferred without developing large rotations. This is due to the fact that, in flush end-plate connections, the contribution of the beam web level for the transfer of compressive forces by contact was added to the "beam flange in compression" component. Consequently, these two contributions must be shared in two different components in header plate connections: 'BILIN_COMP' fibres for the contact at the level of the beam web and the header plate and 'Translated BILIN_COMP' fibres for the contact at the level of beam flanges. This leads to the fibre model described in Figure 6-22. It is noted that the contact at the level of the header plate is divided in 5 to 10 elements in order to obtain a realistic rotational stiffness of the connection.

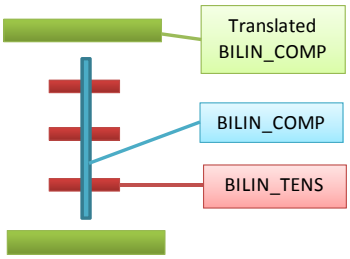

Figure 6-22 : Bilinear Fibre Model for header plate connections after sharing the contact components

This modification induces another possible discontinuity of the joint finite element. The response of the joint subjected to a loading-unloading cycle in compression followed by a loading-unloading cycle in tension is analysed hereafter, under the assumption that the section remains elastic.

1) Application of a compressive force transferred by the "contact fibres" situated at the level of the header plate.

2) Unloading of the section. The "contact fibers" are unloaded and the axial force is 0 in all the fibres of the section.

3) Application of a tensile force transferred by the 'BILIN_TENS' fibres situated at the level of the bolt rows.

4) Unloading of the section. The "contact fibers" are unloaded and the axial force is 0 in all the fibres of the section.

Assuming that the behaviour of all the fibres of the section remains elastic, the activation of the 'BILIN_TENS' fibres matches with the unloading of the "contact fibers". If plastic deformations are developed, the same sequence of loading-unloading cycles becomes:

1) Application of a compressive force transferred by the "contact fibres" situated at the level of the header plate. Development of plastics strains in these fibers.

2) Unloading of the section. The "contact fibres" are unloaded and all the axial force is 0 in all the fibres of the section. Plastic strains are kept constant.

3) Sudden variation of the plastic strains and comeback to the initial state. At that moment, the 'BILIN_TENS' fibres are activated.

4) Application of a tensile force transferred by the 'BILIN_TENS' fibres situated at the level of the bolt rows.

5) Unloading of the section. The “contact fibers” are unloaded and all the axial force is 0 in all the fibres of the section.

This demonstrates that the transition between the two subsequent loading-unloading cycles is not reflected in a realistic way. The contact between beam and column flanges could occur in case of yielding of the “contact fibres” situated at the header plate level but this would not have any influence on this discussion.

This problem is solved by modifying the material law of the fibres representing the action of the bolt rows. The ‘BILIN_BOLTS’ material law is used instead of the ‘BILIN_TENS’ material law. By use of the latter one, the fibres representing the action of the bolt rows will be activated as soon as the compressive force starts to decrease and no discontinuity will occur at any moment of the loading cycle. One additional condition must be fulfilled in order to get a realistic distribution of internal forces between the fibres: the order of magnitude of the stiffness of the “contact fibres” must be higher than the order of magnitude of the fibres representing the action of the bolt rows. If this condition is fulfilled, the axial force is approximately equal to zero in all the fibers after the loading-unloading cycle in compression.

Under natural fire, axial restraints induce compressive forces during the heating phase and tensile forces during the cooling phase and this corresponds to the analysed sequence of axial loadings. It should be noted that a similar discontinuity would be obtained if i) the loading-unloading cycle in tension is followed by compressive forces and ii) plastic strains have been developed in tension.

Finally, the Bilinear Fibre Model used for header plate connections is given in Figure 6-23, with ‘BILIN_BOLTS’ fibres at the level of bolt rows.

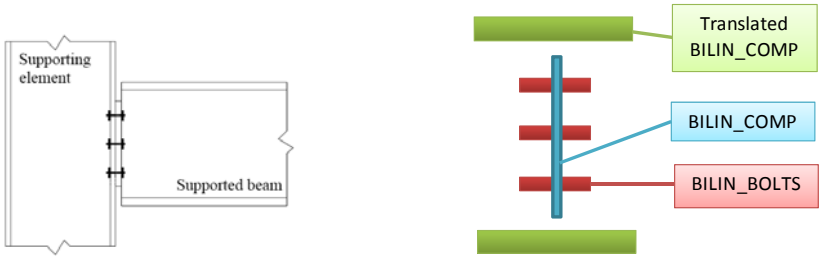

Figure 6-23 : Header plate connections (left) and Bilinear Fibre Model (right)

6.4.3.4 Double web cleats connections

The components activated in double web cleats connections are a combination of those mentioned in the two previous types of connections. The behaviour of bolts connecting the web cleats to the column

is similar to the behaviour of bolts in header plate connections. The connection between the beam and the web cleats activates the same components than fin plate connections but the bolts have two shear planes in double web cleats connections, instead of one.

The use of two consecutive elements reflecting the two bolted connections is not acceptable because of the direct contact between the beam and column flanges when large rotations develop. In the proposed model, all the components situated at the same level are considered in a unique fibre. The behaviour in tension and compression is quite different so that the use of 'BILIN_ASYM' material laws is needed. The contact between the beam and column flange is identical to those already presented for fin plate and header plate connections.

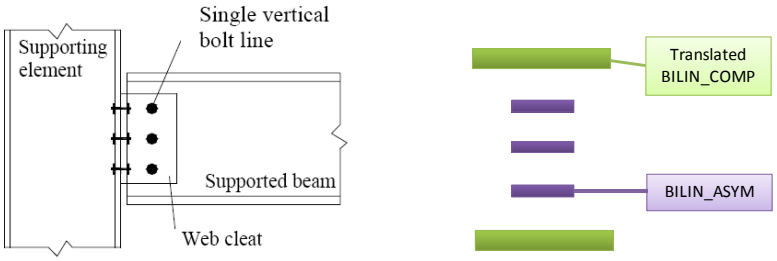

Figure 6-24 : Double web cleats connection (left) and Bilinear Fibre Model (right)

6.4.4 Numerical simulation of the tests performed in Metz

The complete sub-structure tested in Metz has been modelled in the numerical simulation of these tests. The protected part of the column (blue section) and the part of the beam situated outside the furnace (green section) have been supposed to remain at 20°C during the complete test. The self-weight of the sub-structure (not represented on Figure 6-25 to make the figure clear) and the measured value of the point load have been applied. The out-of-plane displacement and the torsion of the section where the point load is applied are avoided because of these degrees of freedom are blocked by the loading device. The sub-structure providing axial restraints has been substituted by an elastic spring (see at the right extremity of the beam).

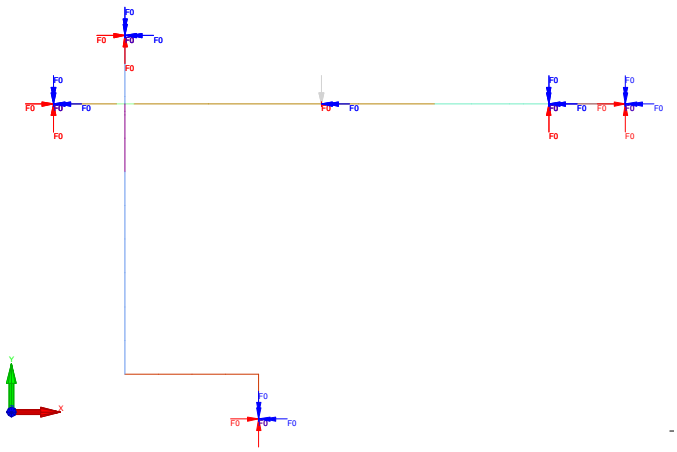

Figure 6-25 : Numerical modelling of the sub-structure tested in Metz

The two tests have been modelled with two different values of the yield strength of carbon steel: 235 MPa and 355 MPa. Structural elements are made of Grade S235 carbon steel but, unfortunately, no coupon tests have been performed on these elements. Theoretically, the yield strength should be approximately equal to 235 MPa but the real yield strength usually exceeds significantly this value. The real yield strength should remain lower than 355 MPa, the yield strength of the upper class. Consequently, the simulations have been run with the extreme values 235 MPa and 355 MPa. The ultimate resistance of bolts considered is the mean value of the four measurements realised on Grade 8.8 bolts at room temperature by Centro Sviluppo Materiali (Table 4-2), i.e. 956 MPa.

In Test n°1, the failure is reached when the furnace temperature is equal to 797°C (t = 4185 sec ≈ 70 min). In the numerical simulations, the failure is obtained a little bit earlier with S235 (61 min) and S355 (65 min) steel grades for carbon steel so that the phase after unloading can not be reached. The failure mode is a plastic beam mechanism: two plastic hinges appear in the studied joint and the section where the vertical loading is applied (Figure 6-26). The comparisons between numerical and experimental values of the vertical displacement at the jack position and the horizontal displacement at the beam extremity are good (Figure 6-27). The evaluation of the resistance of all the components activated in the bolt rows shows that the two weakest components are the “column in bending” and the “flush end-plate in bending”. In spite of the stronger reduction of resistance of bolts, this component is not critical at any moment of the fire and the risk of bolt failure is avoided. The bending deformations of the column flange and plate after the fire test can be observed on Figure 6-29b.

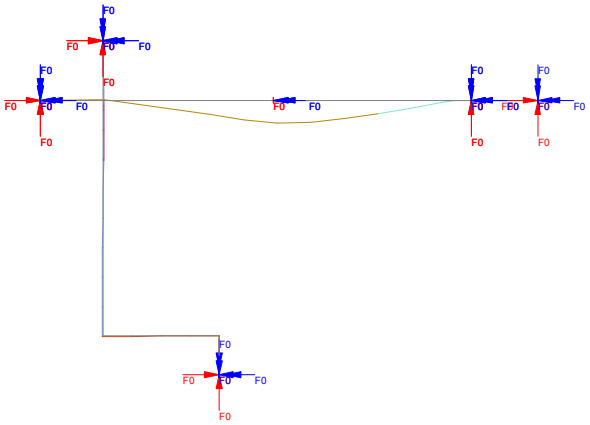

Figure 6-26 : Test n°1 – Grade S235 – Displacements of the sub-structure at failure time (Scale Factor = 3)

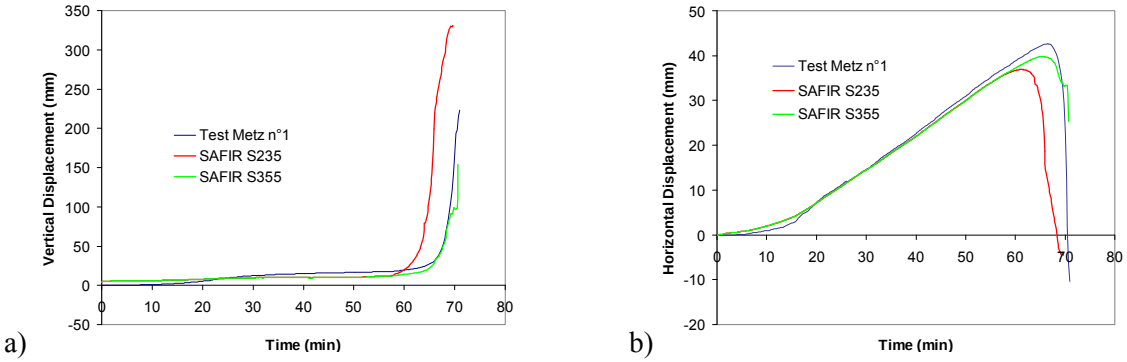

a) b)

Figure 6-27 : Test n°1 – (a) Loading jack: Vert. Deflection - (b) Beam extremity: Horiz. Displacement

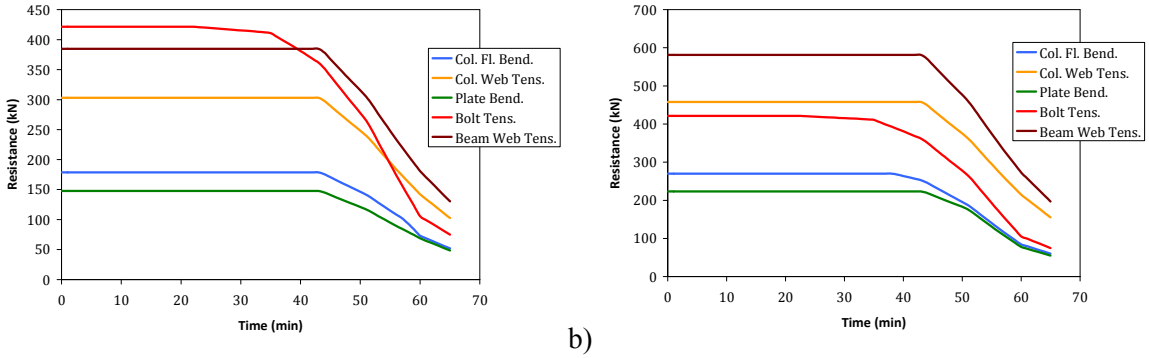

a) b)

Figure 6-28 : Test n°1 - Evolution of the resistance of the components activated in bolt rows: S235 Steel Grade (a) - S355 Steel Grade (b)

a)  b) 

Figure 6-29 : Test n°1 – Beam-to-column joint before (a) and after the test (b) [Efectis France, 2007a]

In Test n°2, no failure is observed until the end of the test (12550 sec = 209 min). The horizontal displacement of the beam extremity obtained numerically with the yield strength of steel equal to 355 MPa follows the experimental curve with good accuracy (Figure 6-30b). The prediction of the joint rotation and the vertical deflection of the beam are good during the heating phase but, during the cooling phase, these two experimental results remained constant (Figure 6-30a).

(a) 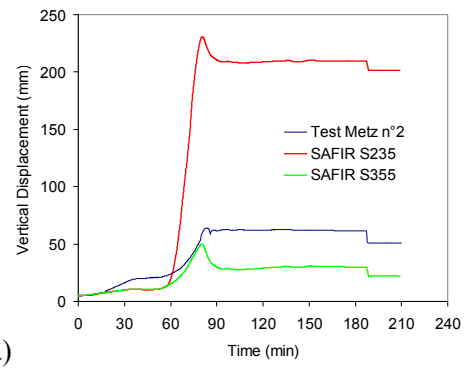

(b) 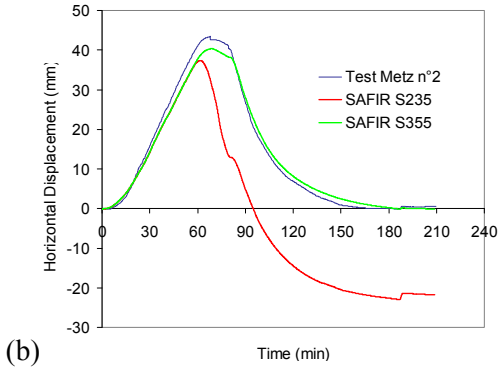

Figure 6-30 : Test n°2 – (a) Loading jack: Vert. Deflection - (b) Beam extremity: Horiz. Displacement

6.4.5 Numerical simulation of the tests performed in Delft

6.4.5.1 Failure Criteria

In literature and design recommendations, it is difficult to find a clear definition of failure criteria for steel joints. At room temperature, the ultimate bending moment $M_{u,joint}$ of a joint is obtained when the ultimate resistance of one component (brittle or ductile) is reached: bolt failure, weld failure, detachment or tearing off of the connecting element, etc. The global failure of the joint is initiated by a local failure and the bending moment in the joint can not exceed $M_{u,joint}$. In addition, the serviceability criterias (deformations) are probably not respected when the bending moment reaches $M_{u,joint}$ in the joint. Under natural fire, the occurrence of a local failure does not automatically induce a global failure: the redistribution of bending moments and/or the activation of catenary action may ensure the

stability of the structure. The probability to "survive" to a local failure is higher if this failure occurs during the cooling phase than during the heating phase because the beam has recovered partially or completely its resistance and stiffness, allowing a redistribution of the internal forces. As an (exaggerated) illustration to this, the Delft test n°1 has demonstrated that the beam was still supported to the column after the three bolts of the fin plate connection have failed.

In the numerical models for connections presented previously, the compression and bolt rows have a bilinear behaviour. The failure of connection components is not taken into account and can not be predicted by the numerical model. Some failure criterias have been defined on the basis of the evolution of the resistance of the components in bolts rows and the yielding of fibres representing the action of bolts in the numerical model.

As a preparation of the input data for the numerical model, the evolution of the resistance of all the components are calculated during the natural fire considered. The components of a bolt row can be divided into brittle and ductile components. For ductile components, the plastic and ultimate resistances are calculated. At any moment of the natural fire, the class of ductility of one bolt row can be classified as A, B or C as follows:

- The bolt row is class A if the resistance of the weakest brittle component is higher than the ultimate resistance of the weakest ductile component.

- The bolt row is class B if the resistance of the weakest brittle component is higher than the plastic resistance of the weakest ductile component and lower than the ultimate resistance of the weakest ductile component.

- The bolt row is class C if the resistance of the weakest brittle component is lower than the ultimate resistance of the weakest ductile component.

The failure criteria of a joint are depending on the classes of ductility of the bolt rows of that joint. Obviously, the criteria can be different at two different instants of a natural fire because the resistances of bolt, weld and carbon steel components evaluate differently with temperature (see Chapter 4). Two failure criteria are defined for joints modelled by Bilinear Fibre Models are:

***Failure Criterion 1*:** At least one fibre representing the action of a class C bolt row is yielded ;

***Failure Criterion 2*:** All the fibres representing the action of bolt rows are yielded and at least one bolt row is class B.

6.4.5.2 Pre-treatment of the experimental results

During the fire tests performed in Delft, the thermal and mechanical data measured are:

- the furnace temperature, the temperature in the mid-span section of the beam, in the connection components and in the part of the column exposed to fire;
- the vertical loading applied to the sub-structure;
- the vertical deflection at the beam mid-span and the horizontal elongation of the spring frame.

As the stiffness of the spring frame has been measured by a specific test (17 kN/mm), the axial force in the beam is extrapolated from the measurement of the horizontal elongation of the spring frame. However, this horizontal elongation remained equal to 0 during 5 minutes in test n°1 (fin plate connections) and 10 minutes in test n°2 (double web cleats connections) and increased slowly afterwards. After 15 minutes, the average temperature of the beam is respectively around 200°C and 250°C and the spring displacements are only 3 mm and 1 mm.

In the elastic domain, the axial force N_t induced in a restrained beam by an elevation of temperature ΔT is given by Eq. 3-5. By example, the displacement d_{spring} obtained for an IPE300 beam heated to 200°C with K_A = 17 kN/mm is given by Eq. 6-35.

$$d_{spring} = \frac{N_t}{K_A} = \frac{\varepsilon_t L}{\left(1 + \frac{K_A}{K_{A,beam}}\right)} = 9.57\,mm \qquad \textbf{6-35}$$

This shows that the experimental spring displacements much lower than expected. Such a difference can not be explained only by the displacements in the bolts working in shear due to the difference between the bolt size and the dimension of the hole. This could be explained by:

1) The disclosings of connection clearances in the sub-structure that provides axial restraints so that the beam elongates freely without development of axial force in the beam and the spring.

2) The stiffness of the restraining frame has been modified between the specific test at room temperature and the tests performed on sub-structures under natural fire.

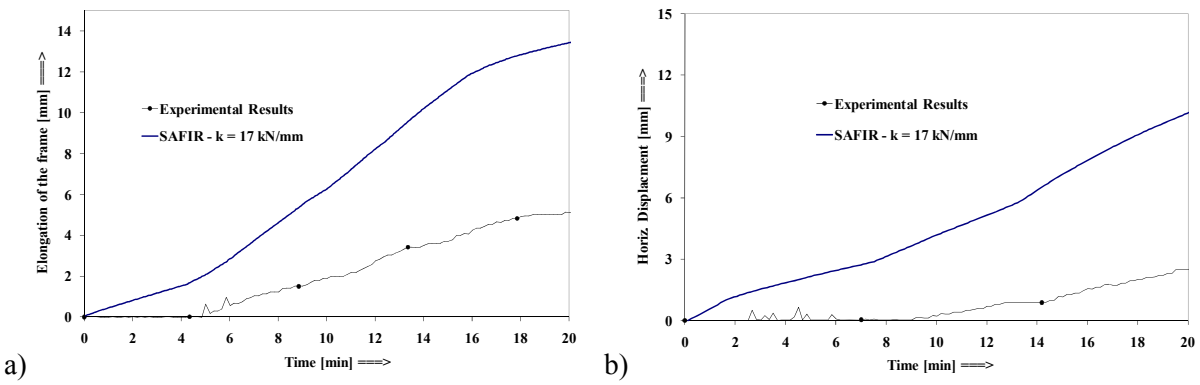

Figure 6-31 : Experimental and expected values of the spring elongation in test n°1 (a) and test n°2 (b)

On the basis of these differencies, the boundary conditions have been adapted in order to approach the real conditions of the test and the real internal forces in the joint zone. For the numerical simulations of the Delft tests, the spring element has been removed and the displacement at the beam extremity has been imposed during the fire test:

- During the first period of time where no horizontal elongation of the frame has been measured experimentally, the displacement imposed in the numerical simulation just equilibrates the thermal elongation of the beam so that no axial force is created in the beam. These imposed displacements have been obtained by a preliminary simulation where the beam can elongate freely.

- During the rest of the test, the horizontal displacements measured experimentally are translated by a value equal to the displacement imposed at the end of the first period.

The numerical model used to perform the numerical simulations of the Delft tests is plotted on Figure 6-32.

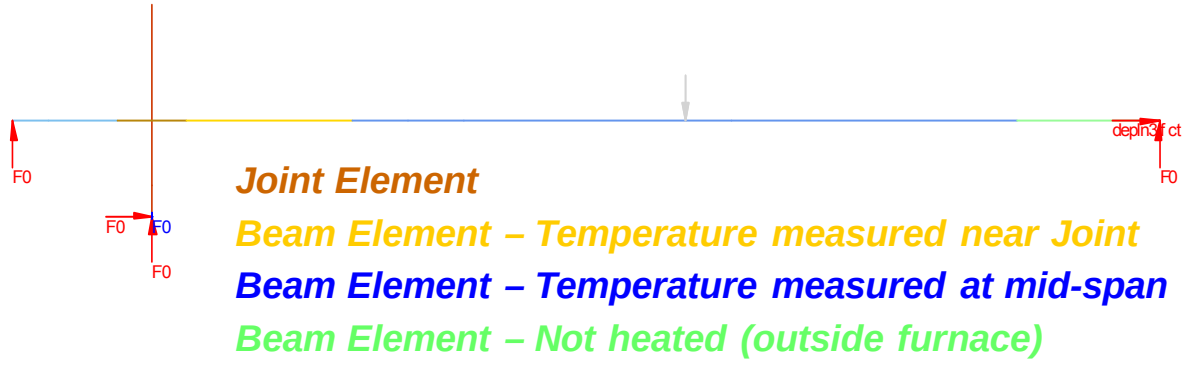

Figure 6-32 : Numerical model of the sub-structures tested in Delft

6.4.5.3 Fin plate connections

The design resistances of all the components activated in the bolt rows have been calculated analytically as a function of time (Figures 6-33 to 6-35). The weakest component is the "beam web in bearing" component and the ultimate resistance of that component has also been evaluated (Eq. 6-36) on the basis of the formula proposed by Pietrapertosa [2004]. During around 30 minutes, the resistance of bolts in shear remains higher than the ultimate resistance of the beam web in bearing and the risk of bolt failure is avoided. After this, the resistance of bolts in shear is situated between the design resistance and the ultimate resistance of the beam web in bearing and bolts could fail after large deformations of the plate.

$F_{bear,u} = 1.25\, F_{bear,Rd}$	**6-36**

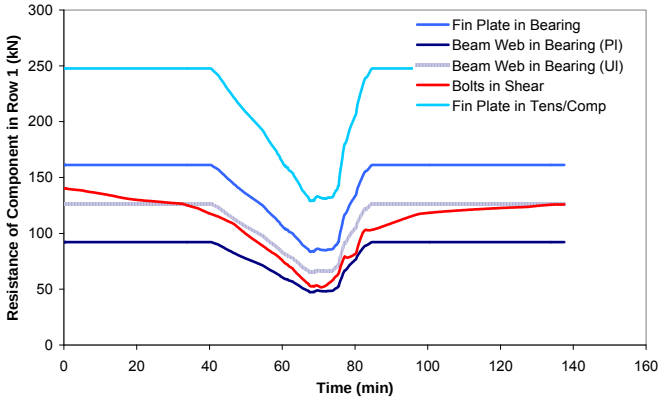

Figure 6-33 : Resistance of components in bolt row n°1 (top row)

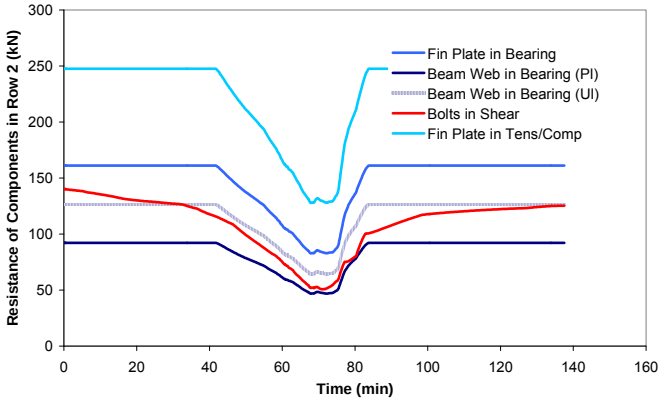

Figure 6-34 : Resistance of components in bolt row n°2 (middle row)

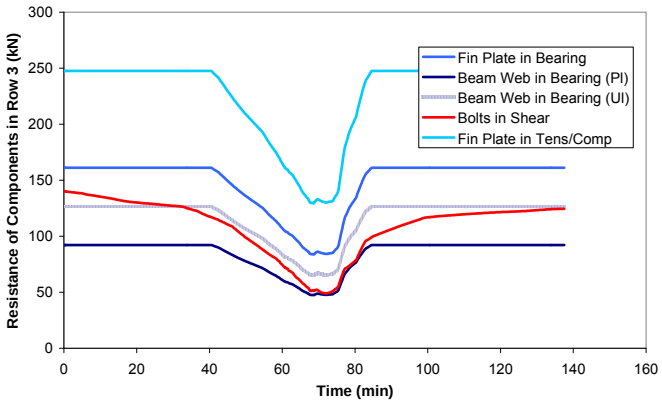

Figure 6-35 : Resistance of components in bolt row n°3 (bottom row)

In the Bilinear Fibres Model, the material law allocated to the fibres representing the action of bolts is bilinear and the yield strength is defined so that the fibre stress reaches this value when the bolt row is subjected to the design resistance of the weakest component. The analysis of numerical results shows that the two top bolt rows are yielded. The contact between the beam and column flanges increases significantly the joint stiffness and limits the joint rotation. During the cooling phase, the contact between the beam and column flanges disappears and, after 119 minutes, the three bolt rows are yielded. In the test, the failure of the fin plate connection has been observed after 127 minutes. The failure of bolts is caused by the decrease of the joint stiffness and the appearance of large deformations in the bolt rows. On Figure 6-66, the runaway failure of the heating phase obtained numerically starts earlier than during the test. For the reasons exposed in § 6.3.2, the furnace temperature and the steel temperature increase very slowly (2-3°C/min) at the end of the heating phase. The difference between experimental and analytical results is consequently amplified on Figure 6-66.

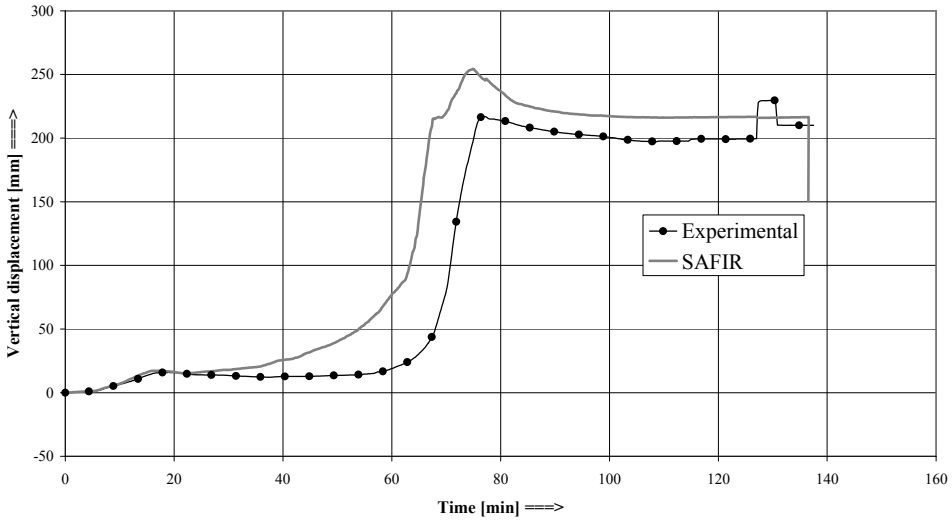

Figure 6-36 : Test n°1 - Comparison between vertical deflections obtained experimentally and numerically

The yield strength of the S235 steel beam measured by coupon tests at room temperature is around 345 MPa. If the yield strength of the beam had been closer to 235 MPa, the risk of bolt failure during the cooling would have been reduced for two reasons:

- the runaway failure of the heating phase would have occurred earlier and the temperature reached at the end of the heating phase would have been lower;
- the resistance of bolts would have been higher than the ultimate resistance of the beam web in bearing during the cooling phase and the ductility of the joint would have been increased.

6.4.5.4 Web cleats connections

In the Bilinear Fibres Model for web-cleat connections, the resistance in compression of one fibre is the minimal value of the components of the connection between the web cleats and the beam. The resistance in tension is the minimal value of the components activated in the connection between the web cleats and the beam and in the connection between the web cleats and the column.

The evolutions of the resistance of all these components are given in Figures 6-37 to 6-39 as a function of time. In order to reduce the number of superposed curves, the resistances of the components of the column are not represented. The resistance of these components is high and does not influence the resistance of the connection. The components “bolts in shear” and “T-Stub Mode 3 - bolts in tension” are fragile components. The component “T-Stub Mode 2”, formed by plastic hinges in the column and bolt failure, has a limited ductility. The other components, represented in blue, are ductile.

The double web cleats connections remain ductile for the complete duration of the test.

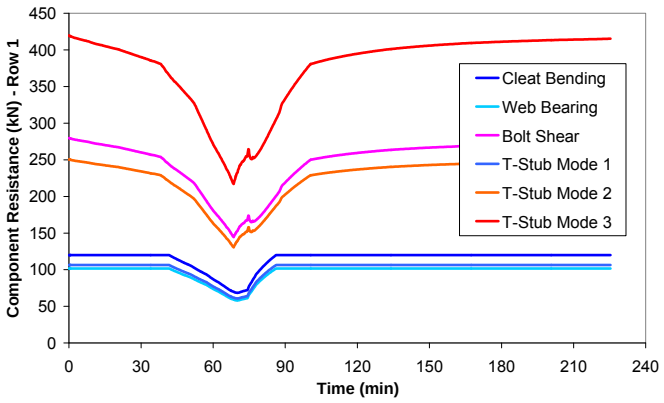

Figure 6-37 : Resistance of components in bolt row n°1 (top row)

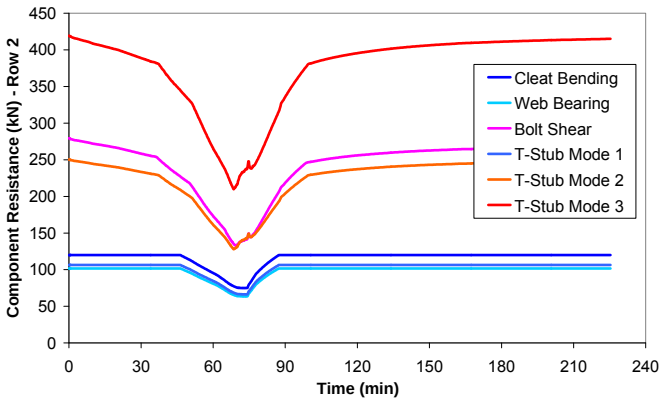

Figure 6-38 : Resistance of components in bolt row n°2 (middle row)

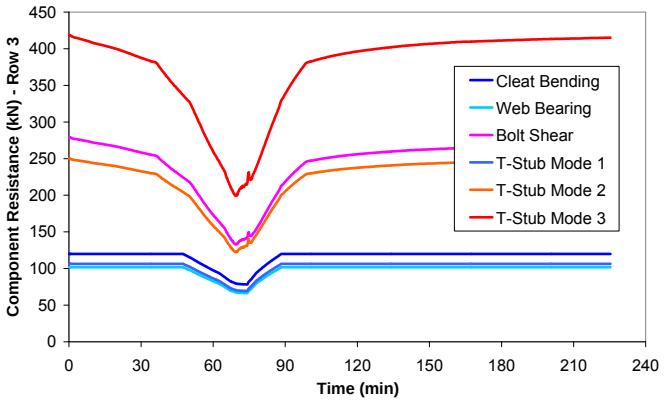

Figure 6-39 : Resistance of components in bolt row n°3 (bottom row)

In the numerical simulation of this test, the yielding of the fibres representing the action of the bolts has been analysed. The number of yielded fibres remains equal or lower than 2 during the complete duration of the test. Bolt failures are avoided and this is in agreement with the experimental observations. The comparison between the experimental and numerical vertical deflections is good, especially during the heating phase (Figure 6-40). The prediction of the moment where the runaway failure of the beam occurs is good. The stabilisation of the vertical displacements during the cooling phase is a little bit different.

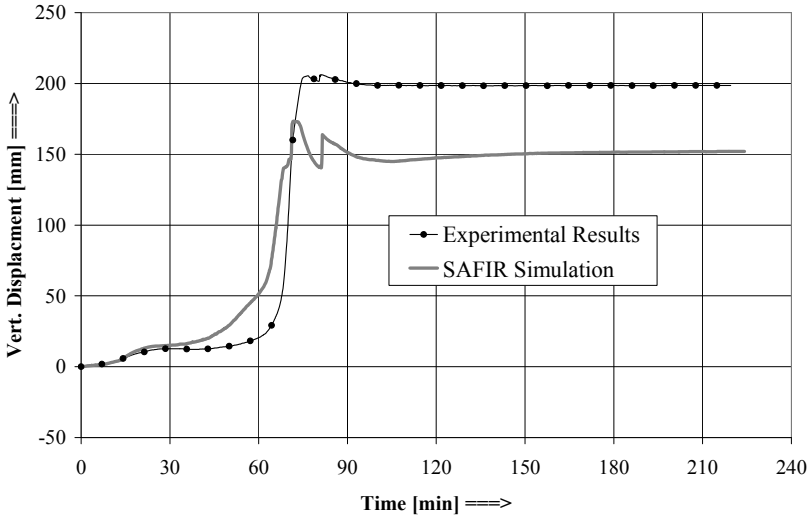

Figure 6-40 : Test n°2 - Comparison between vertical deflections obtained experimentally and numerically

6.4.6 Parametric analyses

6.4.6.1 Introduction

Experimental tests do not provide sufficient information to deduce global conclusions about the behaviour of steel connections under natural fire. The numerical simulations of the two tests performed in Delft have given confidence in the models developed for fin plate and web cleat connections but the validation of these models necessitates more comparisons with reference data. For header plate connections, no test has been simulated. Thus, a large amount of numerical analyses have been run with, on one side, the simple models developed in SAFIR and, on the other side, complex finite element models including 3D solid elements and contact elements. The numerical complex models have been built and run by CTICM (ANSYS software) and by Corus (Abaqus software). Additional parametrical simulations have been achieved to provide a sufficient amount of results for the definition of a simple design procedure.

6.4.6.2 Validation of the Bilinear Fibres Model against other Finite Element Models

6.4.6.2.1 Definition of the geometrical, thermal and mechanical data

The geometrical and mechanical properties of connections and connected elements used for parametric analyses are given in Figure 6-41 and Table 6-5. These data are fixed for all the cases analysed.

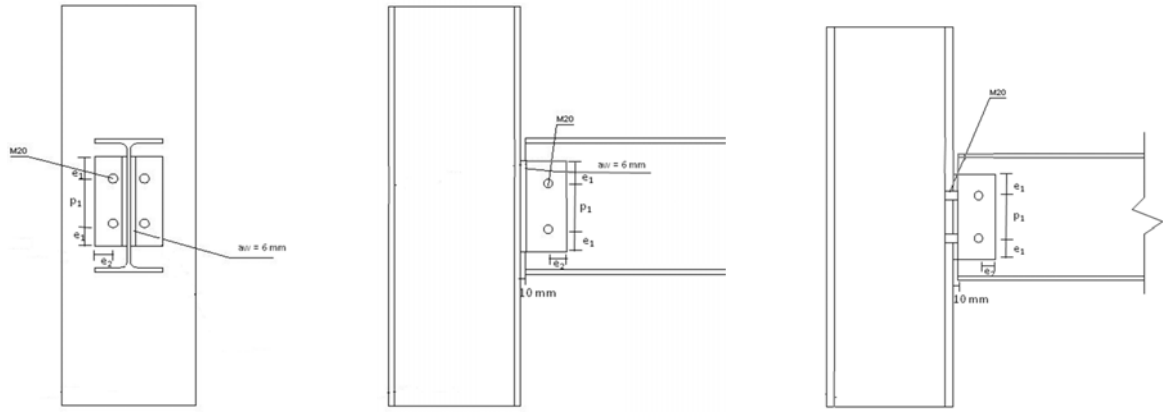

Figure 6-41 : Notations of geometrical data of header plate, fin plate and double web cleats connections

Span (m)	Beam	Column	$M_{pl,Rd,beam}$ (kN.m)	Joint (S275)						
				Case	Dimensions (mm)	Bolt	Bolt rows	e_1 (mm)	e_2 (mm)	p_1 (mm)
6	IPE 300 (S275)	HEA 300 (S275)	172.8	Web Angle	90x90x10 (Depth = 210)	M20 G 8.8	3	35	35	70
				Fin Plate	210x90x10	M20 G 8.8	3	35	35	70
				End Plate	210x150x10	M20 G 8.8	3	35	35	70
12	IPE 550 (S235)	HEM 300 (S275)	654.9	Web Angle	100x100x10 (Depth = 360)	M20 G 8.8	5	40	40	70
				Fin Plate	360x100x10	M20 G 8.8	5	40	40	70
				End Plate	360x210x10	M20 G 8.8	5	40	40	70

Table 6-5 : Geometrical and mechanical properties of connections and connected elements

The parametric studies are focused on the load ratio (w = 0.3, 0.5 or 0.7), the level of axial restraints K (K_A/K_{beam} = 3%, 10% or 15%) and the speed of heating (quick or slow fire). The axial restraints due to the presence of a surrounding frame are represented by a spring that has a constant stiffness during the fire. In the short-quick fires, the fire curves follows the parametric temperature-time curve defined in the Annex A of the EN 1991-1-2 with $\Gamma = 1$ during the heating and cooling phases so that the maximal temperature of the beam reaches 95% of the critical temperature (defined as the temperature at which the simply-supported beam fails). For long-slow fires, the parameter Γ is adapted so that this temperature is obtained after 60 minutes (Figure 6-42). However, the beams failed during the heating phase in 9 cases out of 12 because of the combination between bending moments and thermally-induced axial thrusts (IPE 300 under slow fire - IPE 550 under quick and slow fires). Consequently, temperatures have been reduced in such a way that the temperature of the beam bottom flange at the end of the heating phase is given in Table 6-6 (Eq. 6-37 and Figure 6-43).

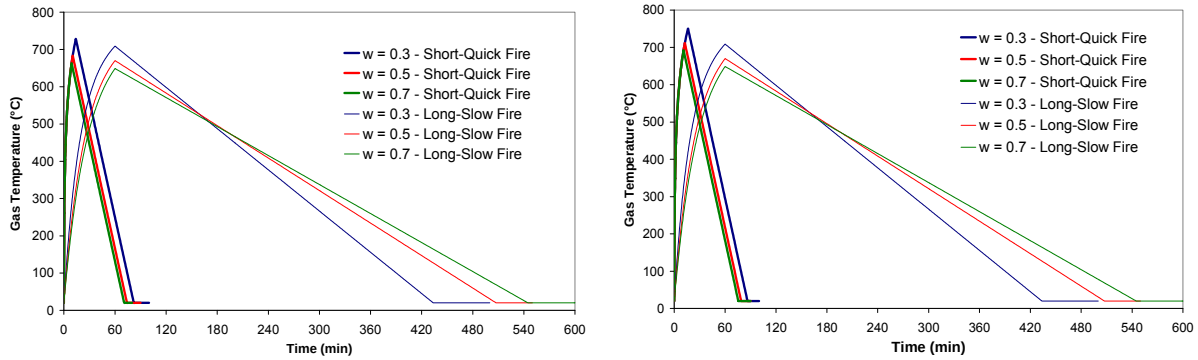

Figure 6-42 : Fire curves used for the parametric analyses with 6-metre long and 12-metre long beams

Steel section	Quick Fire	Slow Fire
IPE300 - w = 0.3	**670**	670
IPE300 - w = 0.5	**606**	606
IPE300 - w = 0.7	**578**	578
IPE550 - w = 0.3	693	660
IPE550 - w = 0.5	623	586
IPE550 - w = 0.7	569	533

Table 6-6 : Temperature of the beam bottom flange at the end of the heating phase

$$\theta_{mod,any} = 20 + \frac{\left(\theta_{mod,any} - 20\right)}{\left(\theta_{ini,any} - 20\right)} \theta_{ini,any} \qquad \textbf{6-37}$$

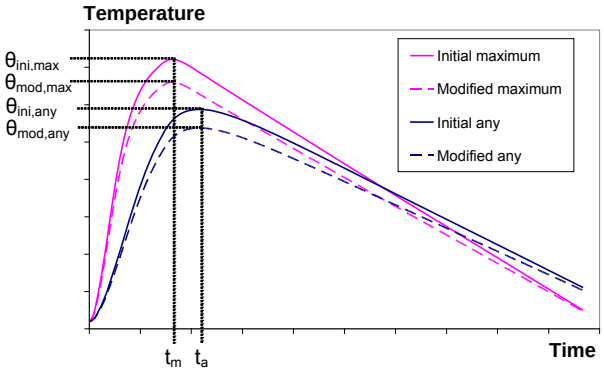

Figure 6-43 : Modification of the temperatures in order to avoid beam failures during the heating phase

6.4.6.2.2 Fin plate connections

The analytical calculation of the resistance of the two critical components (beam web in bearing and bolts in shear) shows that the risk of bolt failures is important, especially at the end of the heating phase. The classes of ductility of the bolt rows at the end of the heating and cooling phases are listed

in Table 6-7. The risk of bolt failures is higher for the "low vertical loads – high temperatures" cases because the resistance of bolts is divided by 2.5 between 500°C and 600°C (instead of 1.6 for carbon steel components), see Figure 6-44. The connections of the 12-metre long IPE 550 beam are more exposed to the risk of bolt failures because the beam thickness t_{wb} is higher in more massive profiles. For identical bolt diameters (M20 in all cases), the ratio "resistance of the bolt in shear divided by the resistance of the beam web in bearing" and the ductility of the connection are smaller for thicker beam webs. The non-reversibility of the resistance of bolts has been taken into account according to recommendations of Chapter 4.

	IPE 300			IPE 550		
	Tmax,bolt	Hot	Cold	Tmax,bolt	Hot	Cold
Case 1 Short Fire w = 0.3	625	C	A	590	C	B
Case 2 Short Fire w = 0.5	560	B	A	520	C	B
Case 3 Short Fire w = 0.7	530	A	A	460	B	B
Case 4 Long Fire w = 0.3	655	C	A	630	C	B
Case 5 Long Fire w = 0.5	595	B	A	560	C	B
Case 6 Long Fire w = 0.7	555	B	A	510	B	B

Table 6-7 : Class of ductility of bolt rows in fin plate connections

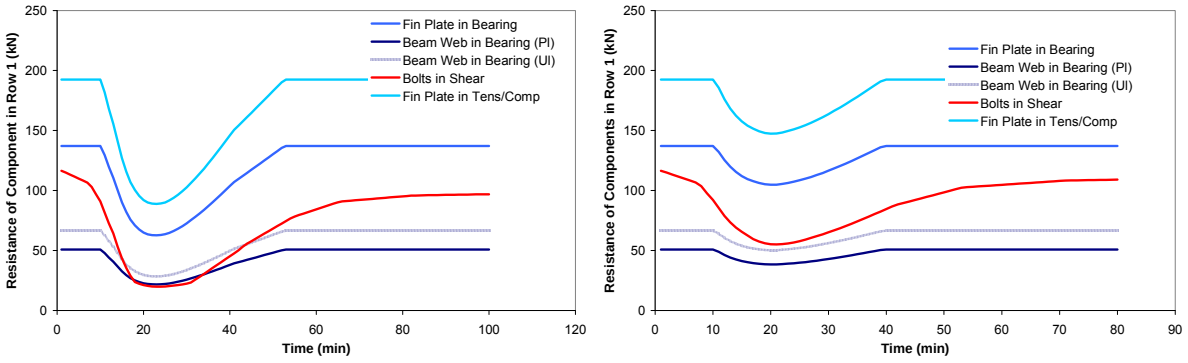

Figure 6-44 : Evolution of the resistance of components activated in the top bolt row of IPE 300 configuration (left : Case 1 – right : Case 3)

With the complex finite element model, the bolt failures are obtained during the (beginning of the) cooling phase of the fire in "low vertical loading – high temperatures" cases with high axial restraints. It should be noticed that the position of the bolts have been modified for the simulations of 12-meter long IPE 550 beams performed with Abaqus software, following the recommendations mentioned in the Green Book [SCI/BSCA, 2002]. This modification increases the resistance of the joint during the

heating phase but also causes a reduction of the resistance during the cooling phase where the joint is subjected to sagging moments (Figure 6-45).

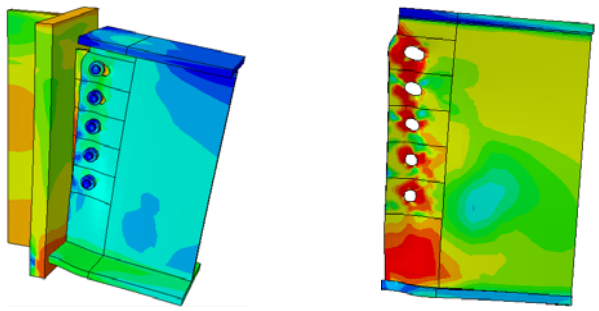

Figure 6-45 : Plots showing the modified position of the bolts in the detailed FEM (Source: Corus Ltd)

The temperature of the beam bottom flange is the same under short and long fire curves but the distribution is more uniform and the bolts temperatures are higher under long fires. The use of the Bilinear Fibre Model leads to bolt failure in more numerous cases. The failure criteria are conservative and seem to under-estimate the ductility of fin plate connections (Table 6-8). The evolutions of the mid-span deflection obtained with the two types of models are given in Appendix C.

	IPE 300				IPE 550		
	K = 3%	K = 10%	K = 15%		K = 3%	K = 10%	K = 15%
Case 1 Short Fire w = 0.3	Fail. HOT	Fail. HOT	Fail. HOT	Case 1 Short Fire w = 0.3	Fail. HOT	Fail. HOT	Fail. HOT
Case 2 Short Fire w = 0.5	No Failure	No Failure	No Failure	Case 2 Short Fire w = 0.5	Fail. HOT	Fail. HOT	Fail. HOT
Case 3 Short Fire w = 0.7	No Failure	No Failure	No Failure	Case 3 Short Fire w = 0.7	No Failure	No Failure	No Failure
Case 4 Long Fire w = 0.3	Fail. HOT	Fail. HOT	Fail. HOT	Case 4 Long Fire w = 0.3	Fail. HOT	Fail. HOT	Fail. HOT
Case 5 Long Fire w = 0.5	No Failure	No Failure	No Failure	Case 5 Long Fire w = 0.5	Fail. HOT	Fail. HOT	Fail. HOT
Case 6 Long Fire w = 0.7	No Failure	No Failure	No Failure	Case 6 Long Fire w = 0.7	No Failure	No Failure	No Failure

	IPE 300				IPE 550		
	K = 3%	K = 10%	K = 15%		K = 3%	K = 10%	K = 15%
Case 1 Short Fire w = 0.3	No Failure	Fail. COOL	Fail. COOL	Case 1 Short Fire w = 0.3	Fail. HOT	Fail. HOT	Fail. HOT
Case 2 Short Fire w = 0.5	No Failure	No Failure	No Failure	Case 2 Short Fire w = 0.5	Fail. HOT	No Failure	Fail. HOT
Case 3 Short Fire w = 0.7	No Failure	No Failure	No Failure	Case 3 Short Fire w = 0.7	No Failure	No Failure	No Failure
Case 4 Long Fire w = 0.3	No Failure	Fail. COOL	No Failure	Case 4 Long Fire w = 0.3	Fail. HOT	Fail. HOT	Fail. HOT
Case 5 Long Fire w = 0.5	No Failure	No Failure	No Failure	Case 5 Long Fire w = 0.5	Fail. HOT	No Failure	No Failure
Case 6 Long Fire w = 0.7	No Failure	No Failure	No Failure	Case 6 Long Fire w = 0.7	No Failure	No Failure	No Failure

Table 6-8 : Occurrence of bolt failures predicted by Bilinear Fibre Model (left) and Abaqus (right)

6.4.6.2.3 Double web cleats connections

For the geometrical and mechanical data considered in this parametric analysis, the weakest ductile and fragile components of the bolt rows are the “beam web in bearing” and the “bolts in shear” components (like for fin plate connections). In comparison with fin plate connections, the ratio “resistance of the bolts in shear divided by resistance of the beam web in bearing” is multiplied by two in double web cleat connections because the bolts linking the beam to the web cleats are have two shear planes. The ductility of the bolt rows in double web cleat connections is consequently higher than those of fin plate connections (Table 6-9).

	IPE 300		IPE 550	
	Hot	Cold	Hot	Cold
Case 1 Short Fire w = 0.3	B	A	B	A
Case 2 Short Fire w = 0.5	A	A	B	A
Case 3 Short Fire w = 0.7	A	A	B	A
Case 4 Long Fire w = 0.3	B	A	B	A
Case 5 Long Fire w = 0.5	A	A	B	A
Case 6 Long Fire w = 0.7	A	A	B	A

Table 6-9 : Class of ductility of bolt rows in double web cleats connections

Due to the low rotational stiffness of double web-cleats connections, the formation of the plastic hinge in the mid-span section of the beam occurs at lower temperatures than with other types of connections and the failure of the beam occurs during the heating phase. In the numerical simulations performed with ANSYS, some failures are also obtained at the beginning of the cooling phase for 6-meter long IPE 300 beam under low vertical loading (w = 0.3) and long-slow fire. Globally, the results given by the Bilinear Fibre Model are similar to the results given by ANSYS model but less bolt failures are obtained with the first model (Table 6-10). In fact, the rotational stiffness and the resisting bending moment of the joint are over-estimated in the Bilinear Fibre Model because the material law assigned to the "beam flange in compression" component is bilinear and the buckling of the bottom flange during the heating phase is not taken into account. Figure 6-46 shows that the vertical deflection of the beam mid-span exceeds L/20 for the IPE 300 under high vertical loading (w = 0.7) and long-slow fire. Even if the Bilinear Fibre Model does not predict any failure, such important vertical deflections should be rejected or considered as a failure.

	IPE 300				IPE 550		
	K = 3%	K = 10%	K = 15%		K = 3%	K = 10%	K = 15%
Case 1 Short Fire w = 0.3	No Failure	No Failure	No Failure	Case 1 Short Fire w = 0.3	No Failure	No Failure	No Failure
Case 2 Short Fire w = 0.5	No Failure	No Failure	No Failure	Case 2 Short Fire w = 0.5	No Failure	No Failure	No Failure
Case 3 Short Fire w = 0.7	No Failure	No Failure	No Failure	Case 3 Short Fire w = 0.7	No Failure	Fail. HOT	Fail. HOT
Case 4 Long Fire w = 0.3	No Failure	Fail. HOT	Fail. HOT	Case 4 Long Fire w = 0.3	No Failure	Fail. HOT	Fail. HOT
Case 5 Long Fire w = 0.5	No Failure	No Failure	No Failure	Case 5 Long Fire w = 0.5	No Failure	Fail. HOT	Fail. HOT
Case 6 Long Fire w = 0.7	No Failure	No Failure	No Failure	Case 6 Long Fire w = 0.7	No Failure	Fail. HOT	Fail. HOT

	IPE 300				IPE 550		
	K = 3%	K = 10%	K = 15%		K = 3%	K = 10%	K = 15%
Case 1 Short Fire w = 0.3	No Failure	No Failure	No Failure	Case 1 Short Fire w = 0.3	No Failure	No Failure	No Failure
Case 2 Short Fire w = 0.5	No Failure	No Failure	No Failure	Case 2 Short Fire w = 0.5	No Failure	Fail. HOT	No Failure
Case 3 Short Fire w = 0.7	No Failure	No Failure	No Failure	Case 3 Short Fire w = 0.7	Fail. HOT	Fail. HOT	Fail. HOT
Case 4 Long Fire w = 0.3	No Failure	Fail. COOL	Fail. COOL	Case 4 Long Fire w = 0.3	Fail. HOT	Fail. HOT	Fail. HOT
Case 5 Long Fire w = 0.5	Fail. COOL	No Failure	No Failure	Case 5 Long Fire w = 0.5	Fail. HOT	Fail. HOT	Fail. HOT
Case 6 Long Fire w = 0.7	No Failure	Fail. HOT	Fail. HOT	Case 6 Long Fire w = 0.7	Fail. HOT	Fail. HOT	Fail. HOT

Table 6-10 : Occurrence of bolt failures predicted by Bilinear Fibre Model (left) and ANSYS (right)

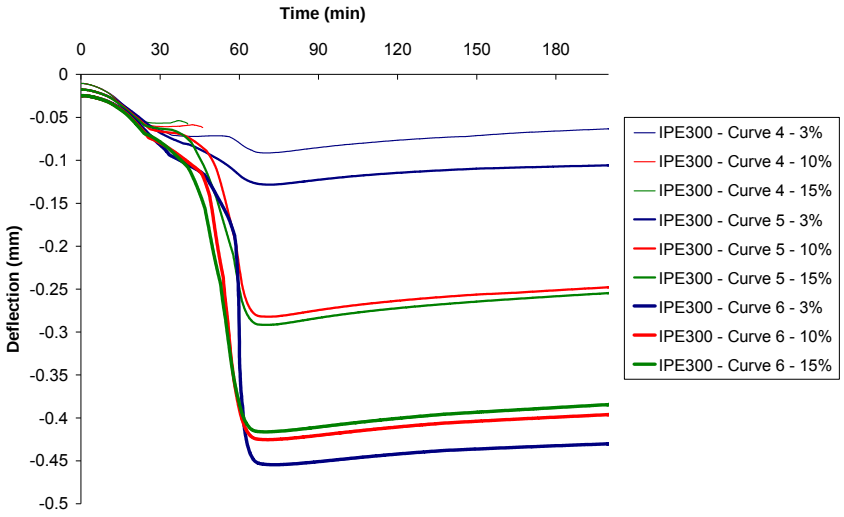

Figure 6-46 : Vertical deflections for 6-meter long IPE 300 subjected to long-slow fire

The evolutions of the mid-span deflection obtained with the two types of models are given in Appendix D.

6.4.6.2.4 Header plate connections

The model for header plate connections, presented previously (§ 6.4.3.3), uncouples the transfer of tensile and compressive forces at the level of bolt rows. Under tensile forces, the total resistance of welds in shear is divided into individual (equal or inequal) contributions related to each bolt row of the connection. In header plate connections, the weld failures are initiated at the top of the weld fillet and extend to the rest of the fillet or induce a failure in the connected members. Following the failure criteria described previously, the components "weld in shear" and "bolts in tension" are the two fragile components of the bolt rows. The resistances of these two components are compared to the resistances of the ductile components and the failure occurs when one of two failure criteria are respected (see § 6.4.5.1). As a result of these comparisons, the class of the bolt rows has been established for the all the parametric analyses. They are given at the end of the heating and cooling phases in Table 6-11. In all cases, the weakest fragile component is the "weld in shear" component. The risk of failure is higher in the cases with the 12-meter long IPE 550 beam because the weld fillet remains identical (a_w = 6 mm) while the resistances of the ductile components increase. The risk of failure is also higher for combinations "low vertical loading – high temperatures" because the weld strength at elevated temperatures reduces faster than the one of carbon steel. The non-reversibility of the weld strength has been taken into account.

	IPE 300		IPE 550	
	Hot	Cold	Hot	Cold
Case 1 Short Fire w = 0.3	B	A	C	B
Case 2 Short Fire w = 0.5	A	A	C	B
Case 3 Short Fire w = 0.7	A	A	B	A
Case 4 Long Fire w = 0.3	C	A	C	B
Case 5 Long Fire w = 0.5	B	A	C	B
Case 6 Long Fire w = 0.7	A	A	C	B

Table 6-11 : Class of ductility of bolt rows in header plate connections

In the configuration with the 6-meter long IPE 300 beams, the Bilinear Fibre Model only predicts two failures of the welds. These failures occur during the cooling phase of the long-slow fire for high axial restraints (K = 10% or 15%) under the combination "low vertical loads – high temperatures". In the configuration with 12-meter long IPE 550 beams, the Bilinear Fibre Model predicts much more weld failures, mainly during the heating phase. The results of the simulations performed with Abaqus are more "disorganized" and the trend is less clear (Table 6-12). However, the general trend is quite similar with the two models. The same thickness of weld fillets in the two joints causes a strong difference of ductility between them because the resistance of ductile components is much higher for massive sections. In the configuration with the 12-meter long beam, the lack of ductility induces failures in the joint for low vertical deflections at the beam mid-span (200 mm to 300 mm). The evolutions of the mid-span deflection obtained with the two types of models are given in Appendix E.

	IPE 300				IPE 550		
	K = 3%	K = 10%	K = 15%		K = 3%	K = 10%	K = 15%
Case 1 Short Fire w = 0.3	No Failure	No Failure	No Failure	Case 1 Short Fire w = 0.3	Fail. HOT	Fail. COOL	Fail. COOL
Case 2 Short Fire w = 0.5	No Failure	No Failure	No Failure	Case 2 Short Fire w = 0.5	Fail. HOT	Fail. HOT	Fail. HOT
Case 3 Short Fire w = 0.7	No Failure	No Failure	No Failure	Case 3 Short Fire w = 0.7	No Failure	No Failure	No Failure
Case 4 Long Fire w = 0.3	No Failure	Fail. COOL	Fail. COOL	Case 4 Long Fire w = 0.3	Fail. HOT	Fail. HOT	Fail. HOT
Case 5 Long Fire w = 0.5	No Failure	No Failure	No Failure	Case 5 Long Fire w = 0.5	Fail. HOT	Fail. HOT	Fail. HOT
Case 6 Long Fire w = 0.7	No Failure	No Failure	No Failure	Case 6 Long Fire w = 0.7	Fail. HOT	Fail. HOT	Fail. HOT

	IPE 300				IPE 550		
	K = 3%	K = 10%	K = 15%		K = 3%	K = 10%	K = 15%
Case 1 Short Fire w = 0.3	Fail. COOL	No Failure	Fail. COOL	Case 1 Short Fire w = 0.3	Fail. HOT	Fail. HOT	No Failure
Case 2 Short Fire w = 0.5	No Failure	Fail. COOL	No Failure	Case 2 Short Fire w = 0.5	Fail. HOT	Fail. HOT	Fail. HOT
Case 3 Short Fire w = 0.7	No Failure	Fail. COOL	No Failure	Case 3 Short Fire w = 0.7	No Failure	Fail. HOT	No Failure
Case 4 Long Fire w = 0.3	Fail. COOL	No Failure	Fail. COOL	Case 4 Long Fire w = 0.3	Fail. HOT	Fail. HOT	Fail. HOT
Case 5 Long Fire w = 0.5	No Failure	No Failure	No Failure	Case 5 Long Fire w = 0.5	No Failure	Fail. HOT	Fail. HOT
Case 6 Long Fire w = 0.7	No Failure	No Failure	No Failure	Case 6 Long Fire w = 0.7	Fail. HOT	No Failure	No Failure

Table 6-12 : Occurrence of bolt failures predicted by Bilinear Fibre Model (left) and Abaqus (right)

6.4.7 Effect of shear forces

6.4.7.1 Introduction

The effect of shear forces can not be included directly into the Bilinear Fibre Model. In the present work, the resistance of the bolt rows has been reduced analytically. For bolts working in shear (fin

plate and beam to web cleats connections), the reduced resistance of one bolt row to axial forces $F_{v,Rd,red}$ is obtained by Eq. 6-38, where $F_{v,Rd}$ is the resistance of the bolt row, n_{rows} is the number of bolt rows and V_{Ed} is the shear force. For bolts working in tension and shear (header plate and web cleats to column connections), the resistance of one bolt row to tensile forces are obtained by the interaction criterion defined in the Eurocodes (Eq. 6-39).

$F_{v,Rd,red} = \sqrt{F_{v,Rd}^2 - \left(\frac{V_{Ed}}{n_{rows}}\right)^2}$	**6-38**
$F_{t,Rd,red} = 1.4\, F_{t,Rd}\left(1 - \frac{V_{Ed}}{n_{rows}\, F_{v,Rd}}\right)$	**6-39**

Up to now, the influence of shear forces on the reduction of resistance of bolt rows has always been limited because the order of magnitude of the resistance of bolt rows always remained higher than the order of magnitude of shear forces. The horizontal forces induced by the combination of axial thrusts and bending moments are crucial for the occurrence of connection failures.

However, failures due to excessive shear forces have already been observed experimentally. The test performed recently at the University of Coimbra on a steel sub-structure with header plate connections is one example. This test is shortly described and discussed hereafter.

6.4.7.2 Test performed on header plate connection under natural fire in Coimbra [Santiago, 2008b]

6.4.7.2.1 Presentation of the test

The sub-structure used for the tests performed in Coimbra is composed of a 5.7-metre long IPE 300 steel beam connected to HEA 300 columns. The column is thermally-protected and provide a level of axial restraints K = 12 %. The beam is loaded by two 20 kN point loads corresponding to a load ratio equal to 0.2. The thickness of the header plate is 8 mm and the geometry of the connection is given in Figure 6-47. The steel grades of header plates and steel sections are respectively S275 and S355. The fire curve applied to the beam and the connections is aimed at reproducing the thermal conditions measured during the 7th Cardington test but, for safety reasons, has been limited to 900°C.

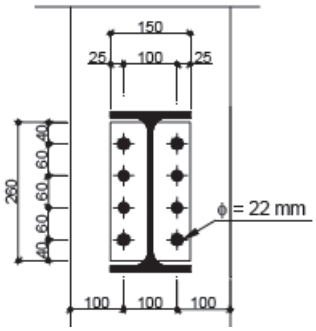

Figure 6-47 : Geometry of the tested header plate connection [Santiago, 2008b]

6.4.7.2.2 Experimental results of the test

The header plate broke along the beam web welds when the temperature reached 850°C in the joint zone, at the level of the bottom flange (Figure 6-48). At the failure time, the vertical deflection of the mid-span beam is 450 mm (≈ L/12). The evolution of temperature in the joint zone and beam deflections are given in Figure 6-49. No damage of the bolts was observed.

Figure 6-48 : Failures of the two joints by header plate and beam web tearing [Santiago, 2008b]

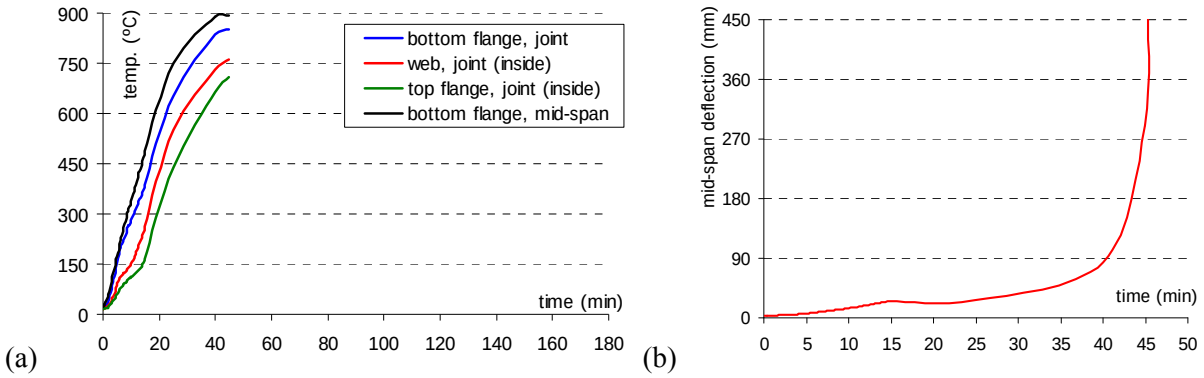

Figure 6-49 : Evolution of temperature in the joint zone (a) and mid-span deflections (b) [Santiago, 2008b]

6.4.7.2.3 Discussion about the test

At room temperature, header plate connections are usually considered as pinned connections. In simply-supported beams, the failure of a beam subjected to fire occurs when the reduction factor for yield strength of steel becomes lower than the load ratio. In the present case, the load ratio is 0.2 and the failure temperature would be around 760°C for a simply-supported beam. The deflections of the beam start to increase significantly after 40 minutes (Figure 6-49). At that time, the beam temperatures measured in the mid-span section and near the joint (200 mm from the connection) are given in Table 6-13. This shows that the fire resistance of the beam has significantly been enhanced by the presence of header plate connections with regard to the simply-supported case. The presence of axial restraints allows membrane action for high deflections but, in the present case, the increase of fire resistance is due to the rotational stiffness and the resistance of the header plate connection to hogging moments.

(°C)	Mid-span	Joint Zone
Top Flange	882	827
Web	845	737
Bottom Flange	743	681

Table 6-13 : Distribution of temperature at mid-span and near the joint after 40 minutes

At such temperatures, the reduction factor for yield strength of carbon steel reduces much (k_y = 0.1 at 700°C) and the order of magnitude of the resistance of bolt rows is similar to the one of the applied shear force. The transfer of shear force is limited to the web welds and is not sufficient anymore.

This shows that the design of the connection at room temperature was sufficient to avoid any failure of the connection under fire conditions if, in the meanwhile, the fire resistance of the beam had not been enhanced significantly by the rotational stiffness of the joint.

6.4.8 Proposal of a new design procedure for simple connections under natural fire

6.4.8.1 Introduction

The parametric analyses presented in § 6.4.6.2 shows that the Bilinear Fibre Model leads to similar results to those given by more complicated and time-consuming models. These analyses also enable to draw the first conclusions about the parameters governing the risk of failures during the heating and cooling phases of a natural fire. As a first recommendation, it should be imposed that the bolt rows have a class of ductility A or B during the complete duration of the fire, allowing a redistribution of internal forces between the bolt rows. For bolt rows in the class of ductility B, the failure of bolts or welds during the cooling phase of the natural fire is linked to the vertical loading, the level of axial restraints and the ability of the beam and the connection to resist during the heating phase. The present

results do not provide sufficient information to deduce simple design procedures able to predict the occurrence of failures. Thus, additional parametric analyses have been run with the Bilinear Fibre Model. The objective of the design procedure is, for a given configuration, to predict the minimal duration of the heating phase leading to failures of the beam or the connection during the heating phase and the minimal duration of the heating phase leading to a failure of the connection during the cooling phase. These two values of the heating phase represent the boundaries of the zone characterized by a failure during the cooling phase (orange zone on Figure 6-50).

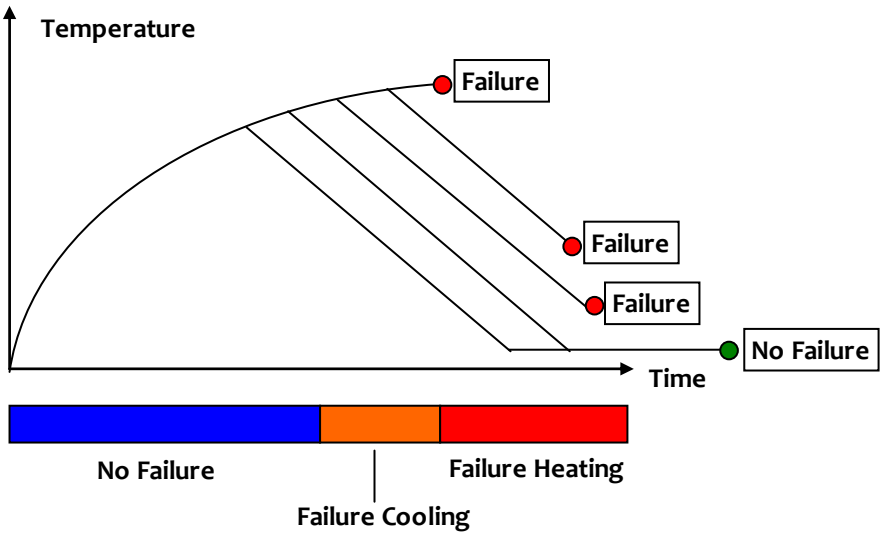

Figure 6-50 : Division of the duration of the heating into three domains

6.4.8.2 Additional parametric analyses

The additional parametric analyses are focused on the configuration with the 6-metre long IPE 300 beam. The fire curve considered for these analyses is the parametrical fire curve of the Annex A with $\Gamma = 1$ and many differents values of the heating phase have been considered. The class of ductility of bolt rows is supposed to be class B so that the failure criteria is the yielding of all the fibres representing the action of bolts. The failure of the beam during the heating phase is assumed to occur when the vertical deflection of the beam mid-span section reaches L/20.

The results of the parametric analyses are given in Figures 6-51 to 6-56. Beam failures are independent of the type of connection and the level of axial restraints. Connection failures occur for low load ratios, high axial restraints and during the cooling phase except for fin plate connections because:

- During the heating phase, axial restraints induce compressive forces in the beams. In fin plate connections (and web cleat connections), the “bolts in shear” component is activated

under compressive forces while these forces are directly transferred by contact in header plate connections.

- The rotational stiffness of fin plate connections is higher than web cleats connections. The vertical deflection of the mid-span beam reaches L/20 before the bolts fail in web cleat connections.

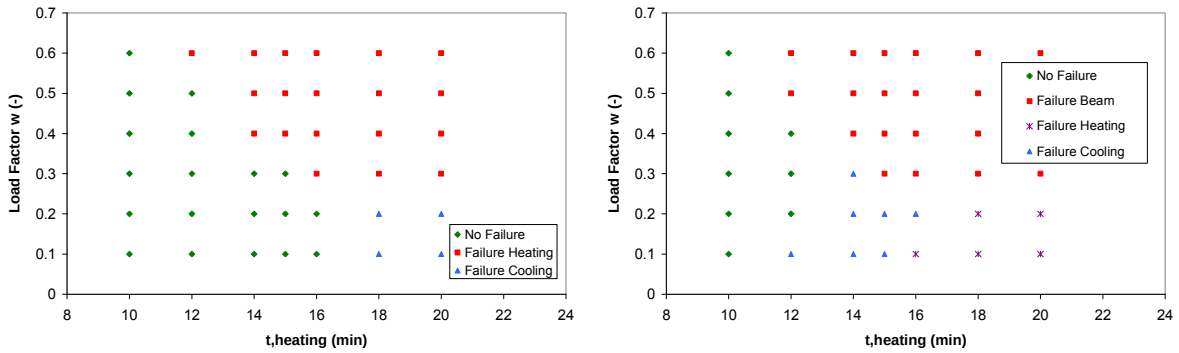

Figure 6-51 : Beam and connections failures – Fin plate connections – K = 2% (left) and K = 5% (right)

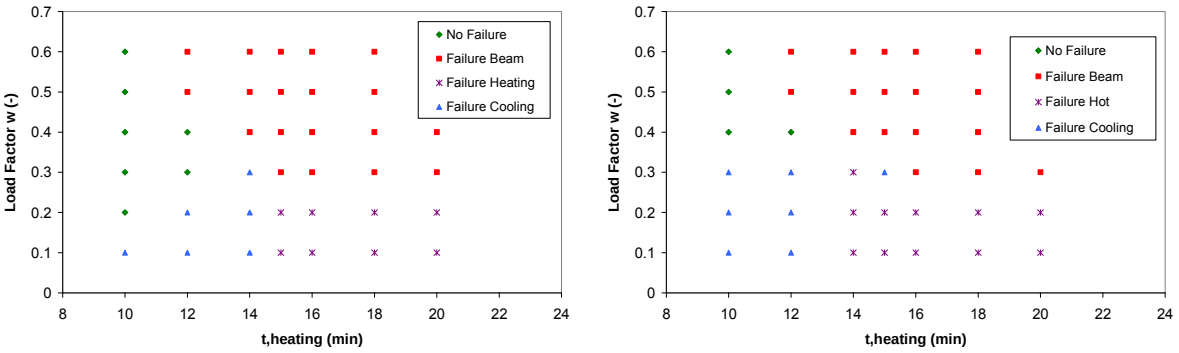

Figure 6-52 : Beam and connections failures – Fin plate connections – K = 10% (left) and K = 15% (right)

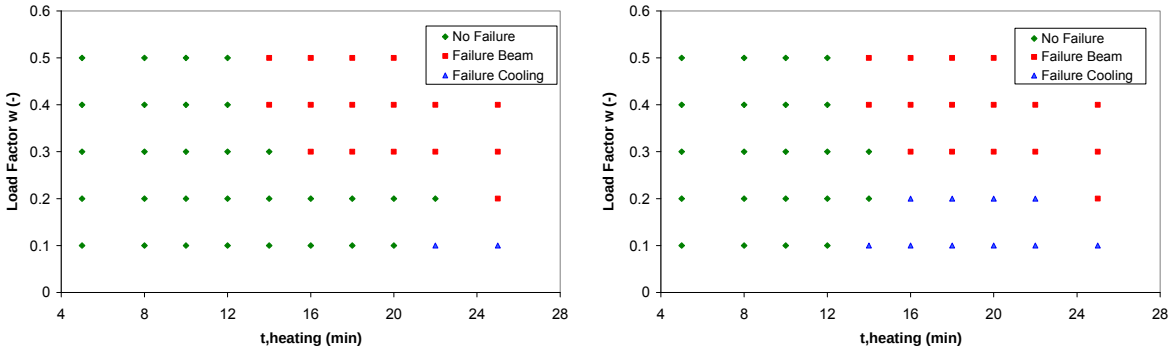

Figure 6-53 : Beam and connections failures –Web cleats connections – K = 2% (left) and K = 5% (right)

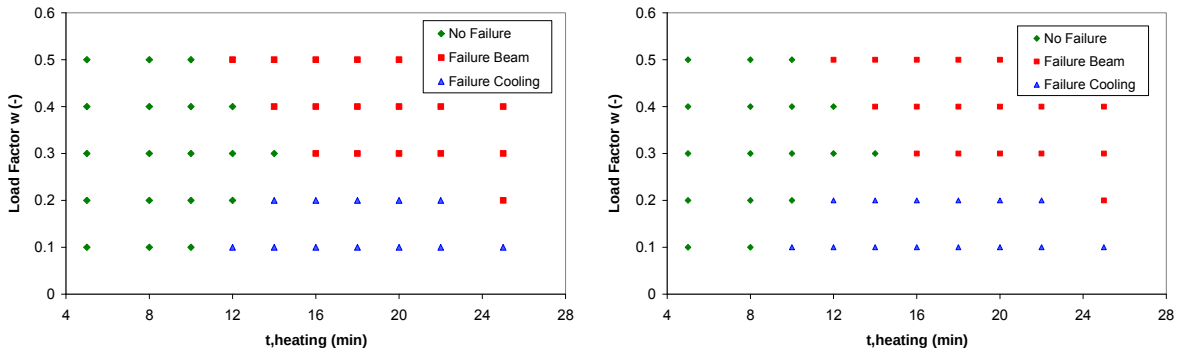

Figure 6-54 : Beam and connections failures – Web cleats connections – K = 10% (left) and K = 15% (right)

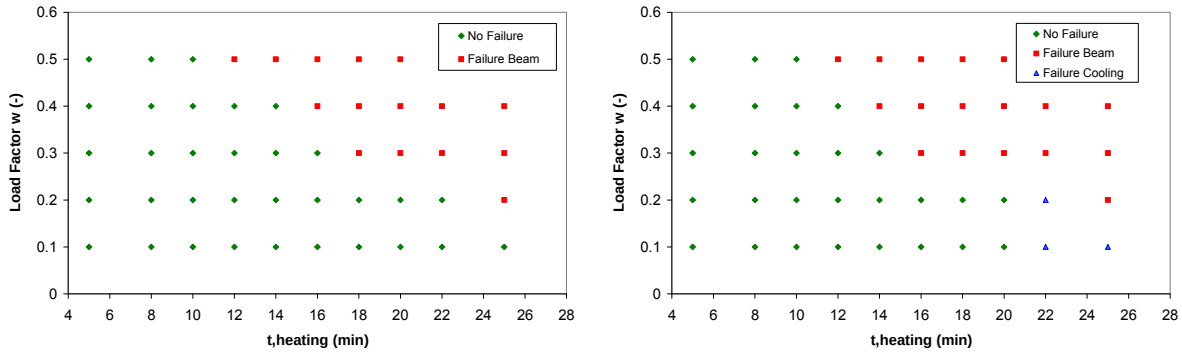

Figure 6-55 : Beam and connections failures – Header plate connections – K = 2% (left) and K = 5% (right)

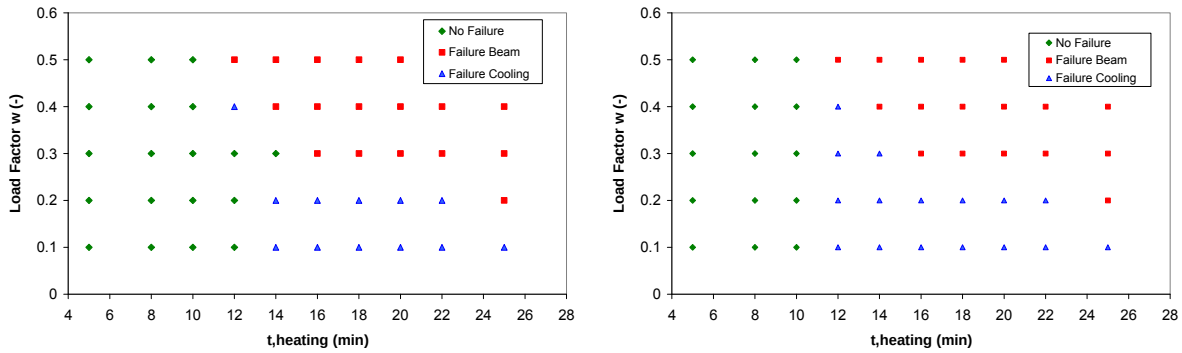

Figure 6-56 : Beam and connections failures – Header plate connections – K = 10% (left) and K = 15% (right)

6.4.8.3 Definition of a procedure for the design of simple connections

On the basis of the experimental and analytical investigations on the behaviour of fin plate, web cleats and header plate connections presented in this chapter, a simple procedure is proposed hereafter for the

design of these connections in order to prevent the failures during both the heating and cooling phases of a natural fire.

6.4.8.3.1 Resistance of the restrained steel beam and connections under natural fire

The design of steel beams is not the objective of the present thesis. However, beams are usually designed under heating fire curves and the effect of axial restraints is not always taken into account. It is proposed to calculate the maximal duration of the heating phase without beam failure as follows:

- In the Eurocode recommendations, a reduction factor κ_1 is applied to the loading to take into account the heat transferred from the steel section to the concrete slab*. This factor is taken as equal to 1 (this effect is neglected) and the load factor w is multiplied by 1.1 to include the effect of axial restraints (Step 1) ;

- The fire resistance of the beam, assumed as unrestrained ans simply-supported is calculated according to the Eurocode recommendations under the load ratio obtained in Step 1 and a fire with no cooling phase (Step 2) ;

- The time of fire resistance is multiplied by a reduction factor $\kappa_{cooling}$ that is given in Figure 6-57 to take into consideration that the temperature keeps increasing during a couple of minutes after the gas temperature starts decreasing (Step 3) ;

- The time obtained in Step 3 must be higher than the duration of the heating phase of the fire curve considered (Step 4).

Figure 6-57 : Values of $k_{cooling}$ as a function of the time of fire resistance calculated at Step 2

* The values of the reduction factor κ_1 given in the EN 1993-1-1 are 0.7 for unprotected beams heated on three sides and 0.85 for protected beams heated on three sides.

6.4.8.3.2 Resistance of the connection under natural fire

Recommendation n°1

The design resistance of all the fragile components of the bolt rows should be higher than the design resistance of the weakest ductile component multiplied by 1.2. The effect of the non-reversible behaviour of bolts and welds is taken into consideration (Criterion 1).

Recommendation n°2

One of the three following should be fulfilled:

- The load ratio w is higher than the critical load ratio w_{lim} (Criterion 2a). The critical load ratio is equal to 0.25 for web cleats connections, 0.35 for fin plate connections and 0.45 for header plate connections.

- The temperature of the bottom flange (calculated by use of the recommendations of the EN 1994-1-2) remains lower than the critical temperature T_{lim} (Criterion 2b). This critical temperature depends on the type of connections and on the level of axial restraints (Table 6-14).

- In all bolts rows and for the complete duration of the natural fire, the resistance of the fragile components remains higher than the ultimate resistance of the weakest ductile component multiplied by 1.2 (Criterion 2c).

Fin Plate Connections		Web Cleats Connections		Header Plate Connections	
K [%]	T_{lim} [°C]	K [%]	T_{lim} [°C]	K [%]	T_{lim} [°C]
2	710	2	740	2	780
5	640	5	680	5	740
10	580	10	620	10	660
15	540	15	580	15	600

Table 6-14 : Values of the critical temperature of the beam bottom flange

Criteria 1 and 2c are ductility criteria and are independent of the internal forces in the joint. The term 1.2 is used to take into consideration that the yield strength of carbon steel members is sometimes largely under-estimated. The yield strength of the steel beams tested in Delft was 345 MPa instead of 235 MPa and the numerical simulations of the tests performed in Metz have demonstrated that the yield strength of the S235 beam steel was closer to 355 MPa than to 235 MPa.

The level of axial restraints K in a beam is evaluated as follows. The beam considered is removed from the frame and unitary point loads are applied at the extremities of that beam. The level of axial

restraints K is given by Eq. 6-40, where d_1 and d_2 are the horizontal displacements at the two extremities under unitary loads.

$$K = \frac{L_{beam}}{(d_1 + d_2)(EA)_{beam}} \qquad \textbf{6-40}$$

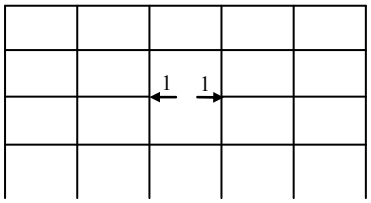

Figure 6-58 : Evaluation of the axial stiffness applied at beam extremities due to surrounding frame

The level of axial restraints K has been calculated in a frame with IPE 300 beams and 3-metre high HEB 260 columns (Tables 6-15 and 6-16). Three different beam spans have been considered: 5 m, 8 m and 10 m.

- There is a large difference between axial restraints applied to beams located in intermediary spans of lower storeys and those applied to off-centered spans of the upper levels. In the case of braced frames, beams situated near the bracing system are much more restrained than other beams.

- The stiffness of the surrounding structure is not modified much when considering different spans. This is due to the fact that the most influent parameter on the horizontal restraints is the column stiffness in bending, which is constant in all cases considered. Consequently, the ratio between the extensional stiffness of the beam and the extensional stiffness of the surrounding frame when considering each span length differs mainly because of the eigen extensional stiffness of the beam.

Beam/Span	5 m	8 m	10 m
1 & 3	7.51	11.27	13.64
2	12.79	18.25	21.48
4 & 6	5.84	8.45	10.04
5	10.01	13.56	15.64
7 & 9	4.94	6.95	8.19
8	9.33	12.42	14.14
10 & 12	0.81	1.18	1.41
11	3.1	3.81	4.17

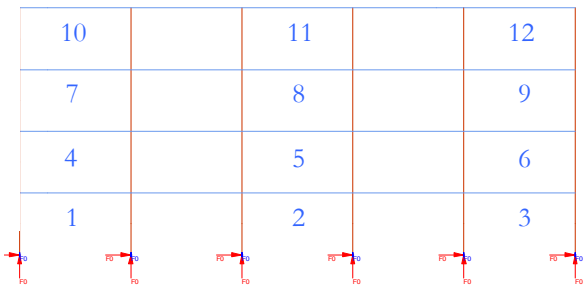

Table 6-15 : Level of axial restraints K (%) in a moment resisting frame (rigid joints)

Beam/Span	5 m	8 m	10 m
1	28.36	38.9	44.92
2	15.97	21.65	24.93
3	7.49	11.22	13.53
4	18.44	24.33	27.65
5	10.82	14.33	16.33
6	5.44	8.02	9.6
7	15.1	20.46	23.54
8	8.81	11.96	13.7
9	4	5.95	7.16
10	2.75	3.84	4.47
11	1.66	2.33	2.27
12	0.69	1.04	1.25

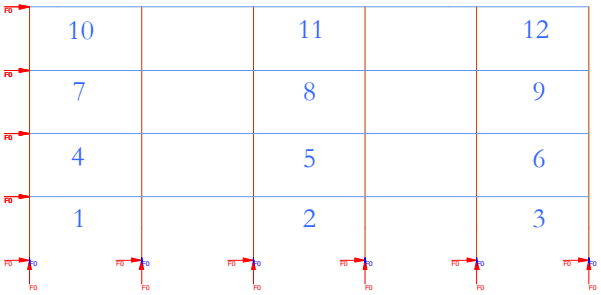

Table 6-16 : Level of axial restraints K (%) in a braced frame (pinned joints)

6.4.8.4 Application of the Criteria 2a and 2b to bolt rows with a class of ductility B

Recommendation n°1 avoids the class of ductility C for bolt rows and the complete duration of the natural fire considered. For the class of ductility A, failures of the fragile components are prevented. The validity of criteria 2a and 2b have been verified for class of ductility B (Figures 6-59 to 6-61).

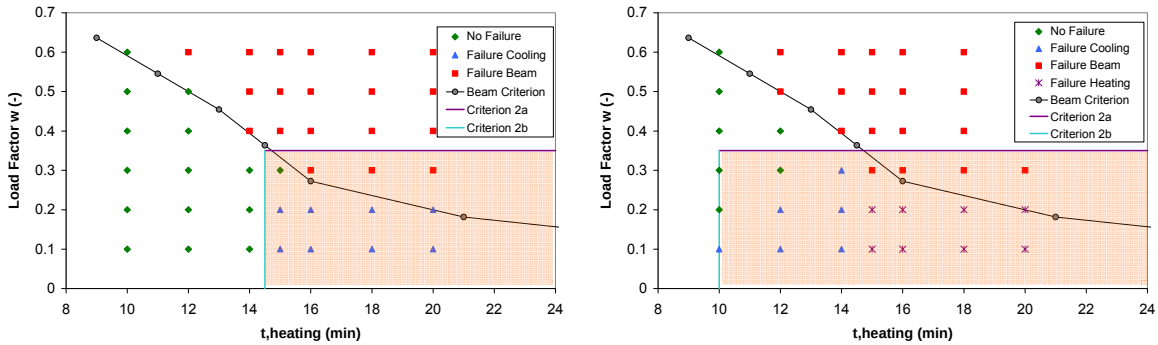

Figure 6-59 : Failure domain for fin plate connections – K = 3% (left) and 10% (right)

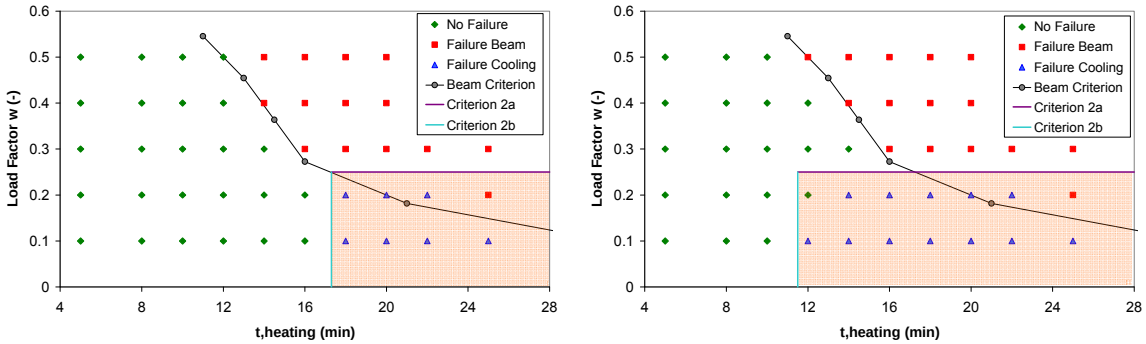

Figure 6-60 : Failure domain for double web cleats connections – K = 3% (left) and 10% (right)

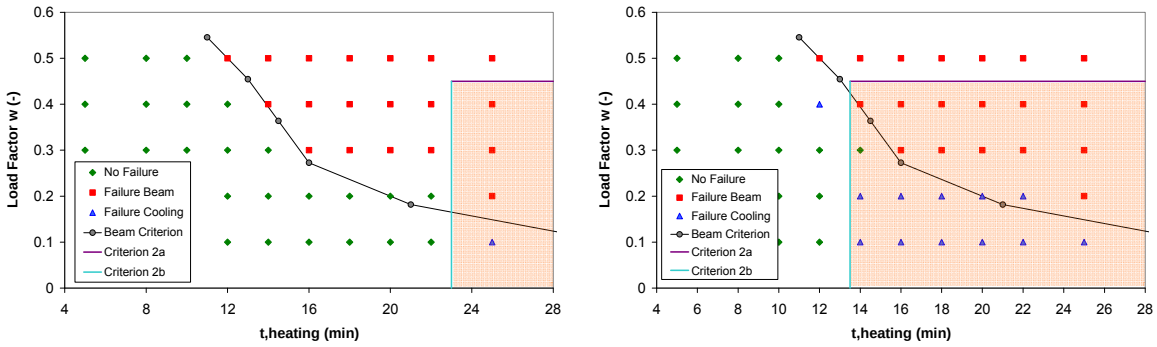

Figure 6-61 : Failure domain for header plate connections – K = 3% (left) and 10% (right)

6.5 Model for connections under natural fire: Nonlinear Fibres

6.5.1 Introduction

The Bilinear Fibres Model is a light and simple model to represent the action of connections in a global frame or a sub-structure. The main advantage of this model is the low calculation time. Very large parametric analyses and simulations of large-scale structures are conceivable with such a model. Concerning the degree of difficulty for the programmation, the Bilinear Fibres Model has just necessitated two types of modifications to the SAFIR program: i) an adjustment to make possible the direct definition of the reduction of resistance and stiffness of a fibre as a function of time and ii) the definition of a few generic material laws.

On the other side, the Bilinear Fibres Models has several drawbacks. Firstly, the preparation of the input files and definition of the data can be relatively fastidious for the user. The evolution of the resistance and the stiffness of each component identified by the Component Method must be calculated for the complete duration of the fire and an algorithm is necessary to prepare partially or completely the input files. Secondly, the joints are represented by beam elements composed of fibres. This type of element does not allow accounting accurately for the presence of shear forces and the existence of group effects. The resistance of the components is reduced as safe approach. Finally, the definition of the failure criteria is a quite difficult and time-consuming operation. It consists in two operations: i) comparing the resistance of ductile and fragile components during the fire and ii) analysing step-by-step the yielding of the fibres. The Nonlinear Fibres Model is aimed at predicting more accurately the failure of connections in the numerical models.

6.5.2 Description of the Nonlinear Fibres Model

In the Nonlinear Fibres Models, the material laws allocated to the fibres of an element representing the action of joints are similar to the stress-strain diagram of steel defined in the EN 1993-1-2 (Figure 6-62). In comparison with the bilinear diagrams used previously, this stress-strain diagram includes an elliptic branch between the proportional limit $f_{p,\theta}$ and the elastic limit $f_{y,\theta}$ and a descending branch after the yield plateau. Consequently, the occurrence of a bolt failure will automatically be taken into account by the program when the deformation of one bolt row is higher than the limiting strain for yield stress $\varepsilon_{t,\theta}$.

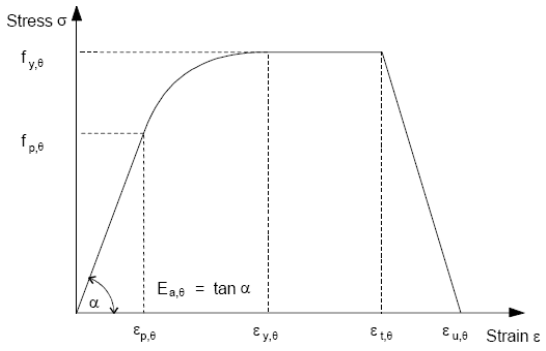

Figure 6-62 : Stress-strain relationship for carbon steel at elevated temperatures

A preliminary work is necessary to evaluate the parameters $f_{p,\theta}$, $f_{y,\theta}$, $\varepsilon_{p,\theta}$, $\varepsilon_{y,\theta}$, $\varepsilon_{t,\theta}$ and $\varepsilon_{u,\theta}$ of the material laws. For one row, the force-displacement diagrams of all the components of that row must be known so that each component can be represented by a truss or beam finite element with adequate geometrical and mechanical properties. The global force-displacement diagram of one row is obtained by assembling the finite elements of all the components in one row and by gradually increasing the displacement at the extremity of the row of finite elements. The transformation of a force-displacement diagram into a stress-strain diagram and inversely is function of the length and the cross-section of the finite element.

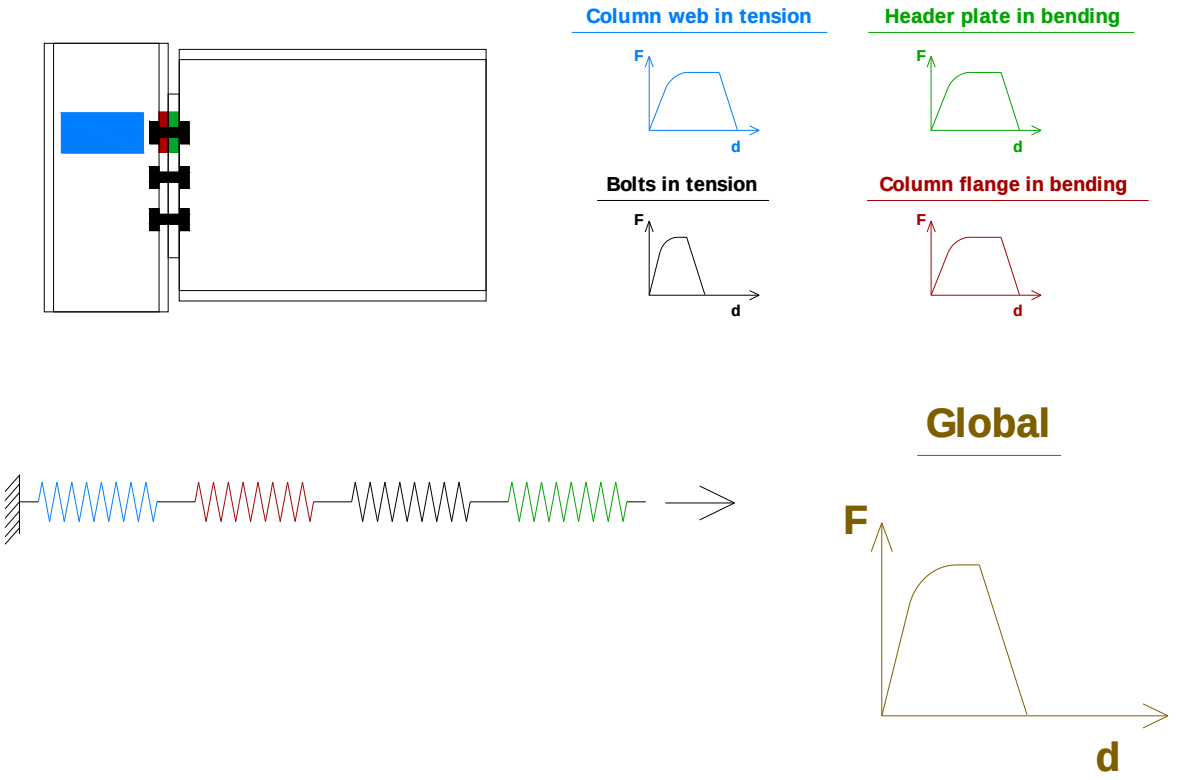

Figure 6-63 : Global force-displacement diagram of a bolt row in a header plate connection

At constant temperature, the parameters of the material law are constant but this is not true anymore under anisothermal conditions. The use of this model under fire conditions necessitate to reiterate the procedure at a sufficient number of temperatures in order to get the evolution of the parameters during the fire. If some components have a non-reversible behaviour during the cooling of fire, the parameters will be function of the maximal temperature of the heating phase T_{max} and the temperature T.

The general material law defined in the SAFIR software for the Nonlinear Fibres Model includes two additional adaptations in order to represent more accurately the behaviour of bolt rows:

- In almost all types of connections, bolt rows only work in tension or have different behaviour in tension and compression domains. Consequently, the general law has been programmed in order to allow the definition of asymmetric material laws.

- For connections with bolts working in shear, forces are transmitted by friction during the first phase of the loading and before the two plate are in contact with the bolt shank. The defined material law for the Nonlinear Fibres Model also enables to account for this phenomenon by translation of the elastic branches. The stiffness of friction has not been defined as equal to 0 because i) the real value of the friction stiffness is not 0 and ii) such a simplification implies

that the rotational stiffness of the connection is 0 at the initial time step and it causes problems of convergence.

The general material law allocated to the fibres of the Nonlinear Fibres Model is plotted on Figure 6-64. The unloading is parallel to the elastic branch (in tension or compression).

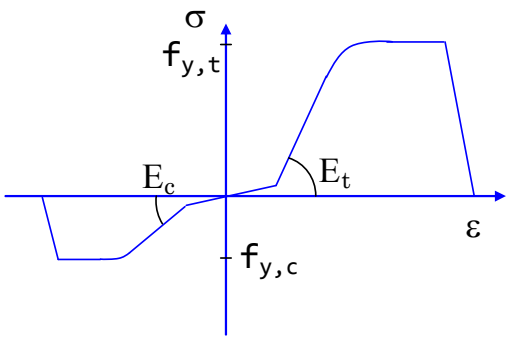

Figure 6-64 : General material law for fibres used in the Nonlinear Fibres Model

6.5.3 Application of the Nonlinear Fibres Model to Fin Plate Connections

6.5.3.1 Introduction

In the present thesis, the Nonlinear Fibres Model has been developed for fin plate connections. The components identified in a bolt row of a fin plate connection are: the plate in bearing, the beam web in bearing, the bolt in shear, the fin plate in tension or compression, the beam web in tension or compression and the weld in shear. In general, the resistance and the stiffness of the bolt row only depend on the resistance and the stiffness of the first three components mentioned. In this work, the resistance and stiffness of the connected elements (resistance in section) and of the welds is assumed to have a negligible influence on the resistance and the stiffness of the bolt rows. The behaviour of bolts rows is almost symmetric in fin plate connections and this assumption was made in the Bilinear Fibre Model. In the present section dedicated to the Nonlinear Fibre Model, the behaviour of bolt rows under tensile and compressive forces has been considered separately.

6.5.3.2 Characterisation of the "bolt in shear" component

The mechanical behaviour of bolts in shear has been analysed in § 4.4.3. The model proposed by Henriques for a wide range of bolts in shear at room temperature has been reported and the model for grade 8.8 bolts has been discussed. On the basis of this work and of the discussion, a modified model has been proposed by the author for grade 8.8 M12 bolts at room temperature and at elevated temperatures (including the cooling phase of natural fire). The validation against results of the

experimental tests performed at the Centro Sviluppo Materiali has shown a good agreement. However, the model has not been extended to other steel grades and diameters. The use of grade 8.8 bolts is very common but the most commonly used bolt sections are the M16, M20 and M24 bolts.

In the model of Henriques, the ratio η between the elastic displacement δ_b and the ultimate displacement $\delta_{u,b}$ is the unique parameter that is assumed to vary with the bolt diameter. However, the values of η proposed by Henriques are slightly underestimated because of the difference between the elastic resistances R_b obtained experimentally in Moscow tests and predicted by the Eurocode recommendations (Figure 4-40). If the elastic resistance predicted by the EN 1993-1-2 is ignored, the ratio η obtained graphically from Figure 4-40 is approximately equal to 4 for M20 bolts. The value $\eta = 4$ is the same as the one considered by the author in the case of grade 8.8 M12 bolts. Consequently, the values of the parameters considered in the modified model for grade 8.8 M12 bolts at room and elevated temperatures has been kept identical for M20 bolts.

6.5.3.3 Characterisation of the "plate/bolt in bearing" components

The resistance and the initial stiffness of the beam web and the fin plate in bearing are defined in the EN 1993-1-8 (see § 6.4.3.2.3). No recommendation is mentioned in the Eurocode about the post-elastic behaviour of the "plate/bolt in bearing" component. An expression of the strain-hardening stiffness $S_{st,bear}$ is suggested by Jaspart [1991] for the "plate/bolt in bearing component" at room temperature (Eq. 6-41). The ultimate resistance of this component has recently been defined as a function of the design resistance given in the Eurocodes [Pietrapertosa, 2004] and the ultimate displacement can be deduced (Eqs 6-42 & 6-43). However, the value 1.25 is a safe assumption and the real ratio depends on the failure mode.

$S_{st,bear} = \frac{S_{bear}}{40}$	**6-41**
$F_{bear,u} = 1.25\, F_{bear,Rd}$	**6-42**
$\delta_{u,b} = 11 \frac{F_{bear,Rd}}{S_{bear,b}}$	**6-43**

When a fin plate connection is only submitted to the combination of an axial force N and a bending moment M, the top and bottom bolts respectively transfer horizontal forces. Two different values of the spacing e_1 must be considered for evaluating the resistance in bearing resistance of the beam web depending if the transferred force is a tensile or compressive force (Figure 6-65). In presence of a shear force V, the force transferred by the bolts are not horizontal anymore and the spacings should be adapted (Figure 6-65). In case of fire, the evolutions of the internal forces M, N, V with time are

different and quite difficult to predict. This short discussion underlines that a special attention should be paid to the evaluation of the spacings influencing the resistance of plates in bearing. The same considerations also apply to pitches p_1, p_2 and transversal spacings e_2. It is noted that for the beam web, the presence of the flanges avoids some failure modes and the spacings e_1 may become meaningless (like for the the bottom bolt on Figure 6-65).

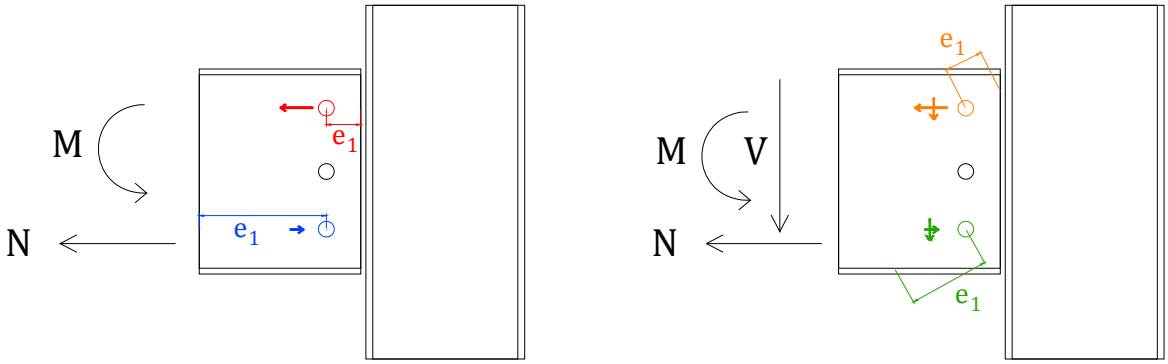

Figure 6-65 : Spacings to be considered for the bearing resistance in top and bottom bolts

6.5.3.4 Description of the tests performed on fin plate connections in Sheffield

Recently, a project conducted at the Universities of Sheffield and Manchester has investigated the robustness of common types of steel connections when subjected to fire. Test results on fin plate connections have been reported in [Yu, 2009c]. These tests are briefly described in this paragraph.

In the 14 isothermal tests performed, UB 305 x 165 x 40 beams are connected to UC 254 x 254 x 89 columns by 200 mm-deep and 8 mm-thick fin plates with three rows of bolts (Figure 6-66). The columns are fixed to a support beam and the loading is applied gradually by an articulated system to allow the development of large rotations (Figure 6-67). The loading is an excentrated and oblique force that induces a combination of tensile force, shear force and bending moment in the joint. The influence of parameters such as the temperature, the angle between the beam longitudinal axis and the applied force, the number of bolt(s) by row (designs 1 and 2 on Figure 6-66) and the bolts properties have been investigated (Table 6-17).

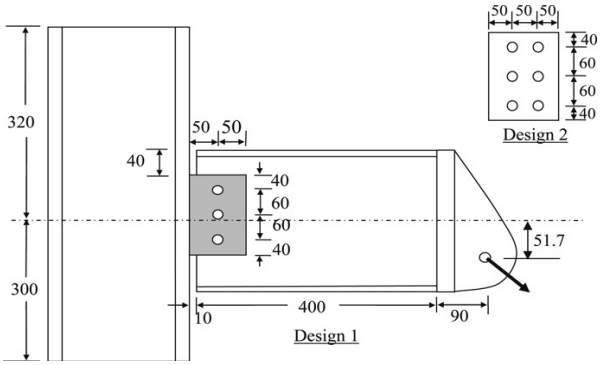

Figure 6-66 : Geometry of the tested fin plate connection in Sheffield tests [Yu, 2009c]

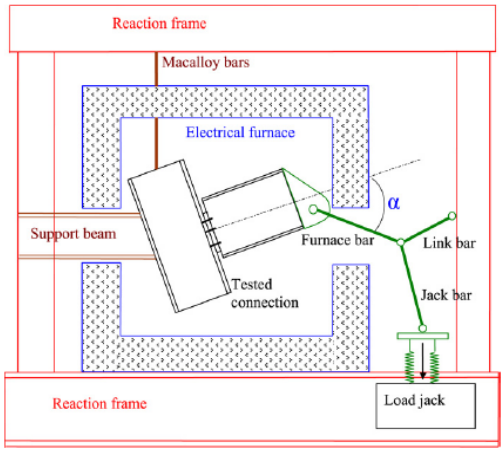

Figure 6-67 : Test set-up used for tests on fin plate connections at University of Sheffield [Yu, 2009c]

n°	1	2	3	4	5	6	7	8	9	10	11	12	13	14
Temp. (°C)	20	450	550	650	20	450	550	650	550	550	20	550	20	550
α (°)	55	55	55	55	35	35	35	35	35	55	35	35	35	35
Grade	8.8	8.8	8.8	8.8	8.8	8.8	8.8	8.8	8.8	8.8	10.9	10.9	8.8	8.8
Diam. (mm)	20	20	20	20	20	20	20	20	20	20	20	20	24	24
$n_{bolt(s)/row}$	1	1	1	1	1	1	1	1	2	2	1	1	1	1

Table 6-17 : Values of the parameters investigated in the Sheffield tests

In all the tests, the steel of beams and fin plates were S275 and the steel grade of the columns was S355. At ambient temperature, a tensile test on a specimen cut from the beam flange showed that the yield strength was 356 N/mm², the ultimate strength was 502 N/mm² and the Young's modulus was 176.35 kN/mm². No coupon tests have been performed on steel at elevated temperatures. The bolts were fully-threaded and the average tensile resistance, based on the results of three tests at ambient temperature, was 224 kN (f_{ub} = 914 N/mm²). At elevated temperatures, the reduction of the resistance of bolts in tension approximately follows the Eurocode recommended values. One double-shear test

indicated a single-shear resistance of 155 kN (ratio between the resistances in shear and in tension equal to 0.69, similar to the value of Eq. 4-16). The results of these tests will be described in § 6.5.3.7.

6.5.3.5 Force-displacement diagrams of one bolt row without friction (Sheffield tests)

The procedure for calculating the global force-displacement diagram of a bolt row is developed here for one bolt row of the fin plate connections used in Sheffield tests n°1 to 8. As a first step, the procedure is realised at room temperature under tension.

The elastic resistance of bolts in shear has been obtained by a specific test. The ultimate resistance per shear plane is assumed to be the same for single-shear and double-shear configurations. The diagram of the "bolt in shear" component is plotted on Figure 6-68 and the parameters are calculated in Eq. 6-44 to 6-50.

Parameters of the "bolt in shear" component at room temperature

$R_{u,b,20°C} = 155\,kN$	**6-44**
$R_b = \frac{R_{u,b}}{\kappa} = 129.2\,kN$	**6-45**
$S_{b,20°C} = \frac{8 d^2 f_{ub}}{d_{M16}} = 182.8\,kN/mm$	**6-46**
$\delta_{b,20°C} = \frac{R_{b,20°C}}{S_{b,20°C}} = 0.71\,mm$	**6-47**
$S_{st,b,20°C} = \frac{S_{b,20°C}}{\beta} = 36.6\,kN/mm$	**6-48**
$\delta_{u,b,20°C} = \eta_{20°C} \frac{R_{b,20°C}}{S_{b,20°C}} = 2.83\,mm$	**6-49**
$\delta_{f,b,20°C} = 6\,mm$	**6-50**

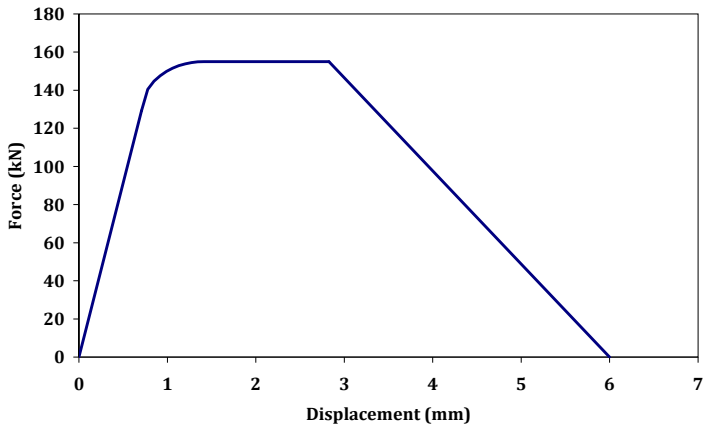

Figure 6-68 : Force-displacement diagram of the "bolt in shear" component

The elastic resistance of the component "beam web in bearing" at room temperature is evaluated in case of tensile forces in the top bolt row. Under pure tensile forces, the horizontal spacing e_1 is 40 mm. The value used here for e_1 has been measured graphically on a picture taken after the test at room temperature with $\alpha = 35°$ (Figure 6-69). The distance between the initial center of the hole and the web extremity in the direction of the hole deformations has been evaluated by scale effect between the longest known distance of the picture $h_i = 283$ mm and the "oblique spacing". A value of 44.7 mm is obtained by this methodology. In the case with $\alpha = 55°$, the spacing e_1 should be longer.

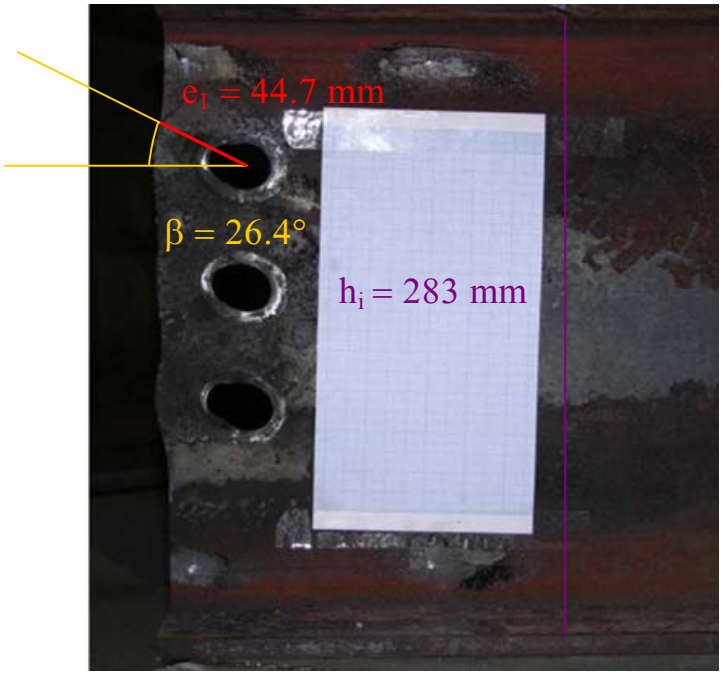

Figure 6-69 : Graphical evaluation of the spacing e_1 in the test 5 (T = 20°C - α = 35°)

The initial stiffness and the elastic resistance of the beam web in bearing have been evaluated by the recommendations of the EN 1993-1-8 (Eqs 6-51 to 6-61). The ultimate resistance of the beam web in bearing is calculated by evaluation of the resistance of the beam to the failure mode showed on Figure 6-70, considering the ultimate strength f_u of the beam steel (Eq. 6-58). The strain-hardening stiffness is calculated by use of Eq. 6-59 [Jaspart, 1997]. The displacement at the end of the descending branch $\delta_{f,bear,bw,20°C}$ is arbitrarily taken as equal to 1.1 times the ultimate displacement $\delta_{u,bear,bw,20°C}$.

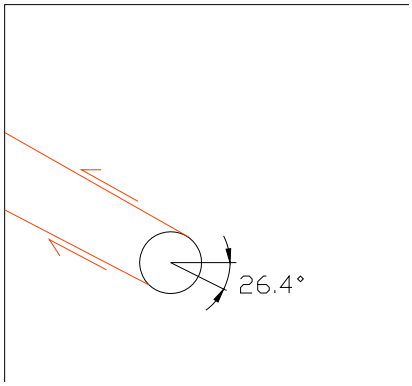

Figure 6-70 : Failure mode of the beam web by bearing at the level of the top bolt

$\alpha_b = \min\left(\frac{e_1}{3d_0};\frac{f_{ub}}{f_u};1\right) = 0.676$	**6-51**
$k_1 = 2.5 \qquad (1\ bolt\ per\ row)$	**6-52**
$F_{bear,bw,Rd,20°C} = \alpha_b\, k_1\, f_u\, d\, t_{wb} = 101.9\,kN$	**6-53**
$k_b = \min\left(\frac{e_1}{4d} + 0.5;\frac{p_1}{4d} + 0.375;1.25\right) = 1.059$	**6-54**
$k_t = \min\left(1.5\frac{t_{wb}}{d_{M16}};2.5\right) = 0.563$	**6-55**
$S_{bear,bw,20°C} = 12\, k_b\, k_t\, f_u\, d = 85.44\,kN/mm$	**6-56**
$\delta_{bear,bw,20°C} = \frac{F_{bear,bw,20°C}}{S_{bear,bw,20°C}} = 1.193\,mm$	**6-57**
$F_{bear,bw,u,20°C} = 2\,\alpha_1\, f_u\, t_{wb} = 155.25\,kN$	**6-58**
$S_{st,bear,bw,20°C} = \frac{S_{bear,bw,20°C}}{40} = 2.136\ kN/mm$	**6-59**
$\delta_{u,bear,bw,20°C} = \delta_{bear,bw,20°C} + \frac{F_{bear,bw,Rd,20°C} - F_{bear,bw,Rd,20°C}}{S_{st,bear,bw,20°C}} = 26.17\,mm$	**6-60**
$\delta_{f,bear,bw,20°C} = 1.1\,\delta_{u,bear,bw,20°C} = 28.79\,mm$	**6-61**

The same procedure is reproduced for the fin plate in bearing at the level of the top bolt in case of a horizontal tensile force. The spacing e_1 is meaningful in the present case because the extremity of the fin plate is welded to the column flange. The elastic resistance of the fin plate in bearing is not reduced by failure modes inducing a tearing off of the fin plate up to a free edge. Consequently, the safe approach of the 1.25 ratio is followed to evaluate the ultimate resistance of the fin plate in bearing (Eqs 6-42 & 6-43). The results obtained for the "fin plate in bearing" component are given in Eqs 6-62 to 6-68.

$F_{bear,fp,Rd,20°C} = \alpha_b \, k_1 \, f_u \, d \, t_{wb} = 200.8\,kN$	**6-62**
$S_{bear,fp,20°C} = 12\,k_b \, k_t \, f_u \, d = 134.5\,kN/mm$	**6-63**
$\delta_{bear,bw,20°C} = \dfrac{F_{bear,fp,20°C}}{S_{bear,fp,20°C}} = 1.493\,mm$	**6-64**
$F_{bear,fp,u,20°C} = 1.25\,F_{bear,fp,u,20°C} = 251\,kN$	**6-65**
$S_{st,bear,fp,20°C} = \dfrac{S_{bear,fp,20°C}}{40} = 3.362\ kN/mm$	**6-66**
$\delta_{u,bear,fp,20°C} = 11\,\dfrac{F_{bear,fp,Rd,20°C}}{S_{bear,fp,20°C}} = 16.42\,mm$	**6-67**
$\delta_{f,bear,fp,20°C} = 1.1\,\delta_{u,bear,fp,20°C} = 18.06\,mm$	**6-68**

The individual force-displacement diagrams of the three components and the global force-displacement diagram are plotted on Figure 6-71. The ultimate resistances of the "bolt in shear" and "beam web in bearing" components are almost identical and large deformations will be developed in these two components. In case of pure tensile forces, the spacing e_1 would have been equal to 40 mm and the failure mode of this row would have been a tearing off of the beam web. The low value of the elastic resistance of the beam web in bearing implies that the bolt row has ductile behaviour before the failure of bolts and that the redistribution of forces between the bolt rows will be increased.

At higher temperatures or after a heating-cooling cycle, the resistance of the "bolt in shear" component is reduced more significantly than the resistance of the other components. Consequently, the failure mode will remain the failure of bolts in shear but the ductility of the row will be deacreased (Figures 6-73 to 6-74).

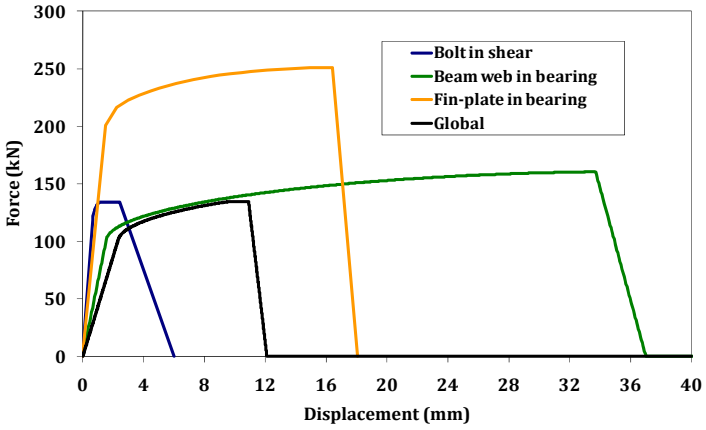

Figure 6-71 : Individual and global force-displacement diagrams of the top bolt – T = 20°C

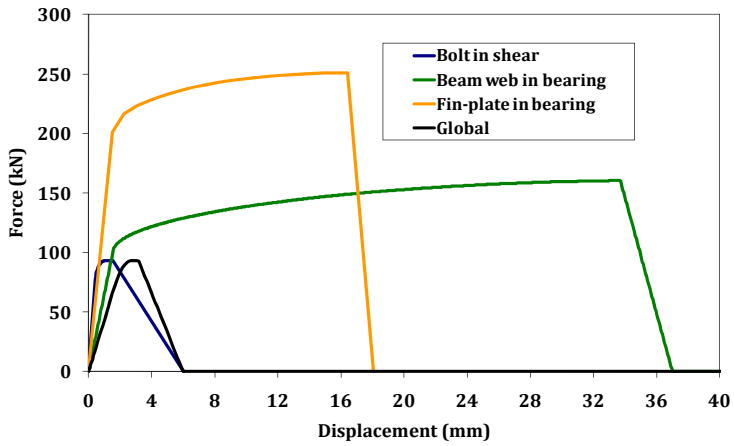

Figure 6-72 : Individual and global force-displacement diagrams of the top bolt – T = 550°C

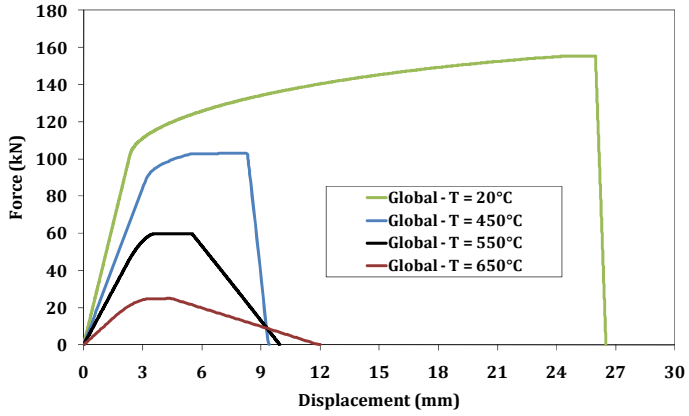

Figure 6-73 : Global force-displacement diagrams of the top bolt at different temperatures

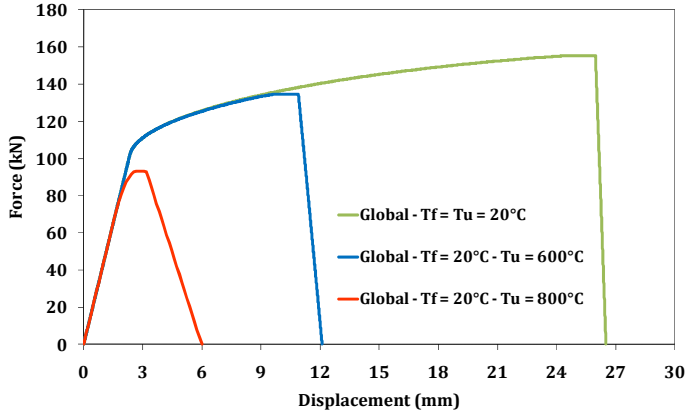

Figure 6-74 : Global force-displacement diagrams of the top bolt at 20°C after different heating phases

6.5.3.6 *Global force-displacement diagrams of bolt rows with friction (Sheffield tests)*

The difference between the diameters of the bolt and the hole implies a translation of the force-displacement diagram (Figure 6-75). This translation is not horizontal because forces are transferred by friction.

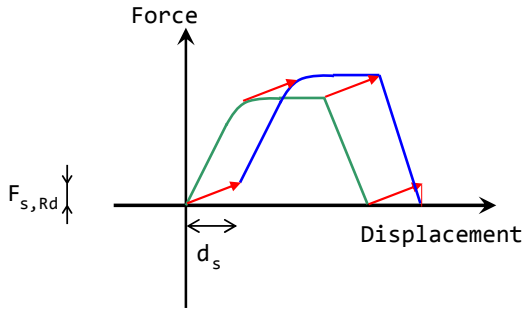

Figure 6-75 : Translation of the force-displacement diagram for friction

The maximal friction force $F_{s,Rd}$ transferred by a non-preloaded bolt has been evaluated by Sarraj [2007] and is given in Eq. 6-69.

$F_{s,Rd} = 0.28\,\mu\, f_{ub}\, A$	**6-69**

where the slip factor μ goes from 0.2 to 0.5 depending on the class of the friction surface, f_{ub} is the bolt ultimate strength and A the tensile stress area of the bolt. In the Sheffield tests, no indication is given about the slip factor or the class of friction surfaces. A good correlation is obtained with μ = 0.5.

The elastic branch starts when the the two plates are in contact with the bolt shank. For M20 bolts, the hole diameter is usually 22mm and the contact is obtained after an initial 2-mm relative displacement. The force-displacement diagrams at different temperatures after integration of the friction are given on Figure 6-76. It is observed that the ductility differs much between tension and compression at 20°C. The values of spacings are different and the weakest components are the 'bolts in shear' under compressive forces and the 'beam web in bearing' under tensile forces. At higher temperatures, the 'bolts in shear' component is always the weakest one.

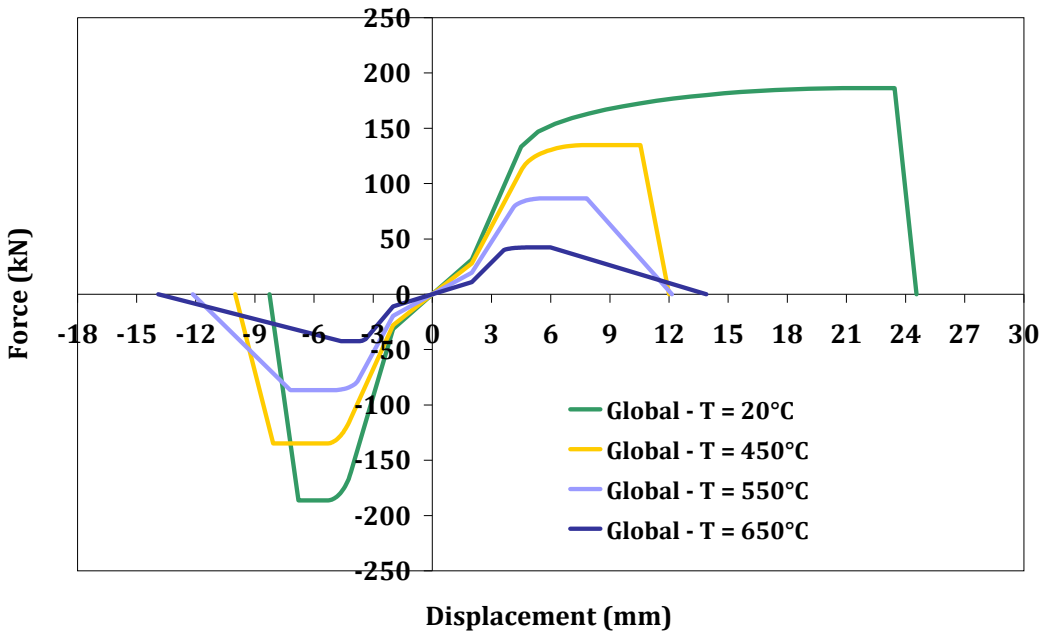

Figure 6-76 : Force-displacement diagram of bolts rows accounting for friction

For fin plate connections, plastic deformations are considered separately in the domains of tension and compression and, in both domains, it is imposed that the plastic deformations can only increase. In fact, this assumption is valid if plastic deformations are developed in the components 'plate/bolt in bearing'. In case plastic deformations are developed in the bolts, considering the behaviours in tension and compression separately is not valid anymore. However, the ductility of bolts is limited and the plastic deformations developed in that component will be small.

In the numerical model, each fibre is characterised by a cross-section area, a length (equal to the length of the beam element) and a stress-strain material law. Figure 6-77 represents the initial stress-strain material law of one fibre and the adapted law after plastic deformations develop in the compression and tension domains.

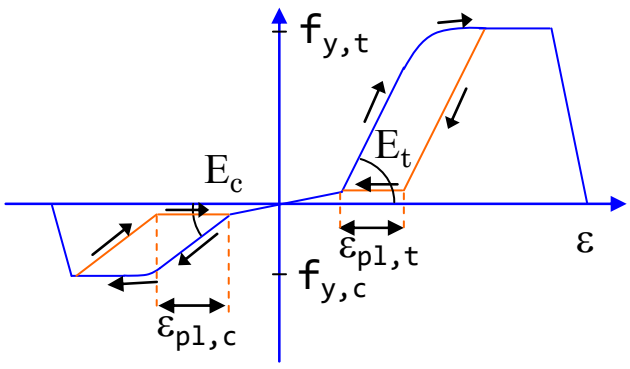

Figure 6-77 : Stress-strain diagram of a fibre after yielding in tension and compression

6.5.3.7 Global behaviour of fin plate connections (Sheffield tests)

The force-displacement diagrams of bolt rows have been described in detail (§ 6.5.3.6). For the contact between the beam and column flanges, a 'Translated BILIN_COMP' material law is used with identical properties to what has been realised in the Bilinear Fibres Models (§ 6.4.3.2.2).

Tests n°1 to 8 performed in Sheffield have been simulated numerically. The loading has been applied step-by-step and the variation of the loading inclination during the tests has been taken into account. No unloading phase has been considered. The comparisons between experimental and numerical rotations of joint are plotted on Figures 6-78 and 6-79. The effect of shear forces has been neglected in these simulations. The reduction of bolts resistance to axial forces due to the presence of shear forces has been calculated analytically in all tests and this reduction always remains lower than 5% at the failure time.

The correlation between rotations of the joint obtained numerically and mechanically is good. The failure of the fin plate connection is correctly predicted, except for test n°7 (Table 6-18). In tests n°7 and 8, a strong discontinuity is obtained when the applied force respectively reaches 30 kN and 15 kN. This is perhaps due to a partial or complete loss of contact between the plates and a reduction of the force transmitted by friction.

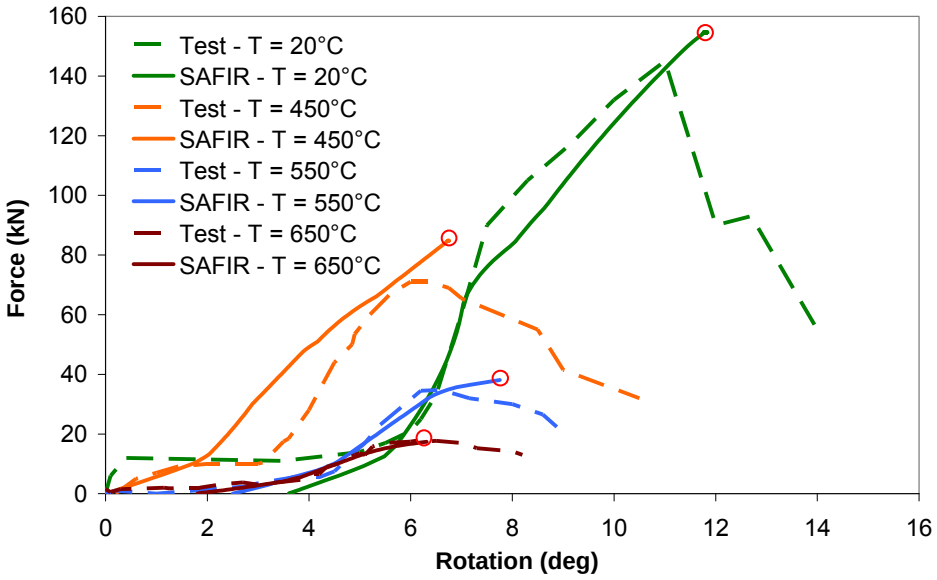

Figure 6-78 : Force-rotation diagram of Sheffield tests n°1 to 4 (α = 55°)

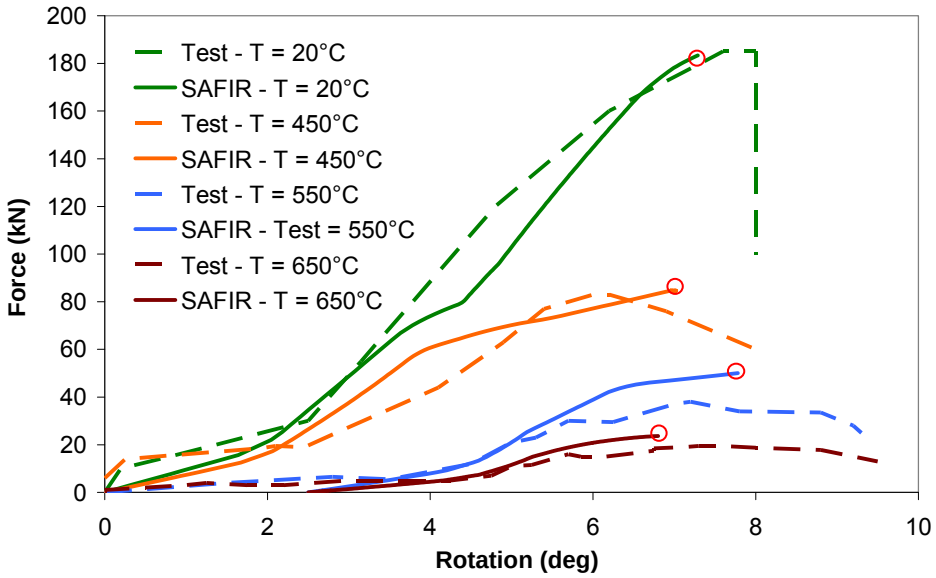

Figure 6-79 : Force-rotation diagram of Sheffield tests n°5 to 8 (α = 35°)

Test n°	Temperature	F_{max} Test	F_{max} SAFIR	Test n°	Temperature	F_{max} Test	F_{max} SAFIR
(-)	(°C)	(kN)	(kN)	(-)	(°C)	(kN)	(kN)
1	20	171.1	154.6	5	20	189.1	183.4
2	450	84.0	84.7	6	450	87.5	84.8
3	550	42.2	38.1	7	550	40.2	50.1
4	650	21.8	17.4	8	650	20.1	23.7

Table 6-18 : Comparisons between the forces causing connection failure in tests and numerical simulations

6.5.3.8 Numerical simulation of Delft test

The test performed in Delft on a steel sub-structure with fin plate connections, presented in § 6.3.2, has been stopped after the failure of bolts during the cooling phase. The evolution of the mid-span deflections predicted numerically with the Bilinear and Nonlinear Fibres Models are plotted on Figure 6-80. In the Bilinear Fibre Model, the three fibres representing the action of the bolt rows are yielded after 119 minutes and, by application of the failure criteria defined in § 6.4.5.1, the failure of the connection occurs at this moment. In the Nonlinear Fibre Model, the convergence is not reached after 126 minutes and this is in agreement with the test observations ($t_{failure}$ = 127 minutes). The evolutions of axial forces obtained with the two models are given in Figure 6-81.

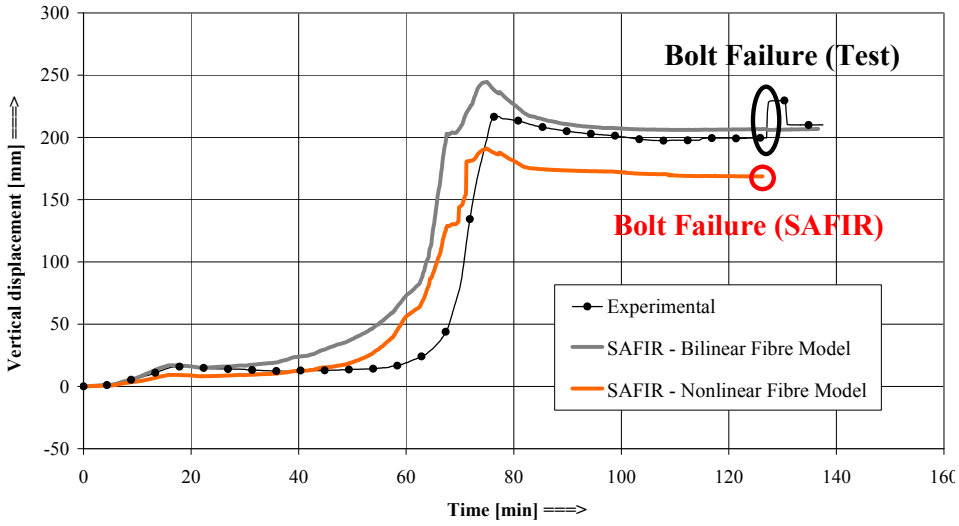

Figure 6-80 : Evolution of the beam deflections during the test of Delft

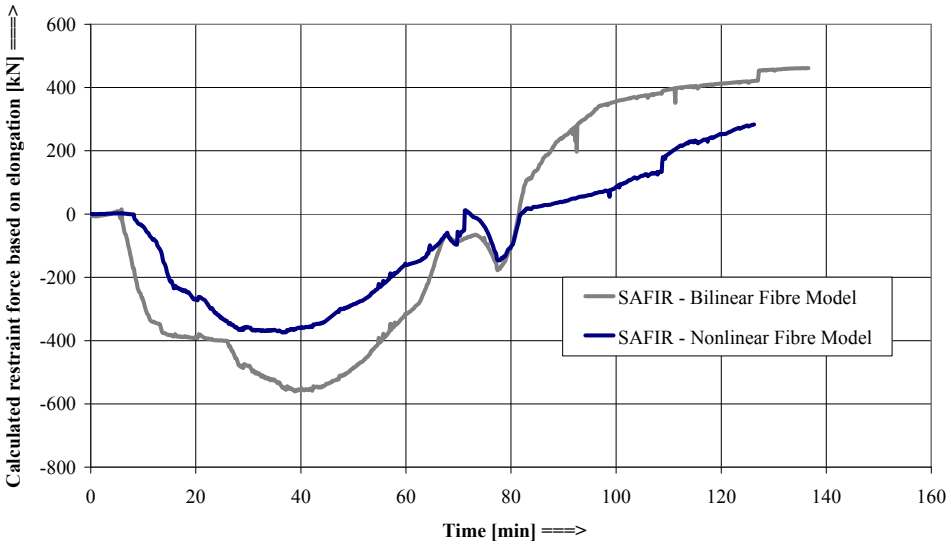

Figure 6-81 : Evolution of axial forces during the test of Delft

6.6 Conclusions

Component-based models and new material laws (bilinear and non linear) have been developed to represent the action of common simple connections in steel sub-structures under fire conditions. The action of the joint is modelled by a fibre beam finite element where the force-displacement relationship of each bolt row or compression row is represented by one fibre. The two models differ by the degree of complexity of the material laws allocated to the fibres. In the Bilinear Fibres Models, bilinear material laws have been assigned to bolt and compression rows to build Bilinear Fibre Models representing the action of connections. Different laws have been defined for rows working only in

tension (e. g.: bolt rows of header plate connections), laws working only in compression (e. g.: contact between beam and column flanges) and symmetric or asymmetric laws working in tension and compression (e. g.: bolt rows of fin plate and double web cleats connections). These models are quite simple but are not able to predict accurately the occurrence of a failure in the connection components. In order to verify the joints against failure, some failure criteria must be added in which the ductility of bolt rows is considered following a simplified approach based on the concept of classes of ductility. The use of these failure criteria is relatively time-consuming and can hardly be extended to large-scale structures. After the failure of one connection is obtained, the rest of the simulation is not valid. The Nonlinear Fibres Models necessitate more work for building the model but allows detecting automatically connection failures, especially in the simulations of a complete building. In the present work, this type of model has only been applied to fin plate connections but the procedure would be completely similar for other types of connections.

The test set-up, recorded measurements and observations of the tests performed recently in Metz and Delft on steel sub-structures under heating and sub-sequent cooling are described in detail in this chapter. The two Delft tests performed on steel sub-structures have been modelled with use of the Bilinear Fibres Model and good correlation was obtained with experimental results. In the first test, the failure of bolts occurred during the cooling phase and is correctly predicted by the failure criteria defined in this work. In the second test, no failure occurred in double web cleats connections and numerical simulations are in agreement with this observation. The validation of the Bilinear Fibres Models for fin plate connections, double web cleats connections and header plate connections has been completed by comparisons with the results of parametric analyses performed by other research centers using complex finite element model (Abaqus models by Corus and Ansys models by CTICM). The Nonlinear Models have been used to model isothermal tests performed on isolated joints in Sheffield and the first test of Delft. Good results have been obtained by use of the Nonlinear Fibres Models.

The possibility of failure in simple connections during the heating and cooling phases of a fire is strongly dependent of the rotational stiffness and the ductility of this connection. Simple connections are usually designed at room temperature to resist shear forces and sometimes to bending moments due to the excentricity between the connection and the center of gravity of the column section. During the heating phase, the rotational stiffness of joints causes a redistribution of bending moments in the beam and hogging bending moments are transferred by simple connections. Consequently, the fire resistance of the beam is increased while joints are subjected to a combination of axial forces, shear forces and bending moments that the connections have usually not been designed for. During the cooling phase, the connection can fail when high temperatures have been reached at the end of the heating phase and the beam has not failed; failure of the connection is more likely to occur for high levels of axial restraints and low vertical loads. Indeed, high temperatures are reached at the end of the

heating phase, i) large plastic strains develop in the beam and large tensile thrusts develop during the cooling phase and ii) the non-reversible behaviour of bolts and welds components implies a reduction of the ductility of the connection. When internal forces induce the yielding of components in bolt and/or compression rows, the failure will occur if the yielded component has not a sufficient ductility to allow a redistribution of internal forces. The design of the joint should be performed in such a way that the weakest components are ductile components during both the heating and cooling phases. The comparisons of components resistances during the fire also necessitates to account for the different reduction factors for carbon steel, bolt and welds components under heating and the non-reversibility of these factors. The risk of failure in double web cleats connections is lower than for the two others types of simple connections studied here because of its low rotational stiffness and its good ductility for the configurations analysed.

A simple procedure has been proposed to predict whether the failure of simple connections, satisfying to the Eurocode recommendations for the design of connections at room temperature, may occur under a natural fire. The concept of class of ductility is crucial in this procedure but other parameters like the type of connection, the maximal temperature of the bottom beam flange under the natural fire considered, the level of axial restraints and the load ratio have also an influence.

7 Case Study

7.1 Introduction

Different models have been proposed and validated within the previous paragraphs for thermal and mechanical analyses of steel simple connections and steel structures under natural fire. Chapter 7 describes the verification of the fire resistance of a steel structure with fin plate connections subjected to a realistic fire scenario. The geometrical and mechanical properties of the beam and the fin-plate connection are identical to those used for the tests performed in Sheffield on isolated joints.

7.2 Description of the case study

The structure analysed here is a six-bays and four-storeys braced frame composed of 6-metre long IPE 300 beams and 3-meter high HEA 300 columns (Figure 7-1). This frame is part of a 36m x 45m x 12m office building and the distance between two consecutive frames is 5 metres. The floors are made of 15-mm thick precast hollow core slab covered by an additional 5-mm thick concrete topping. Beams and columns are connected by fin plate connections (Figure 7-2). The thickness of the fin plate is 10 mm. The columns, beams and fin plates are made of S275 steel and Grade 8.8 M20 bolts are used. The welds connecting the fin plates to the columns are designed so that weld failures are avoided.

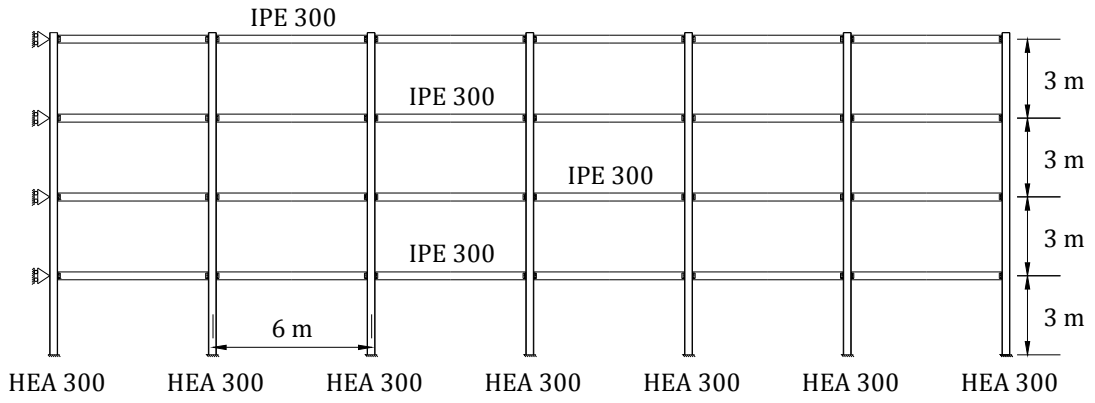

Figure 7-1 : Geometrical properties of the steel frame analysed as a case study

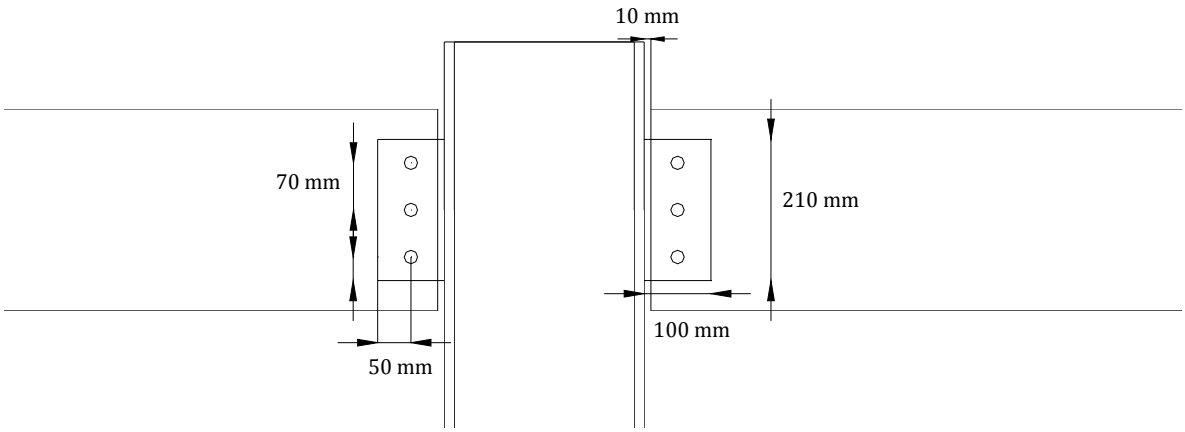

Figure 7-2 : Geometry of the beam-to-column joints (fin plate connections)

The building is divided in 18m x 15m x 3m compartments. The fire scenario chosen for this case study is a fire in a compartment situated at the second floor (Figure 7-3). The two external walls of this compartment are made of concrete blocks and the two internal walls are composed of 100-mm thick glass wool covered by two 14-mm thick gypsum boards (Figure 7-4). No openings are considered in the internal walls and three 2m x 1m windows (sill height = 1 m) are considered in each external wall. The precast concrete hollowcore slabs are covered by gypsum boards on the ceiling side.

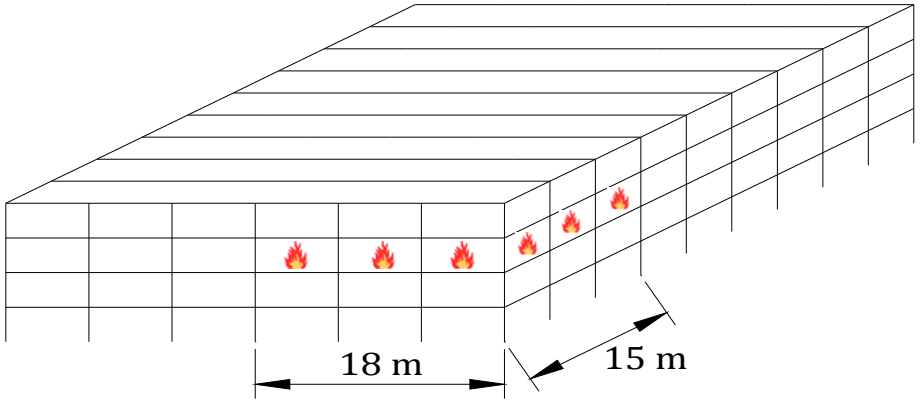

Figure 7-3 : Fire scenario considered for the case study

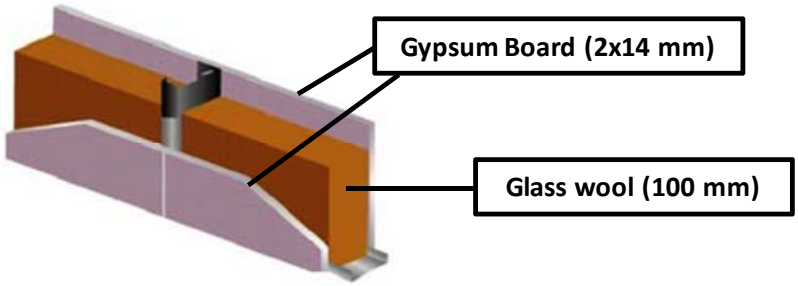

Figure 7-4 : Composition of the internal walls

The time-temperature curve in the compartment has been calculated by use of the Annex A of the Eurocode [CEN, 2002a] in § 7-3.

7.3 Time-temperature curve in the compartment

The expression of the parametrical time-temperature curve depends on two parameters during the heating phase: the opening factor O (Eq. 7-1) and the factor b that characterises the thermal properties of the enclosure. The factors b_i of the ceiling and the two types of walls are calculated by Eq. 7-2. Eq. 7-3 is used to evaluate a global b factor accounting for the individual b factors.

$O = A_v \sqrt{h_{eq}} \big/ A_t = 12\sqrt{1.5}/738 = 0.0199 < 0.02 \;\rightarrow\; O = 0.02$	**7-1**

where A_v, h_{eq} and A_t, are respectively the total area of vertical openings on all walls, the weighted average of window heights on all walls and the total area of enclosure (walls, ceiling and floor). The opening factor must satisfy to $0.02 \leq O \leq 0.2$ and is consequently rounded up to 0.02.

$b_{ext.wall} = b_{floor} = \sqrt{\rho c \lambda} = \sqrt{2300*1000*1.6} = 1918.3 \;\; W^{1/2}/m^2.K$	**7-2**
$b_{int.wall} = \sqrt{60*1030*0.037} = 46.51 \;\; W^{1/2}/m^2.K$	
$b_{ceiling} = \sqrt{\rho c \lambda} = \sqrt{900*1000*0.25} = 474.3 \;\; W^{1/2}/m^2.K$	

where ρ, c and λ are the density, the specific heat and the thermal conductivity of the enclosure surface. For enclosure surfaces with different layers, b is equal to the value b_1 of the exposed layer if b_i is higher than b_1 for other layers of the surface ($i > 1$). The criteria $100 \leq b \leq 2200$ is respected for all the enclosure surfaces.

$b_{compartment} = \left(\sum_i b_i \, A_i \right) \Big/ \left(A_t - A_v \right) = 1126 \;\; W^{1/2}/m^2.K$	**7-3**

The parameter Γ (already mentioned in Eq. 2-10) is given by Eq. 7-4 and the gas temperature in the compartment exposed to fire is given by Eq. 7-5 where t* is the fictive time expressed in hours (Eq. 7-6).

$\Gamma = \left(O/b\right)^2 \big/ \left(0.04/1160\right)^2 = 0.265$	**7-4**
$\theta_{gas} = 20 + 1325 \left(1 - 0.324\, e^{-0.2 t^*} - 0.204\, e^{-1.7 t^*} - 0.472\, e^{-19 t^*}\right)$	**7-5**
$t^* = t\,\Gamma$	**7-6**

The fictive duration of the heating phase t^*_{max} is related to the parameter Γ, equal to the ratio between the floor area and the total enclosure surface and the design value of the load density $q_{t,d}$.

The design value of the fire load $q_{f,d}$ is defined by Eq. 7-7.

$$q_{f,d} = q_{f,k}\, m\, \delta_{q1}\, \delta_{q2}\, \delta_n = 511*0.8*1.5*1*0.302 = 185.31 \;\; MJ/m^2 \qquad \textbf{7-7}$$

Where the characteristic fire load density $q_{f,k}$ is given in Table 7-1, m is the combustion factor, the factors δ_{q1} and δ_{q2} respectively take into account the fire activation risk due to the size of the compartment and the type of occupancy (Table 7-2), and d_n take intoaccount the active fire fighting measures (Eq. 7-8 and Table 7-3). The condition $50 < q_{t,d}$ (MJ/m²) < 1000 is respected. In the present case study, the active fire fighting measures adopted are: the presence of automatic water extinguishing system ($\delta_{n1} = 0.61$), automatic fire detection by smoke and alarm ($\delta_{n4} = 0.73$), automatic alarm transmission to fire brigade ($\delta_{n5} = 0.87$) and an off site brigade ($\delta_{n7} = 0.78$). The other δ_{ni} parameters are equal to 1.

Occupancy	Average	80% Fractile
Dwelling	780	948
Hospital (room)	230	280
Hotel (room)	310	377
Library	1 500	1 824
Office	420	511
Classroom of a school	285	347
Shopping centre	600	730
Theatre (cinema)	300	365
Transport (public space)	100	122
NOTE Gumbel distribution is assumed for the 80 % fractile.		

Table 7-1 : Fire load densities $q_{f,k}$ [MJ/m²] for different occupancies

Compartment floor area A_f [m²]	Danger of Fire Activation δ_{q1}	Danger of Fire Activation δ_{q2}	Examples of Occupancies
25	1,10	0,78	artgallery, museum, swimming pool
250	1,50	1,00	offices,residence, hotel, paper industry
2 500	1,90	1,22	manufactory for machinery & engines
5 000	2,00	1,44	chemical laboratory, painting workshop
10 000	2,13	1,66	manufactory of fireworks or paints

Table 7-2 : Values of the factors δ_{q1} and δ_{q2}

$$\delta_n = \prod_{i=1}^{10} \delta_{ni} = 0.61*1*1*0.73*0.87*1*0.78*1*1*1 = 0.302 \qquad \textbf{7-8}$$

δ_{ni} Function of Active Fire Fighting Measures									
Automatic Fire Suppression		Automatic Fire Detection			Manual Fire Suppression				
Automatic Water Extinguishing System	Independent Water Supplies	Automatic fire Detection & Alarm		Automatic Alarm Transmission to Fire Brigade	Work Fire Brigade	Off Site Fire Brigade	Safe Access Routes	Fire Fighting Devices	Smoke Exhaust System
	0 | 1 | 2	by Heat	by Smoke						
δ_{n1}	δ_{n2}	δ_{n3}	δ_{n4}	δ_{n5}	δ_{n6}	δ_{n7}	δ_{n8}	δ_{n9}	δ_{n10}
0,61	1,0 | 0,87 | 0,7	0,87 or 0,73		0,87	0,61 or 0,78		0,9 or 1 or 1,5	1,0 or 1,5	1,0 or 1,5

Table 7-3 : Values of the factors δ_{ni}

Finally, the duration of the heating phase t_{max} is obtained by Eqs 7-9 & 7-10.

$$q_{t,d} = q_{f,d}\frac{A_f}{A_t} = 185.31 * \frac{18*15}{738} = 67.8 \ MJ/m^2 \qquad \textbf{7-9}$$

$$t_{\max} = \max\left[\left(2*10^{-4} * q_{t,d}/O\right); t_{\lim}\right] = 0.68 \ h = 40.7 \ \text{min} \qquad \textbf{7-10}$$

During the cooling phase, the gas temperature is given by Eq. **Erreur ! Source du renvoi introuvable.** ($t^*_{max} = 0.68$).

$$\theta_{gas} = \theta_{\max} - 250\left(3 - t^*_{\max}\right)\left(t^* - t^*_{\max} x\right) \quad [°C] \qquad for \quad 0.5 \le t^*_{\max} \le 2 \qquad \textbf{7-11}$$

The correlation between the compartment temperatures obtained by use of a Zone model [Cadorin, 2003] and the parametric curve calculated from the EN 1991-1-2 is good during the heating phase and the maximal temperatures obtained with these two methods are similar (around 700°C). The compartment temperature decreases much quicker in the Zone model (Figure 7-5).

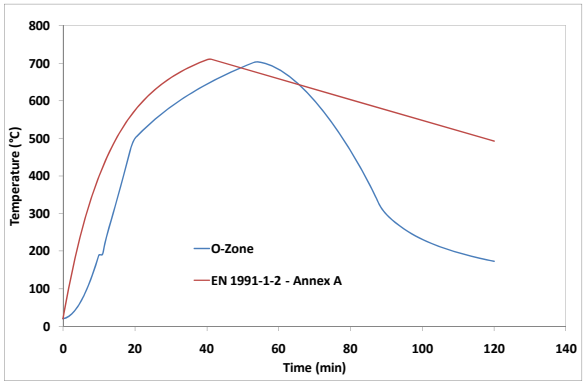

Figure 7-5 : Comparison between gas temperatures obtained by a zone model and parametric curves

The curve obtained by use of the Annex A of EN 1991-1-2 will be considered for the present study case.

7.4 Distribution of temperature in structural elements

Different simple methods have been described in Chapter 2 to predict the distribution of temperature in beams and joints covered by a flat concrete slab. In the present case, the proposed simple methods have been used and, for the 2D beam sections, have been compared to the results given by SAFIR. The two adapted versions of the Lumped Capacitance Method for predicting the temperature of the beam bottom flange give very good results (Figure 7-6a), as observed previously. Concerning the evolution of temperature in the top flange, the Heat Exchange Method (with ϕ_{150} = 14 kW/m² and ϕ_{475} = 20 kW/m²) give better predictions than the Component Method during both the heating and cooling phases (Figure 7-6b). The delay before the cooling down of the Component Method had already been observed previously. The under-estimation of temperature during the heating phase with this method is due to the low value of Γ in the present case; the evolution of the thickness of the concrete slab integrated in the heated section should be adapted in that way for very slow or very fast fires. For the distribution of temperature in the joint zone, the temperature at the level of the bottom and top beam flanges has respectively been evaluated by the Lumped Capacitance A2 (ratio $(A_m/V)_{beam}$ divided by 2) and the Heat Exchange Method (Figure 7-6).

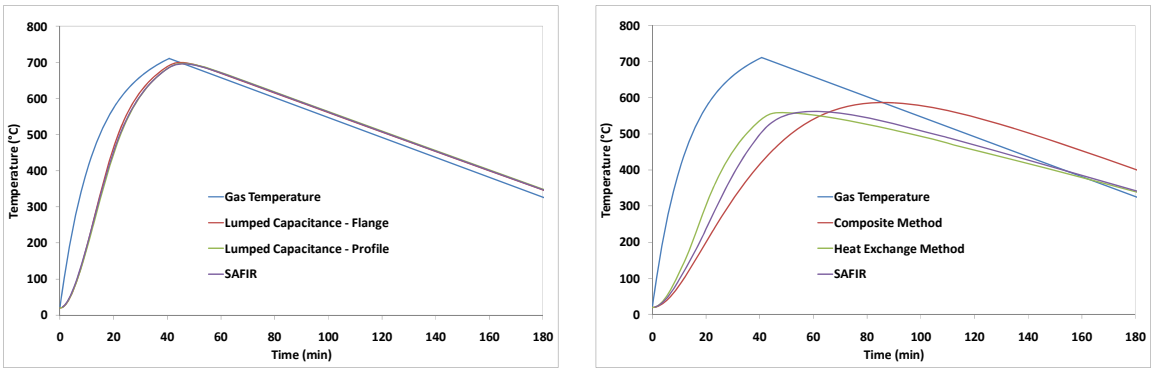

Figure 7-6 : Temperature in the beam flanges (left: bottom – right: top)

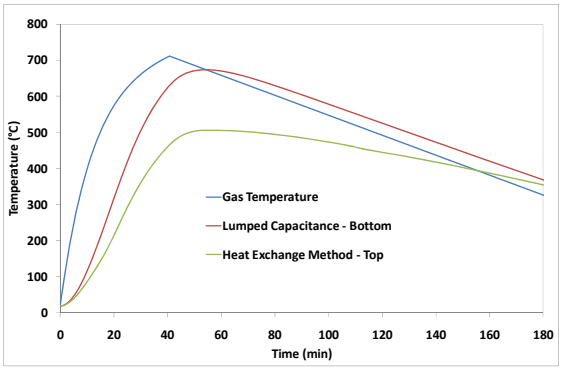

Figure 7-7 : Temperature in the joint zone at the levels of the bottom and top beam flanges

7.5 Verification of the resistance of structural elements

7.5.1 Design procedure for structures under fire according to European standards

Following the recommendations of Eurocodes, the design of structures is based on the concept of limit states, i. e. states beyond which the structure no longer satisfies the design performance requirements [Franssen, 2009]. These limit states are divided into ultimate limit states (failures, instabilities, etc) and serviceability limit states (excessive deflections, vibrations, etc). Eurocodes considers the fire event as an accidental load case and only requires verifications against ultimate limit state. The semi-probabilistic approach imposes that the design resistance of the structure remains higher than the effects induced in the structure by the design actions. In accidental load cases, the partial safety factor applied to materials and loads are equal to 1.

7.5.2 Analytical and numerical results with different load ratios

In order to compare the numerical results obtained with the Nonlinear Fibres Models and the recommendations enunciated on the basis of parametric analyses performed with the Bilinear Fibres Models, a large number of load ratios have been used in the present section.

The force-displacement diagrams of the top bolt row during the heating and cooling phases are given on Figures 7-8 and 7-9. The maximal temperature of bolts is 673°C (bottom joint zone) and the diagrams related to T = 700°C are given as an informative data. The ductility of this row is high during the heating phase until 400°C. Until temperature comes back to 400°C, the shear resistance of bolts is approximately equal to the plastic resistance of the "beam web in bearing" components (Figure 7-10). The ductility class of the bolt row is C during the heating phase (T > 575°C) and the cooling phase (T > 400°C), what is not in agreement with the recommendations proposed in § 6.4.8.3. At the end of the cooling phase, the reduction factor for the non-reversible behaviour of bolts is 0.76.

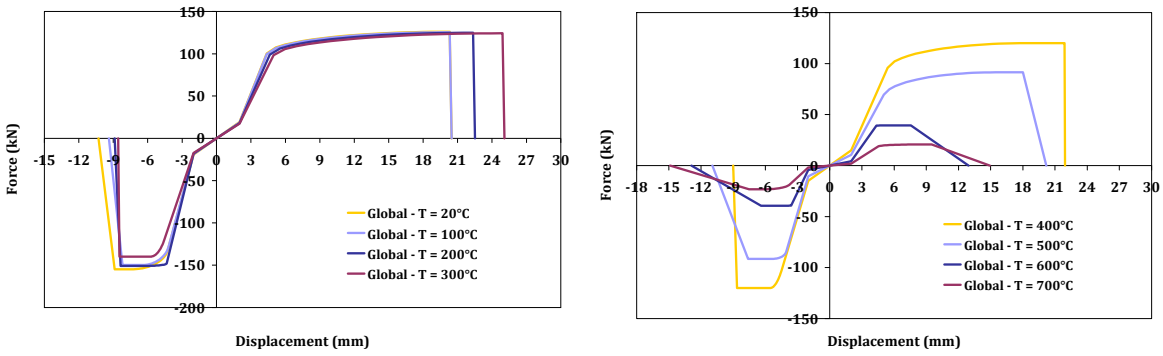

Figure 7-8 : Global force-displacement diagrams of the top bolt during the heating phase

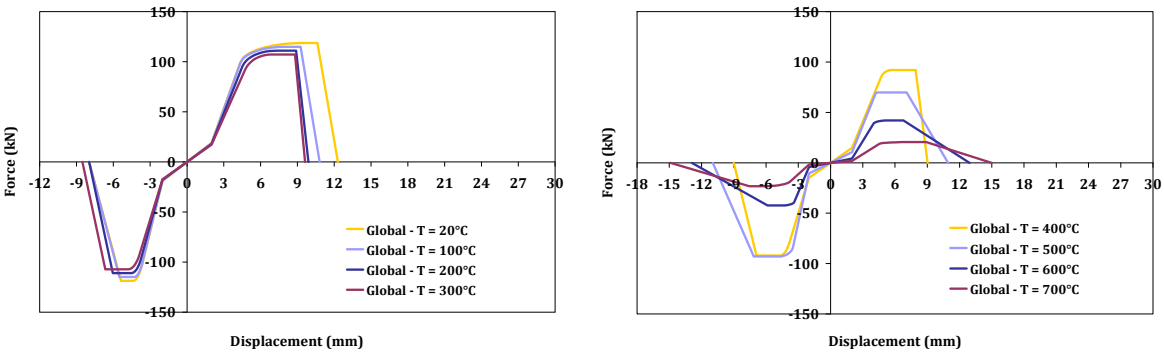

Figure 7-9 : Global force-displacement diagrams of the top bolt during the cooling phase

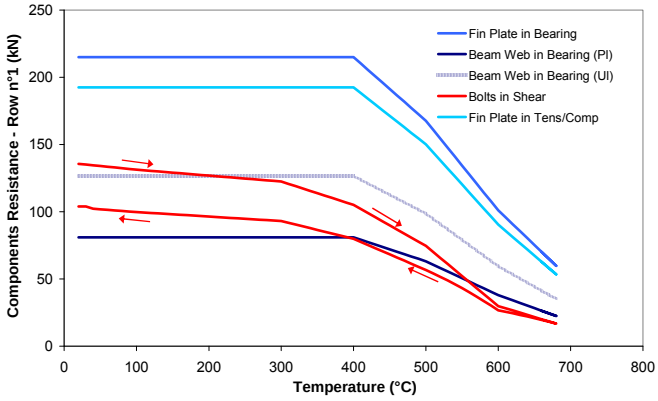

Figure 7-10 : Resistance of components in bolt row n°1

The analysed frame is braced and fire attacks three beams and four columns (Figure 7-11). No horizontal loads are applied to the structure. The maximal temperatures in the bottom and top flanges are respectively obtained after 45 and 60 minutes. The distributions of temperature at these times are given in Figure 7-12. The maximum weighted average temperature $T_{beam,aver}$ (Eq. 7-12) is 651°C and, in case of uniform distribution of temperature, this corresponds to a reduction factor for yield strength $k_y = 0.35$. The level of axial restraints K, calculated by application of Eq. 6-40, is 3.8 %. Following the recommendations proposed in § 6.4.8.3 to account for second order effects, the failure of the beam during the heating phase occurs for load ratios higher than 0.318 (Eq. 7-13). During the cooling phase, the failure is avoided if one of the three following statements is respected: i) the load ratio is higher than w_{lim} (0.35 for fin plate connections), ii) the temperature of the beam bottom flange remains lower than T_{lim} at the end of the heating phase (670°C for fin plate connections and K = 3.8%) and iii) the class of ductility of the bolt rows is A during the complete fire. It appears than none of the three statements are respected for cases where the beam does not fail during the heating phase ($w < 0.318$) and that the failure of the connection should occur during the cooling phase.

The results of the numerical simulations are reported on Figure 7-13. The frame resists to the fire for two domaines of the load ratio: w < 0.12 and 0.26 < w < 0.32. The failure of the beam is correctly predicted by the proposed recommendations (w ≥ 0.318). The first domaine with no failure is rarely encountered, even under fire conditions, because the self-weight of the beam and the floor usually induce higher vertical loadings. The absence of failure for 0.26 < w < 0.32 is due to the combination of low axial restraints and a vertical deflections that induce large deflections without beam failure. This domaine is quite narrow and the proposed recommendations are conservative. It should also be noted that beam temperature has not yet come back to 20°C at the end of the simulation ($T_{mid\text{-}span} \approx 180°C$) and that the failure could still happen after more than 240 minutes. The duration of such a numerical simulation until t = 240 minutes goes from 2 hours to 3 hours.

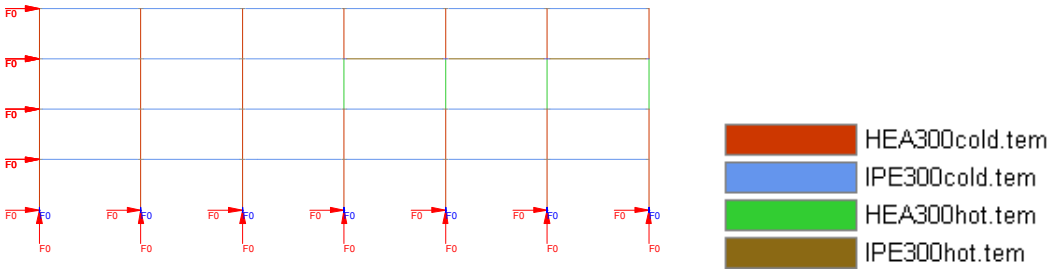

Figure 7-11 : Boundary conditions and geometrical properties of the frame

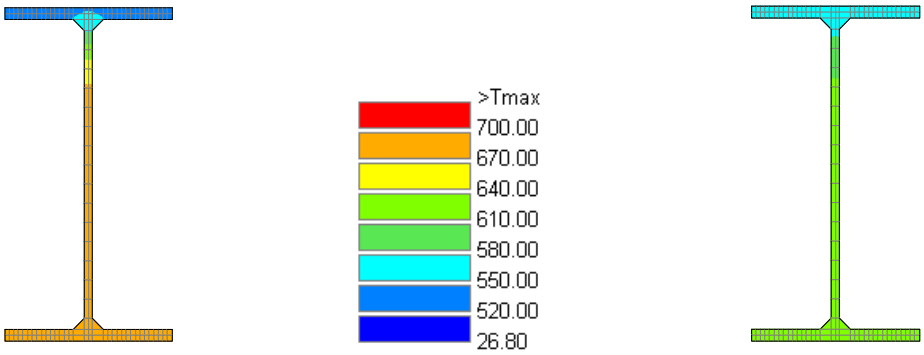

Figure 7-12 : Distribution of temperature in the beam profile after 45 minutes (left) and 60 minutes (right)

$T_{beam,aver.} = \frac{\sum_i A_i T_i}{\sum_i A_i}$	**7-12**
$w_{max,heating} = \frac{k_{y,T=T_{max}}}{1.1} = 0.315$	**7-13**

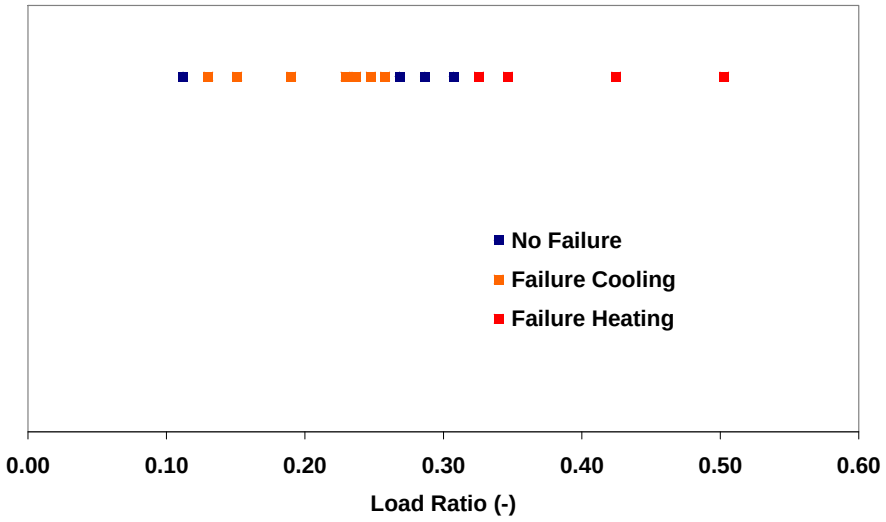

Figure 7-13 : Results of the numerical simulations with Nonlinear Fibres Model

7.6 Conclusions

The present chapter aimed at describing briefly the different steps of the fire design of a steel structure with a special focus on the behaviour of fin plate connections. This application refers to existing and new methods for the distribution of temperature in the joint zones and members. By modelling the action of fin plate connections with Nonlinear Fibres Model, the transient behaviour of the structure has been evaluated automatically by SAFIR software until collapse, without any need of a definition of failure criteria in the joints and detection of failures by the user. The results of these simulations are in agreement with the recommendations proposed on the basis of the parametric analyses performed with the Bilinear Fibres Model.

The geometrical and mechanical properties of the fin plate connections used in the present analysis are identical to the one designed for the eight first tests performed on isolated joints in Sheffield. The fact that the resistance of bolts in shear is the weakest component during the main part of the fire influences significantly and negatively the ductility of the joint during the heating and cooling phases. The occurrence of numerous connection failures during the cooling phase of the fire still underlines the necessity to include some ductility requirements into the design of simple connections under natural fire.

8 Personal contributions, general conclusions and perspectives for future researches

In collaboration with European research centres, investigations have recently been undertaken at the University of Liège on the behaviour of common steel connections subjected to natural fire. As mentioned within the present thesis, the contribution of the University of Liege does not include the realisation of experimental tests but is globally composed of the following tasks:

- the analysis and the post-treatment of experimental results performed on bolts, welds and sub-structures under fire conditions ;
- the creation of numerical models in SAFIR software for thermal and mechanical analyses and the realisation of parametric numerical investigations ;
- the development of simplified analytical methods calibrated on the results of experimental and numerical investigations, aimed at predicting the behaviour of simple connections under natural fire ;
- the definition of design recommendations for simple connections subjected to natural fire.

The present thesis briefly describes the experimental tests resulting from this collaborative project and other recent tests performed in Europe. It presents in detail the analytical and numerical developments realised by the author and an application of the new proposed method to a complete frame.

The personal contributions of the author to the enhancement of the understanding of the thermo-mechanical behaviour of simple connections under natural fire are highlighted in the present chapter. Then, the global conclusions of the present work are summarized. Some phenomena are not accounted for and all the configurations are not covered by this work. Modifications and improvements that should be developed in the future in order to account for phenomena neglected in this work and/or extend the applicability of the proposed methods to configurations that are still uncovered.

8.1 Personal contributions

The present work includes bibliographic studies, the presentation of experimental and analytical work carried out by other research centers and the complete description of the contributions of the author. The personal contributions of the author are listed hereafter.

- Numerical models for the prediction of temperature in 2D-beam sections and 3D-joint zones covered by a concrete flat slab

- Proposal of new simple methods for the prediction of temperature in 2D-beam sections and 3D-joint zones covered by a concrete slab and calibration of this method on the numerical results

- Validation of a model built in SAFIR against experimental tests performed at the University of Manchester for the prediction of deflections and internal forces in axially and rotationally-restrained beams under fire conditions.

- Adaptations to the simplified method developed by Yin and Li for predicting bending moments profiles in axially and rotationally-restrained beams during heating and cooling phases of a fire and extension to joints with a bilinear moment-rotation diagram

- Treatment of the results of the tests performed on bolts and welds under natural fire conditions

- Development of analytical models for bolts (in tension or in shear) and welds during the heating and cooling phases of a fire.

- Definition of new material laws and of two models for modelling the action of simple steel connections under natural fire conditions

- Definition of failure criteria for the Bilinear Fibres Models and validation of these models against results of experimental tests and against numerical simulations performed with complex finite element models

- Realisation of parametric analyses using the Bilinear Fibres Models for fin plate, double web cleats and header plate connections aimed at detecting the parameters governing the risk of connection failures in steel structures; definition of design procedures to avoid these connection failures

- Development of Nonlinear Fibre Models for fin plate connections, validation against experimental results of isothermal tests performed on isolated joints (Sheffield) and of a fire test performed on a sub-structure (Delft)

- Application of the Nonlinear Fibre Models to a complete frame structure and comparison of the results to the design procedures proposed on the basis of parametric analyses performed with the Bilinear Fibres Model

8.2 General conclusions and main achievements

8.2.1 Numerical models for the prediction of temperature in 2D-beam sections and 3D-joints zones covered by a concrete flat slab

The prediction of the distribution of temperature in beams and joints according to the current methods of the Eurocodes are based on the Lumped Capacitance Method or extrapolated from the temperature of the beam bottom flange in the mid-span section. Thermal models have been built in SAFIR software in order to provide some reference results of temperature in beams and joints under natural fire. The thermal properties of steel and concrete are taken from the Eurocodes recommendations and the fire curves considered for these analyses are the parametric fire curves of the EN 1991-1-2 – Annex A. The comparison between the results obtained numerically and those predicted by the Lumped Capacitance Method has underlined the limitations and the sources of imprecision of this last analytical method. The results of these simulations have also been used to calibrate the new simple methods described in § 8.2.2 for the prediction of temperature in 2D-beam sections and 3D-joint zones under natural fire.

8.2.2 Proposal of new simple methods for the prediction of temperature in 2D-beam sections and 3D-joint zones covered by a concrete slab

The application of the Lumped Capacitance Method and the comparison with numerical results has shown that this method leads to a good prediction of temperature at the level of the bottom flange (2D and 3D cases). For the prediction of temperature at the level of the top flange, the accuracy of the Lumped Capacitance Method remains acceptable during a limited duration of the heating phase, mainly because the heat fluxes between the top flange and the concrete slab are not taken into consideration. Two different methods based on the Lumped Capacitance Method have been proposed and calibrated on the results obtained from numerical simulations to obtain better predictions of the temperature at the level of the top flange. The Composite Section Method consists in integrating a part of the concrete slab into the heated zone considered in the Lumped Capacitance Method. This first proposed method gives very good results during the heating phases but a long delay is observed before the cooling down of the top flange. This imprecision is due to the omission of the heat fluxes between the top flange and the rest of the steel section. The Heat Exchange Method considers separately the three heat fluxes between, on one side, the top flange and, on the other side, the hot gases, the other steel parts and the concrete slab. This second proposed method gives some very correlations with numerical results, at least for parametric fire curves from EN 1991-1-2 – Annex A.

8.2.3 Validation of a model built in SAFIR against experimental tests performed at the University of Manchester for the prediction of deflections and internal forces in axially and rotationally-restrained beams under fire conditions.

A series of experimental tests was performed at the University of Manchester on 'rugby goal post' sub-structures in order to investigate the effect of axial restraints on the eventual catenary action, which may prevent the beam from running away at elevated temperatures [Liu, 2002]. These tests have been simulated in SAFIR software in order to validate a numerical model able to reproduce the mechanical behaviour of restrained beams under natural fire. The creation of this numerical model is aimed at guiding the analytical investigations of the author for developing an existing simplified method predicting the deflections and internal forces induces by the combination of mechanical and thermal actions in axially and rotationally restrained beams (see § 8.2.4).

8.2.4 Adaptations to the simplified method developed by Yin and Li for predicting bending moments profiles in axially and rotationally-restrained beams during heating and cooling phases of a fire and extension to joints with a bilinear moment-rotation diagram

A simple method developed successively by Yin and Li is able to predict with reasonable accuracy the evolutions of axial force and vertical deflections in axially and rotationally-restrained steel beams during the heating and cooling phases of a natural fire. The author has contributed to add some modifications to this method in order to obtain good predictions of bending moment profile. The action of joints has been represented by a rotational spring with a bilinear force-displacement diagramme.

The objectives of the modifications proposed by the author are:

- Accounting for the elliptic branch of the stress-strain diagram for carbon steel at elevated temperatures in the evaluation of internal forces from beam deformations. For this, the prediction of the axial force has been adapted and an analytical method has been developed to obtain the moment-curvature diagram of a beam section subjected to an axial force and a non-uniform elevation of temperature.

- Evaluating the thermally-induced bending moments applied to the beam extremity by expressing the compatibility of rotations at the extremity of the beam and in the rotational spring. The bending resisting moment of joints has also been taken into consideration.

- Accounting for the variation of the beam axial stiffness as a function of mid-span vertical deflections.

- Deducing a new coefficient of interpolation for the deflection profile from the equation of equilibrium between the bending moment in extremity beam section and the rotational spring.

The influence of these modifications on the predictions of deflections and internal forces has been separately analysed and it is demonstrated that, except for the variation of the beam axial stiffness with mid-span deflections, all the modifications have a significant and favourable influence on the results predicted by this analytical method.

The modifications made to this method have yet induced a higher degree of complexity for its application while assumptions on the vertical deflection profile and the mechanical behaviour of joints are still necessary. Including completely the real behaviour of joints subjected to natural fire (M-N interaction, different and non-reversible reduction factors for bolts, welds and carbon steel components, contact between beam and column flanges in simple connections, influence of shear forces,…) is beyond practical reach. Finite element methods appear as more adapted tools for the resolution of such analyses and the development of the Modified Method has not been developed further.

8.2.5 Treatment of the results realised during the tests performed on bolts and welds under natural fire conditions

On the basis of tests performed on bolts and welds in the 90's [Latham, 1993 and Kirby, 1995], reduction factors for bolts and welds have been included in the Eurocodes. However, no recommendations are given for the cooling phase of a fire. Series of tests have recently been performed by the Centro Sviluppo Materiali on Grade 8.8 bolts and welded specimens in order to characterise the mechanical behaviour of bolts and welds under cooling. These tests are presented in this work and the experimental results have been pre-treated and treated by the author. The pre-treatment has consisted in evaluating the spurious displacements inherent to the testing procedures. The analysis of the tested specimens led to the elimination of the results given by 3 tensile tests performed on bolts. The welded specimens have not been made available and could not be inspected but the analysis of the test results nevertheless tends to demonstrate that specimens failed by insufficient resistance of the welds. After pre-treatment, test results are represented by force-displacement diagrams. The analysis of the experimental results shows that the loss of resistance of bolts and welded specimens during cooling reached respectively 40% and 20% of the resistance at the same temperature during heating. This loss of resistance is negligible below 500°C for bolts and below 600°C for welded specimens. An evolution of the shape of the force-displacement diagrams is observed when temperature exceeds 500°C: a yield plateau appears and the descending branch is reached after high deflections have developed.

8.2.6 Development of analytical models for bolts (in tension or in shear) and welds during the heating and cooling phases of a fire.

The non-reversible behaviour of bolts (in tension or shear) and welds has been quantified by a new coefficient k_{nr} depending on the temperature reached at the end of the cooling phase T_u and on the test temperature T_f. This coefficient has the same values for bolts in tension and in shear but is significantly lower for bolts than for welds. Analytical models, calibrated on the tests results, have been proposed to characterise the force-displacement relationships for Grade 8.8 bolts in tension or in shear. These models can be used into component-based models or finite element models representing the action of connections.

8.2.7 Definition of new material laws and of two models for modelling the action of simple connections under natural fire conditions

Bilinear Fibres Models and Nonlinear Fibres Models have been developed to represent the action of simple connections (fin plate, double web cleats and header plate connections) in steel structures under natural fire. These two models are based on the Component Method: the action of the joint is modelled by a beam finite element where the force-displacement relationship of each bolt row or compression row is represented by one fibre. The two models differ by the degree of complexity of the material laws allocated to the fibres. In the Bilinear Fibres Models, the behaviour of the fibres are elastic-plastic. Different laws have been defined for rows working only in tension, rows working only in compression and rows working symmetrically or asymmetrically in tension and compression. In the Nonlinear Fibres Models, the material laws allocated to bolt rows are not symmetric and contain an elastic branch, an elliptic branch, a yield plateau and a descending branch in the two domains. The definition of the parameters for Nonlinear Fibres Models is more time-consuming than for Bilinear Fibres Models but the descending branch allows considering more accurately and automatically the real ductility of connections. For large-scale structures with a unique type of connection, the time used to build a component-based model (Bilinear of Nonlinear) is rapidly counter-balanced by a large reduction of the time for the simulation compared to complex finite element models based on solid and contact elements.

8.2.8 Definition of failure criteria for the Bilinear Fibres Models and validation of these models against results of experimental tests and against numerical simulations performed with complex finite element models

Bilinear Fibres Models do not allow an automatic detection of the connections failures (bolts, welds and carbon steel components). Consequently, some failure criteria have been defined by the author to judge whether a connection failure occurs or not. When a connection failure is obtained by such a

failure criterion, the rest of the simulation is considered as meaningless and the post-failure behaviour of the structure can not be analysed. However, the failure of one row usually corresponds to the initiation of the global connection failure and it is not certain that the complete structure could survive this complete failure of the connection.

The definition of failure criteria is based on the concept of classes of ductility for bolt rows and on the number of yielded fibres representing the action of bolt rows. The classes of ductility of a bolt row depend on the comparison between, on one side, the resistance of the weakest brittle component (bolts, welds components) of the bolt rows and, on the other side, the plastic and ultimate resistance of the weakest ductile component (other components) of the bolt row. The class of ductility of one bolt row varies during the fire due to the different reduction factors for bolt, weld and carbon steel components. The class of ductility of the connection is linked to the class of ductility of all bolt rows and influences the number of yielded fibres for which the connection failure is observed by the failure criterion.

Two fire tests performed recently by Efectis Netherlands, in Delft, on two steel sub-structures with fin plate connections and web cleats connections [Efectis NL, 2009] have been modelled by use of the developed Bilinear Fibres Models. In the first test, bolts of the fin plate connection failed during the cooling phase (after 127 minutes) and the numerical model led to a good correlation with experimental results and observations. In the second test, no failure occurred in the double web cleats connections and the numerical simulation of this test is in agreement with this. The Bilinear Fibre Models for fin plate connections, double web cleats connections and header plate connections have been validated by comparisons of the results obtained for parametric analyses with numerical simulations performed by research centers in more complex 3-D finite element models of joints with contact and solid elements (Abaqus models by Corus and Ansys models by CTICM). The correlation between the results given by the component-based models (SAFIR) and complex finite element models (Abaqus and Ansys) shows a good agreement in terms of time-deflection evolutions. Failure criteria appear to give good predictions of connection failures and to be a safe approach.

8.2.9 Realisation of parametric analyses using the Bilinear Fibres Models for fin plate, double web cleats and header plate connections aimed at detecting the parameters governing the risk of connection failures in steel structures and definition of design procedures to avoid these connection failures

The influence of vertical loading, level of axial restraints and fire loading on the occurrence of connection failure has been analysed using the Bilinear Fibres Models. During the heating phase, the rotational stiffness of joints causes a redistribution of bending moments in the beam and hogging bending moments are transferred by simple connections. Consequently, the fire resistance of the beam is increased while joints are subjected to a combination of axial forces, shear forces and bending

moments that the connections have usually not been designed for. When these internal forces induce the yielding of components in bolt and/or compression rows, the failure will occur if the yielded component has not a sufficient ductility to allow a redistribution of internal forces. The rotational stiffness of header plate connections and fin plate connections is higher than the rotational stiffness of double web cleats connections, which induces higher internal forces in the joint section. This reduces the risk of insufficient capacity of the beam but increases the risk of connection failures during the heating phase. In addition, bolts have two shear planes in double web cleats instead of one in fin plate connections so that the ductility of the first type of connections is lower than the ductility of the latter one.

During the cooling phase, connection failure may occur under low vertical loading, high axial restraints and if high temperatures have been reached at the end of the heating phase. When high temperatures are reached at the end of the heating phase, i) large plastic strains develop in the beam and large tensile thrusts develop during the cooling phase and ii) the non-reversible behaviour of bolts and welds components implies a reduction of the ductility of the connection.

On the basis of these observations, a simple procedure has been proposed in order to predict if the failure of simple connections, satisfying to the Eurocode recommendations for the design of connections at room temperature, may occur under a natural fire. Obviously, the concept of class of ductility is crucial but this procedure also accounts for other parameters like the type of connection, the maximal temperature of the bottom beam flange under the natural fire considered, the level of axial restraints and the load ratio.

8.2.10 Development of a Nonlinear Fibres Model for fin plate connections, validation of this model against experimental results of isothermal tests performed on isolated joints (Sheffield) and of a fire test performed on a sub-structure (Delft)

The Nonlinear Fibres Models necessitate a time-consuming building of the model for the designer. In the present work, these types of models have only been applied to fin-plate connections. The force-displacement diagrams of bolt rows at various temperatures have been obtained by combination of the individual diagrams of three components: the “beam web in bearing”, “bolts in shear” and “fin plate in bearing” components. A part of the tests realised recently at the University of Sheffield [Yu, 2009c] at constant temperature (from 20°C to 650°C) have been modelled and have validated the use of Nonlinear Fibres Models for the prediction of failures in fin-plate connections. The test performed in Delft on a steel sub-structure with fin plate connections has also been modelled with the Nonlinear Fibres Models and the failure predicted numerically has a very good correspondance with experimental observations.

8.2.11 Application of the Nonlinear Fibres Models to a complete frame and comparison of the results with the design procedures proposed on the basis of parametric analyses performed with the Bilinear Fibres Model

The different models developed for representing the action of simple connections in a steel structure exposed to fire are presented in Chapters 2 to 6. In Chapter 7, these concepts are applied to a complete steel structure with fin plate connections modelled by 2-D beam elements for columns and beams as well as for the semi-rigid connections. A compartment of the building has been subjected to a parametric fire curve evaluated on the basis of the Annex A of EN 1991-1-2 [CEN, 2002a]. The distribution of temperature in beams and joints is realised by use of the developed analytical methods. In the structural analysis, a Nonlinear Fibres Model has been build to represent the action of fin-plate connections. The structure has been subjected to a large variety of uniform vertical loadings. The influence of the load ratio on the occurrence of beam and connection failures has confirmed the validity of the design procedure proposed on the basis of the results rising from parametric analyses performed with Bilinear Fibres Model.

8.3 Perspectives

8.3.1 Validation of the new methods aimed at predicting the distribution of temperature in steel beams and joints covered by a concrete slab against experimental results

The validation of the Composite Section Method and the Heat Exchanges Method for predicting the distribution of temperature in steel beams and joints covered by a flat concrete slab has been realised by comparing the results given by these two analytical methods to temperatures predicted by 2-D (beam) and 3-D (joint) numerical simulations performed in SAFIR software. The complete validation of these methods for the fields of application mentioned in Chapter 2 would also require a comparison with experimental results. Such experimental results are difficult to realise because boundary condition are often non-uniform, especially in the joint zones, because the majority of existing tests performed on joints are not focused on the cooling phase and/or because the test configurations do not reproduce the real exposure or boundary conditions (tests performed on isolated joints, concrete slab substituted by insulating material, etc). For tests realised recently in Metz and Delft Fire Laboratories, the heating of the tested structure is very slow and the difference of temperature between the gases and the structure is not important.

The contact between the steel beam and the concrete slab, supposed to be perfect in the numerical simulations and in the analytical evaluation of the heat flux between the beam top flange and the concrete slab, should be analysed for real applications with flat concrete slabs or composite slabs (steel corrugated sheets covered by concrete). An over-estimation of the contact between steel beams and concrete slabs may lead to an unsafe prediction of temperature at the level of the beam top flange.

The prediction of the distribution of temperature in thermally-protected steel beams and joints has not been considered within the present thesis. The risk of connection failures in protected configurations has been analysed by considering very slow fire curves. It should be verified that the Composite Section Method and the Heat Exchange Method could be extended to protected configurations by substituting the general equation of the Lumped Capacitance Method for unprotected members into the general equation of the Lumped Capacitance Method for protected members.

In the Composite Section Method, the relationship between the height of concrete slab integrated into the "Heated zone" should be function of the speed of heating of the gases and the presence of thermal protection.

8.3.2 Analysis of the reversibility of deformations in carbon steel elements subjected to a heating-cooling cycle

In the Metz test n°2 (flush end-plate connection, T_{max} = 700°C) and in the test of Delft n°2 (double web cleat connections), the vertical deflections of the beam during the cooling phase are under-estimated by the numerical models. In the two tests, the connections have not failed under the heating and cooling phases and the vertical deflections remain approximately constant during the cooling phase although the beam (and the connections) recover, partially or completely, their stiffness. This tends to show that the behaviour of carbon steel member is not reversible in terms of stiffness after such heating-cooling cycles. This aspect should be investigated in detail because plastic deformations have a significant influence on the distribution of internal forces in an axially and rotationally-restrained beam (and, by consequent, in joints) subjected to natural fire.

8.3.3 Integration of group effects, of instability phenomena in beam flanges and of the interaction of shear forces with axial forces and bending moments on the resistance of simple connections into numerical models

The Bilinear Fibres Model and Nonlinear Fibre Model developed to represent the action of simple connections are based on several assumptions. Group effects and the interaction of shear forces with axial forces and bending moments on the resistance and the stiffness of the connections can not be taken into account automatically in these two component-based models. In the present work, these

phenomena are neglected when their influence on the results is limited and considered by use of safe approximations otherwise. This problem is also encountered for component-based models at room temperature. The instability of beams flanges, often observed during the experimental tests should be considered. The allocation of a material law with a descending branch to the fibres representing the transfer of compressive forces at the level of beam flanges is a solution to investigate.

8.3.4 Definition of an adimensional beam element for representing the action of joints following the Component Method

In the present work, the elements representing the action of joints are fibre finite elements with a finite length and two Gauss nodes. The material laws allocated to the fibres are defined under stress-strain diagrams adapted to the cross-section area and the element length in order to obtain the correct force-displacement diagram for each fibre. In SAFIR, stresses are expressed under the Piola-Kirchhoff form. As the length of the joint elements is quite small, the ratio between the initial and final lengths of the element can be significantly different from 1 and the resistance of the fibres in the deformed configuration can be significantly different from the one in the intial configuration.

One solution to this problem would be the definition of a new type of fibre element that has no dimension and where force-displacement diagrams are directly allocated to the fibres representing the action of bolt rows and compressive rows. This new type of element would also avoid to obtain two different distributions of internal forces in the two Gauss nodes of one joint element, as in the case with beam elements.

8.3.5 Extension of this work to composite joints

The Component Method also applies to composite joints and the experimental tests performed in Delft have been accompanied by four tests on composite sub-structures with fin plate, web cleats, header plate and extended end-plate connections. The present work focused on steel sub-structures should be continued to analyse the behaviour of simple composite connections under natural fire condition. A special attention should be paid to the definition of the collaborating width in beam and joint sections because of the development of large compressive and tensile forces under fire conditions. The reversibily of the mechanical properties of concrete after heating-cooling cycles should also be investigated.

9 References

Abaqus (2009) "Abaqus User's Manual, version 6.6", Providence, RI, USA, 2009

Al-Jabri K.S. (1999) "The behaviour of steel and composite beam-to-column connections in fire", K.S. Al-Jabri, PhD Thesis, Department of Civil and Structural Engineering, University of Sheffield, 2000.

Al-Jabri K.S. (2004) "Component-based model of the behaviour of flexible end-plate connections at elevated temperature", Composite Structures, Vol. 66, pp. 215-221, 2004

Anderson D. (1999) "Composite steel-concrete joints in frames for buildings: Design provisions". COST C1 – semi-rigid behaviour of civil engineering structural connections, Luxembourg, 1999.

Anderson K. (2009) "Investigation into Methods for Predicting Connection Temperatures", K. Anderson, M. Gillie, Czech Technical University Publishing House, Acta Polytechnica Vol. 49 No. 1, 2009.

Ang K.M. (1984) "Analysis of 3-Dimensional Frames with Flexible Beam-Column Connections", K.M. Ang and G.A. Morris, Canadian Journal of Civil Engineering, Vol. 11, pp. 245-254, 1984.

Atamaz Sibai W. (1993) "New Semi-Rigid Joint elements for non-linear analysis of flexibly connected frames", W. Atamaz Sibai and F. Frey, Journal of Constructional Steel Research, Volume 25, pp. 185-199, 1993.

Bailey C.G. (1996) "Analysis of the effects of cooling and fire spread on steel-framed buildings", C.G. Bailey, I.W. Burgess, R. Plank, Fire Safety Journal, Vol. 26, pp. 273-293, 1996.

Bailey C.G. (1999) "Design of steel framed buildings without applied fire protection", C.G. Bailey, G.M. Newman, W.I. Simms. The Steel Construction Institute P197, 1999.

Bailey C.G. (2000) "The tensile membrane action of unrestrained composite slabs simulated under fire conditions", C.G. Bailey, D.S White and D.B. Moore. Engineering Structures, Vol. 22, Issue 12, pp 1583-1595, December 2000.

Bailey C.G. (2000) "The structural behaviour of steel frames with composite floors slabs subject to fire – Part 1 Theory", C.G. Bailey, D.B. Moore, Structural Engineering, Vol. 78(11), pp. 19-27, 2000.

Bailey C.G. (2004) "Structure fire design: Core or specialist subject?", C.G. Bailey, The Structural Engineer, Vol. 32, May 2004.

Bažant Z.P. (1996) "Concrete at High Temperatures: Material Properties and mathematical Models", Z.P. Bažant and M.F. Kaplan, Longman Group Ltd, Essex, England, 1996.

Bayo E. (2006) "An effective component-based method to model semi-rigid connections for global analysis of steel and composite structures", E. Bayo, J.M. Cabrero and B. Gil, Engineering Structures, Vol. 28, pp. 97-108, 2006.

Beg, D. (2004) "On the rotation capacity of moment connections", D. Beg, E. Zupančič and I. Vayas, Journal of Constructional Steel Research, Vol. 60, pp. 601-620, 2004.

Block F.M. (2006) "Development of a Component-based Finite Element for Steel Beam-to-Column Connections at Elevated Temperatures", F.M. Block, Department of Civil and Structural Engineering, University of Sheffield, December 2006.

Block F.M. (2007) "Development of a component-based finite element for steel beam-to-column connectionelement for end-plate connections in fire", F.M. Block, I.W. Burgess, J.B. Davison, R.J. Plank, Fire Safety Journal, Vol. 42, pp. 498-506, 2007.

Blundell R. (1976) "The Properties of Concrete Subjected to Elevated Temperatures", R. Blundell, C. Diamond and R.G. Browne, Technical Note No 9, CIRIA Inderwater Engineering Group, London, UK, 1976.

B.S. (1982) "The performance of beam-to-column and beam-to-beam connections in the BS476: 8 fire tests", British Steel, Reports T/RS/1380/33/82D and T/RS/1380/34/82D, 1982.

B.S. (1990) "Fire resistance of steel structures, modern fire protection systems and design methods", British Steel General Steel, 1990.

Buchanan A. (1999) "Structural Design for Fire", A. Buchanan, University of Canterbury, New Zealand, 1999.

Browne R.D. (1972) "Concrete", R.D. Browne, Vol. 6, No 11, 1972.

Cadorin J.-F. (2003) "Compartment Fire Models for Structural Engineering", J.-F. Cadorin, PhD Thesis, Faculty of Applied Sciences, University of Liège, 2003.

CEC (1999) "Competitive Steel Buildings through Natural Fire Safety Concept", CEC Agreement 7210-SA/125/126/213/214/323/423/522/623/839/937, Final Report, Profil ARBED Research, March 1999.

CEN (1995), ENV 1993-1-2 – Eurocode 3 "Design of steel structures" – Part 1-2: Structural fire design, European Committee for Standardization, Brussels, 1995.

CEN (2002a), EN 1991-1-2 – Eurocode 1 "Actions on structures – Part 1-2: General actions – Actions on structures exposed to fire", European Committee for Standardization, Brussels, November 2002.

CEN (2002b), EN 1990 – Eurocode – Basis of structural design, European Committee for Standardization, Brussels, April 2002.

CEN (2004a), EN 1993-1-2 – Eurocode 3 "Design of steel structures" – Part 1-2: Structural fire design, European Committee for Standardization, Brussels, June 2004.

CEN (2004b), EN 1994-1-1 – Eurocode 4 "Design of composite steel and concrete structures" – Part 1-1: General rules and rules for building, European Committee for Standardization, Brussels, November 2004.

CEN (2004c), EN 1992-1-2 – Eurocode 2 "Design of concrete structures – Part 1-2: General rules - Structural fire design", European Committee for Standardization, Brussels, December 2004.

CEN (2005a), EN 1993-1-8 – Eurocode 3 "Design of steel structures" – Part 1-8: Design of joints, European Committee for Standardization, Brussels, May 2005.

CEN (2005b), EN 1994-1-2 – Eurocode 4 "Design of composite steel and composite structures" – Part 1-2: General rules – Structural fire design, European Committee for Standardization, Brussels, August 2005.

Cerfontaine F. (2004) "Etude de l'interaction entre moment de flexion et effort normal dans les assemblages boulonnés" F. Cerfontaine, PhD Thesis (in French), Faculty of Applied Sciences, University of Liège, 2004.

CoP : www.connectionprogram.com

Corus "Welding", www.corusconstruction.com, Architectural Teaching Resources.

Dai X. (2007) "Temperature Distribution in Unprotected Steel Connections in Fire", X. Dai, Y.C. Wang, C. Bailey, Proceedings of the Third International Conference on Steel and Composite Structures, Manchester, UK, 2007.

De Lima L.R.O. (2004) "Behaviour of extended end-plate beam-to-column joints subjected to bending and axial force", L.R.O. De Lima, L. Simões da Silva, P.C.G. Da S. Vellasco and S.A.L. De Andrade, Engineering Structures, Vol. 26, pp. 1333-1347, 2004.

Demonceau J.-F. (2008) "Steel and composite building frames: sway response under conventional loading and development of membrane effects in beams further to an exceptional action". PhD Thesis, Faculty of Applied Sciences, University of Liège, 2008**.**

Dotreppe J.-C. (1983) "Résistance au feu des structures – Principes généraux et recommandations à l'usage des auteurs de projets", Commission Nationale Belge de Recherche Incendie, 1983

ECSC (1988) "Practical design tools for composite steel-concrete construction elements submitted to ISO-fire considering the interaction between axial load N and bending moment M", Final report, European Coal and Steel Community, Contract ECSC 7210 SA 504, 1988.

ECSC (1995a) "Fire resistance of composite concrete slabs with profiled steel sheet and of composite steel concrete beams", Final report, European Coal and Steel Community, Contract ECSC 7210 SA 509, July 1995.

ECSC (1995b) "Buckling curves of hot rolled H steel sections submitted to fire Fire resistance of composite concrete slabs with profiled steel sheet and of composite steel concrete beams", Final report, European Coal and Steel Community, Contract ECSC 7210 SA 316/515/931/618, 1995

ECSC (1999) "Behaviour of a multi-storey steel framed building subjected to fire", Final report, European Coal and Steel Community, Contract ECSC 7215 CA 306, December 1999.

ECSC (2000) "Demonstration of real fires in car parks and high buildings", Final report, European Coal and Steel Community, Contract PP 025, December 2000.

Efectis France (2007a) "Résistance au feu des elements de construction – Note de Laboratoire n° 07-U-077", Efectis France, Mars 2007.

Efectis France (2007b) "Résistance au feu des elements de construction – Note de Laboratoire n° 07-U-087", Efectis France, Mars 2007.

Efectis NL (2009) "Test Report COSSFIRE WP3 fire tests", Efectis Nederland Report 2009-Efectis-R0609, A.J. Breunese and C. Both, June 2009.

El-Houssieny O.M. (1998) "Behavior of Extended End plate Connections at High Temperature", O.M. El-Houssieny, S. Abdel Salam, G.A.M. Attia and A.M. Saad, Journal of Constructional Steel Research, Vol. 46, Issues 1-3, pp. 299, Paper no 172, 1998.

El-Rimawi J.A. (1996) "The treatment of Strain Reversal in Structural Members During the Cooling Phase of a Fire", J.A. El-Rimawi, I.W. Burgess and R.J. Plank, Journal of Constructional Steel Research, Vol. 37, Issue 2, pp.115-135, 1996.

El-Rimawi J.A. (1997) "The influence of connection stiffness on the behaviour of steel beams in fire", J.A. El-Rimawi, I.W. Burgess and R.J. Plank, Journal of Constructional Steel Research, Vol. 43, Issue 1, pp.1-15, 1997.

Ferrario, F. (2004) "Analysis and modelling of the seismic behaviour of high ductility steel-concrete composite structures"**,** PhD Thesis, University of Trento, February 2004.

Finet L. (1994) "Influence de l'effort normal sur le calcul des assemblages semi-rigides", Diploma Work (in French), CUST, Clermont-Ferrand, 1994.

Franssen J.-M. (1990) "The Unloading of Building Material", J.-M. Franssen, Fire Safety Journal, Volume 16, pp. 213-227, 1990.

Franssen J.-M. (2003) "SAFIR A Thermal/Structural Program Modelling Structures under Fire", J.-M. Franssen, Proceedings NASCC 2003, A.I.S.C. Inc., Baltimore, 2003.

Franssen J.-M. (2004) "Numerical determination of 3D temperature fields in steel joints", J.-M. Franssen, Fire and Materials, Vol. 28, No 2, pp. 63-82, 2004.

Franssen J.-M. (2005) "SAFIR A Thermal/Structural Program Modelling Structures under Fire", J.-M. Franssen, Engineering Journal, A.I.S.C., Vol. 42, No. 3, pp. 143-158, 2005.

Franssen J.-M. (2009) "Designing steel structures in Fire", J.-M. Franssen, R. Zaharia and V. Kodur, Taylor & Francis Group, London, UK, 2009.

Girão Coelho A.M. (2001) "A ductility model for steel connections", A.M. Girão Coelho and L. Simões da Silva, Journal of Constructional Steel Research, Vol. 57, pp. 1169-1195, 2001.

Girão Coelho A.M. (2004) "Ductility analysis of end plate beam-to-column joints", A.M. Girão Coelho, L. Simões da Silva and F.S.K. Bijlaard, Proceedings of the 4th European Conference on Steel and Composite Structures, Maastricht, The Netherlands, 2005.

Gonzalez F. (2008) "Material Behaviour of high strength Grade 10.9 bolts under fire conditions", F. Gonzalez and J. Lange, 5th European Conference on Steel and Composite Structures, Graz, Austria, September 2008.

Guisse S. (1997) "Application of the component method to column bases. Experimentation and development of a mechanical model for characterization", S. Guisse, D. Vandegans and J.-P. Jaspart, CRIF Report, MT 295, CRIF, Liège, 1997.

Haller M. (2006) "Development of a method to calculate the temperature of a column exposed to localized fire, according to the EC1 and EC3 fire parts", M. Haller, A. Kay and L.-G. Cajot, Proceedings of the Fourth International Workshop Structures in Fire, Aveiro, 2006.

Hasemi Y. (1995) "Numerical Analysis of structures exposed to localized fire", A. Ptchelinstev, Y. Hasemi, M. Nikolaenko, ASIAFLAM's 95, 1995.

Henriques J.A.G. (2007) "Ductility requirements in shear bolted connections", Master Thesis, Universidade de Coimbra, 2007.

Hermann J. (1997) "Méthodes simplifiées de calcul des assemblages en acier entre profilés reconstitués par soudage", Diploma Work (in French), University of Liège, 1997.

Hoffmann J.-P. (1993) "Eurocode 3 - Calcul des assemblages de portiques rigides faits de profilés reconstitués soudés", Diploma Work (in French), CUST, Clermont-Ferrand, 1993.

Incropea F.P. (2005) "Fundamentals of Heat and Mass Transfer", F.P. Incropea, D.P. DeWitt, T.L. Bergma,, A.S. Lavine, John & Wiley Sons, Hoboken, USA, Sixth Edition, 2005.

Jaspart J.-P. (1991) "Etude de la semi-rigidité des noeuds poutre-colonne et son influence sur la résistance et la stabilité des ossatures en acier", PhD Thesis (in French), Faculty of Applied Sciences, University of Liège, 1991.

Jaspart J.-P. (1994), "Numerical simulation of a T-stub – Experimental Data", COST C1, Numerical Simulation Working Group, Doc C1WD6/94-09, 1994.

Jaspart J.-P. (1997), "Contributions to recent advances in the field of steel joints, column bases and further configurations for beam-to-column joints and beam splices", Aggregation Thesis, University of Liège, 1997.

Jaspart J.-P. (1999), "Recent advances in the field of structural steel joints and their representation in the building frame analysis and design process", Semi-rigid behaviour of civil engineering structural connections, COST C1, Jean-Pierre Jaspart, University of Liège, 1999.

Jaspart, J.-P. (2008) "European design recommendations for simple joints in steel structures", J.-P. Jaspart and J.-F. Demonceau, Journal of Constructional Steel Research, Vol. 64, pp. 822-832, 2008.

Karmalin V.V. (1989) "Load capacity and deformativity of bearing and friction-bearing connections", V.V. Karmalin and A.B. Pavlov, Proceedingd of the International Colloquium on Bolted and Special Structural Connections, Moscow, USSR, May 1989.

Kirby B.R. (1995) "The Behaviour of High-Strength Grade 8.8 Bolts in Fire", Journal of Constructional Steel Research, Vol. 33, pp 3-38, 1995.

Kirby B.R. (1998) "Behaviour of a multi-storey steel framed building subjected to fire attack, experimental data". Technical report, British Steel, 1998.

Kruppa J. (1976) "Résistance au feu des assemblages par boulons haute résistance", Centre Technique et Industriel pour la Construction Métallique, France, 1976.

Kumar S. "Welding and welded connections", S.R.S. Kumar and A.R.S. Kumar, Design of Steel Structures, Indian Institute of Technology Madras.

LaMalva K. J. (2009) "Failure Analysis of the WTC 5 Building", K.J. LaMalva, J.R. Barnett and D.O. Dusenberry, Journal of Fire Protection Engineering, Vol. 19, No 4, pp 261-274, 2009.

Latham D.J. (1993) "Elevated Temperature Behaviour of Welded Joints in Structural Steelwork", D.J. Latham and B.R. Kirby, Contract ECSC 7210 SA 824, November 1993.

Lapwood D.G. (1980) "The Effect of Fire Damage on the Mechanical Properties of Structural Steels Assessed Using Laboratory Heat Treatment Simulations", British Steel Report No. T/RS/1189/8/80/C.

Law R. (1997) "A Review of Formulae for T-Equivalent", R. Law, Proceedings of the Fifth International Symposium on Fire Safety Science, Australia, 1997.

Lawson R.M. (2001) "Fire engineering design of steel and composite buildings", Journal of Constructional Steel Research, Vol. 57, pp. 1233-1247, 2001.

Leston-Jones L.C. (1997) "The influence of semi-rigid connections on the performance of steel framed structures in fire", L.C. Leston-Jones, PhD Thesis, Department of Civil and Structural Engineering, University of Sheffield, 1997.

Li G.-Q. (2006) "Analysis of restrained heated steel beams during cooling phase", G.-Q. Li and S.-X. Guo, Proceedings of the Fourth International Workshop Structures In Fire, Aveiro, Portugal, May 2006**.**

Liew J. R. (2004) "Composite joints subject to reversal of loading – Part 2: analytical assessments", J.R. Liew, T.H. Teo and N.E. Shanmugam. Journal of Constructional Steel Research, Vol. 60, Issue 2, pp. 247-268, February 2004.

Liu T.C.H. (1996) "Finite element modelling of behaviour of steel beams and connections in fire", T.C.H. Liu. Journal of Constructional Steel Research 35(3), pp 181-199, 1996.

Liu T.C.H. (1998) "Effect of connection flexibility on fire resistance of steel beams" T.C.H. Liu, Journal of Constructional Steel Research 45(1), pp. 99-118, 1998.

Liu T.C.H. (1999a) "Fire resistance of unprotected steel beams with moment connections" T.C.H. Liu, Journal of Constructional Steel Research 51, pp. 61-77, 1999.

Liu T.C.H. (1999b) "Moment-rotation-temperature characteristics of steel/composite connections", T.C.H. Liu, Journal of Structural Engineering 125(10), pp. 1188-1197, 1999.

Liu T.C.H. (2002) "Experimental investigation of behaviour of axially restrained steel beams in fire", T.C.H. Liu, M.K. Fahad and J.M. Davies. Journal of Constructional Steel Research 58, pp. 1211-1230, 2002.

Lou G.B. (2006) "Nonlinear finite element modelling of behaviour of extended end-plate bolted moment connections in fire", G.B. Lou and G.Q. Li, Proceedings of the Fourth International Workshop "Structures in Fire", pp. 327-343, Aveiro, Portugal.

Olenick S.M. (2003) "An Updated International Survey of Computer Models for Fire and Smoke", S.M. Olenick and D.J. Carpenter, SFPE – Journal of Fire Protection Engineering, Vol. 13(2), pp. 87-110, 2003.

Pettersson O. (1976) "Fire Engineering Design of Structures", O. Pettersson, S.E. Magnusson, J. Thor, Swedish Institute of Steel Construction, Publication 50, Lund, Sweden, 1976.

Pietrapertosa, C. (2004) "Ductility requirements in shear bolted connections", C. Pietrapertosa, E. Piraprez and J.-P. Jaspart, ECCS/AISC Workshop: Connections in steel structures V: Behaviour, Strength and Design, Amsterdam, The Netherlands, June 3-4, pp. 335-345.

Poggi C. (1988) "A finite element model for the analysis of flexible connected steel frames", C. Poggi, International Journal for Numerical Methods in Engineering, Vol. 26, pp. 2239-2254, 1988.

Qian Z.-H. (2009) "Numerical and analytical investigations of steel beam-to-column joints at elevated temperatures", Z.-H. Qian, K.-H. Tan, I.W. Burgess, Journal of Constructional Steel Research, Vol. 65, pp. 1043-1054, 2009.

Ramli Sulong N.H. (2005), "Behaviour of steel connections at elevated temperatures", PhD Thesis, Imperial College, University of London, 2005.

Ramberg W. and Osgood W.R. (1943) "Description of Stress-Strain Curves by Three Parameters", National Advisory Committee for Aeronautics, Technical Report 902, Washington D.C., 1943.

Riaux H. (1980), "Comportement à l'incendie des assemblages simples boulonnés" (in French), PhD thesis, INSA of Rennes, 1980.

RFCS (2008) "Connections of Steel and Composite Structures under Natural Fire Conditions: Mid-term Report", Research Programme of the RFCS, Technical Report No3, RFSR-CT-2006-00028, B. Zhao et al., 2008.

Richard R.M. (1980) "The Analysis and Design of Single Plate Framing Connections", R.M. Richard, P.E. Gillett, J.D. Kriegh and B.A. Lewis, Engineering Journal, AISC, Vol. 17, Issue 2, 1980.

Santiago A. (2008a) "Numerical study of a steel sub-frame in fire", A. Santiago, L. Simões da Silva, P. Vila Real, M. Veljkovic, Computers and Structures, Vol. 86, pp. 1619-1632, 2008.

Santiago A. (2008b) "Experimental evaluation of the influence of connection typology on the behaviour of steel structures under fire", A. Santiago, L. Simões da Silva, P. Vila Real, A. Gameiro Lopes, G. Vaz, Engineering Journal, AISC, 2008.

Santiago A. (2008c) "Effect of Joint Typologies on the 3D Behaviour of a Steel Frame under a Natural Fire", A. Santiago, L. Simões da Silva, P. Vila Real, A. Gameiro Lopes, G. Vaz, Proceedings of the Fifth International Conference "Structures in Fire", pp. 205-216, Singapore, 2008.

Santiago A. (2008d) "Behaviour of beam-to-column steel joints under natural fire", PhD Thesis, Department of Civil Engineering, University of Coimbra, April 2008.

Sarraj M. (2006) "Finite element modelling on fin plate steel connections in fire", M. Sarraj, I.W. Burgess, J.B. Davison and R.J. Plank, Proceedings of the Fourth International Workshop "Structures in Fire", pp. 327-343, Aveiro, Portugal, 2006.

Sarraj. M. (2007) "The behaviour of Steel Fin Plate Connections in Fire", PhD Thesis, Department of Civil and Structural Engineering, University of Sheffield, 2007.

Schneider U. (1988) "Concrete at high temperatures: A general review", U. Schneider, Fire Safety Journal, 1988, Vol. 13, pp. 55-68.

SCI/BSCA (2002) "Joints in steel construction: Simple Connections", jointly published by The Steel Construction Institute & The British Constructional Steelwork Association, Publication P212, 2002**.**

Simões da Silva L. (2000) "Equivalent post-buckling models for the flexural behaviour of steel connections", L. Simões da Silva, A. Girão Coelho and E.L. Neto, Computers and Structures, Vol. 77, pp.615-624, 2000.

Simões da Silva L. (2001a) "A component model for the behaviour of steel joints at high temperatures", L. Simões da Silva, A. Santiago and P. Vila Real, Journal of Constructional Steel Research, Vol. 57, pp 1169-1195, 2001.

Simões da Silva L. (2001b) "An analytical evaluation of the response of steel joints under bending and axial force", L. Simões da Silva and A. Girão Coelho, Computers and Structures, Vol. 79, pp. 873-881, 2001.

Simões da Silva L. (2004) "Behaviour of flush end-plate beam-to-column joints under bending and axial force", L. Simões da Silva, L.R.O. De Lima, P.C.G. Da S. Vellasco and S.A.L. De Andrade, Steel and Composite Structures, Vol. 4, No 2, pp. 77-94, 2004.

Sokol Z. (2008) "Column Behaviour during Localised Fire Test", Z. Sokol, F. Wald, P. Kallerová and N. Bonnet, Proceedings of the Fifth International Conference Structure in Fire, pp. 24-31, Singapore, 2008.

Spyrou S. (2002) "Development of a component-based model of steel beam-to-column joints at elevated temperatures", PhD Thesis, Department of Civil and Structural Engineering, University of Sheffield, 2002.

Spyrou S. (2004a) "Experimental and analytical investigation of the 'compression zone' component within a steel joint at elevated temperatures", S. Spyrou, J.B. Davison, I.W. Burgess, R.J. Plank, Journal of Constructional Steel Research, Vol. 60, pp. 841-865, 2004.

Spyrou S. (2004b) "Experimental and analytical investigation of the 'tension zone' components within a steel joint at elevated temperatures", S. Spyrou, J.B. Davison, I.W. Burgess, R.J. Plank, Journal of Constructional Steel Research, Vol. 60, pp. 867-896, 2004.

Spyrou S. (2004c) "Experimental and analytical studies of steel joint components at high tempature", S. Spyrou, J.B. Davison, I.W. Burgess, R.J. Plank, Fire and Materials, Vol. 28, pp. 83-94, 2004.

Tschemmernegg F. (1988), "The Design of Structural Steel Frames under Consideration of the Nonlinear Behaviour of Joints", F. Tschemmernegg and C. Humer. Journal of Constructional Steel Research, Vol. 11, pp. 73-103, 1988.

Tschemmernegg F. (1994), "The Nonlinear Behavior of Composite Joints", F. Tschemmernegg, COST C1, Proceedings of the First State-of-the-Art Workshop, pp. 146-169, 1994.

Wainman D.E. (1995) "Summary of data obtained during tests on bolted beam-to-column and beam-to-beam connections", D.E. Wainman, BS476: Part 21 Fire Resistance Tests, British Steel plc, Report No SL/HED/R/S2442/2/95/C, October 1995.

Wald F. (2001) "Experiments with end-plate joints subjected to moment and normal forces", F. Wald and M. Švarc., Contribution to Experimental Investigation of Engineering Material and Structures, Czech Technical University Reports No 2-3, pp. 1-13, 2001.

Wald F. (2003) "Tensile membrane action and robustness of structural steel joints under natural fire", F. Wald, A. Santiago, M. Chladná, T. Lennon, I. Burgess and M. Beneš, Internal Report, Part 1 – Project of Measurements; Part 2 – Prediction; Part 3 – Measured data; Part 4 – Behaviour, BRE, Watford, 2003.

Wald F. (2005) "Calculation of fire resistance of structures", F. Wald et al., ISBN 80-0103157-8, Czech Technical University in Prague, p 336, 2005.

Wald F. (2006) "Experimental behaviour of steel structure under natural fire", F. Wald, L. Simões da Silva, D. Moore, T. Lennon, M. Chladná, A. Santiago, M. Beneš and L. Borges, New Steel Construction 13(3), pp. 24-27, 2006.

Wang Y. C. (1998) "Composite beams with partial fire protection", Y.C. Wang, Fire Safety Journal, Volume 30, Issue 4, pp. 315-332, June 1998.

Yin Y. Z. (2005a) "Analysis of catenary action in steel beams using a simplified hand calculation method, Part 1 : theory and validation for uniform temperature distribution", Y.Z. Yin and Y.C. Wang, Journal of Constructional Steel Research 61 (2005), pp. 183-211.

Yin Y. Z. (2005b) "Analysis of catenary action in steel beams using a simplified hand calculation method, Part 2 : theory and validation for non-uniform temperature distribution", Y.Z. Yin and Y.C. Wang, Journal of Constructional Steel Research 61 (2005), pp. 213-234.

Yu H. (2008) "Experimental Investigation of the Behaviour of Flush Endplate Connections in Fire", H. Yu, I.W. Burgess, J.B. Davison and R.J. Plank, Proceedings of the Fifth International Conference Structures in Fire, pp. 150-157, Singapore, 2008

Yu H. (2009a) "Tying capacity of web cleat connections in fire, Part 1: Test and finite element simulation", H. Yu, I.W. Burgess, J.B. Davison and R.J. Plank, Engineering Structures, Vol. 31, pp. 651-663, 2009.

Yu H. (2009b) "Tying capacity of web cleat connections in fire, Part 2: Development of component-based model", H. Yu, I.W. Burgess, J.B. Davison and R.J. Plank, Engineering Structures, Vol. 31, pp. 697-708, 2009.

Yu H. (2009c) "Experimental investigation of the behaviour of fin plate connections in fire", H. Yu, I.W. Burgess, J.B. Davison and R.J. Plank, Journal of Constructional Steel Research, Vol. 65, pp. 723-736, 2009.

Yu H. (2009d) "Development of a yield-line model for endplate connections in fire", H. Yu, I.W. Burgess, J.B. Davison and R.J. Plank, Journal of Constructional Steel Research, Vol. 65, pp. 1279-1289, 2009.

Zoldners N. (1971) "Thermal properties of concrete under sustained elevated temperatures", N.Z. Zoldners, Temperature and Concrete, ACI Special Publication No 25, Paper SP 25-1, American Concrete Institute, Detroit, pp 1-31, 1971.

Zoetemeijer P. (1983) "Summary of the Research on Bolted Beam-to-Column Connections period 1978 – 1983)", P. Zoetemeijer, Report No 6-85-M, Seven Laboratory, Delft, 1983.

10 Appendices

Appendix A Evaluation of the plastic bending moment of an I-section under axial force and non-uniform distribution of temperature

Six configurations have been identified for the evaluation of the plastic bending moment M_{pl} of an I-section under axial force F_T and non-uniform distribution of temperature. These configurations differ by the position of the neutral axis y_P under the non-uniform distribution of temperature, before and after application of the axial force F_T. The equations are developed here for cases where the top flange is colder than the bottom flange, under compressive forces and hogging bending moments. The adaptation to other cases is very simple.

Configuration 1

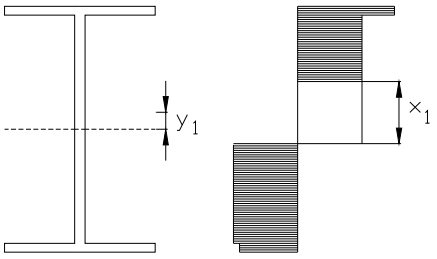

$$y_1 = \frac{b t_f \left(k_{y,1} - k_{y,3}\right)}{2 t_w k_{y,2}} \quad ; \quad x_1 = \frac{F_T}{t_w k_{y,2} f_y}$$

If $y_1 \le \frac{h}{2} - t_f + l_{rc}$ *and* $y_1 + \frac{x_1}{2} \le \frac{h}{2} - t_f + l_{rc}$ *, then*

$$M_{pl,1} = f_y k_{y,1} b t_f \left(\frac{h}{2} - \frac{t_f}{2} - y_1\right) + f_y k_{y,3} b t_f \left(\frac{h}{2} - \frac{t_f}{2} + y_1\right) + f_y k_{y,2} \left(\frac{h}{2} - t_f + y_1 - \frac{x_1}{2}\right) t_w \frac{1}{2} \left(\frac{h}{2} - t_f + y_1 + \frac{x_1}{2}\right)$$
$$+ f_y k_{y,2} \left(\frac{h}{2} - t_f - y_1 - \frac{x_1}{2}\right) t_w \frac{1}{2} \left(\frac{h}{2} - t_f - y_1 + \frac{x_1}{2}\right) + f_y k_{y,2} l_{rc} t_w \left(h - 2 t_f - \frac{2 r_c}{3}\right)$$

$$M_{th,pl,1} = F_T y_1$$

Configuration 2

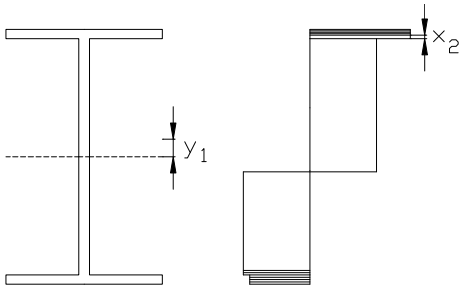

$$y_1 = \frac{b\,t_f\left(k_{y,1} - k_{y,3}\right)}{2\,t_w\,k_{y,2}} \quad ; \quad x_2 = \frac{\frac{F_T}{2} - f_y\,k_{y,2}\,t_w\left(\frac{h}{2} - t_f - y_1\right) - f_y\,k_{y,2}\,l_{rc}\,t_w}{t_w\,k_{y,1}\,f_y}$$

If $y_1 \le \frac{h}{2} - t_f + l_{rc}$, $y_1 + \frac{x_1}{2} > \frac{h}{2} - t_f + l_{rc}$ *and* $y_1 - \frac{x_1}{2} \ge -\frac{h}{2} + t_f - l_{rc}$, *then*

$$M_{pl,2} = f_y\,k_{y,1}\,b\left(t_f - x_2\right)\left(\frac{h}{2} - \frac{t_f}{2} - y_1 + \frac{x_2}{2}\right) + f_y\,k_{y,3}\,b\,t_f\left(\frac{h}{2} - \frac{t_f}{2} + y_1\right) + f_y\,k_{y,2}\left(\frac{h}{2} - t_f + y_1 - \frac{x_1}{2}\right)t_w\,\frac{1}{2}\left(\frac{h}{2} - t_f + y_1 + \frac{x_1}{2}\right)$$
$$+ f_y\,k_{y,2}\,l_{rc}\,t_w\left(\frac{h}{2} - t_f + y_1 - \frac{r_c}{3}\right)$$

$$M_{th,2} = f_y\,k_{y,2}\,\frac{x_1}{2}\,t_w\left(y_1 - \frac{x_1}{4}\right) + f_y\,k_{y,2}\left(\frac{h}{2} - t_f - y_1\right)t_w\,\frac{1}{2}\left(\frac{h}{2} - t_f + y_1\right) + f_y\,k_{y,1}\,b\,x_2\left(\frac{h}{2} - t_f + \frac{x_2}{2}\right) + f_y\,k_{y,2}\,l_{rc}\,t_w\left(\frac{h}{2} - t_f - \frac{r_c}{3}\right)$$

Configuration 3

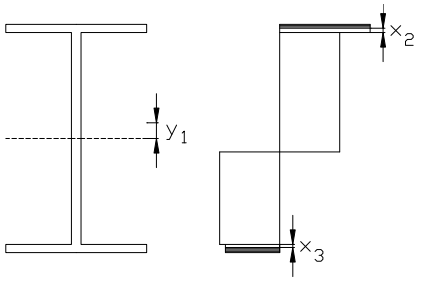

$$y_1 = \frac{b\,t_f\left(k_{y,1} - k_{y,3}\right)}{2\,t_w\,k_{y,2}} \quad ; \quad x_3 = \frac{\frac{F_T}{2} - f_y\,k_{y,2}\,t_w\left(\frac{h}{2} - t_f + y_1\right) - f_y\,k_{y,2}\,l_{rc}\,t_w}{t_w\,k_{y,1}\,f_y}$$

If $y_1 \le \frac{h}{2} - t_f + l_{rc}$, $y_1 + \frac{x_1}{2} > \frac{h}{2} - t_f + l_{rc}$ *and* $y_1 - \frac{x_1}{2} < -\frac{h}{2} + t_f - l_{rc}$, *then*

$$M_{pl,3} = f_y\,k_{y,1}\,b\left(t_f - x_2\right)\left(\frac{h}{2} - \frac{t_f}{2} - y_1 + \frac{x_2}{2}\right) + f_y\,k_{y,3}\,b\left(t_f - x_3\right)\left(\frac{h}{2} - \frac{t_f}{2} + y_1 - \frac{x_3}{2}\right)$$

$$M_{th,3} = f_y\,k_{y,1}\,b\,x_2\left(\frac{h}{2} - t_f + \frac{x_2}{2}\right) + f_y\,k_{y,3}\,b\,x_3\left(-\frac{h}{2} + t_f - \frac{x_3}{2}\right)$$

Configuration 4

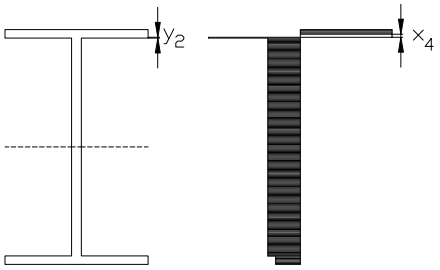

$$y_2 = \frac{b t_f \left(k_{y,1} + k_{y,3} - 2k_{y,2}\right) + A k_{y,2}}{2 t_w k_{y,1}} \quad ; \quad x_4 = \frac{F_T}{b k_{y,1} f_y}$$

If $y_1 > \frac{h}{2} - t_f + l_{rc}$ *and* $\frac{x_4}{2} \le y_2$ *, then*

$$M_{pl,4} = f_y k_{y,1} b\left(t_f - y_2 - \frac{x_4}{2}\right)\left(\frac{t_f}{2} - \frac{y_2}{2} + \frac{x_4}{4}\right) + f_y k_{y,1} b\left(y_2 - \frac{x_4}{2}\right)\left(\frac{y_2}{2} + \frac{x_4}{2}\right)$$
$$+ f_y k_{y,3} b t_f \left(h - \frac{3t_f}{2} + y_2\right) + f_y k_{y,2}\left(A - 2bt_f\right)\left(\frac{h}{2} - t_f + y_2\right)$$

$$M_{th,4} = F_T\left(\frac{h}{2} - \frac{t_f}{2} + y_2\right)$$

Configuration 5

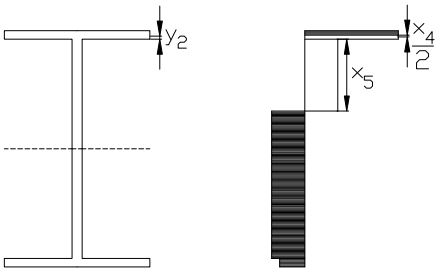

$$y_2 = \frac{b t_f \left(k_{y,1} + k_{y,3} - 2k_{y,2}\right) + A k_{y,2}}{2 t_w k_{y,1}} \quad ; \quad x_5 = \frac{F_T/2 - f_y k_{y,1} b y_2}{t_w k_{y,2} f_y}$$

If $y_1 > \frac{h}{2} - t_f + l_{rc}$, $\frac{x_4}{2} > y_2$ *and* $x_5 \le h - 2t_f + 2l_{rc}$, *then*

$$M_{pl,5} = f_y k_{y,1} b\left(t_f - y_2 - \frac{x_4}{2}\right)\left(\frac{t_f}{2} - \frac{y_2}{2} + \frac{x_4}{2}\right) + f_y k_{y,3} b t_f \left(h - \frac{3t_f}{2} + y_2\right)$$
$$+ f_y k_{y,2} t_w \left(h - 2t_f + 2l_{rc} - x_5\right)\left(y_2 + x_5 + \frac{1}{2}\left(h - 2t_f + 2l_{rc} - x_5\right)\right)$$

$$M_{th,5} = f_y k_{y,1} b\left(y_2 + \frac{x_4}{2}\right)\left(\frac{h}{2} - t_f + \frac{y_2}{2} + \frac{x_4}{4}\right) + f_y k_{y,2} t_w x_5 \left(\frac{h}{2} - t_f - \frac{x_5}{2}\right)$$

Configuration 6

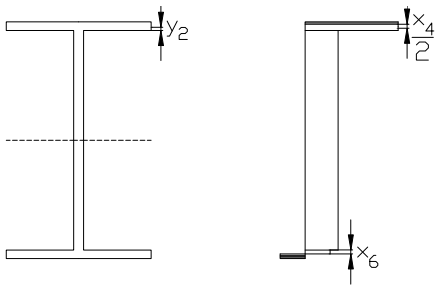

$$y_2 = \frac{b t_f \left(k_{y,1} + k_{y,3} - 2k_{y,2}\right) + A k_{y,2}}{2 t_w k_{y,1}} \quad ; \quad x_6 = \frac{F_T/2 - f_y k_{y,1} b y_2 - f_y k_{y,2} t_w \left(h - 2t_f - 2l_{rc}\right)}{b k_{y,3} f_y}$$

If $y_1 > \frac{h}{2} - t_f + l_{rc}$, $\frac{x_4}{2} > y_2$ *and* $x_5 > h - 2t_f + 2l_{rc}$, *then*

$$M_{pl,6} = f_y k_{y,1} b\left(t_f - y_2 - \frac{x_4}{2}\right)\left(\frac{t_f}{2} - \frac{y_2}{2} + \frac{x_4}{2}\right) + f_y k_{y,3} b\left(t_f - x_6\right)\left(h - \frac{3t_f}{2} + y_2 + \frac{x_6}{2}\right)$$

$$M_{th,6} = f_y k_{y,1} b\left(y_2 + \frac{x_4}{2}\right)\left(\frac{h}{2} - t_f + \frac{y_2}{2} + \frac{x_4}{4}\right) + f_y k_{y,3} b x_6\left(-\frac{h}{2} + t_f - \frac{x_6}{2}\right)$$

Appendix B Evaluation of the beam extensional stiffness of the beam as a function of the mid-span vertical deflection

The shape of the bending moment and axial force diagrams including second-order effects are given in Figure B-1. The terms of the virtual works equilibrium are developed hereafter.

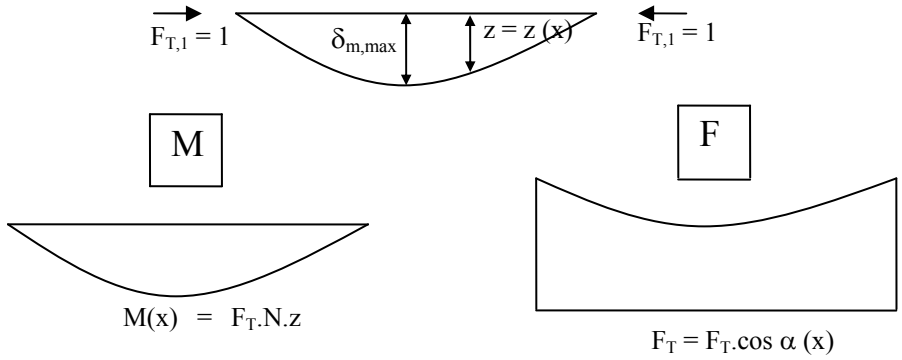

Figure B-1 : Bending moment and axial force accounting for second order effects

Simply-supported beams deflection profile

$$\int_0^L \frac{M.M_1}{EI}\,dx = \frac{1}{EI}\int_0^L \left(\frac{16\,\delta_{m,\max}}{5L}\right)^2 \left(\frac{x^4}{L^3} - \frac{2x^3}{L^2} + x\right)^2 dx$$

$$= \frac{1}{EI}\left(\frac{16\,\delta_{m,\max}}{5L}\right)^2 \int_0^L \left(\frac{x^8}{L^6} + \frac{4x^6}{L^4} + x^2 - \frac{4x^7}{L^5} - \frac{4x^4}{L^2} + \frac{2x^5}{L^3}\right) dx$$

$$= \frac{1}{EI}\left(\frac{16\,\delta_{m,\max}}{5L}\right)^2 \left[\frac{x^9}{9L^6} + \frac{4x^7}{7L^4} + \frac{x^3}{3} - \frac{4x^8}{8L^5} - \frac{4x^5}{5L^2} + \frac{2x^6}{6L^3}\right]_0^L$$

$$= \frac{1}{EI}\left(\frac{16\,\delta_{m,\max}}{5L}\right)^2 . L^3 . \left[\frac{1}{9} + \frac{4}{7} + \frac{1}{3} - \frac{4}{8} - \frac{4}{5} + \frac{2}{6}\right]$$

$$= \frac{3968\,.\,\delta_{m,\max}^2\,.L}{7875\,EI}$$

$$\int_0^L \frac{F_T.F_{T,1}}{EA}\,dx = \frac{1}{EA}\int_0^L \left(1-\left(\frac{16\,\delta_{m,\max}}{5L}\right)^2\left(\frac{4x^3}{L^3}-\frac{6x^2}{L^2}+1\right)^2\right)\,dx$$

$$= \frac{L}{EA} - \frac{1}{EA}\left(\frac{16\,\delta_{m,\max}}{5L}\right)^2 \int_0^L \left(\frac{16x^6}{L^6}+\frac{36x^4}{L^4}+1-\frac{48x^5}{L^5}-\frac{12x^2}{L^2}+\frac{8x^3}{L^3}\right)dx$$

$$= \frac{L}{EA} - \frac{1}{EA}\left(\frac{16\,\delta_{m,\max}}{5L}\right)^2 \left[\frac{16x^7}{7L^6}+\frac{36x^5}{5L^4}+x-\frac{48x^6}{6L^5}-\frac{12x^3}{3L^2}+\frac{8x^4}{4L^3}\right]_0^L$$

$$= \frac{L}{EA} - \frac{1}{EA}\left(\frac{16\,\delta_{m,\max}}{5L}\right)^2 . L . \left[\frac{16}{7}+\frac{36}{5}+1-\frac{48}{6}-\frac{12}{3}+\frac{8}{4}\right]$$

$$= \frac{L}{EA} - \frac{4352\,.\,\delta_{m,\max}^2}{875\,EA\,.L}$$

Finally,

$$\int_0^L \frac{M.M_1}{EI}\,dx + \int_0^L \frac{F_T.F_{T,1}}{EA}\,dx = \frac{L}{EA} + \frac{3968\,.\,\delta_{m,\max}^2\,.L}{7875\,EI} - \frac{4352\,.\,\delta_{m,\max}^2}{875\,EA.L}$$

Fully fixed beams deflection profile

$$\int_0^L \frac{M.M_1}{EI}\,dx = \frac{1}{EI}\int_0^L \left(\frac{16\,\delta_{m,\max}}{L^2}\right)^2\left(\frac{x^4}{L^2}-\frac{2x^3}{L}+x^2\right)^2\,dx$$

$$= \frac{1}{EI}\left(\frac{16\,\delta_{m,\max}}{L^2}\right)^2 \int_0^L \left(\frac{x^8}{L^4}+\frac{4x^6}{L^2}+x^4-\frac{4x^7}{L^3}-\frac{4x^5}{L}+\frac{2x^6}{L^2}\right)dx$$

$$= \frac{1}{EI}\left(\frac{16\,\delta_{m,\max}}{L^2}\right)^2 \left[\frac{x^9}{9L^4}+\frac{4x^7}{7L^2}+\frac{x^5}{5}-\frac{4x^8}{8L^3}-\frac{4x^6}{6L^2}+\frac{2x^7}{7L^2}\right]_0^L$$

$$= \frac{1}{EI}\left(\frac{16\,\delta_{m,\max}}{L^2}\right)^2 . L^5 . \left[\frac{1}{9}+\frac{4}{7}+\frac{1}{5}-\frac{4}{8}-\frac{4}{6}+7\right]$$

$$= \frac{128\,.\,\delta_{m,\max}^2\,.L}{315\,EI}$$

$$\int_0^L \frac{F_T.F_{T,1}}{EA}\,dx = \frac{1}{EA}\int_0^L \left(1-\left(\frac{16\,\delta_{m,\max}}{L^2}\right)^2\left(\frac{4x^3}{L^2}-\frac{6x^2}{L}+2x\right)^2\right)\,dx$$

$$= \frac{L}{EA} - \frac{1}{EA}\left(\frac{16\,\delta_{m,\max}}{L^2}\right)^2 \int_0^L \left(\frac{16x^6}{L^4}+\frac{36x^4}{L^2}+4x^2-\frac{48x^5}{L^3}+\frac{16x^4}{L^2}-\frac{24x^3}{L}\right)dx$$

$$= \frac{L}{EA} - \frac{1}{EA}\left(\frac{16\,\delta_{m,\max}}{L^2}\right)^2 \left[\frac{16x^7}{7L^4}+\frac{36x^5}{5L^2}+\frac{4x^3}{3}-\frac{48x^6}{6L^3}-\frac{16x^5}{5L^2}+\frac{24x^4}{4L}\right]_0^L$$

$$= \frac{L}{EA} - \frac{1}{EA}\left(\frac{16\,\delta_{m,\max}}{L^2}\right)^2 . L^3 . \left[\frac{16}{7}+\frac{36}{5}+\frac{4}{3}+\frac{16}{5}-8-6\right]$$

$$= \frac{L}{EA} - \frac{512\,.\,\delta_{m,\max}^2}{105\,EA\,.L}$$

Finally,

$$\int_0^L \frac{M.M_1}{EA}\,dx + \int_0^L \frac{F_T.F_{T,1}}{EA}\,dx = \frac{L}{EA} + \frac{128\,.\,\delta_{m,\max}^2\,.L}{315\,EI} - \frac{512\,.\,\delta_{m,\max}^2}{105\,EA\,.L}$$

Appendix C Time- beam deflection diagrams of the parametrical analyses : Fin plate connections

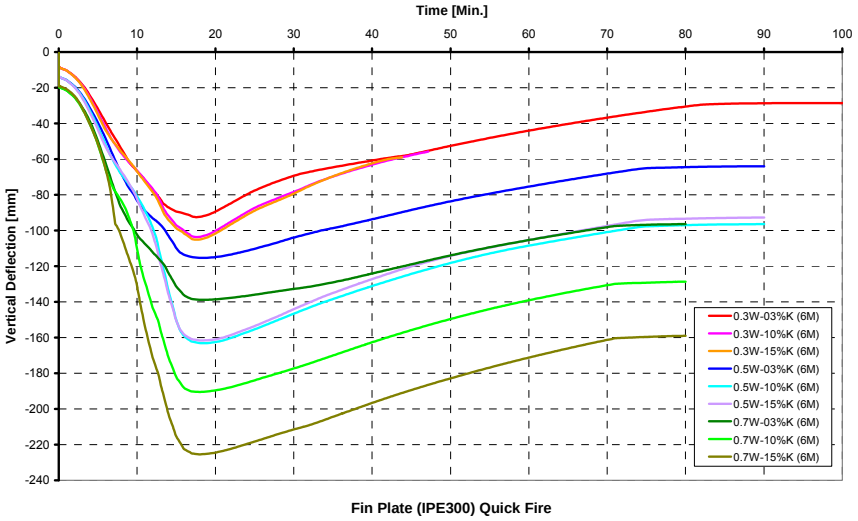

Figure C-1 : Vertical deflections of the 6-metre long IPE 300 beams under short-quick fire (Abaqus)

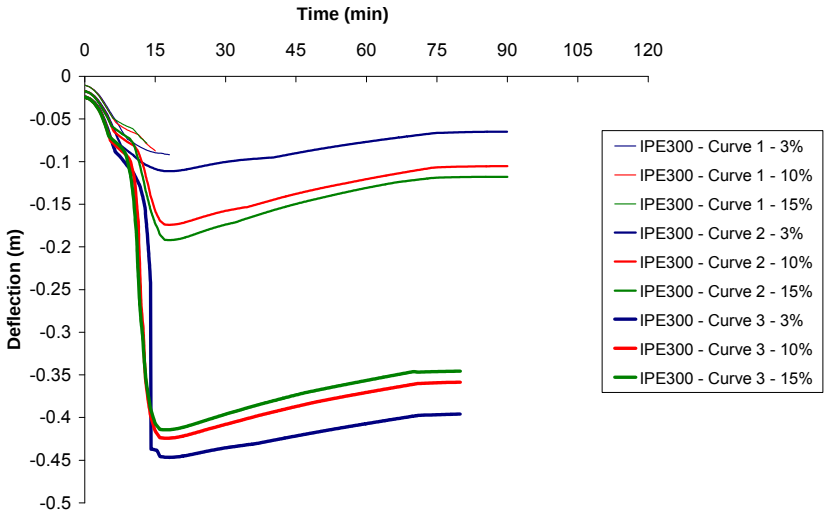

Figure C-2 : Vertical deflections of the 6-metre long IPE 300 beams under short-quick fire (SAFIR)

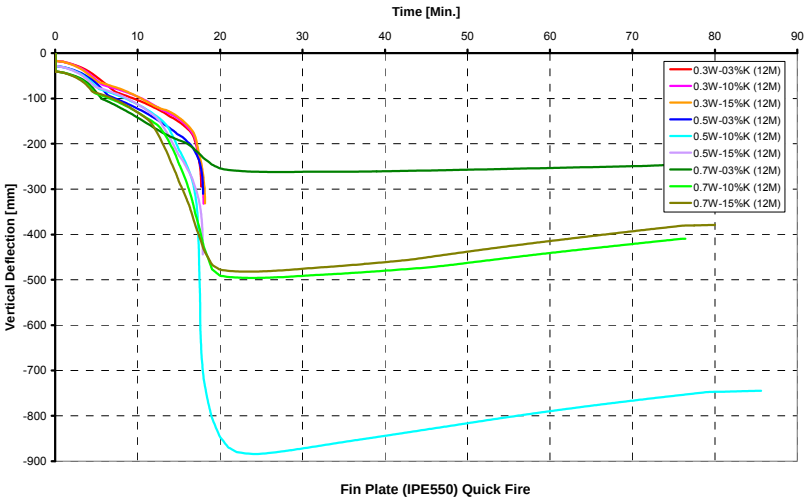

Figure C-3 : Vertical deflections of the 12-metre long IPE 550 beams under short-quick fire (Abaqus)

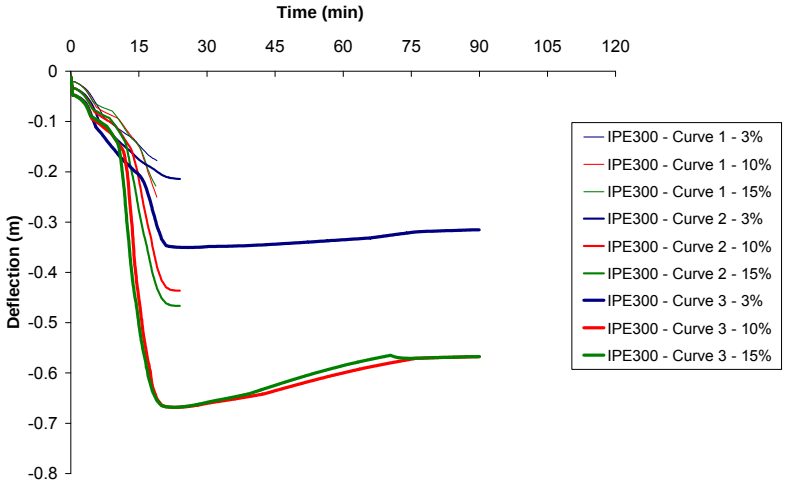

Figure C-4 : Vertical deflections of the 12-metre long IPE 550 beams under short-quick fire (SAFIR)

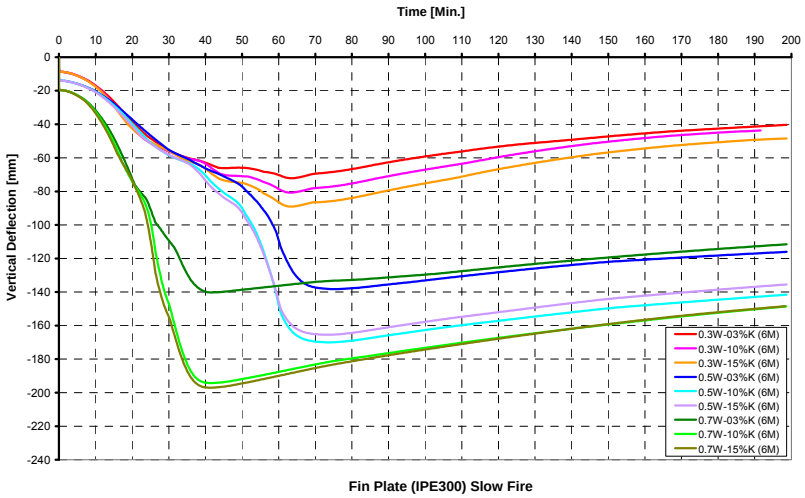

Figure C-5 : Vertical deflections of the 6-metre long IPE 300 beams under long-slow fire (Abaqus)

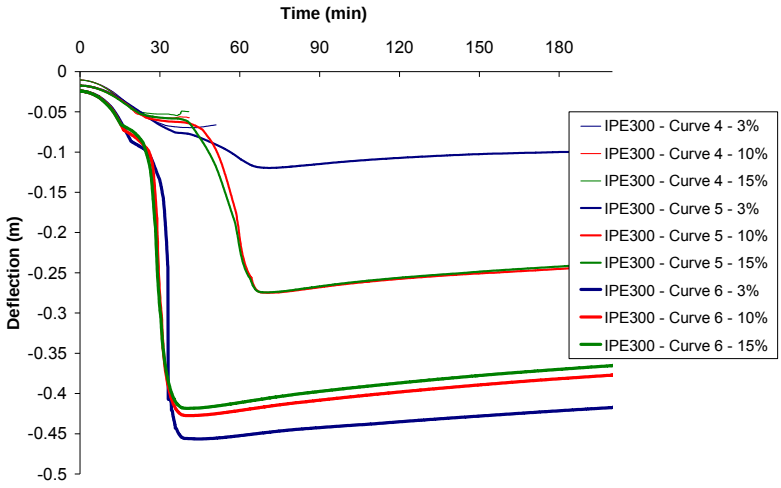

Figure C-6 : Vertical deflections of the 6-metre long IPE 300 beams under long-slow fire (SAFIR)

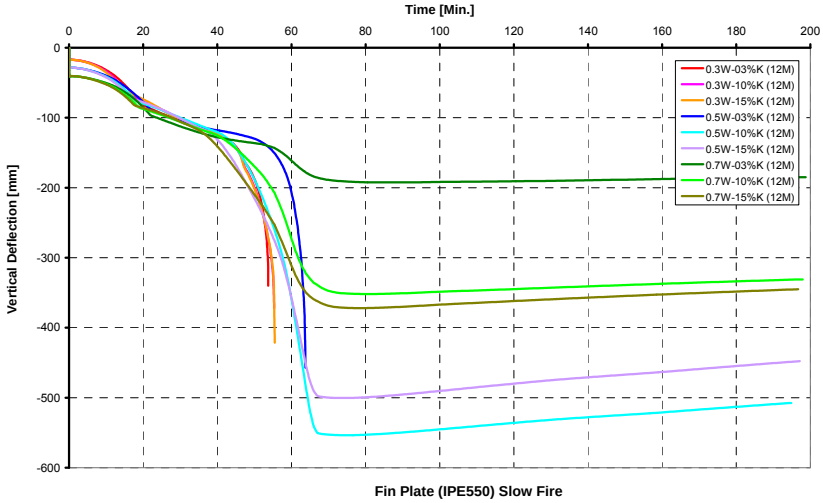

Figure C-7 : Vertical deflections of the 12-metre long IPE 550 beams under long-slow fire (Abaqus)

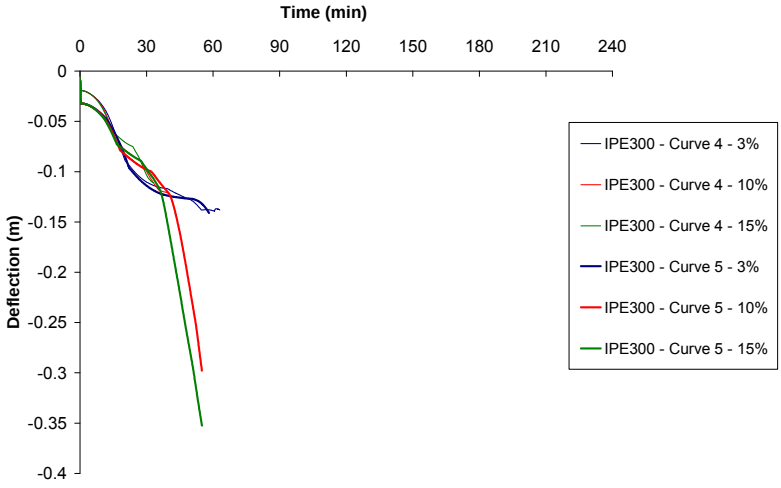

Figure C-8 : Vertical deflections of the 12-metre long IPE 550 beams under long-slow fire (SAFIR)

Appendix D Time- beam deflection diagrams of the parametrical analyses : Double web cleats connections

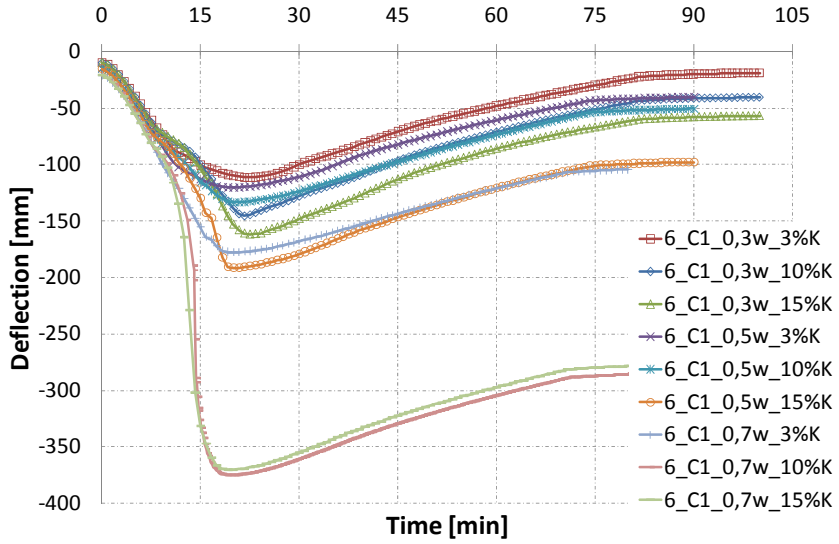

Figure D-1 : Vertical deflections of the 6-metre long IPE 300 beams under short-quick fire (ANSYS)

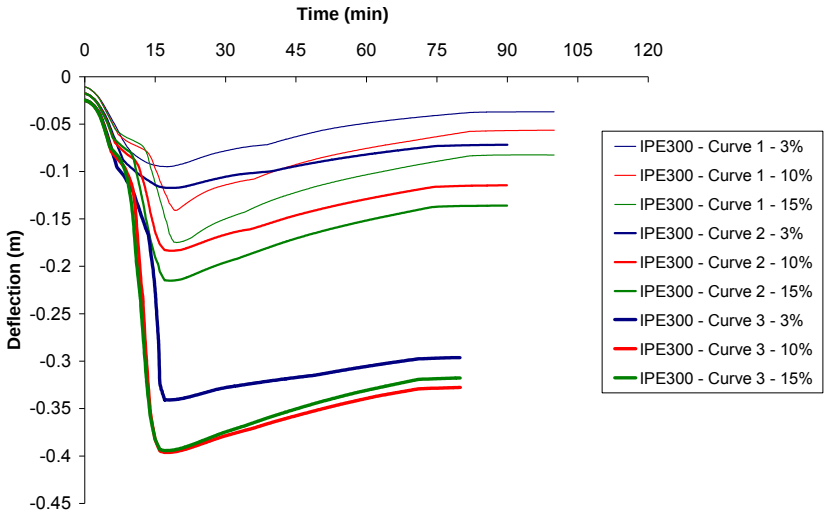

Figure D-2 : Vertical deflections of the 6-metre long IPE 300 beams under short-quick fire (SAFIR)

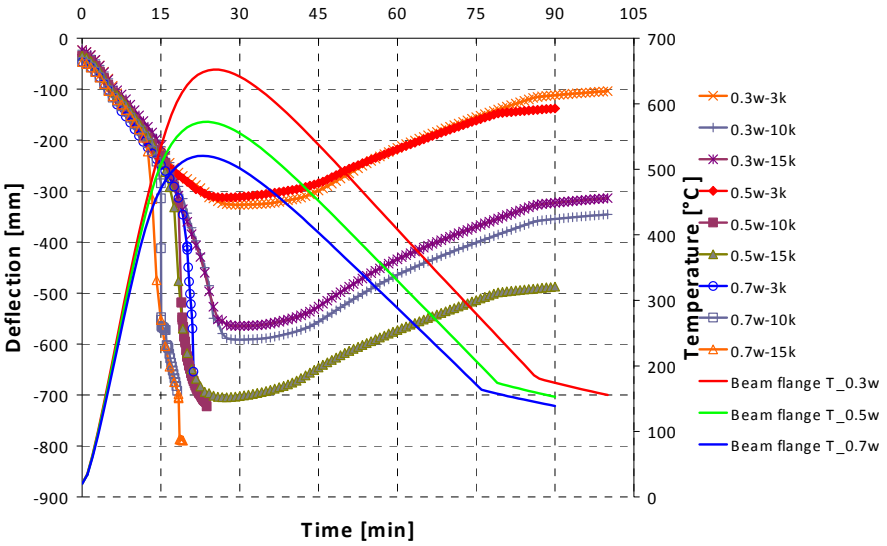

Figure D-3 : Vertical deflections of the 12-metre long IPE 550 beams under short-quick fire (ANSYS)

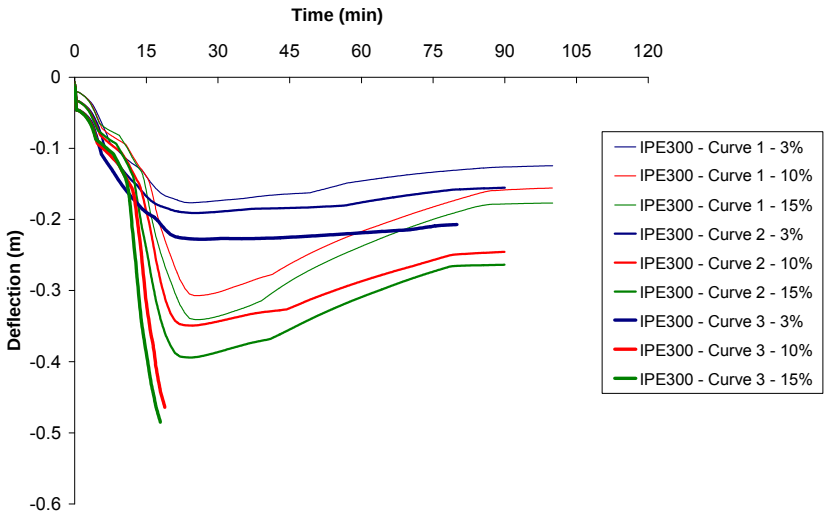

Figure D-4 : Vertical deflections of the 12-metre long IPE 550 beams under short-quick fire (SAFIR)

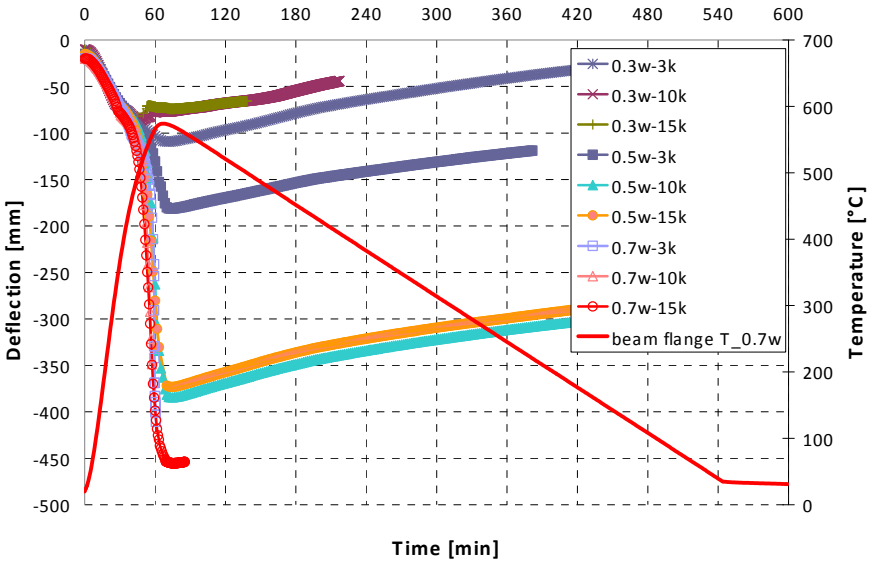

Figure D-5 : Vertical deflections of the 6-metre long IPE 300 beams under long-slow fire (ANSYS)

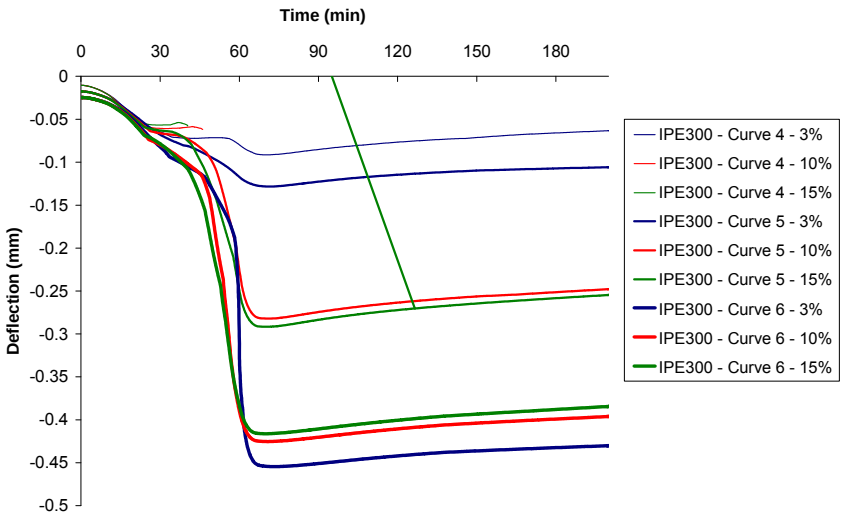

Figure D-6 : Vertical deflections of the 6-metre long IPE 300 beams under long-slow fire (SAFIR)

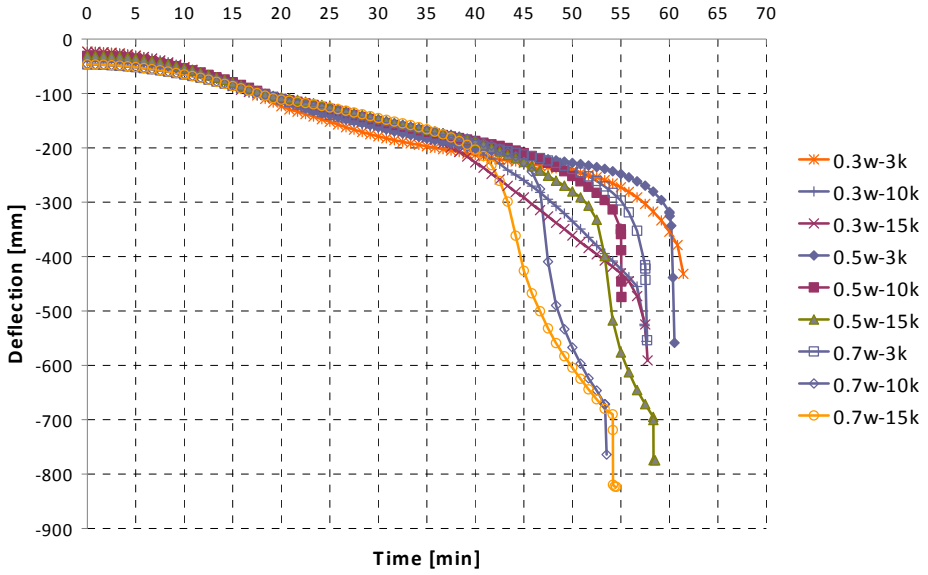

Figure D-7 : Vertical deflections of the 12-metre long IPE 550 beams under long-slow fire (ANSYS)

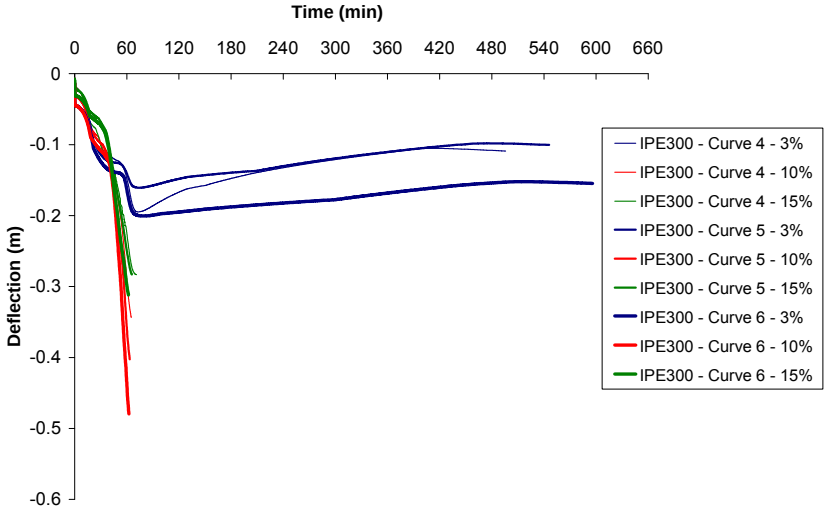

Figure D-8 : Vertical deflections of the 12-metre long IPE 550 beams under long-slow fire (SAFIR)

Appendix E Time- beam deflection diagrams of the parametrical analyses : Header plate connections

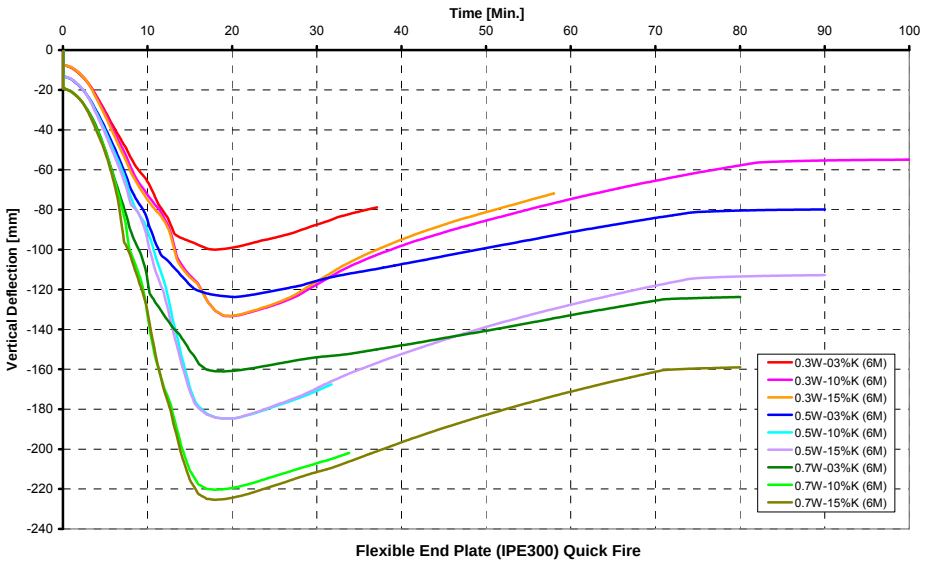

Figure E-1 : Vertical deflections of the 6-metre long IPE 300 beams under short-quick fire (Abaqus)

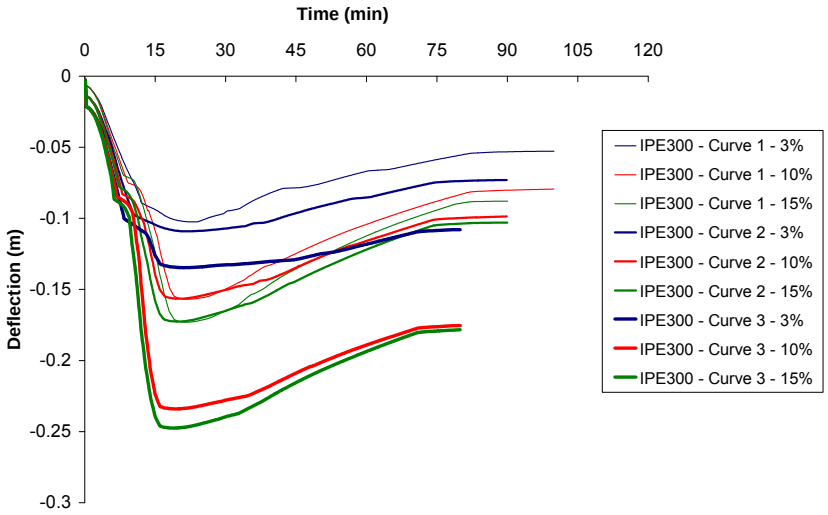

Figure E-2 : Vertical deflections of the 6-metre long IPE 300 beams under short-quick fire (SAFIR)

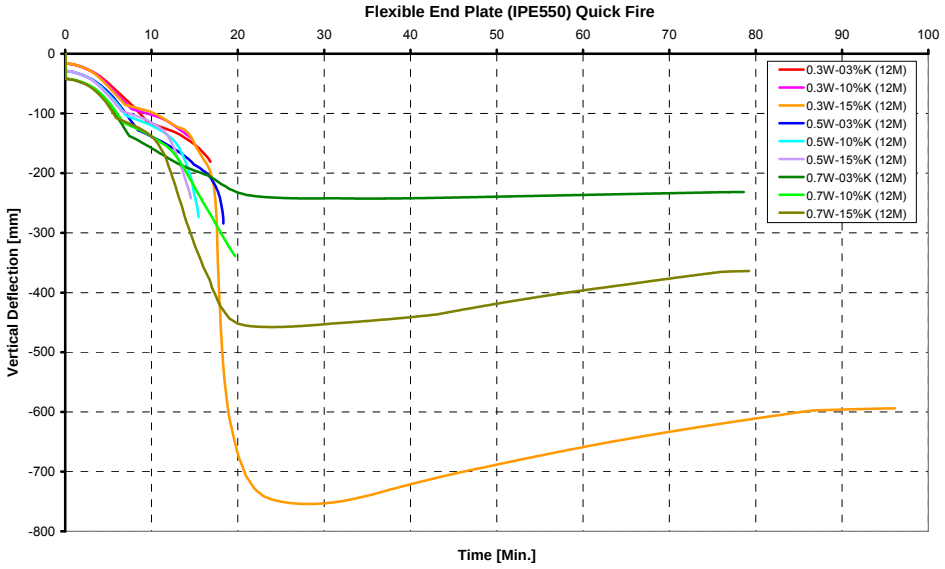

Figure E-3 : Vertical deflections of the 12-metre long IPE 550 beams under short-quick fire (Abaqus)

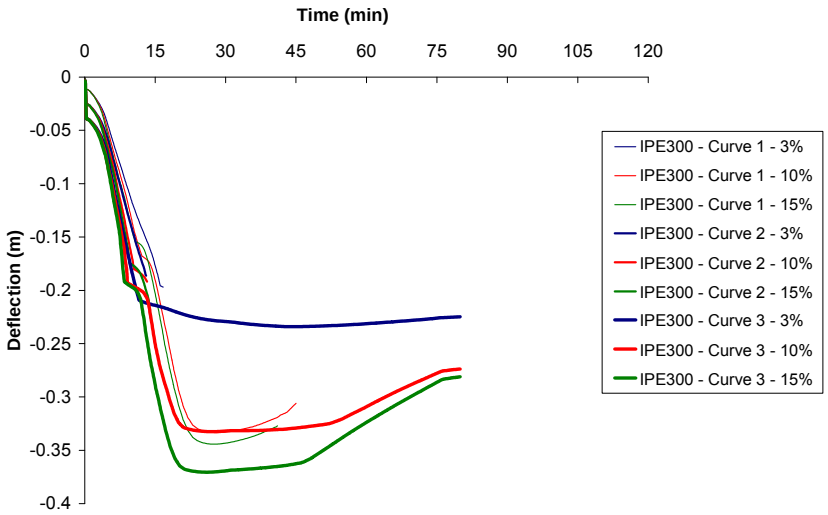

Figure E-4 : Vertical deflections of the 12-metre long IPE 550 beams under short-quick fire (SAFIR)

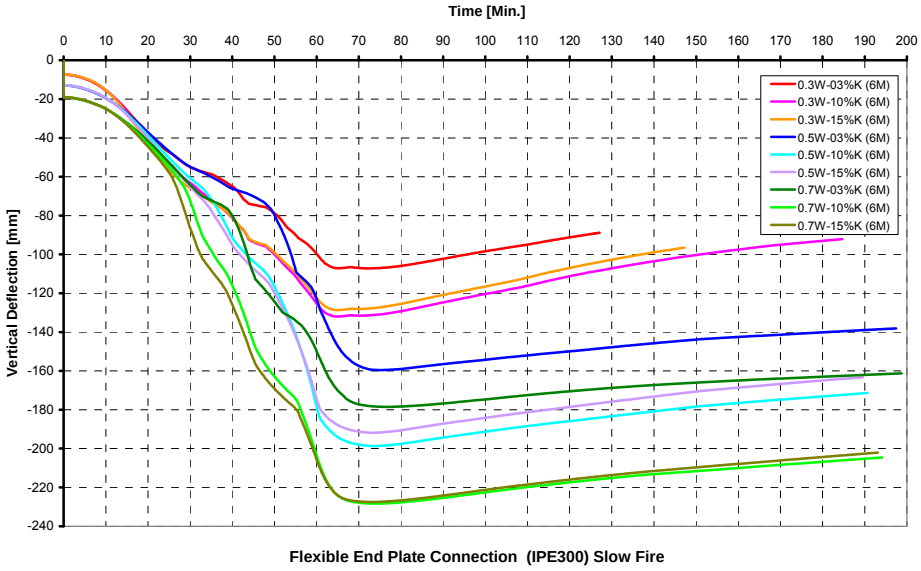

Figure E-5 : Vertical deflections of the 6-metre long IPE 300 beams under long-slow fire (Abaqus)

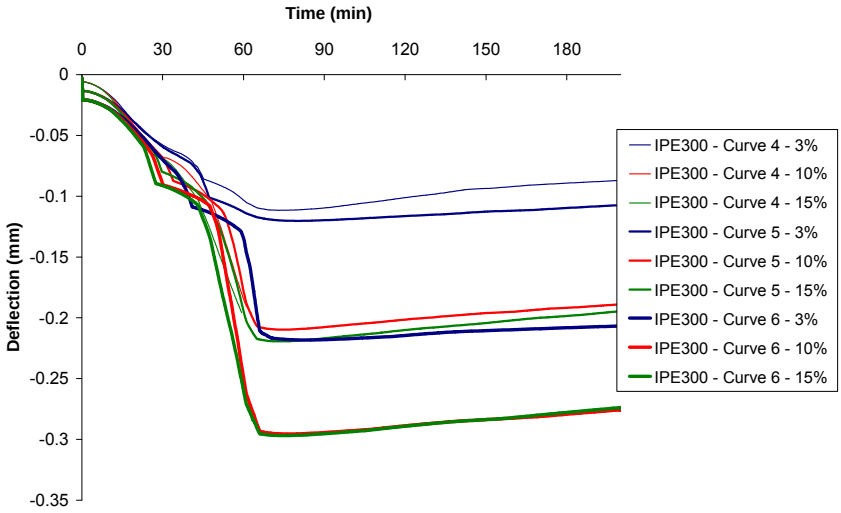

Figure E-6 : Vertical deflections of the 6-metre long IPE 300 beams under long-slow fire (SAFIR)

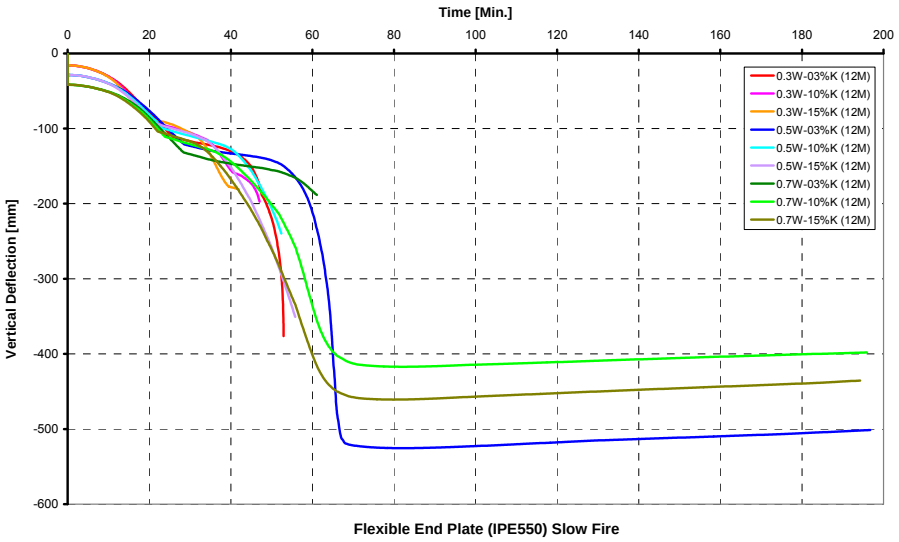

Figure E-7 : Vertical deflections of the 12-metre long IPE 550 beams under long-slow fire (Abaqus)

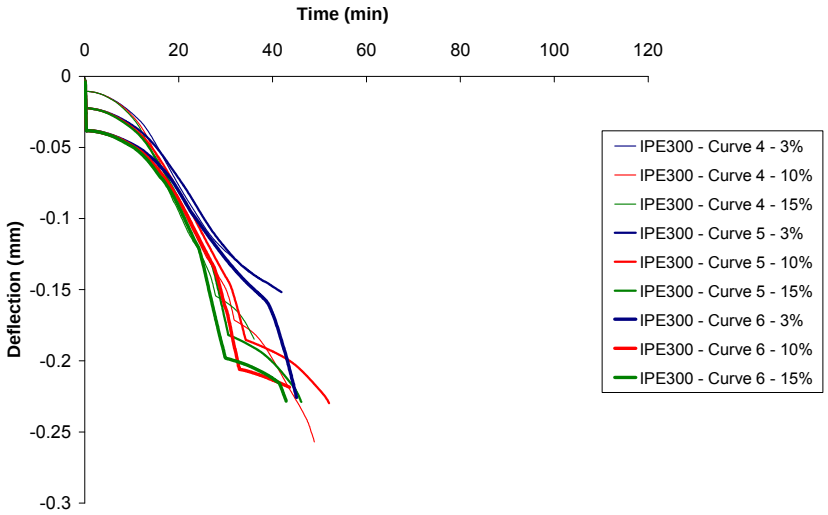

Figure E-8 : Vertical deflections of the 12-metre long IPE 550 beams under long-slow fire (SAFIR)